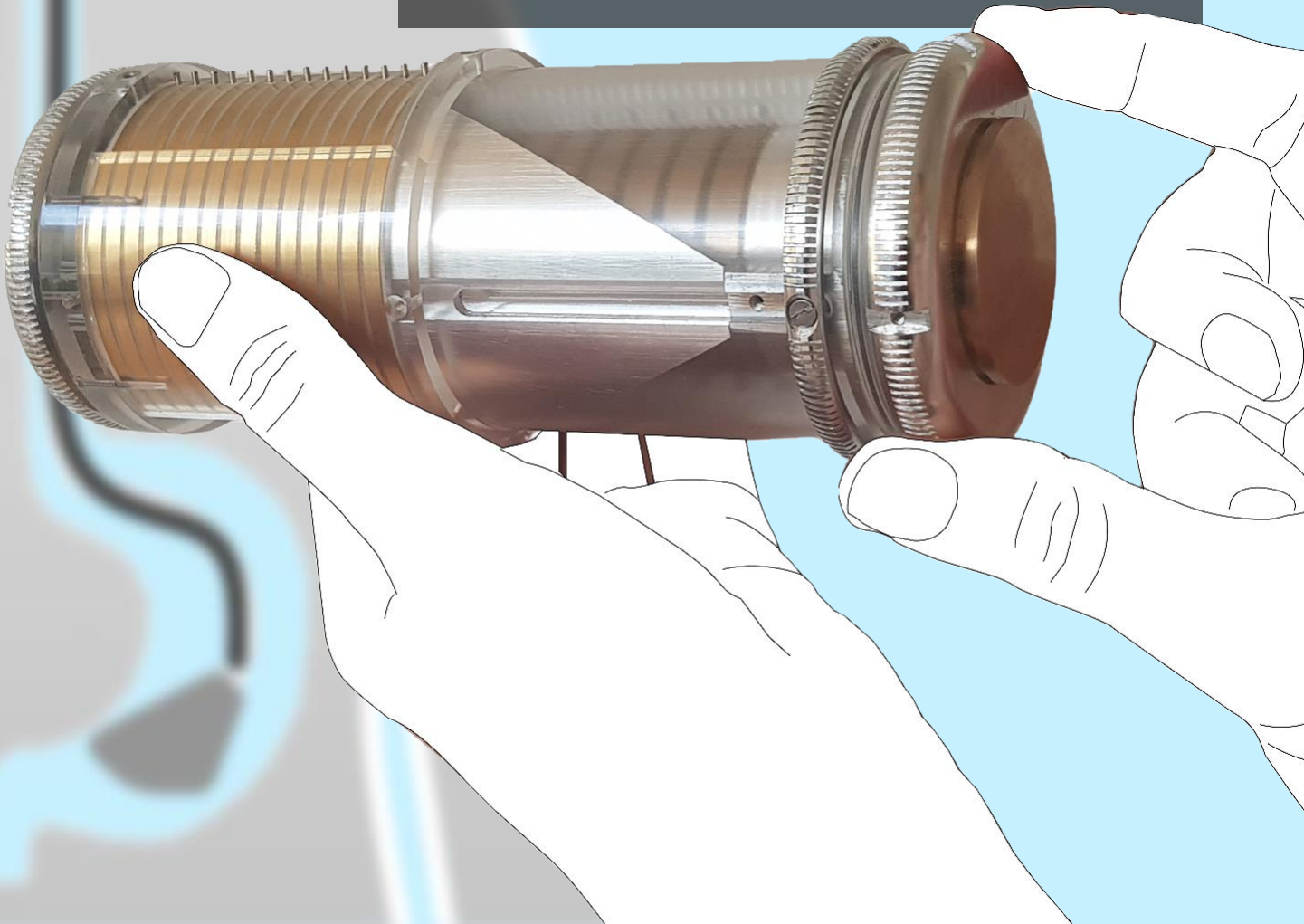


Cryptex Programmable Memory Mechanism

A mechanically programmable
path mechanism for minimally
invasive surgery tools

P.M. van Zaanen

20-01-2021



Cryptex Programmable Memory Mechanism

**Mechanically programmable path mechanism
for minimally invasive surgery tools**

by

P.M. van Zaanen

to obtain the degree of Master of Science
at the Delft University of Technology,
to be defended publicly on the 27th of January 2021.

Student number: 4349806
Thesis committee: Prof. dr. ir. P. Breedveld, TU Delft, supervisor
Ir. F. Trauzettel, TU Delft, supervisor
Dr. ir. J.F.L. Goosen, TU Delft, committee

This thesis is confidential and cannot be made public until 20/01/2023

After 20/01/2023, an electronic version of this thesis is available at
<http://repository.tudelft.nl/>.

Acknowledgements

I would like to acknowledge everyone who has contributed to this thesis and helped me accomplish these results. First and foremost, I would like to express my sincere gratitude towards my professor and supervisor, Prof.dr.ir. P. Breedveld. With his enthusiasm and expertise in mechanical mechanisms and path-planning devices, he has motivated and guided me throughout the whole process. The weekly discussions and brainstorm sessions at the beginning of the project have provided me with a lot of new insights and knowledge. I would also like to express my sincere appreciation to my daily PhD-supervisor ir. F. Trauzettel, for his continuous support throughout the whole process of forming this thesis. The weekly meetings provided me with valuable feedback, ideas and encouragement. Finally, I would like to thank the precision technicians from DEMO: D. Jager and R. van Starckenburg. Not only did they manufacture a beautiful prototype, but I could also always go to them to consult and discuss different design options.

Thank you.

Abstract

In the history of medicine and surgery, a slow transition is made from open surgery to minimally invasive surgery. Nowadays, natural orifice transluminal endoscopic surgery (NOTES) is investigated and tested. NOTES is a new development in surgery methods that includes flexible instruments, which are inserted through natural orifices such as the mouth, nose, anus or vagina. The instrument then passes transluminally towards the areas of interest [5]. Benefits of this surgery method compared to conventional open surgery include, among others: the reduction in tissue trauma, no external scar tissue, less blood loss and a shorter recovery period [1][37]. However, the method requires highly advanced medical devices that are slender and able to bend and form different paths to reach the area of interest. Bio-inspired by the movement and the propulsion of a snake, new instruments are being developed that provide a follow-the-leader motion (FTL-motion). In a follow-the-leader mechanism, the user steers the tip of the instrument. The position given to the tip is stored and passed on proximally from segment to segment. The control of the shaft segments can be done with a robotic or mechanical design. Robotics for such a complex task seem promising. However, robotics in surgery tools is still under discussion, because of high costs and the chance of system failures [2]. Therefore, this thesis aims to improve the existing mechanically controlled FTL-mechanisms, in which the shaft is controlled with four-cable control.

In this research, a cylindrical mechanical path-planning module is designed and manufactured: the Cryptex Programmable Memory Mechanism (CPMM). The prototype is designed to provide a follow-the-leader motion in a compliant shaft with 15 segments. The cylindrical shape improves cable-control, as it can simultaneously steer one cable and its antagonist, and control the motion of a compliant shaft in one plane. The design exists out of input elements and output elements. The orientation of multiple input rings is controlled by the user. The relative orientations of the input rings form a path. After that, the given orientations are locked and transferred by a guiding element to the output rings. The rotation of the output rings causes the pulling and releasing of cables that actuate the rotation of segments. As part of this research, a modified 3D printed version has been manufactured as well. Both designs were manually tested in four phases: individual components and subassemblies; the key component solely; integrated design excluding the key component; completely integrated design. It is concluded that the design of the 3D printed prototype is limited by the accuracy of the parts and the material properties. With a lot of play and jamming, the 3D printed prototype is deemed insufficient. The machined prototype shows promising results, as it can form diagonal and curved paths as an output. However, optimisation is required for the guiding element to improve the performance of the prototype. Even though the performance of the CPMM prototype leaves room for improvement, it does validate that the proposed concept can provide the follow-the-leader motion.

Contents

List of Figures	xi
List of Tables	xv
1 Introduction	1
1.1 Developments in surgery methods	1
1.1.1 Open surgery	2
1.1.2 Minimally invasive surgery	2
1.1.3 Natural orifice transluminal endoscopic surgery	2
1.2 Instruments for surgical procedures	3
1.2.1 Snake-like surgical instruments	4
1.2.2 Mechanically and electrically controlled instruments	6
1.3 Problem statement and goal	7
1.4 Structure of this thesis	7
2 State of the Art	9
2.1 Cable-driven FTL-mechanisms	9
2.2 Fixed path FTL-mechanisms	12
2.2.1 MemoFlex I	12
2.2.2 MemoFlex II	13
2.3 Programmable path FTL-mechanisms	14
2.3.1 MemoSlide	14
2.3.2 MemoBox	16
2.4 Evaluation of the state of the art	18
3 Design process	21
3.1 Introduction	21
3.2 Engineering design process	21
3.2.1 Problem definition	21
3.2.2 Information gathering	22
3.2.3 Solution generation	22
3.2.4 Analysing and selecting one solution	22
3.2.5 Developing, testing and implementing	23
3.3 CPMM design phase and timeline	23
4 Mechanism design	25
4.1 Design objectives and requirements	25
4.2 First sketch	27
4.3 Concept generation	30
4.3.1 Path input: shafts and memory rings	31
4.3.2 Path output: reading rings	33
4.3.3 Path transmission: guidance	33
4.3.4 Path insertion: translational motion	35
4.3.5 Cable guidance	36
4.3.6 Exclusion of solutions	37
4.3.7 Basic idea of the concepts	39
4.3.8 Concepts	40
4.4 Concept selection	45
4.5 Final design	46
4.5.1 Design of possible critical parts	46
4.5.2 Overview of the parts	54
4.5.3 Dimensioning	54

5	Integrated functioning: working principle	59
5.1	Path input	59
5.2	Path output	60
5.3	User input and the instrument's shaft output relations	65
5.4	Ergonomics	68
6	Proof of concept: Machined prototype	71
6.1	Introduction	71
6.2	Materials	72
6.3	Testing the key component: H-beam	72
6.3.1	Testing different H-beams	73
6.3.2	H-beam evaluation	76
6.4	Testing the prototype	76
6.4.1	Test method	76
6.4.2	Test phase 1: individual parts and subassemblies	77
6.4.3	Test phase 2: prototype without H-beam	78
6.4.4	Test phase 3: path input	79
6.4.5	Test phase 4: complete prototype	81
6.4.6	Changes made during the test phases	85
6.5	Design evaluation	86
7	Proof of concept: 3D printed prototype	87
7.1	Purpose	87
7.2	Parts and differences with the machined prototype	88
7.3	3D printers and materials	89
7.4	Dimensioning	90
7.5	Testing the prototype	92
7.5.1	Test method	92
7.5.2	Test phase 1: individual parts and subassemblies	92
7.5.3	Test phase 2: prototype without H-beam	93
7.5.4	Test phase 3: path input	94
7.5.5	Test phase 4: complete prototype	96
7.6	Design evaluation	97
7.6.1	Functionalities of the 3D printed prototype	97
7.6.2	Benefits and downsides of 3D printing	97
8	Design implementation	99
8.1	CPMM in a surgical instrument	99
8.2	Incorporated design	100
9	Discussion	103
9.1	Machined prototype	103
9.1.1	Performance of the prototype	103
9.1.2	Design limitations and recommendations for improvements	105
9.1.3	Overview of recommendations for further research.	110
9.2	3D printed prototype	111
9.2.1	Performance of the prototype	111
9.2.2	Limitations of the prototype	112
9.2.3	Comparison of the two prototypes	115
9.2.4	Overview of recommendations for further research.	116
9.3	CPMM in a medical instrument	116
9.3.1	Incorporated design	116
9.3.2	Safety	117
9.3.3	Sterilisability	118
9.3.4	Recommendations for the CPMM in a medical instrument.	118

10 Conclusion	119
Bibliography	121
A Design process	125
B Integrated functioning	131
C H-beam	133
D Machined prototype	137
E 3D printed prototype	159
F MATLAB scripts	185

List of Figures

1.1	Surgery methods categorised based on invasiveness	1
1.2	Follow-the-leader mechanism bio-inspired by the movement of a snake	4
1.3	The Flex system and MemoFlex I	5
2.1	Four cable control of a segmented shaft	9
2.2	State of the art: the four existing prototypes	11
2.3	Working principle of the MemoFlex I	12
2.4	Working principle of the MemoFlex II	13
2.5	Working principle of the MemoSlide	15
2.6	Working principle of the MemoBox	17
3.1	Engineering design cycle	22
3.2	Design process of the CPMM prototype	24
4.1	One of the first sketches from the CPMM prototype	29
4.2	Sketch of the main components of the prototype	30
4.3	Solution tree for the path input	31
4.4	Solution tree haptic feedback for path input	32
4.5	Solution tree for guiding	34
4.6	Solution tree for continuous rail guidance	34
4.7	Solution tree for the translational motion of the input elements	35
4.8	Solution tree of haptic feedback mechanism while translating the input elements	36
4.9	Solution tree of the guiding of the cables	37
4.10	Guidance design challenges	39
4.11	Basic idea of the concepts	40
4.12	Concept 1	41
4.13	Concept 2	42
4.14	Concept 3	43
4.15	Concept 4	44
4.16	CAD final design	46
4.17	Calculation critical part: teeth profile of input elements	48
4.18	Calculation of critical part: disk friction of the output rings	50
4.19	H-beam deformation, change in length	51
4.20	Torsion of the H-beam	53
4.21	Exploded view of the complete design	55
4.22	Exploded view of the shaft assembly	56
4.23	Exploded view of the memory rings with the translational motion mechanism	56
4.24	Exploded view of the reading rings and the frame	57
4.25	Exploded view of the casing components	57
4.26	Bill of materials	58
5.1	Working principle of the translational motion mechanism of the CPMM	60
5.2	Working principle: path input	61
5.3	Working principle: H-beam	62
5.4	Working principle: path output	63
5.5	Working principle of the reading rings and antagonist cables	64
5.6	Four cable control of the shaft	66
5.7	Input Output relations	67
5.8	Ergonomics of the prototype	69

6.1	Pictures of the machined prototype	71
6.2	H-beam dimensions	73
6.3	H-beam testing and optimisation 1	74
6.4	H-beam failure modes	74
6.5	H-beam testing and optimisation 2	75
6.6	Test phase 1: individual parts and subassemblies	77
6.7	Test phase 2: without H-beam	78
6.8	Test phase 3: path input	79
6.9	Test results: input function of the machined prototype	80
6.10	Test phase 4: complete prototype	81
6.11	Path output: diagonal shape	82
6.12	Path output: curved shape	83
6.13	Path output: multi-curved shape	84
6.14	H-beam failure in test 3	85
6.15	Summary machined prototype evaluation	86
7.1	Picture of the 3D printed prototype	87
7.2	3D printers available for this project and their specifications	89
7.3	3D printed prototype spacing for geared profile	90
7.4	Test phase 1: individual parts and subassemblies	93
7.5	Test phase 2: without H-beam	94
7.6	3D printed prototype play in reading rings	94
7.7	Test phase 3: input function of the 3D printed prototype	95
7.8	Test phase 3: path input	96
7.9	Test phase 4: complete prototype	96
7.10	Fails in 3D printing	98
8.1	Concepts for CPMM incorporated in surgical instrument	99
8.2	Incorporated design	101
9.1	Performance of the prototype compared to the functional requirements	104
9.2	Performance of the prototype compared to the design requirements	106
9.3	Failure mode of the H-beam due to compression and buckling	108
9.4	Alternatives for the guiding elements	109
9.5	Reading ring frame design recommendation	110
9.6	Performance of the 3D printed prototype compared to the functional requirements	112
9.7	Performance of the 3D printed prototype compared to the design requirements	113
9.8	Comparison of the prototypes	115
A.1	Solution space of the main functions	126
A.2	Solution space of the haptic feedback mechanisms	127
A.3	Concept 1 with Hirth coupling	128
A.4	Reading ring frame concepts (1)	129
A.5	Reading ring frame concepts (2)	130
B.1	Alternative solution for steering	131
C.1	H-beam test method	135
C.2	Test results H-beam test 3	135
C.3	Test results H-beam test 4	136
D.1	Construction drawings of the inner shaft - Machined prototype	138
D.2	Construction drawings of the inner shaft part 2 - Machined prototype	139
D.3	Construction drawings of the inner shaft part 3 - Machined prototype	139
D.4	Construction drawings of the inner shaft part 4 - Machined prototype	140
D.5	Construction drawings of the fixed shaft - Machined prototype	141
D.6	Construction drawings of the input shaft - Machined prototype	142

D.7	Construction drawings of the input knob - Machined prototype	143
D.8	Construction drawings of the input knob pins - Machined prototype	143
D.9	Construction drawings of the end knob - Machined prototype	144
D.10	Construction drawings of a memory ring - Machined prototype	145
D.11	Construction drawings of the H-beam - Machined prototype	146
D.12	Construction drawings of the translational motion main part - Machined prototype	147
D.13	Construction drawings of the translational motion front part - Machined prototype	148
D.14	Construction drawings of the connection pin connecting the two translational motion parts - Machined prototype	148
D.15	Construction drawings of the translational motion input knob - Machined prototype	149
D.16	Construction drawings of the pin connecting the translational motion mechanism to the translational motion input knob - Machined prototype	149
D.17	Construction drawings of the reading ring - Machined prototype	150
D.18	Construction drawings of the reading ring frame rings in between - Machined prototype	150
D.19	Construction drawings of the reading ring frame outside ring- Machined prototype	151
D.20	Construction drawings of the reading ring frame pin - Machined prototype	151
D.21	Construction drawings of the casing front part - Machined prototype	152
D.22	Construction drawings of the casing middle part - Machined prototype	153
D.23	Construction drawings of the casing end part - Machined prototype	154
D.24	Machined prototype: picture of the three building assemblies	155
D.25	Picture of the input knob and the input shaft from the machined prototype	156
D.26	Picture of the translational motion mechanism from the machined prototype	156
D.27	Picture of the memory ring from the machined prototype	157
D.28	Picture of the reading ring assembly from the machined prototype	157
D.29	Picture of the casing assembly from the machined prototype	158
E.1	Exploded view of 3D printed prototype	160
E.2	Bill of materials 3D printed prototype	161
E.3	Machined vs. 3D printed prototype 1/3	162
E.4	Machined vs. 3D printed prototype 2/3	163
E.5	Machined vs. 3D printed prototype 3/3	164
E.6	Construction drawings of the inner shaft - 3D Printed prototype	165
E.7	Construction drawings of the inner shaft part 2 - 3D Printed prototype	166
E.8	Construction drawings of fixed shaft and the end knob combination - 3D Printed prototype	167
E.9	Construction drawings of input shaft and the input knob combination - 3D Printed prototype	168
E.10	Construction drawings of the pins of the input knob - 3D Printed prototype	168
E.11	Construction drawings of the memory ring- 3D Printed prototype	169
E.12	Construction drawings of the H-beam - 3D Printed prototype	170
E.13	Construction drawings of translational motion main part - 3D Printed prototype	171
E.14	Construction drawings of translational motion front part - 3D Printed prototype	172
E.15	Construction drawings of translational motion input knob - 3D Printed prototype	173
E.16	Construction drawings of the reading ring - 3D Printed prototype	174
E.17	Construction drawings of the reading ring frame in between - 3D Printed prototype	174
E.18	Construction drawings of the reading ring frame outside rings - 3D Printed prototype	175
E.19	Construction drawings of the reading ring frame holder - 3D Printed prototype	176
E.20	Construction drawings of the casing front part - 3D Printed prototype	177
E.21	Construction drawings of the casing middle part - 3D Printed prototype	178
E.22	Construction drawings of the casing end part - 3D Printed prototype	179
E.23	3D printed shaft and memory ring version 3	180
E.24	3D printed prototype, rectangular teeth.	180
E.25	Picture of the inner shaft from the 3D printed prototype	181
E.26	Picture of the input knob-shaft and the end knob and fixed shaft from the 3D printed prototype.	181
E.27	Picture of the translational motion parts from the 3D printed prototype	182
E.28	Picture of the translational motion parts and the memory rings from the 3D printed prototype	182
E.29	Picture of the memory rings from the 3D printed prototype	183

E.30 Picture of the reading rings in their frame from the 3D printed prototype	183
E.31 Picture of the casing components of the 3D printed prototype	184
F.1 MATLAB script for the input output relations of the CPMM	185

List of Tables

2.1	Characteristics of the state of the art	19
4.1	Functional requirements	26
4.2	Element design requirements	28
4.3	Selection criteria	38
4.4	Concept selection	45
5.1	Working principle: input output relations	67
5.2	Working principle: stepwise input output relations	67
6.1	Machined prototype parts and materials used	72
7.1	3D printed prototype parts, printing technique and materials	90
7.2	Spacing used for the printed shaft and memory rings	91
7.3	Spacing between the 3D printed parts	92
9.1	Possible failure modes of the CPMM prototype and their occurrence in the machined prototype	107
9.2	Possible failure modes of the 3D printed CPMM prototype and their occurrence	114
C.1	Test results and characteristics of H-beams	134

Nomenclature

<i>CPMM</i>	Cryptex Programmable Memory Mechanism
<i>DEMO</i>	Dienst Elektronische en Mechanische Ontwikkeling
<i>DOF</i>	Degrees Of Freedom
<i>EDM</i>	Electrical Discharge Machining
<i>FDM</i>	Fused Deposition Modeling
<i>FTL</i>	Follow-The-Leader
<i>MIS</i>	Minimally Invasive Surgery
<i>NOTES</i>	Natural Orifice Transluminal Endoscopic Surgery
<i>SILS</i>	Single-Incision Laparoscopic Surgery
<i>SLA</i>	Stereolithography
<i>SSL</i>	Single-Site Laparoscopy

Introduction

1.1. Developments in surgery methods

For ages, surgery has played an essential role in the healing of humans and animals. Over time, surgery methods have changed significantly. This is caused by the increased knowledge in anatomy and physiology, but mostly by the increasing role of technology in surgery. The development in surgery procedures is guided by the introduction of new technology in combination with the expanding skill set of the surgeon.

The Cambridge Dictionary defines surgery as: *(medical operation) "The treatment of injuries or diseases in people or animals by cutting open the body and removing or repairing the damaged part"* [12].

Reflecting on this definition, surgery includes cutting open the body to create space and access to the diseased or damaged tissue. Meaning, it is an invasive procedure. However, with the new developments in the medical field, surgical procedures can be categorised based on their degree of external invasiveness. A distinction can be made between open surgery, minimally invasive surgery and natural orifice transluminal surgery. These groups also represent the medical progress in surgery methods over time. In the history of surgery, a slow transition is made from open surgery to minimally invasive surgery. Nowadays, surgery methods are investigated that do not require any external incisions. The three groups of surgery methods are shown in Figure 1.1 and further elaborated in this chapter.

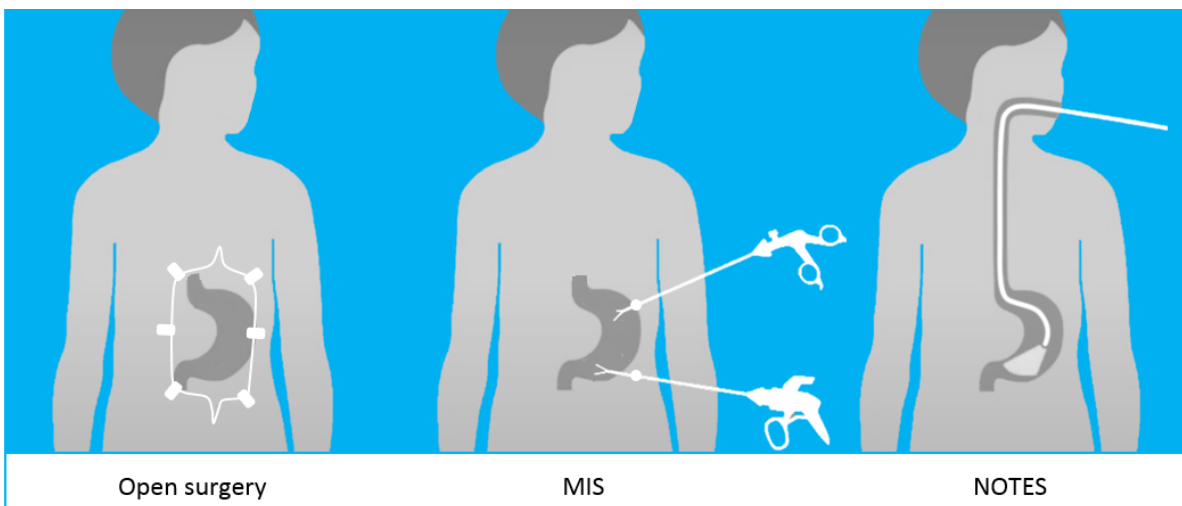


Figure 1.1: Surgery methods categorised based on external invasiveness. For open surgery, a relatively large incision is made. Clamps are used to fold this incision open and expose all the target issue. Minimally invasive surgery (MIS) includes one or multiple small incisions for the insertion of slender surgical instruments. For a NOTES procedure (Natural Orifice Transluminal Endoscopic Surgery), the medical device is inserted via a natural orifice, in this case the mouth.

1.1.1. Open surgery

The first operations on humans and animals were conducted with open surgery methods. During open surgery, relatively large incisions are made to expose the target tissue to the surgeon's direct view and to create space for the surgical instruments. Often, clamps are used to hold the incision open, creating a large hole. Therefore, open surgery is an invasive method, causing large wounds and much tissue trauma for significant procedures. Large surgical procedures that require large incisions can be very tough on the human body. The skin and underlying tissue endure a lot of trauma. Therefore, the recovery period can be long and much scar tissue can be a result. The first image in Figure 1.1 is a schematic representation of open surgery on the stomach. A vertical incision is spread open by clamps and the full stomach can be accessed with conventional surgery tools. The surgeon can directly view the stomach and has a lot of workspace to examine or treat the tissue.

1.1.2. Minimally invasive surgery

With the development of new surgical instruments and improved skills of the surgeon, minimally invasive surgery methods were developed to reduce the patient's tissue trauma. The introduction of minimally invasive surgery (MIS) was a significant development in the history of medicine. The method can be described as a medical procedure that allows surgeons to operate on the human body, using only small incisions for the insertion of cameras and slender instruments into a body cavity. The incision size varies typically between 8 and 19 mm [24]. This runs counter to classical open surgery where incisions can be relatively large to expose the tissue to the surgeon's direct view and to create space for surgical instruments. In most minimally invasive procedures, multiple small incisions are made, so surgical instruments are inserted into the body cavity from different locations and angles (multi-port surgery). The second image in Figure 1.1 shows two entry points, but three or four entry points are also a common quantity [31]. Single-port minimally invasive surgery also exists: the surgeon operates through one single entry point in the body. Terms used for this procedure are, among others: single-incision laparoscopic surgery (SILS) and single-site laparoscopy (SSL) [32]. In this case, the navel is frequently used as an entry point.

MIS is an umbrella term for several different medical procedures, such as laparoscopy and arthroscopy. Laparoscopy is derived from the Greek word *lapara*, meaning "flank", and *scope*, meaning "an instrument for observation". It can be defined as a surgical technique in which a slender camera, called a laparoscope, is inserted through a small incision in the abdominal wall to perform a procedure [33][34]. Laparoscopy usually requires at least two incisions: one for the laparoscope and the other for the surgical tool. Arthroscopy is an MIS-method used to operate on a joint. For example, the knee or shoulder joint. Generally, three entry points are required for an arthroscope (slender camera) and two tools to examine and treat the damage in the joint [25]. Laparoscopy, arthroscopy and other minimally invasive methods have become very common and are, if applicable, preferred over open surgery.

Minimally invasive surgery has many benefits. For the patient, the reduction in incision size minimises blood loss and tissue trauma [1][37], ultimately reducing the recovery period and the scar tissue formed as a result of the operation. Furthermore, the chance of postoperative complications, like pain, infection and dehiscence, is generally lower when compared to conventional surgical techniques [1]. Minimally invasive surgery also has a positive impact on society. As the recovery period is shorter, the hospital time is reduced, which makes the method cheaper. A faster recovery means that the patient can pick up his or her everyday life and start working again [15]. However, the size limitation of the instrument in combination with the limitation in motion range, limits surgeons performing MIS to choosing devices that are specifically designed for this kind of procedure. Thus, MIS procedures require specialised instruments and advanced skills of the surgeon.

1.1.3. Natural orifice transluminal endoscopic surgery

Because minimally invasive surgery has many benefits, surgeons and technicians seek ways to improve this method. The goal is to minimise the number and the size of the incisions, or in the case of natural orifice transluminal endoscopic surgery (NOTES), to eliminate all external incisions [4]. NOTES is a new development in surgery methods that includes flexible instruments, which are inserted through natural orifices such as the mouth, nose, anus or vagina. The instrument then passes transluminally

towards the areas of interest [5]. No external incisions are made; therefore, it is non-invasive externally. Of course, during the operations, incisions are made inside the body to repair or remove tissue. For a NOTES procedure, an existing flexible endoscope is used in combination with functional end-effectors, such as graspers, clamps and scissors. The endoscope used is a thin, flexible rod, containing a light and small camera that can visualise the inside of the patient's body [34].

In the right image of Figure 1.1, an example is shown in which a medical instrument is inserted via the mouth towards the stomach. This is an example of transesophageal endoscopy (TE): from the mouth through the oesophagus towards the area of interest. Many NOTES procedures exist, such as transvaginal endoscopy (TVE). For example, transvaginal cholecystectomy: removing the gallbladder via the vagina. Endoscopic Endonasal Surgery (EES) is also a kind of NOTES procedure in which the base of the skull is examined, using the nostrils as entry port. For example, tumours or abnormalities of the pituitary gland can be treated with this method.

The advantages of a NOTES procedure over the open surgery or laparoscopic approach comes from the fact that no external incision has to be made. Common complications are eliminated, such as wound infections or for example, a hernia in the case of abdominal surgery [5][26]. However, the method requires advanced instruments that can provide multiple degrees of freedom and are able to reach the target tissue. For example, the path the endoscope has to make from the mouth to the stomach is not straight. The medical instrument should bend in the pharynx to move from the mouth into the oesophagus. Also, entering and examining the inside of the stomach requires movement of the shaft and the end-effector of the instrument. Another example is Endoscopic Endonasal Surgery (EES). With straight, rigid surgery tools, the surgeon cannot reach all the areas of the pituitary gland. This is because the nostrils are small, and the bony walls restrict the movement of the instruments. As a result, the tools are limited in size, have a highly restricted sideways movement and also the insertion angle is not variable [19]. Thus, performing a surgery by inserting the tools via natural orifices requires highly advanced medical devices that are able to form different paths.

1.2. Instruments for surgical procedures

The incision made for open surgery is relatively large. By opening this incision with clamps, the surgeon has enough space for surgical tools. Therefore, the instruments used for open surgery are conventional and are not heavily restricted in size. The surgical instruments and their end-effectors do not need to provide many degrees of freedom, because the surgeon has enough space to translate and rotate the complete tool.

Minimally invasive surgery instruments on the other hand, like laparoscopic devices, are limited in size because of the small entry point. Typically the tools have a maximum diameter of 10 mm. Laparoscopy involves the use of long and slender, yet rigid instruments which are inserted into the body via trocars. Besides being the insertion point of the surgeon's instruments, the trocar also functions as a fulcrum around which the instrument can rotate. This fulcrum acts as a lever mechanism: the angular motion made by the surgeon are amplified or reduced in the end-effector, depending on how deep the tool is inserted into the body. This lever mechanism also causes the translational motions of the tool to be in the opposite direction. When the surgeon steers to the left, the end-effector of the surgical tool moves to the right. The limited workspace leaves less room for instrument manoeuvrability. However, the location of the incision can be chosen by the surgeon: selecting the most optimal location and angle for the tool to reach the targeted tissue. While most minimally invasive instruments have rigid shafts, the end-effectors of certain devices, such as the LaproFlex (DEAM b.v. Amsterdam, The Netherlands) or the Da Vinci EndoWrist (Intuitive Surgical, Inc, Sunnyvale, CA, USA), can provide multiple degrees of freedom, to better reach tissues and fulfil surgical tasks. The EndoWrist exists out of two planar joints, enabling the end-effector to rotate in two directions perpendicular to each other. In this way, the mechanism provides steerability to the end-effector, while the shaft of the instrument is straight and rigid.



Figure 1.2: Follow-the-leader mechanism bio-inspired by the movement of a snake. The left figure is adapted from the BITE website [6] and shows how the new developments of FTL-mechanisms in surgical instruments are based on the motion of a snake. The right figure shows the famous game Snake, here on a Nokia 3310 phone (Nokia, Espoo, Finland).

NOTES requires the most advanced tools. Using straight and rigid instruments, even though the end-effector is steerable, is not sufficient for this operation method. The majority of the surgical procedures where a natural orifice is used as an entry point, the path towards the area of interest is not straight and requires the complete tool to make curved paths. A solution is the use of flexible endoscopes during a NOTES procedure. Flexible endoscopes contain a steerable tip and a flexible shaft. The tip is actively controlled by the surgeon through the curvy lumen. The shaft of the endoscope is passively guided by the surrounding tissue. This method requires the surrounding anatomy to be relatively strong and stiff, in order to support the guidance of the shaft. However, soft or fragile tissues, can not provide sufficient support and may possibly damage. In these cases, there is a need for having instruments with a flexible shaft, that is capable of self-guidance. Present-day developments to improve the NOTES methods are towards snake-like instruments, in which the complete surgical instrument can be steered transluminally towards the areas of interest.

1.2.1. Snake-like surgical instruments

Bio-inspired by the movement and the propulsion of a snake, new instruments are being developed that provide a follow-the-leader motion (FTL). Burgner-Kahrs et al. define an FTL-mechanism as: *"Stating that these devices must operate in a so-called follow-the-leader manner where the body conforms approximately to the path taken by its end-effector without relying on anatomical interaction forces."* [27]

In a follow-the-leader motion, the user steers the most distal part of the instrument (the tip of the tool). The position given to the tip is stored and passed on proximally from segment to segment. The orientation of the tip corresponds to the location of the tip at that moment. When a follower segment is at that specific location, it makes the orientation the tip had at that position. Therefore, the tip of the tool is the leader, and the remainder of the shaft are the followers: they follow the trajectory made by the leader. The FTL-mechanism is similar to a famous video game called Snake, in which the user controls the movement of the head of the snake and the body segments follow this movement. The user manoeuvres the snake towards food and to avoid obstacles. This can be seen in Figure 1.2.

FTL-motion requires high steerability of the complete shaft. Several types of follow-the-leader instruments have already been designed and developed. Generally, these robots were designed for exploring and inspection purposes, not for medical applications. For example, a snake-like robot developed by the robotics lab of Carnegie Mellon University was used as a rescue robot after Mexico City's Deadly Earthquake in September 2017 [40]. Equipped with a camera, the snake-like robot is able to move in confined places under debris of collapsed buildings to inspect the area and track people that are trapped. The follow-the-leader motion designs available now can be categorised into two groups, based on their working principle: telescoping and shape-shifting mechanisms.

Telescoping robots can provide the follow-the-leader motion with a telescoping mechanism: a working principle based on concentric parts that can slide and rotate into each other. The FTL-motion is achieved by extending and providing an angular displacement to the tip of the shaft, while the shape of the remainder of the shaft is secured. The first telescoping FTL-robot is developed by Webster et al. at the Vanderbilt University [39]. This design includes concentric tubes that have a predefined curvature. The concentric tubes can rotate and translate relative to each other. The overall shape of the instrument's shaft is determined by how the pre-curved tubes are concentrically placed with respect to each other. Because of the pre-curved tubes, the design is limited to making only some specific paths. Another telescoping design is provided by Neumann et al. [28]. They replaced the pre-curved tubes with flexible tubes, enabling them to realise more shapes in the shaft. The flexible tubes are steered with cables that are connected to actuators. A more advanced telescoping robot is designed by Degani et al. [29], which includes an alternating telescoping mechanism. This design consists out of two flexible concentric shafts that can advance, deform and stiffen in an alternating fashion to form the desired path [29]. The tube that is locked memorises the current shape, while the flexible tube is advanced and steered in a new position. This is continuously repeated. An existing alternating telescoping robot that is designed for medical applications, is the Flex System (Medrobotics Corp., Raynham, MA, USA). It is the only FTL-mechanism that is available for surgical procedures. Figure 1.3A shows the Flex system.

In shape-shifting mechanisms, the shaft of the instrument is built out of many segments. The user controls the direction of the most distal segment of the shaft (the first segment). The surgeon manoeuvres this segment along a path through the lumina of the patient. The computer saves these positions of the first segment and ensures that the follower segments make the same displacements at the right location. In this case, the computer has the complex task of controlling all the follower segments and their motions. An example of a shape-shifting mechanism to provide an FTL-motion is a design by Tappe et al. [35], consisting of actuators incorporated in the shaft segments. By implementing a transmission mechanism to the segments, like cables, the actuators can also be placed externally. Motors are placed outside the robot and can still control the sliding and rotation of the tubes over one another. The Bio-Inspired Technology group of the Technical University of Delft developed shape-shifting mechanisms that are fully mechanically controlled. Each shaft segment is controlled by two sets of antagonist cables: one set for the motion in the horizontal direction and one set for the motion in the vertical direction. The upper and lower cable control the up and down movement of the shaft segment. Similarly, the left and right cable can let the segment rotate to the left or right. Pulling one cable and releasing its antagonist cable, causes an angular displacement of that particular segment. Two designs developed by the BITE group included fixed-path mechanisms: the MemoFlex I [21] and the MemoFlex II [19]. The shaft of the instrument could only make one predefined shape. The MemoFlex I is shown in Figure 1.3B. Newer designs, the MemoSlide [20] and MemoBox [11], are programmable path FTL-mechanisms. These prototypes allow the user to continuously adjust the path in real-time. The MemoSlide and MemoBox are proof of principles for the FTL-motion. The path-controllers have not been incorporated into a surgical instrument, steering a compliant shaft. The current design would require four path-planning modules in the surgical instrument: one module for each group of cables. The prototypes are promising, but optimisation is necessary to incorporate it into a surgical instrument.



Figure 1.3: The Flex system (Medrobotics, Raynham, MA, USA) and MemoFlex I (BITE, Delft, The Netherlands). Figure A is the Flex system. Inside the black tube, two concentric tubes can rotate and translate with respect to each other. It is an alternating telescoping robot, that is designed for medical applications. Figure B shows the MemoFlex I. It is a shape-shifting mechanism that is fully mechanically controlled with cables. The images are adapted from Medrobotics Corp. [9] and BITE group [6].

1.2.2. Mechanically and electrically controlled instruments

The existing FTL-mechanisms can be categorised based on being mechanically and electronically controlled. Mechanical actuation means that the instrument is manually controlled and the shaft segments are steered with transmission elements. No motors and controllers are incorporated into the system. There is relatively more design freedom regarding the size and form of the instrument when the mechanism is independent of mechatronic elements. The latter group, electronically controlled FTL-mechanisms, comprises robotic solutions and includes electric actuators controlling the shaft. Generally, the shaft exists out of multiple segments that are connected with joints, enabling them to move relative to each other. Each segment's or element's motion is controlled by a separate actuator, often a small electric motor. The first designs included *intrinsic actuation*, where all the individual actuators are embedded inside the shaft segments. In other words, the shaft itself is active. The problem that arises with an intrinsic actuation design is that the diameters of these robots become too large for minimally invasive surgery procedures [35]. Thus, intrinsic actuation is insufficient for minimally invasive surgery tools, as the diameter of the shaft is difficult to minimise with the actuators positioned inside. To solve this problem, surgical robots with *extrinsic actuation* have been designed. The actuation of the segments is not located in the shaft of the instrument, but in for example the handle of the instrument. The actuators are always located outside the patient's body. This means that the shaft of the instrument can be miniaturised, making it suitable for minimally invasive procedures. Concluding, both extrinsic electrical actuation and manual actuation are promising to provide FTL-motion in a surgical instrument. Each method has advantages and disadvantages.

To electronically control a shaft with multiple shaft segments, requires many components like actuators, sensors and controllers. An advantage of mechatronic solutions is that the controlling is done by a computer. Thus the difficult tasks, such as memorising the path and shifting the shape from the tip of the tool to the shaft's proximal side, are regulated by a computer. The surgeon only has to provide the path input. However, there are some downsides to the use of actuators, sensors and controllers to steer the shaft of the instrument. One downside is that every additional component to a system affects the reliability of the complete mechanism. Alemzadeh et al.(2016) describe that, despite robotic systems are more commonly used and adopted for minimally invasive surgery, a non-negligible number of technical complications still occur [2]. Every additional mechatronic component accumulates to the overall error, and the chance of system failure increases. Another downside is that mechatronic designs tend to be expensive compared to designs with mechanical actuation. The components need to be small and highly reliable: electric components that are used in medical settings need to meet many requirements based on ISO-norms. A comprehensive quality management system and procedure (ISO 13485, Medical devices) have to be followed for the design and manufacturing of parts for medical devices [16], causing the parts to be relatively costly compared to conventional parts. Besides that, there are additional costs for maintenance and service of the instrument.

Manual actuation, with the use of mechanical transmissions towards the shaft of the instrument, has many benefits. The benefits are mainly based on the relatively low costs and the possibility to minimise the size of the instrument's shaft. Also, the chance of system failure is lower, as the method is independent of electrical components. However, the main downside is that controlling a shaft with multiple segments is very challenging. Functions, such as saving the positions of the tip of the tool and passing it on to the next segment, has to be covered by a mechanical memory mechanism. Recent designs like the MemoFlex (I and II), MemoSlide and MemoBox show promising results for mechanical control of an FTL-motion.

1.3. Problem statement and goal

The new development in surgery methods, namely surgery done via natural orifices (NOTES), has shown many benefits. To support the shift from open surgery to methods with reduced invasiveness, it is desired to improve the instruments that can be used during a NOTES procedure. These procedures require advanced instruments: the shaft of the instrument should be able to make variable multi-curved paths and should execute a follow-the-leader motion. The FTL-motion ensures that the instrument moves its way through the lumen towards the area of interest, without support from the anatomical surroundings. The mechanism requires the control of many shaft segments: implementing a path beginning at the tip of the tool and shifting it proximally to the remainder of the shaft. The control of the shaft segments can be done with extrinsic electric actuation, a robotic design, but also mechanically. Robotics for such a complex task seems promising. However, robotics in surgery tools is still under discussion, because of high costs and the chance of system failures. Therefore, this thesis aims to improve the existing mechanically controlled FTL-mechanisms.

The mechanically controlled MemoFlex I, MemoFlex II, MemoSlide and MemoBox show promising functionalities. They will be further elaborated in the State of the Art, Chapter 2 in this report. The MemoFlex I and MemoFlex II can only form one path in the shaft of the instrument, because the path input is a predefined shape. The MemoSlide and MemoBox are programmable path-planning mechanisms, in which the surgeon can adjust the shape of the shaft in real-time. The latter is desired for a NOTES procedure. The MemoSlide and the MemoBox are proof of concepts, to show how a path can be planned and how the FTL-propagation is controlled. The prototypes have not been incorporated into a surgical instrument. The current designs are rectangular and four of those path-planning modules are required to provide a 3D motion in the shaft of the surgical instrument: one module for each group of cables. Meaning, all the upper cables are controlled by one module, all the left cables are steered with another module, and the same applies to the lower and right cables. Not only is this not space efficient, also additional control is necessary to synchronise the antagonist cables. Making the path-planning module cylindrical is a solution. The cylindrical shape is easier to incorporate in a handle of a surgical tool. Most important, by making the design cylindrical, one path-planning module can provide the motion of one type of cable including its antagonist. With a cylindrical design, the movement of the antagonist cables is synchronised and has the same magnitude but inverse. Consequently, only two path-planning mechanisms are required to provide a 3D motion: one for the horizontal motion and another for the vertical motion. The cylindrical design is more space efficient and easier to control, as only two path-planning modules need to be steered rather than four. In conclusion, manually actuating a surgical instrument with the MemoSlide or MemoBox is promising, but optimisation of the prototypes by making them cylindrical, is desired to incorporate it into a surgical instrument.

The goal of this thesis is:

To introduce a cylindrical, mechanically controlled follow-the-leader mechanism, that can control one cable and its antagonist to steer a compliant shaft of a surgical instrument

1.4. Structure of this thesis

This thesis comprises the design and testing of an FTL-prototype, starting from a state of the art and finishing with a prototype, results and recommendations. The next chapter, the State of the Art, elaborates on the existing mechanically controlled FTL-mechanisms. The state of the art is used to determine the design requirement and functional requirements for the refined path-planning mechanism. Chapter 3 describes the design process that is necessary to reach the goal set in Section 1.3. It first explains a typical engineering design cycle. After that, the design phase and timeline of this project are elaborated. The remainder of the thesis is constructed in the same sequence of the design cycle. Chapter 4 elaborates the progress from functional requirements, to conceptualisation, to design selection and eventually, the final design. The working principle of the prototype is described in Chapter 5. Chapter 6 and 7 include the proof of concepts for the machined prototype and the 3D printed prototype respectively. As the concept is only to prove the FTL-motion, Chapter 8 shows additional CAD-drawings and explains how this prototype can be incorporated into a surgical instrument. Finally, the results are discussed in Chapter 9 and conclusions are drawn in Chapter 10.

2

State of the Art

2.1. Cable-driven FTL-mechanisms

This thesis aims to refine a mechanically controlled path-following mechanism that can provide a follow-the-leader motion in the shaft of a surgical tool. The design is based on four existing mechanisms, developed by the Bio-Inspired Technology (BITE) group from the Technical University of Delft: the MemoFlex I, MemoFlex II, MemoSlide and the MemoBox.

The existing prototypes are cable-driven FTL-mechanisms. The prototypes are designed to control the motion of a segmented shaft by steering the segments with cables. All segments are connected in series and are able to rotate relative to each other, making the shaft compliant. The shaft can be assembled from metal parts, such as the HelixFlex [18]. The BITE group also developed a 3D printed shaft, that can be printed as one part: the HelicoFlex [10]. Each segment of the shaft is steered by two sets of antagonist cables, as can be seen in Figure 2.1A. The upper (U) and lower (D) cable provide the motion in the vertical direction: rotating upwards or downwards. The left (L) and right (R) cable provide the rotation of that segment in the horizontal plane. By pulling one cable and releasing its antagonist cable, the segment rotates in the pulling direction. This principle is shown in Figure 2.1A on the right.

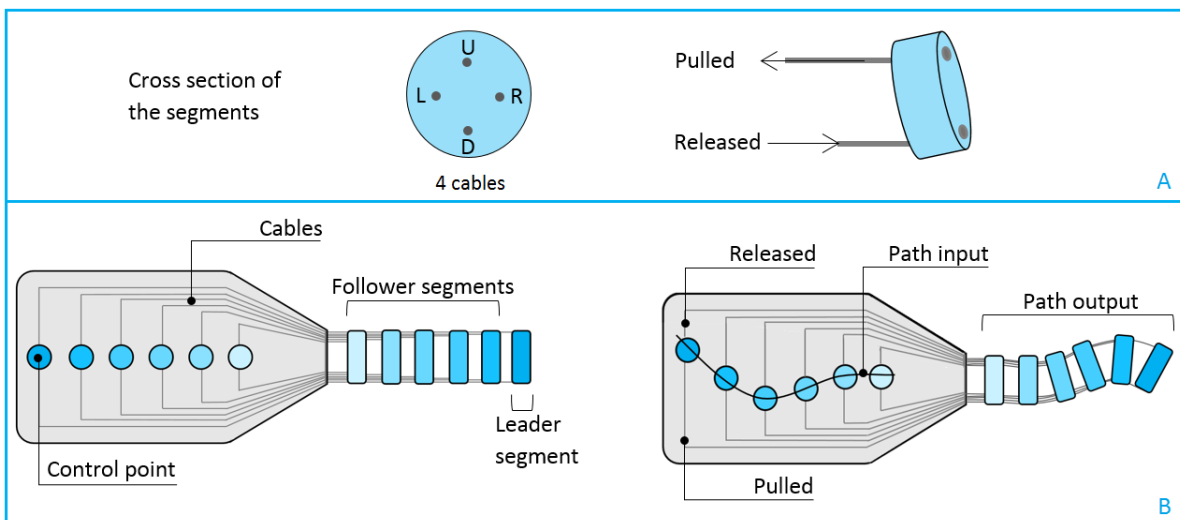


Figure 2.1: Steering a segmented shaft with four cables. The cross-section of one segment is provided in Figure A, showing the two sets of antagonist cables. The upper (U) and lower (D) cable provide the motion in the vertical direction. The left (L) and right (R) cable provide the rotation in the horizontal plane. By pulling one cable and releasing its antagonist cable, the segment rotates in the pulling direction. Figure B is a simplified image of the working principle. It shows how the vertical motion of a shaft is provided. A control point is connected to a segment by the antagonist cables. The control point and its corresponding segment are coloured in the same shade of blue. Moving a control point pulls one cable and releases its antagonist. This results in a rotation of the shaft segment.

Figure 2.1B shows the working principle of how a segmented shaft is steered with antagonist cables. It is a simplified image, representing the side view of the steering mechanism. The image only displays the antagonist cables that provide the movement in the vertical plane. Each shaft segment is represented by a control point. Attached to these control points are the antagonist cables. The cables are the mechanical transmission, connecting the control points to the shaft segments. In the figure, the control point and the corresponding shaft segment are presented by the same shade of blue. One cable is pulled by translating a control point, while its antagonist is released with the same magnitude. The pulling and releasing of the antagonist cables cause the corresponding segment to rotate. For example, the most left control point is translated upwards. Therefore, the lower cable is pulled and the upper cable is released. As a result, the leader segment rotates clockwise. Additional control points are necessary to provide the same working mechanism in the horizontal plane. Thus, each shaft segment is connected to at least two control points: the combination of the displacement of these control points causes a 3D motion of that specific segment. The magnitude and direction of the pulling and releasing of the cables control the movement of the shaft segments.

In a follow-the-leader mechanism, the orientation given to the tip of the tool (the leader segment) is passed on to the follower segments. This requires a mechanism that controls the orientation of the most distal segment and passes it from segment to segment towards the proximal side of the instrument. In other words, a controller is necessary to provide a follow-the-leader motion of the control points. The MemoFlex I, MemoFlex II, MemoSlide and MemoBox include different types of mechanisms that enable a follow-the-leader motion in the control points. The MemoFlex I and MemoFlex II are complete instruments: the prototypes include the path controller, the compliant shaft, cables, a casing and a base. The MemoSlide and MemoBox are prototypes of the FTL-controllers solely. They are proof of principles, showing how an FTL-motion can be implemented and controlled. Therefore, the prototypes are not integrated into a surgical tool and do not include the compliant shaft, cables and casing.

The four prototypes can be divided into two groups: fixed path and programmable path FTL-mechanisms. The MemoFlex I and MemoFlex II are fixed path FTL-mechanisms, while the MemoSlide and the MemoBox are programmable. The fixed path mechanisms make use of a predefined path. Therefore, the device can only provide one path in the shaft of the surgical instrument during the procedure. The MemoFlex I includes a fixed spatial track: a multi-curved physical 3D track. The design is a mechanical master-slave system, that captures the shape of the fixed track and copies it to the compliant shaft of the surgical instrument. The physical track is predetermined, so a new track needs to be introduced to make a different path. The MemoFlex II has four fixed 2D tracks, rather than one 3D track. Each cable is represented by its own control point. This means that the tracks of the antagonist cables are each other's inverse. The control points are guided by the fixed tracks. To change the path of in the compliant shaft, the fixed tracks need to be replaced by other tracks. Programmable path mechanisms on the other hand, allow the user to continuously adjust the path while using the instrument. For these mechanisms, the user steers the tip of the tool. It requires a complex mechanism that continuously controls the orientation of tip, saves the given orientation and passes it towards the proximal side of the instrument. The MemoSlide and the MemoBox discretize the predefined continuous track into smaller, movable elements. In the MemoSlide the user only steers the first element, which is the input element. For the MemoBox, the user controls the position of all the elements. Both mechanisms create adaptable 2D tracks and represent the FTL-motion in the control points. The existing mechanisms are further elaborated in this chapter. Pictures of the four prototypes are shown in Figure 2.2.

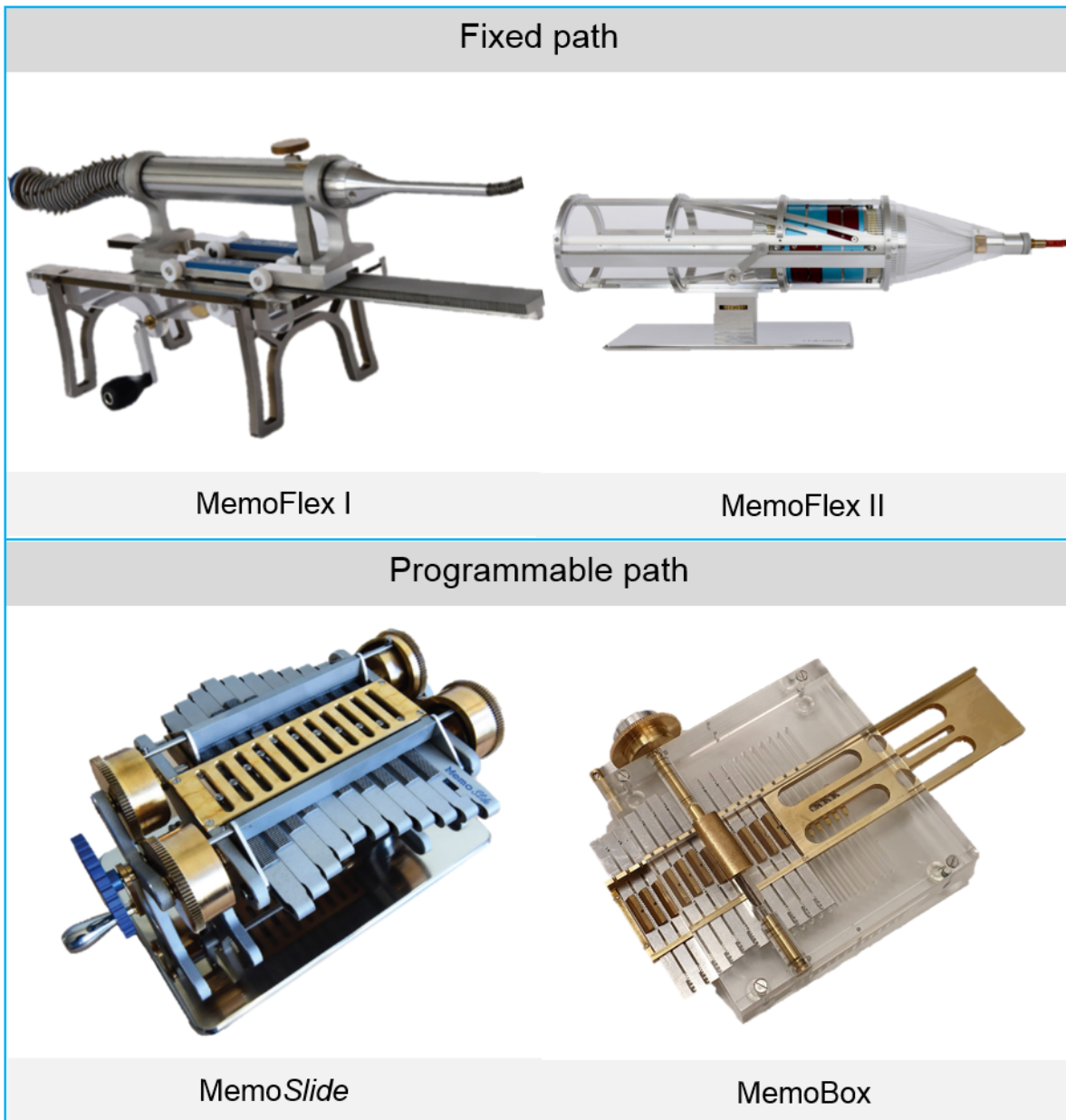


Figure 2.2: Pictures of the four existing prototypes. The four prototypes can be divided into two groups: fixed path and programmable path FTL-mechanisms. The fixed path prototypes include the MemoFlex I and MemoFlex II. Their input is a pre-defined path. Both prototypes are designed by P.W.J. Henselmans. The MemoSlide and MemoBox are programmable path mechanisms. The system allows the user to decide the path in real-time, while the instrument is inserted. The prototypes do not include the complete instrument with a shaft, but are proof of principles showing the follow-the-leader principle in the control points. The MemoSlide is designed by P.W.J. Henselmans, and the MemoBox is designed by C. Culmone. The images of the MemoFlex I and Memoflex II are adapted from Henselmans (2020) [19]. The picture of the MemoSlide is adapted from Henselmans (2017) [20] and the MemoBox from Culmone (not published yet) [11].

2.2. Fixed path FTL-mechanisms

The MemoFlex I and MemoFlex II are prototypes that implement a predetermined path. A fixed track is introduced to the system as input, and the mechanism converts this path into the pulling and releasing motion of antagonist cables. Ultimately, it results in a path as output in the compliant shaft of the surgical instrument.

2.2.1. MemoFlex I

The MemoFlex I is designed by P.W.J. Henselmans [21]. It is a master-slave mechanism, in which the compliant shaft of the instrument follows the path the handle makes. Therefore, the handle is the master, and the compliant shaft is the slave.

Figure 2.3A shows the CAD drawing of the main components of the MemoFlex I prototype. The base is not included in this image. The handle contains a 3D printed helical structure that can compliantly change shape and capture the shape of an inserted track. This structure is called the track-follower and can be seen in Figure 2.3B. The exoskeleton of the handle fixates and guides the cables towards the compliant shaft. The slave is built out of 14 segments, each being controlled by four cables. The segments are connected to each other with hex ball joints, enabling the shaft to bend with minimal stiffness. In the MemoFlex I design, the path input is provided by a prebent steel rod that functions as shape memory mechanism. When the prebent rod is slid through the compliant handle, the helical track-follower will capture the shape. The cables connecting the master and the segments of the slave, enable the slave to follow the path. The proximal side of the handle is connected to the most distal segment of the compliant shaft of the instrument (the tip of the tool). The distal end of the handle is connected to the most proximal segment of the shaft. This enables the follow-the-leader motion, because inserting the fixed track will first engage the tip of the tool, and the shape is passed down the shaft from segment to segment. The master-slave mechanism and path insertion can be seen in Figure 2.3C. The path is fixed: to create a different path, a new prebent steel rod is required.

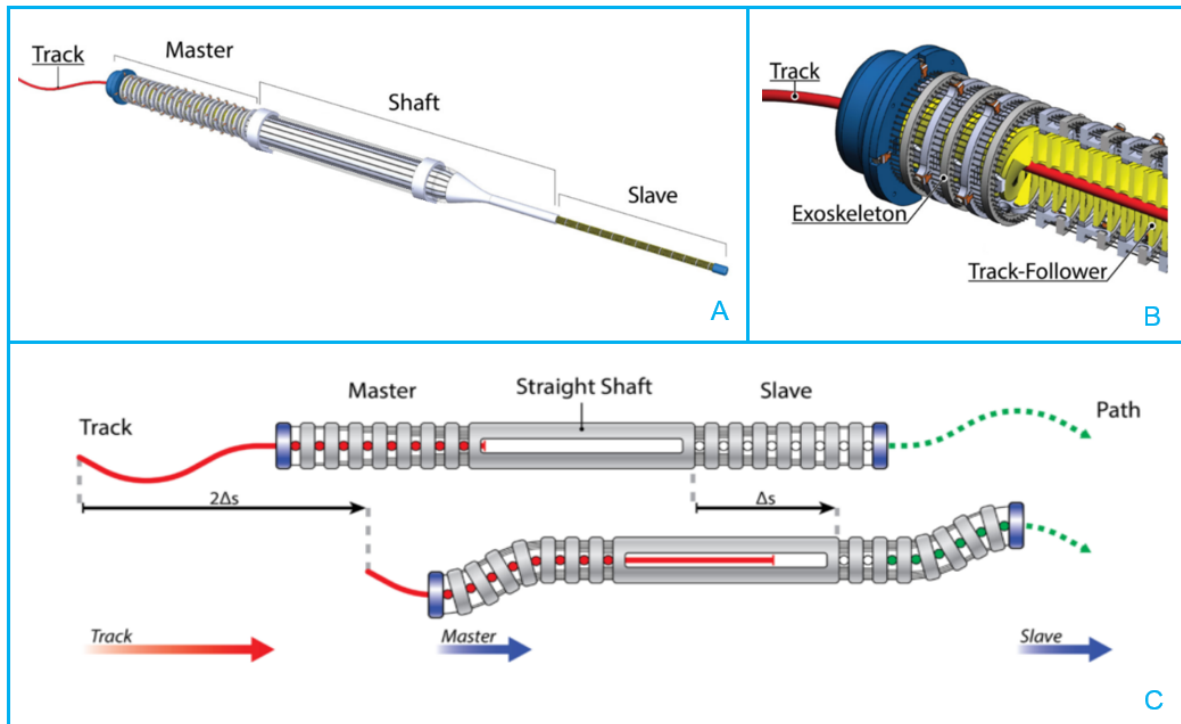


Figure 2.3: CAD images of the MemoFlex I prototype. Figure A shows the main components of the master-slave mechanism. The handle is the master and the compliant shaft is the slave. Figure B is a section of the handle of the tool. The predefined track (red) deforms the track-follower (yellow), ultimately deforming the exoskeleton, incorporating the steering cables. Figure C shows the master-slave mechanism and how the path is inserted and formed. The deformation of the master, because of the inserted track, causes the pulling and releasing of cables attached to the slave's segments. As a result, the slave copies the shape. The images are adapted from Henselmans (2017) [21].

2.2.2. MemoFlex II

The MemoFlex II is shown in Figure 2.4. The mechanism is designed by P.W.J. Henselmans and produced at the central workshop of the Technical University of Delft (DEMO) [19].

The main components of the MemoFlex II are the track-plates, the track ring, control points and the cables, shown in Figure 2.4A. The cables are responsible for the movement of the shaft segments. The cables are attached to control points, each cable having its own control point. These control points, which are small ball bearings, are mounted to straight bars that are contained in horizontal slots. The straight bars are coloured in yellow in the figure. The combination of the straight bars and the slots enables the control points to translate inside the slots while being fixed in the vertical direction. The translational motion of the control points in the horizontal plane causes the pulling and releasing of the cables. Initially, the bearings are kept in a straight track, keeping the shaft of the tool in a straight configuration. Rotating the track-ring will move the track relative to the control points. First, the leader control point enters the track, providing an angular displacement in the leader segment of the shaft (the tip of the instrument, Figure 2.4C). The leader control point and its corresponding segment are coloured in red in Figure 2.4B and 2.4C. As the track-ring is rotated further, the follower control points (blue) also enter the track. One by one, the ball bearings pass from the initial straight groove to the curved groove, as shown in Figure 2.4B. Because of the form of the track, the bearings are forced to translate in the horizontal direction, providing the change in cable length. The MemoFlex II contains four fixed 2D tracks. Each type of cable (upper, lower, left and right), is represented by its own track and control points. This means that the tracks of the antagonist cables are each other's inverse. In total, the MemoFlex II controls 7 shaft elements.

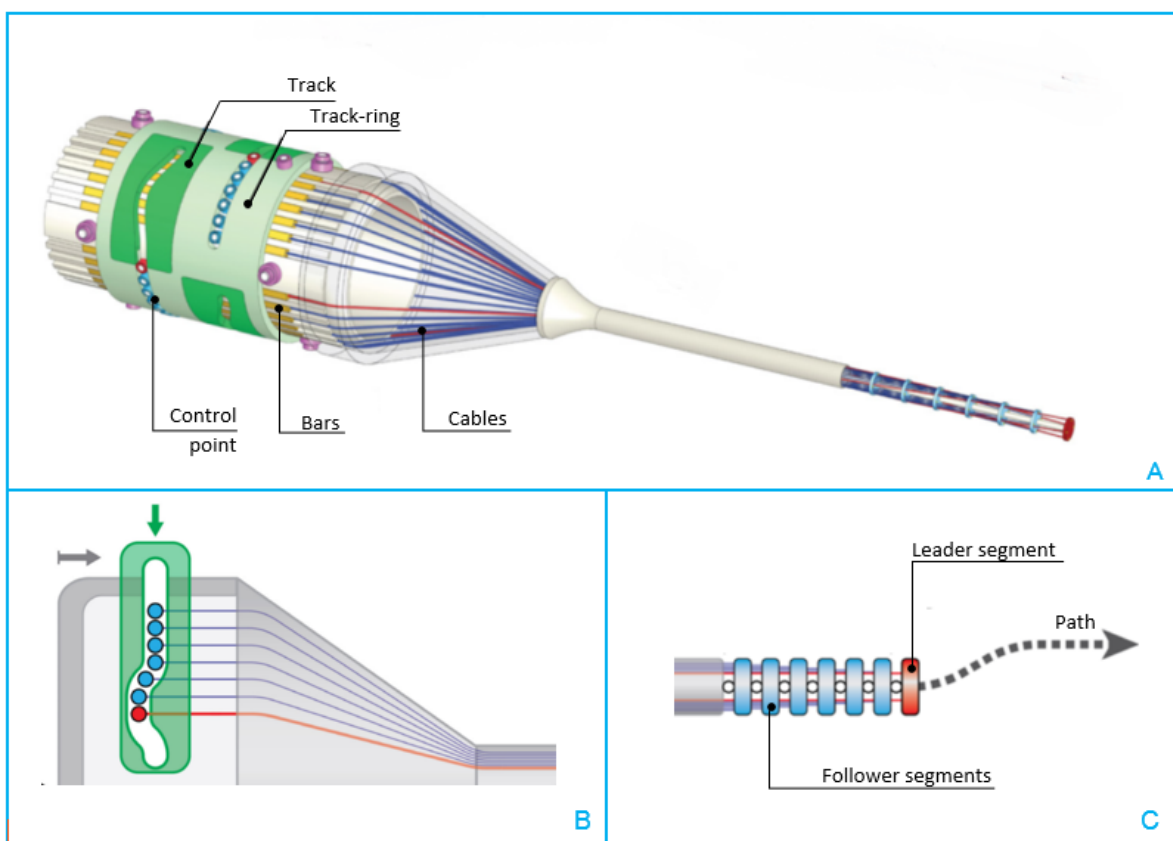


Figure 2.4: CAD images of the MemoFlex II. The images are adapted from Henselmans (2020) [19]. Figure A shows an overview of the main components of the mechanism. This includes four track-plates, a track-ring, control points, straight bars and the cables. Figure B provides a schematic drawing of how the change in cable length is introduced by inserting the track. The introduced track causes the control points to translate in the horizontal direction. Attached to the control points are cables, which are also connected to the segments of the shaft. By translating the control points, the cables are pulled or released, causing the shaft segments to rotate. Figure C shows the compliant shaft of the instrument. The first segment, the tip of the tool, is the leading segment. The other segments are follower segments.

2.3. Programmable path FTL-mechanisms

The *MemoSlide* and the *MemoBox* are both programmable path mechanisms that provide a follow-the-leader motion in a compliant shaft. Instead of a predefined physical track, the track is discretized into multiple steering elements that can translate relative to each other. Locking their new positions forms the input path. The system allows the user to implement the path in real-time, while the surgical instrument is inserted into the patient.

2.3.1. *MemoSlide*

The *MemoSlide* is designed by P.W.J. Henselmans and developed by D. Jager from DEMO, the central workshop of Delft University of Technology. The CAD drawings of the *MemoSlide* prototype can be seen in Figure 2.5. The *MemoSlide* is a proof of principle to show the programmable follow-the-leader motion of the control points. Therefore, the prototype only includes the path-planning mechanism; the shaft and the remainder of the surgery tool are not incorporated in this design.

The *MemoSlide* consists out of two registers, this can be seen in Figure 2.5C. The first register contains a leader element (blue) and follower elements (green). The leader element is the steering element: the user can translate the leader element to the left and right to the desired position. The follower elements form the path made by the leader element step by step and contain the control points. In this design, the control points are small ball bearings, similar to the *MemoFlex II*. The other bank, coloured in yellow, is called the memory mechanism, which consists of multiple memory elements. These elements function as the path retainer, that locks the implemented positions when the path is passed from segment to segment. The memory-bank is able to translate the width of one element forward and backwards, in the longitudinal direction. The other register is fixed. All the elements, blue, green and yellow, can translate from left to right and vice versa when they are unlocked. However, only the position of the blue element is controlled by the user. The control points that are attached to the leader element and follower elements are guided in a wedge-shaped groove in the memory elements, shown in Figure 2.5A.

Implementing the path with the *MemoSlide* is done in four steps that are repeated multiple times. It requires the locking of the memory elements and the control points in an alternating fashion, in order to memorise their position. So, when the memory elements are locked, the control points of the follower elements are free to translate. This also works the other way around: when the follower elements are locked, the memory elements are able to translate. The locking is provided by locking bars (coloured in red), that are form fit with the external teethed structure on the elements. Figure 2.5A shows the four steps of how the path is inputted by the user. First, the memory-bank is unlocked and the follower elements are locked. The leader element is steered by the user to the desired position (1). Then, the memory-bank is locked and the control points are slid one step upwards, by moving the memory-bank with respect to the follower elements (2). The control points align with the locked memory elements, because they are guided in the wedge-shaped groove (3). Now, the control points are locked and the memory elements are released (4). The memory-bank moves back one step and aligns with the control points (4). This sequence is repeated to implement a full path. The teethed structure on top of the elements makes sure that the path input is done in discrete steps. The leader segment is translated in steps of 1 mm and has a range of 4 mm to the left and 4 mm to the right. In total, the *MemoSlide* can control a compliant shaft with 11 segments. One leader segment, the tip of the tool, and 10 follower segments.

The *MemoSlide* is a proof of concept, to show the FTL-principle. The control points of the *MemoSlide* can be connected to cables, which are attached to the shaft segments of the surgical device. The surgical instrument requires four path-planning mechanisms to provide a motion in 3D space: two mechanisms that contain the control points for the upper and lower cables and two mechanisms that contain the control points for the left and right cables. The mechanisms of the *MemoSlides* for the upper and lower cables need to be coupled, as the paths formed should be each other's inverse. The same applies to the path-planning mechanisms for the left and right cables.

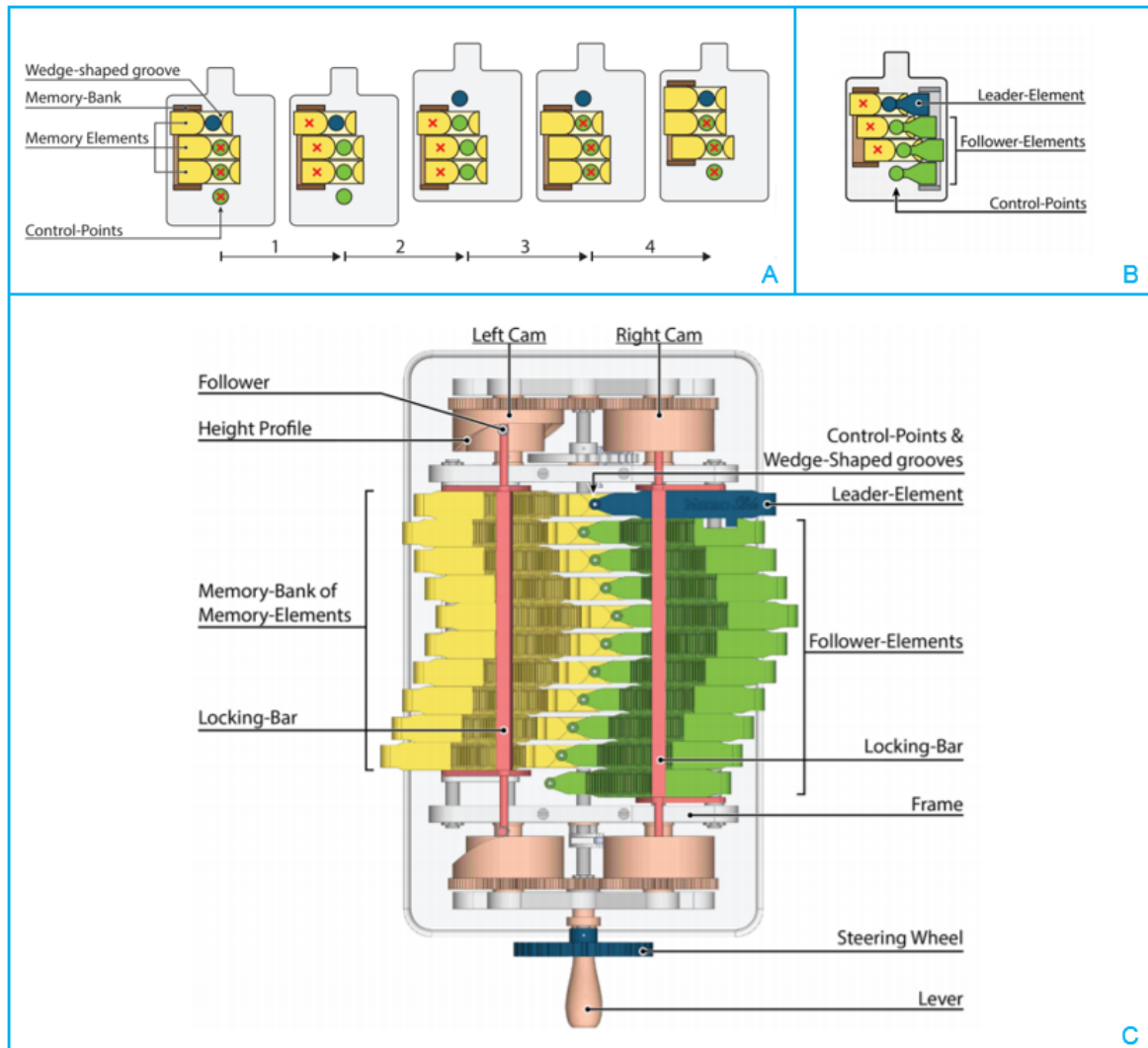


Figure 2.5: Working principle of the MemoSlide. Figure A is a schematic view of the alternating mechanism providing the FTL-motion. The path implementation is done in four steps. The memory-bank and the control points are locked in an alternating way. The working mechanism is described in the text. Figure B shows the leader element and follower elements, containing the control points. The control points are kept inside a wedge-shaped groove in the memory elements. Figure C is a top view of the complete prototype in SolidWorks. The mechanism exists out of two banks: the memory-bank (yellow) and the bank containing the leader- (blue) and follower-elements (green). Locking-bars (red) that are form fit with the teathed profiles on the memory- and follower-elements, alternately lock one of the banks. The images are retrieved from: Henselmans (2017) [20].

2.3.2. MemoBox

The MemoBox is a programmable path mechanism based on the functions of the *MemoSlide*. It is designed by C. Culmone and developed at DEMO by D. Jager [11]. Similar to the *MemoSlide*, the MemoBox includes steering elements and control points. The steering elements provide the path input and the control points represent the path output. The MemoBox is a proof of principle to show the programmable FTL-motion of the control points. Therefore, the prototype only includes the path-planning mechanism; the compliant shaft and the remainder of the surgery tool are not incorporated in this design.

In Figure 2.6 an exploded view of the SolidWorks model is shown. The main components are the steering elements (green), element selector (blue), guiding units (red) and the control points. The steering elements provide the path input. Their translational motion relative to each other creates a path. The steering elements are interlocked by a teeth-like profile on their sides, making the elements form-fit. They are pushed together by a pretensioned leaf spring. The interlocking enables the memorising of the given positions and saves the path of the steering elements. Guiding units are connected to the steering element with a pin, enabling them to rotate around their axis. Each guiding unit includes thin flaps that overlap with the adjacent guiding unit. Therefore, when translating the steering elements in discrete steps of 1 mm, the guiding elements form a continuous path.

Implementing the path is done in four repeated steps. In contrary to the *MemoSlide*, where always the same element is steered by the user, in the MemoBox the path input is given to each steering element individually. The elements are divided into three groups: the future, present and past. The present element corresponds to the element, which is steered at that moment. The user can translate this element. The past corresponds to all the elements that already have the desired position. The future elements correspond to the elements for which the position is yet to be defined by the user. The four steps of the path implementation can be seen in Figure 2.6B. The first step of the path implementation is decoupling the present steering element from the past steering elements, by pressing the steering element selector down. It functions as a wedge and creates space between the past and the present steering elements. The second step is steering: rotating the positioning wheel enables a lateral translation of the present and future steering elements with respect to the past elements. The elements can translate in steps of 1 mm and is limited by 2 mm to the left or 2 mm to the right. When the desired position is achieved, the steering element selector is released and recoupling of the steering elements occurs. By coupling the elements, the new position is locked and memorised. The last step is advancing the steering elements one step. The present steering element becomes the past and the next steering element becomes the present. The sequence is repeated until all steering elements have the desired position and are shifted to the past.

When the steering elements are slid from the present to the past, the control points are guided by the guiding elements. The control points are small ball bearings, that are connected to sliding bars. They can roll inside the guiding element around their own axis. The sliding bars enable the control points to translate sideways inside the slot, but limits the control points to translate in the longitudinal direction. The control points in this prototype represent the connection of one cable. The translational motion of the control point pulls or releases the cable. Similar to the *MemoSlide*, the surgical instrument requires four path-planning mechanisms to provide a motion in 3D space: two mechanisms that contain the control points for the upper and lower cables and two mechanisms that contain the control points for the left and right cables. The path-planning mechanisms for the upper and lower cables need to be synchronised, as the paths formed should be each other's inverse. The same applies to the path-planning mechanisms for the left and right cables.

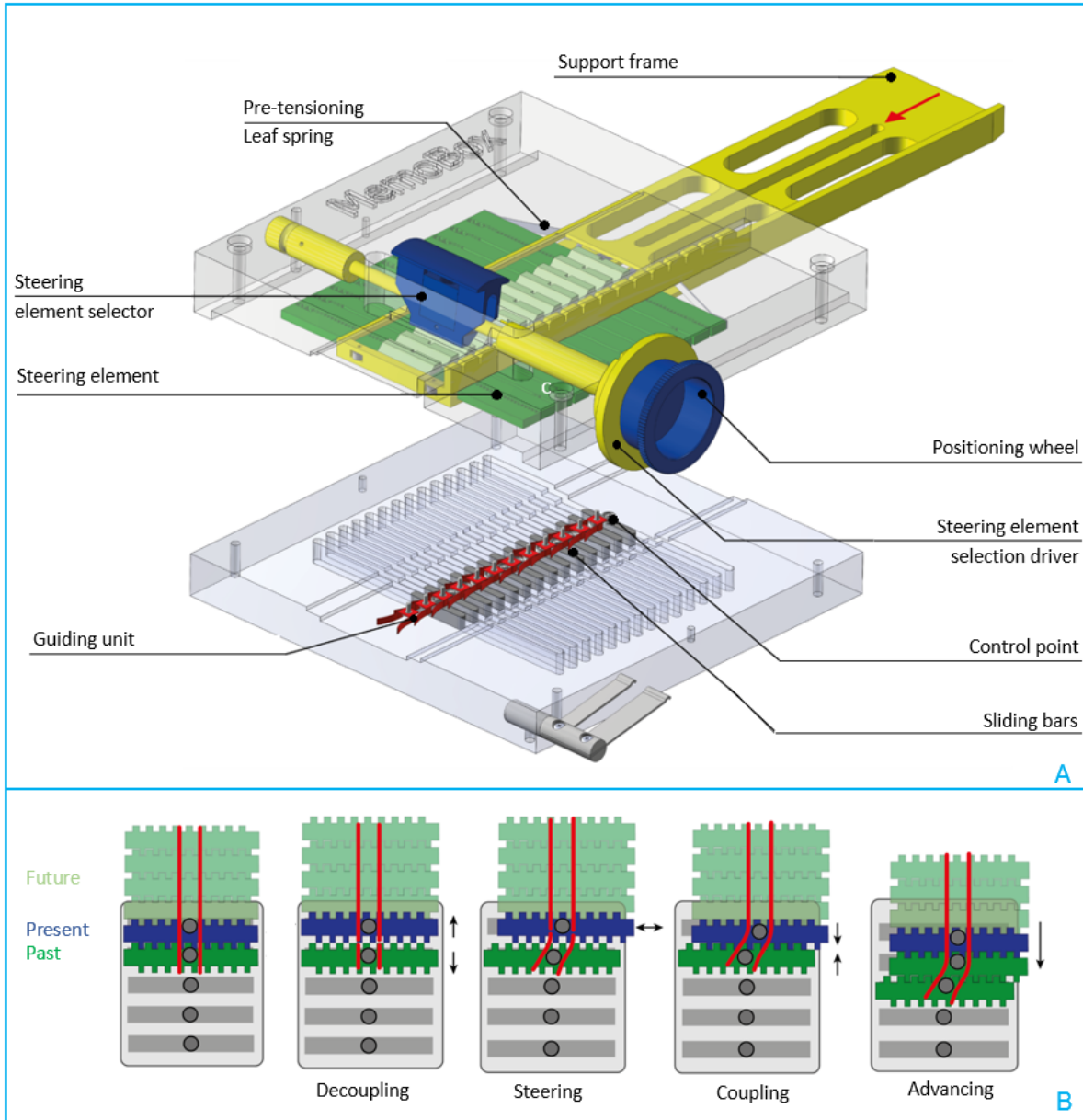


Figure 2.6: Working principle of the MemoBox. Figure A is an exploded view of the MemoBox, showing all the parts present. Figure B shows the memory mechanism and path implementation in three modes: the future, present and past. The working principle is described in the text. The images are adapted from: C. Culmone (not published yet) [11].

2.4. Evaluation of the state of the art

In Table 2.1 on the next page, the specifications of the four designs are shown. The MemoFlex I and MemoFlex II are both fixed path mechanisms, which have a predefined path as input. The MemoFlex I can form a 3D path in the segmented shaft. The compliant shaft copies the shape made by the handle. The handle is deformed by the input of a multi-curved physical 3D track. The MemoFlex II can also output a 3D shape in the shaft of the surgical instrument, by incorporating 4 track-plates. The MemoFlex I and MemoFlex II are complete prototypes, including a compliant shaft, cables towards the shaft, a casing and a base. The MemoFlex I is designed to steer a shaft with 14 segments and the MemoFlex II can steer a compliant shaft with 7 segments. Both prototypes only require one action from the user: inserting the path by sliding the physical track into the handle or rotating the track-plate. The predetermined path has as disadvantage that the surgeon can not adjust the path in real-time: the surgical instrument can output one shape. If another shape is required, the track or track-plates need to be replaced.

The MemoSlide and MemoBox are programmable path prototypes. The designs are made to validate the functionality of programming a path and providing the FTL-motion. Therefore, they do not include a compliant shaft or casing. Four of those mechanisms need to be incorporated in the surgical instrument to create a 3D motion in the compliant shaft. It can be concluded that a programmable path-planning mechanism requires a relatively more complex design, compared to mechanisms using a predefined path. This is because discretising the path input into separate steerable elements, requires additional functions for the steering of those elements and for locking them into their given positions. For minimally invasive surgeries, it is useful to have a device that is able to make multiple paths and can be programmed in real-time, while performing the surgery. Therefore, the MemoSlide and MemoBox have promising working principles.

Comparing the MemoSlide and the MemoBox, the designs have similar functions and components, except for memorising and advancing the path. In both prototypes, the path input is done by translating a steering element. The path output is provided by the movement of control points. Both designs implement the path in steps of 1 mm. The range of the MemoSlide is larger, as the steering element of the MemoSlide has a maximum relative displacement of 4 mm to the left and right, while the range of the MemoBox is 2 mm to the left and right. The alternating mechanism of the MemoSlide is not space efficient. An additional memory-bank and locking bars are necessary to memorise and advance the path input. Rather than having one steering element and advancing that input, the MemoBox design can steer all the elements relative to each other. By interlocking the steering elements, the new positions are fixed. The size of the MemoBox is only 70x85x6 mm and is relatively small compared to the size of the MemoSlide, which is 145x125x25 mm. The smaller size of the MemoBox is advantageous. However, the MemoBox requires more actions from the user to implement a path. The MemoSlide only requires two repeated steps from the user, while the MemoBox requires four repeated steps.

As described above, both designs are made to show the FTL-principle in a programmable mechanism. The proofs of concept were not made for direct use in a surgical instrument. As a result, the MemoSlide and MemoBox are rectangular models, that only provide the motion of one type of control point. Meaning, they only provide the motion of for example all the upper cables, or all the left cables. Therefore, four path-planning mechanisms are necessary to provide a 3D motion in the compliant shaft of the surgical tool. Not only is a cylindrical design desired, because it is easier to incorporate in the handle of a surgical instrument. Also, by making the design cylindrical, one path-planning module can provide the motion of one type of cable including its antagonist. With a cylindrical design, the movement of the antagonist cables is directly synchronised: it has the same magnitude but is each other's inverse. Consequently, only two path-planning mechanisms are required to provide a 3D motion: one for the horizontal motion and one for the vertical motion. Concluding, the cylindrical design is more space efficient and easier to control, as only two path-planning modules need to be steered rather than four. The functions and parts of the MemoSlide and MemoBox are taken into account for the functional and design requirements of this new cylindrical prototype.

Table 2.1: Characteristics of the state of the art

	MemoFlex I	MemoFlex II	MemoSlide	MemoBox
Aesthetics				
Form	Cylindrical	Cylindrical	Rectangular	Rectangular
Path input				
Path	Predefined	Predefined	Programmable	Programmable
Number of input elements	1	1	11	11
Step size	-	-	1 mm	1 mm
Relative steering range	-	-	4 mm	2 mm
Guidance	Helical structure	Slot in track-plate	Groove in memory elements	Guiding units
Path output				
Number of shaft elements	14	7	11	14
Location of the cables inside the shaft	4.5 mm	2.3 mm	2.3 mm	3 mm
Angular displacement per input step	-	-	25 degrees	20 degrees
Usability				
Number of steps	1: Sliding the fixed path distally inside the handle	1: Rotating the track-plate to insert the path	2: Rotating input knob 1 to steer the leading element and rotating input knob 2 to advance the path	4: Decoupling the steering element with the wedge, steering the leading element, remove the wedge for coupling, advancing the element

3

Design process

3.1. Introduction

Based on the problem statement made and the design goal given in the Introduction and the State of the Art, a series of steps have been followed to accomplish the goal. In this chapter, a typical engineering design process is elaborated and the design process towards the final prototype is explained.

3.2. Engineering design process

A design can start from a problem, a need or a creative idea. For the majority of the engineering projects, problem-solving is the main goal. Every engineering project shares common components. The path towards the solution consists out of a basic sequence of steps. As can be seen in Figure 3.1, the five main stages of an engineering design process are [30]:

1. Problem definition
2. Information gathering
3. Solutions generation
4. Analysing and selecting one solution
5. Developing, testing and implementing the solution

A design process is an iterative process: after all the steps are completed, the design is evaluated and a new problem can be defined. The series of steps are continuously repeated over a long period of time; that is why the process is also called a design cycle. Every iteration aims for a better and refined solution, continually improving the product. Even when the product is released on the market, the design cycle can persist. For example, to fulfil the new needs of the society or because of the availability of improved manufacturing methods. While going through the steps, sometimes it is necessary to go back to the previous step or to the begin to redefine the problem. For example, the need to gather additional information or finding out that the chosen concept does not work, are reasons to go back one or multiple steps.

3.2.1. Problem definition

In the first step of the design cycle, the problem is specified and clearly stated. The problem statement includes an identification of the need, showing the actual goal of the design: the design objectives. Three main questions are answered: what is the problem, for who is this a problem and why is it important to solve this problem? A significant part of the problem definition is the design criteria. These criteria are boundaries or limits given to the design: they show which characteristics the end-product must have to be a successful design. Examples of design criteria are: maximum dimensions (geometric constraints), the ability to function in certain types of environment (material properties) and assembling criteria (manufacturing constraints).

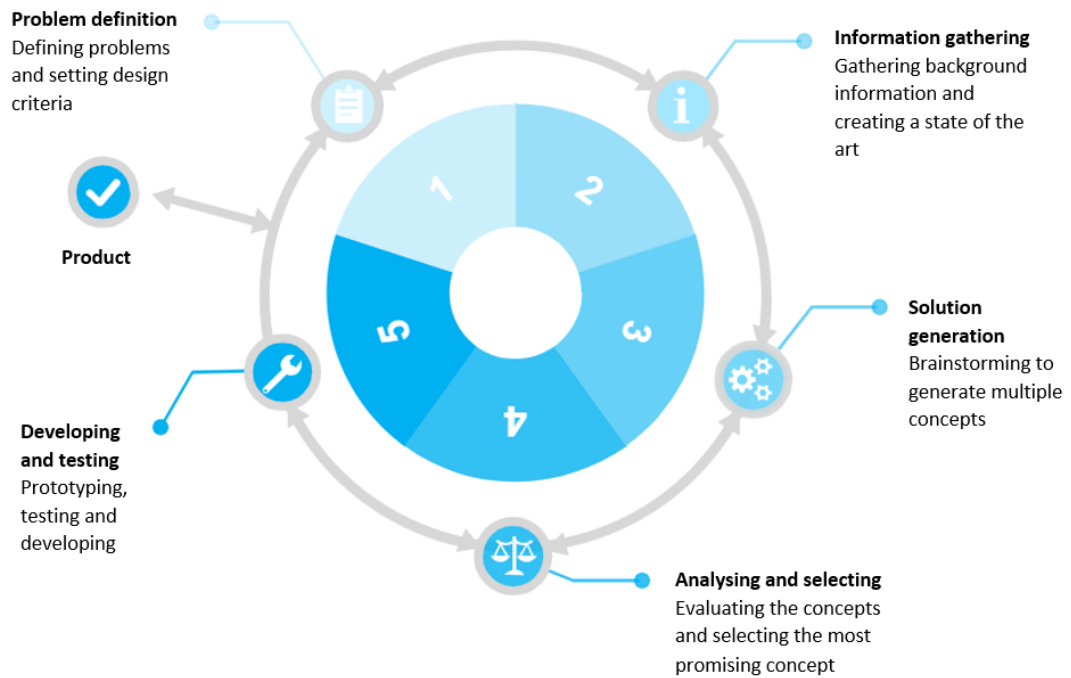


Figure 3.1: The design cycle existing out of five steps: problem definition, information gathering, solutions generation, analysing and selecting a concept and developing, testing and implementing the design. After all the steps are completed, the design is evaluated and a new problem can be defined, repeating the series of steps. Shown by the grey arrows in between the steps, the cycle does not always follow the cycle in one direction. While going through the steps, sometimes it is necessary to go back to the previous step(s).

3.2.2. Information gathering

The second step of the design cycle is doing background research on the subject. First, a general understanding of the situation is necessary. For example, in the case of medical applications, knowledge about the specific body part or surgical procedure is useful to evaluate the design criteria and possibly reassign new criteria. Information gathering is also done to generate a state of the art. By creating a state of the art, the researcher gains knowledge about the different types of solutions which have already been developed and tested before or if there are solutions already available to solve a similar problem. This research is important to see if there is indeed a need for a new solution or if the problem has already been solved. It is also the opportunity to learn from previous designs. Useful information is gathered, like what was wrong with the previous solutions and what were the strengths of the previous solutions. While gathering information, the design criteria and/or the design goal can be altered.

3.2.3. Solution generation

Based on the objectives and the desired functions, multiple solutions are generated. There are several methods for creating solutions. Generating ideas can be done by brainstorming and creating a web of concepts by using knowledge and creativity. However, for mechanical designs often a systematic method is conducted. Some systematic methods for designing include: Functional Decomposition and Synthesis, Morphological Analysis, Theory of Inventive Problem Solving, Axiomatic Design, Design Optimisation and Decision-Based Design [13]. Functional Decomposition and Synthesis is a systematic approach in which the goal of the design is divided into subfunctions and physical behaviour. Concepts are created by the combination of the different solutions per subfunction. Morphological Analysis is a systematic method that explores all the possible solutions by placing them into a multi-dimensional morphological chart. The goal of this method is to fill all the potential gaps in the solution space.

3.2.4. Analysing and selecting one solution

After multiple solutions are generated, the best solution has to be selected to develop further, which is the fourth step in the design cycle. Some designs can be excluded immediately based on technical knowledge, if it is known that the solution is not possible to carry out. An evaluation process is used

for the remaining solutions. Various methods exist. The methods can be based on decision matrices, analytic hierarchy, uncertainty modelling, optimisation or heuristics [23]. Many engineering projects use the structural approach based on decision matrices. With this approach, the criteria for each design are evaluated. Also other factors can be added to the evaluation like manufacturability, safety, costs and ergonomics. Sometimes calculations are necessary to substantiate the choices made.

3.2.5. Developing, testing and implementing

The last step of the design cycle is the step in which the chosen solution is worked out in more detail, prototyped, tested and implemented. The process towards product development is a short design cycle itself. Starting from 2D sketches, more detailed 3D sketches are made. The dimensions are determined and eventually CAD models are made. Prototyping is necessary to generate new information about the design and its working principles. The prototype is not always tested in its entirety, but single parts or subassemblies give insight in what functions can be critical and must be reviewed before the actual design is made. The testing of the product is an important step within the design cycle: the potential solution can be flawed, and revision of previous steps in the design cycle is necessary to get a satisfactory solution.

3.3. CPMM design phase and timeline

For this thesis, a cylindrical mechanically controlled path-planning mechanism is designed for the use in minimally invasive surgery instruments. The previous chapter, the State of the Art, was the first step of the design process. This research is based on existing prototypes, designed and developed by the BITE group of the Technical University of Delft. Three devices are designed by P.W.J. Henselmans and described in the articles published as his doctoral thesis [19]: the MemoFlex I, the MemoFlex II and the MemoSlide. The most recent prototype, the MemoBox, is designed by C. Culmone. With the aim of a refined solution, the design of the Cryptex Programmable Memory Mechanism (CPMM) is initiated. The main goal of the new design was making a mechanism similar to the MemoBox, but in a cylindrical shape. Partly, because most surgical instruments and handles have a cylindrical form for ergonomics. Making the programmable path mechanism in a cylindrical shape, would make it easier to incorporate the prototype into the handle of the surgical instrument. Another reason is that a cylindrical shape will provide better guidance of the cables towards the segmented shaft of the surgical instrument. The main reason is that with a cylindrical design, one module steers a cable and its antagonist cables for multiple segments. In contrary to the MemoSlide and MemoBox, only two modules are necessary rather than four. Consequently, the size of the instrument is reduced and controlling the path-planning is easier.

The problem definition and design criteria are very similar to the designs of the predecessors. Mainly the functions and the mechanisms implemented in the MemoBox are taken into account: with the knowledge of the parts used in the MemoBox and the functions of those parts, the solutions for the CPMM were generated and selected. The concept generation has been done systematically by dividing the complete design into subfunctions and element requirements. Multiple solutions were generated for each element design requirement, resulting in a solution space. During the solution generation and selection of the design, the individual parts and entire design are revised multiple times together with the supervisors, Professor P. Breedveld and PhD researcher F. Trauzettel, and also with the precision technicians D. de Jager and R. van Starckenburg. The parts have been adjusted to improve manufacturability, but also to improve the steerability, ergonomics and aesthetics of the design.

After the design was worked out in detail and all CAD-models were complete, the fourth step of the design cycle started: the design is machined at Dienst Elektronische en Mechanische Ontwikkeling of the TU Delft (DEMO). The majority of the prototype is made out of metal with subtractive manufacturing. Simultaneously, a 3D printed version is developed. To do so, some CAD-files had to be adjusted to create more spacing between the parts in the assembly, reducing friction. Also, some components were simplified for the 3D printed version. Both the metal design as the 3D printed design have been tested and evaluated as last step of the design cycle. In the discussion, Chapter 9 of this report, new problem statements are made, providing recommendations for an updated version of this design as future research. On the next page, in Figure 3.2, the design timeline of this research can be found.

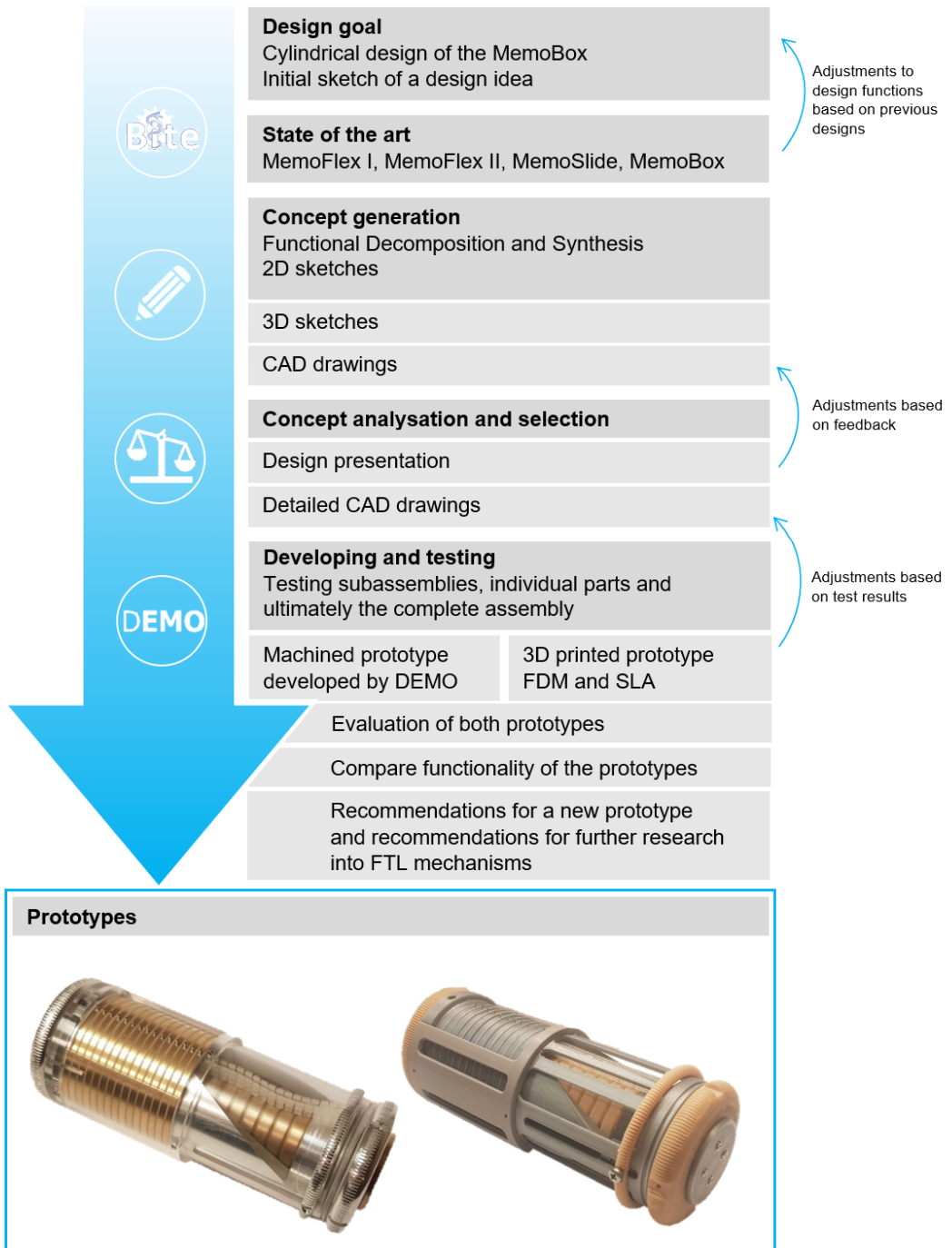


Figure 3.2: Design process of the CPMM prototype. Resulting into two prototypes: a machined version (left) and a 3D printed version (right).

4

Mechanism design

4.1. Design objectives and requirements

The design objectives are divided into functional requirements and product element design requirements. The functional requirements manifest what the overall instrument should be able to do and thus describe the desired behaviour of the mechanism. Since the design is mostly based on the *MemoSlide* and the *MemoBox*, the components required for this path-following mechanism are known. Therefore, the element design requirements are more specific and include what types of components are necessary, their specific functions and the number of components. It is a combination of component-specific functions and non-functional requirements, like physical requirements and manufacturability. Table 4.1 shows the functional requirements and the table on the next page, Table 4.2, is more detailed and includes the product element design requirements. A distinction is made between a must and a wish, depending on the importance of that requirement. Musts are requirements set for the design to be a functioning and satisfactory prototype, while wishes are based on improving the ease of use or aesthetics of the prototype, but are not necessary for the prototype to function properly. As shown in both tables, all functional requirements are important, while the element design requirements also include wishes.

Functional requirements

The mechanically path-planning mechanism should enable the user to insert and repeatedly change the path that is formed in the shaft of the minimally invasive surgery instrument. For that reason, the two main functions of the mechanism are: inserting the desired path by the user (input) and the path formation in the compliant shaft of the surgical instrument (output). The functional requirements are divided into multiple subrequirements in Table 4.1. The subrequirements provide additional information about the input and output functions of the design.

Functional requirement 1 describes that the design is manually steered with mechanical transmissions between the input and output. The mechanism controls a shaft built out of segments, which are controlled by two sets of antagonist cables. The compliant shaft is designed by P. Henselmans and C. Culmone [10]. The user's task is planning the path. Similar to the *MemoBox*, the path implementation exists out of three modes: the past, the present and the future (requirement 2.1). The present is the input element that is steered at that moment, moving it to the orientation of the user's choice: the steering element. The future is the part of the path that still needs to be formed by the user. The input elements representing the future do not have the desired orientation yet: their position is not defined yet. The past represents the element or elements that have already been implemented and locked in their new orientation. The input elements that are in the "past-mode" provide an output in the segmented shaft. A more detailed explanation of the three modes will be given in Chapter 5. The input elements can be converted from future to past and vice versa; repeatedly implementing a new path and locking it. Steering the present input element is done in steps of 1 mm (requirement 2.2). Requirement 2.2 is based on the functions of both the *MemoSlide* and *MemoBox*. In the state of the art, it is explained that the input element of the *MemoSlide* can translate in steps of 1 mm. The *MemoBox* is also controlled in steps of 1 mm, because of the teeth design that interlocks the adjacent input elements.

Requirement 3 comprises the output function of the mechanism. The design must enable the control of a compliant shaft with at least 11 segments (requirement 3.1). Similar to the *MemoSlide*, the FTL-motion and working principle can be shown with 11 segments and is sufficient for the proof of principle. In the actual surgical instrument, more segments may be required. The *MemoBox* assumes that the actuation cables are attached at $r = 3$ mm and the *MemoSlide* at $r = 2.3$ mm. As a result, an input translation of 1 mm causes a segment's angular displacement of 20 degrees and 25 degrees for the *MemoBox* and *MemoSlide* respectively. The same as the *MemoBox*, it is assumed that the actuation cables are attached at $r = 3$ mm from the centreline of the compliant shaft (requirement 1.2). Consequently, requirement 3.4 is set that the output elements of the path-planning mechanism should provide at least a 20 degrees angular displacement of the segment with respect to the previous segment. The compliant shaft of the surgical instrument should be able to make multiple shapes, like S-shapes and a complete change in direction (180 degrees turn). In theory, the compliant shaft should be able to make a 220 degrees turn, based on the number of segments (11) and the amount of angular displacement per segment (20). However, requirement 3.5 is set that the prototype should be able to make a single curvature of at least 170 degrees in the compliant shaft.

Product element design requirements

The product element design requirements overlap with the functional requirements, but are component-specific. The product element design requirements are shown in Table 4.2. The overall design can be divided into 4 main components: the memory elements, the reading elements, path transmission element and a cable guiding element. The memory elements are the input elements, controlled by the user. The reading elements follow the path formed by the memory elements, resulting in a change in cable length of the compliant shaft. Therefore, the reading elements provide the output of the mechanism. A path transmission element is necessary to transmit the path between the input and output elements. Cables attached to the reading elements should be guided towards the compliant shaft of the surgery tool; a cable guiding element is needed.

Table 4.1: Functional requirements

Number	Requirement	Must / Wish	Note	Value
1	Actuation of the total design			
1.1	Mechanically actuated	Must	No additional actuators. A mechanical transmission between the user input and the motion of the flexible shaft.	
1.2	Four cable control of the compliant shaft segments	Must	The compliant shaft of the instrument is built out of segments. The movement of each segment is controlled by two sets of antagonist cables, attached at $r = 3$ mm from the midline of the compliant shaft.	4 cables at $r = 3$ mm
2	Path planning by the user (input)		The user implements the path: path planning.	
2.1	Path planning	Must	The path is not fixed: the path can be changed by the user. The mechanism should exist out of 3 modes: past, present and future. The present is the input at that moment, this element is adjusted by the user. The past includes the part of the path that is already inserted and formed by segments of the compliant shaft. The future is the part of the path that is not yet defined.	
2.2	Stepwise path input	Must	The path input can be done in steps of 1 mm.	1 mm accuracy
3	Path formation in the compliant shaft (output)		Displacement of the output elements provide the change in cable length, ultimately causing an angular displacement of the segments of the flexible shaft	
3.1	Controlling a compliant shaft with at least 11 segments	Must	The mechanism should control a shaft of at least 11 segments. Thus at least 11 sets of cables need to be controlled.	≥ 11 segments
3.2	Cable guidance from path-planning mechanism towards compliant shaft	Must	The output elements of the design should have attachment point or the cables. Guidance of the cables towards the compliant shaft should minimise friction and avoid entanglement of the cables.	
3.3	Improving cable guidance: round or cylindrical shape of the design	Must	Improving cable guidance towards the flexible shaft. The previous model, the <i>MemoBox</i> , was rectangular shaped. The new model should have a round or cylindrical shape.	
3.4	Multiple curvature with 20 degree angle per segment .	Must	The output elements of the path-planning mechanism should provide at least a 20 degree angular displacement of the segment with respect to the previous segment.	≥ 20 degrees
3.5	Single curvature of 170 degrees	Must	The output elements should provide a single curvature of at least 170 degrees in the compliant shaft.	≥ 170 degrees

The main difference of this design compared to the previous models is the cylindrical shape to improve cable control and ergonomics. Because of the shape requirement, the output elements and consequently also the input elements, have a round shape. A minimum of 8 input elements and at least 11 output elements are required in the proof of principle. The number of output elements do not need to match the number of input elements. More reading elements smoothen out the motion in the compliant shaft of the surgery tool.

The memory elements should provide a stepwise input of 1 mm per step, as previously described in the functional requirements but also by design requirement 2.3. For the ease of use, it is wished that the user is provided with haptic feedback, so the user knows how much the memory rings have rotated (design requirement 2.4). In the functional requirements, it is explained that based on the MemoBox, the input elements have three modes: present, future and past. To avoid the implementation of an irregular path, it is necessary that the future elements move along with the present element (design requirement 2.5). By doing this, the present element's rotation is always a relative rotation to the previous element. In design requirement 2.6 is stated that to shift the element between the future mode to the past mode, the elements should be able to translate. The translational motion is relative to the output rings. It is wished that while the rings are translated, the user is provided with haptic feedback. Haptic feedback improves the ease of use, because the user knows when one memory element is shifted from present to past and vice versa. The present element and the future elements are part of the input and thus free to rotate by the user. While the elements in the past are already converted into an output and thus should be locked in that position. Design requirement 2.8 is set about the locking and unlocking of the memory elements: the mechanism should enable the memory elements to rotate while the path is inserted by the user (input). The mechanism should lock the memory elements after the path insertion is complete, and it is transmitted to the reading elements (output).

The transmission of the path from the input to the output is an important function in this mechanism: a guiding element, like a rail, should transmit the rotational input of the memory elements to the reading elements. It has two important characteristics: flexible enough to form the inserted path, stiff enough to provide enough normal force and transmit the path to the reading rings. The guidance must have minimal play (design requirement 4.2), otherwise an error occurs. Due to the play in the guidance, the reading elements will have some play as well. As a result, the cables can move, rotating the shaft elements: the path formed in the shaft is not secured and the shaft of the instrument is not stiff enough. Attached to the reading elements are antagonist cables that steer the segments of the shaft. Each output element should have two attachment points for the sets of antagonist cables (design requirement 3.3). The cables are guided towards the surgery tool. As stated in design requirement 5.2, the cables must be guided towards the segments of the flexible shaft, avoiding friction and tangling of the cables.

Overall, it is important that moving parts should operate with minimal friction. This is the case for the memory elements (design requirement 2.8) and the reading elements (design requirement 3.4). Friction should be minimised to prevent wear, jamming and loss of mechanical energy. Last, some requirements are set for ease of manufacturing: design requirements 6.1 - 6.3. Using standard parts and minimising the number of parts is preferred, to limit manufacturing time. Also, the use of 3D printed parts is preferred to reduce the manufacturing time and the costs of the prototype.

4.2. First sketch

Before the design process started, an initial sketch was introduced with the idea to make the MemoBox in a cylindrical shape. A sketch made on October 3th 2019 is shown in Figure 4.1. Additional comments are added to the sketch. The overall design consists out of two adjustable memory cylinders, C1 and C2: C1 is for the horizontal movement of the compliant shaft and C2 provides the vertical movement of the shaft. The memory cylinders exist out of multiple input elements, and the sketch shows a guiding mechanism forming a path. The path output mechanism is incorporated in the casing of the instrument, including a cable guiding component that guides the cables to the compliant shaft. In this sketch the two mechanisms are placed in line, giving the complete instrument a T-shape.

Table 4.2: Element design requirements

Number	Requirement	Must / Wish	Note	Value
1	Shape of the mechanism			
1.1	Round or cylindrical shape	Must	Previous models were rectangular. The new model should have a round or cylindrical shape to improve the guidance of the cables. A round shape is better suited in the handle of a surgical instrument.	
2	Memory elements			
2.1	Number of memory elements ≥ 8	Must	In the proof of principle at least 8 memory elements are required.	≥ 8 components
2.2	Functioning as path input elements	Must	Existing out of 3 modes: past, present and future. The present is the input, this element's or these elements's orientation can be adjusted.	
2.3	Path input by rotation of memory rings, in steps of 1 mm	Must	To provide a new position as input, the memory elements should be able to rotate per step. Accuracy of this rotation is 1 mm.	1 mm accuracy
2.4	Haptic feedback for rotation input	Wish	The user is provided with haptic feedback, so the user knows how much the memory rings have rotated for ease of use.	
2.5	Future memory elements rotate along with present	Must	To make sure the movement is smooth: meaning the input is a relative movement compared to the input of the memory element in front of that one. The future memory elements should be coupled to the present memory element.	
2.6	Translation of memory elements	Must	To shift the memory element from present to past or the other way around, the memory elements should be able to translate to or away from the input location.	
2.7	Haptic feedback for translational input	Wish	The user is provided with haptic feedback for the ease of use, so the user knows when one memory element is moved from present to past and the other way around.	
2.8	Memory element should rotate and translate with minimal friction	Must	The friction between the memory elements themselves and the other parts should be minimal. To prevent wear, jamming and loss of energy.	
2.9	Locking and unlocking of memory elements	Must	The mechanism should enable the memory elements to rotate while the path is inserted by the user (input). The mechanism should lock the memory elements after the path insertion is complete and it is transmitted to the reading elements (output).	
3	Reading elements			
3.1	Function as path output elements	Must	Attached to the reading elements are the actuation cables for the compliant shaft. Rotation of the reading element provides the pulling on the cables and thus movement of the shaft segments.	
3.2	Number of reading elements ≥ 11	Must	The number of reading elements do not need to match the number of memory elements. More reading elements smoothen out the motion and make path guidance easier. For the proof of principle at least 11 reading elements necessary.	≥ 11 components
3.3	Reading elements include attachment points for the actuation cables	Must	Attachment points on the reading elements for two cables. The distance between the attachment points should be equal on both sides of the reading elements. Meaning, rotation will cause a shortening of one cable equal to the elongation of the other cable.	
3.4	Reading element should rotate with minimal friction	Must	The friction between the reading elements, while rotating, should be minimal. To prevent wear, jamming and loss of energy.	
4	Transmission between input and output elements: Guidance			
4.1	Smooth path by guiding elements	Must	The path formed by the memory elements should be transmitted to the reading elements. A guiding element, like a rail, should transmit the rotational input of the memory elements to the reading elements.	
4.2	Minimal play	Must	The guidance should have minimal play. Otherwise an error occurs: the reading elements can rotate because of the play. As a result, the shaft element will move as well.	
5	Transmission from controller to surgery tool			
5.1	Cables attached to reading elements	Must	Attachment on each reading element for two cables: the antagonist cables.	
5.2	Cables guided towards surgery tool	Wish	Mechanism will be used to steer the flexible shaft surgery instruments. Cables must be guided towards the compliant shaft segments, avoiding friction and tangling of the cables.	
6	Ease of manufacturing			
6.1	Standard parts	Wish	For parts like bearings, pins and fasteners, existing sizes should be chosen.	
6.2	Number of parts	Wish	Minimise number of parts for the ease of manufacturing and assembling.	
6.3	3D printable	Wish	Use of 3D printed parts where possible, to reduce manufacturing time and costs.	

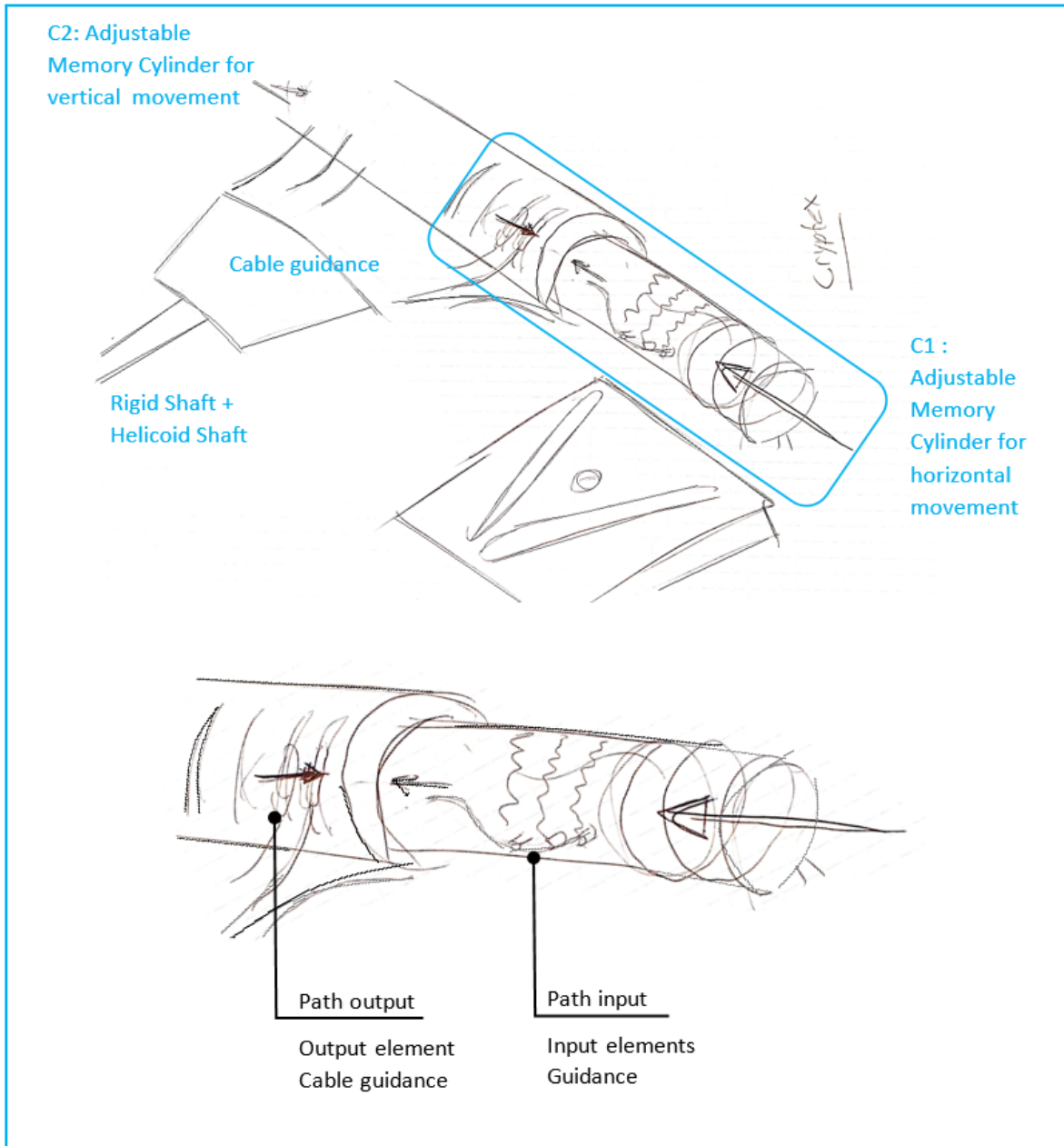


Figure 4.1: Initial design idea. Sketch for a cylindrical programmable path mechanism.

4.3. Concept generation

A more detailed sketch of the design idea is given in Figure 4.2. The sketch shows the main components necessary in the prototype. The design should include input rings (yellow), that are steered by the user. The input rings must be able to rotate and translate. The orientation of the memory rings with respect to each other is the formed path. The output is provided by reading rings (blue), against which the antagonist cables are attached. The path is transferred from the input to the output with a guiding element (red). The guiding element makes a continuous path from the discrete path input of the memory rings. Based on the element design requirements, multiple solutions are generated for each element and its functions. All solutions combined form a solution space. Combinations of these solutions form the concepts that are evaluated in Section 4.4, resulting in a final design.

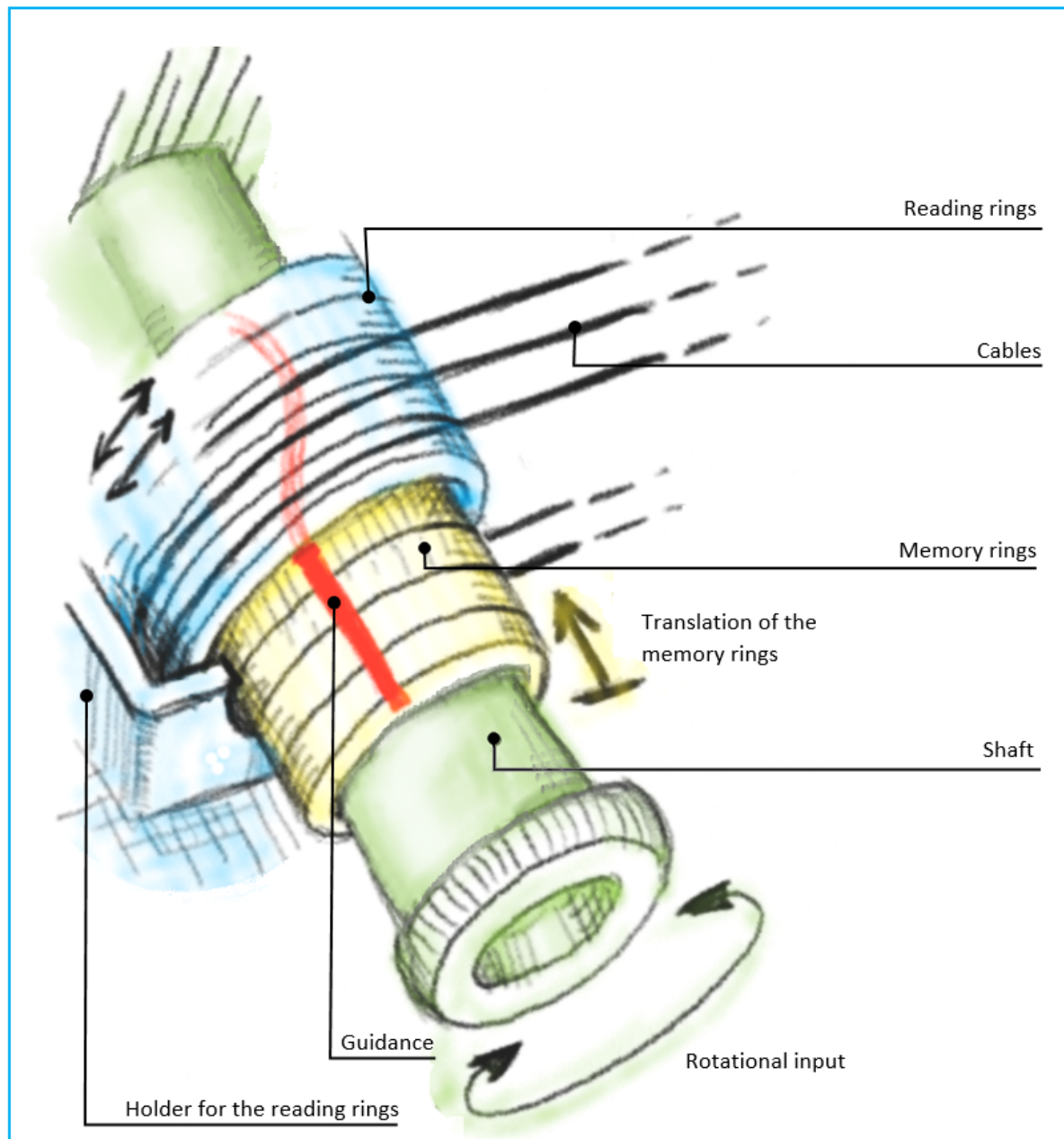


Figure 4.2: Sketch showing the main components necessary in the prototype. The design should include memory rings (yellow), which provide the path input. The rings are steered by the user with a rotational input and a translational input. The path output is given by the rotation of the reading rings (blue). Antagonist cables are connected to the reading rings. A guiding element (red) is necessary to transfer the path input to the output.

4.3.1. Path input: shafts and memory rings

The path input is provided by the memory elements. As the complete design must be cylindrical, it is chosen to make the input elements disk-shaped. Table 4.2 sets multiple design requirements for the memory rings. The solutions for the translational motion of the memory elements and the haptic feedback thereof, are elaborated in subsection 4.3.4.

The most essential function of the memory rings is the input of the path by rotating the rings in steps of 1 mm. Both the *MemoSlide* and the *MemoBox* provide the stepwise input by adding a teathed profile to their input elements. From this, it is assumed that either the inner or the outer circumference of the memory element should have a geared profile to provide the stepwise input. However, the design required for the input rotation is correlated with the locking of the memory elements. To memorise the path, the newly given orientation must be locked and saved. This is described by functional requirement 2.9: the mechanism should enable the memory elements to rotate while the path is inserted by the user (input), and they should lock after the path insertion is complete. The *MemoSlide* and *MemoBox* have locking mechanisms. The *MemoSlide* externally locks the follower elements, by two locking bars that are form fit with the follower elements. When the locking bars are positioned on top of the follower elements, the elements cannot translate anymore. The *MemoBox* has an interlocking mechanism, where the input elements are pushed together with a spring and have a form fit profile to interlock with each other. There are three possible solutions for locking: external locking, interlocking and internal locking. External locking means that an additional part is applied on the external area of the memory ring to lock its position. Interlocking implies that the memory rings lock against each other. The last group, internal locking, includes solutions that lock the memory rings from the inside. The three main groups can be subdivided into form fit and force fit. Form fit comprises a design with a counterpart, that perfectly aligns in shape with the memory rings and can prevent the rotational motion of the memory rings. Force fit mechanisms have an additional part that is pushed against the memory rings, creating enough friction to stop the rotation. The solution tree is shown in Figure 4.3.

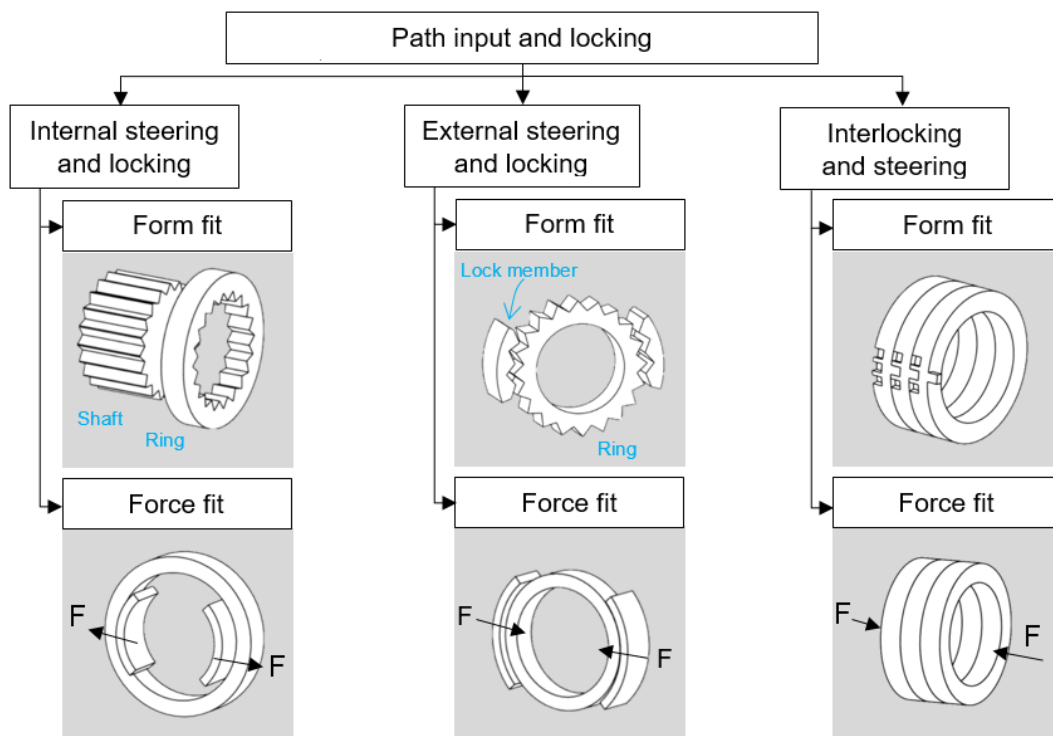


Figure 4.3: Solution tree for the path input and locking mechanism. The path input and locking are correlated. Three groups are made: internal, external and inter. Within the three groups a distinction is made between form fit and force fit. Additional explanation is given in the text.

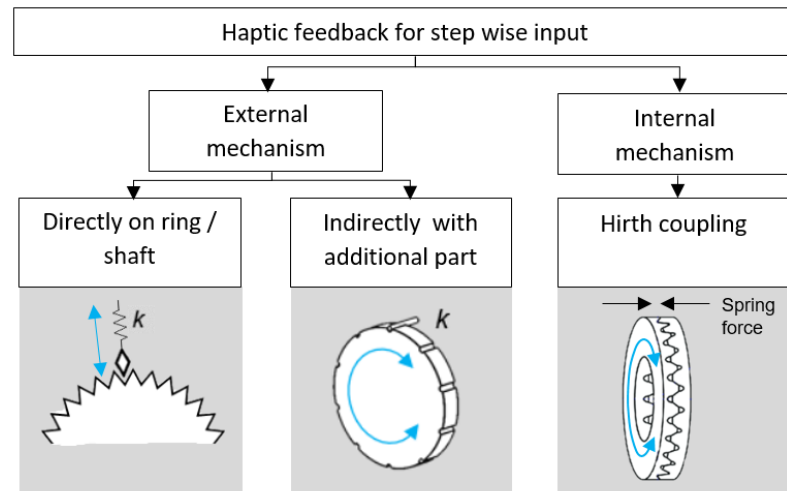


Figure 4.4: Solution tree haptic feedback for path input, stepwise motion. A distinction is made between an external mechanism and an internal mechanism. An external mechanism includes a spring element, operating on the external surface of a part. An internal mechanism is incorporated in the shaft design.

Internal and external locking mechanisms can have different shapes and working principles serving the same function. For example, the locking mechanism can grasp onto only a part of the memory ring or cover the whole circumference. Also, rather than having a locking member that alternately connects and disconnects by moving in/out or up/down, another solution can be that the locking member is stationary and the memory rings translate towards the locking member. Implementing an interlocking mechanism would require a member that can couple and separate the memory rings. For example, a preloaded spring to push the rings together, and a wedge-like member to separate the rings.

The *MemoSlide* and *MemoBox* both limit the amount of steps each input element can make with respect to its adjacent element. This limitation is necessary to avoid creating an irregular path. If the formed path has many sharp curves and is not smooth, it would be unable to guide the control points. The *MemoSlide* can translate 4 steps to the left and 4 steps to the right, while the *MemoBox* is limited by 2 steps to the left and right. A straightforward solution is providing each ring with a slot and a pin. The pin of the first memory ring moves in the slot of the second ring and the pin of the second ring is limited by the slot in the third ring, et cetera.

A wish to improve the ease of use is to provide haptic feedback for the rotational input. So the user knows when the input ring has been rotated with exactly one step. Different solutions will serve this wish. Electrical solutions, such as sensors, are not taken into account. Mechanical haptic feedback will be in the form of a click: a small resistance to the user's input and possibly a click as sound. Different solutions will serve this function; some are shown in Figure 4.4. The mechanism can be an external mechanism or an internal mechanism incorporated in the shaft of the design. A possible solution is a spring element that is force fit with the teathed profile of the input shaft or input ring. A small ball or cone is attached to a preloaded spring: when the ball is positioned above a gap between two teeth, it springs back to its desired position. This mechanism cannot be applied to memory rings that have an interlocking design, as it requires a teathed profile on the outer perimeter of the shaft or the memory ring itself. A similar solution with an external spring mechanism is adding a separate part with indents around its perimeter. A small pin, functioning as leaf spring, is attached to the input knob and moves along the perimeter from indent to indent. A more complex solution is incorporating a Hirth serration in the input shaft. A Hirth coupling is a mechanical connection between two shafts with tapered teeth. The teeth of the Hirth connection are form fit. The Hirth coupling can be pushed together with a spring. Rotating the shafts with respect to each other, requires the shafts to be slightly pulled apart, when the profiles are form fit again the spring will push the shafts together again. This mechanism will provide a small click as haptic feedback.

4.3.2. Path output: reading rings

The reading rings provide the output of the path. They should include two elements: a bearing that can move through the path made by the memory rings and attachment points for the steering cables of the compliant shaft. The design freedom is therefore very limited: the solution for the design of the reading rings is straight forward. However, they should rotate with minimal friction. This is elaborated in section 4.4.1, describing the possible critical parts in this design.

4.3.3. Path transmission: guidance

To transmit the input rotation made by the memory rings to the reading rings as output, a guiding element is necessary. From the previous designs, only the MemoBox has additional guiding elements. The MemoFlex II has a predefined path. The output bearings move in the slot in the track plates: the input and the output are directly in contact with each other. The slot in the input track element is optimised for the guidance of the bearings. The MemoSlide also does not include an additional guiding mechanism. The programmable path of the MemoSlide is formed by translating wedge-shaped grooves in the memory bank. The MemoBox on the other hand, has separate carts attached to the input elements. Each guiding element is connected to the corresponding input element via a pin, enabling them to rotate. The discrete displacement of the input elements in steps of 1 mm is converted into a continuous path. The input elements are v-shaped and include thin-walled flexible lateral flaps. These flaps form a continuous path, because the flaps of one guiding element and the body of the next guiding element overlap. The bearings that form the output of the mechanism, travel through these carts.

In the solution space, only mechanical guiding techniques are taken into account. Other types of guiding methods, for example the use of magnets or shape-memory materials, are not part of the scope. The different solutions for the path transmission can be found in the solution tree in Figure 4.5. A first division is made based on having an additional component or not. Not including an extra guiding component will result in a similar mechanism as the MemoSlide, in which the path is a slot in the input elements. The bearings of the output rings will move in this slot. The second group includes a specific component that fulfils the function as a guide for the bearings. A distinction can be made between separate carts and a continuous rail. A continuous rail is a component that is connected over the complete length. This can be a compliant design made out of one piece, or a design consisting out of multiple rigid parts connected to each other with hinges. Separate carriers are small carts that are connected to the input elements, each input element having its own cart.

The design of the guiding element is variable. If carts are chosen as guiding element, the design can be based on the MemoBox with thin metal flaps overlapping the carriers. Different shapes are possible for a continuous rail. Three potential shapes are the O-, U- and H-shape, shown in the solution tree in Figure 4.6. Both the U-beam and H-beam are designed to keep the bearings inside of the guiding element by the "legs" of the form. Conventional ball bearings can be used in these designs. Having a U-shaped guidance means that only the reading rings include bearings. In contrast to the H-beam, where both the memory rings as the reading rings contain bearings. Instead of a conventional bearing, The bearings should have an hourglass-shape, to be form fit with the guidance. In this case, the guidance is attached to the memory rings and the reading rings contain the bearings. This design is also possible with two O-shaped guiding elements, forming a parallel rail. In that case, the bearings are kept inside the two rods. However, this solution is not given in the solution tree, as it seems most likely not to work. The rods cannot be connected to each other with the hourglass-shaped bearings moving in between, so the distance between those rods will be variable. In curved paths the distance decreases; this will block the bearings and limit the guiding function.

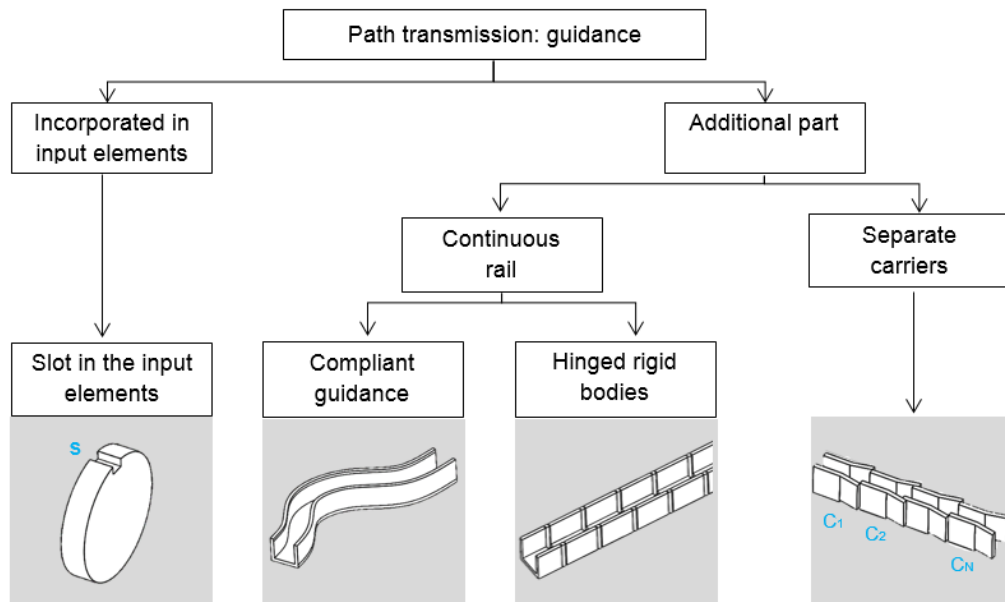


Figure 4.5: Solutions for the guiding mechanism of the bearings. The guidance transmits the path from the input elements to the output elements. Similar to the *MemoSlide*, one solution is to make a slot in the input elements. Consequently, no additional guiding element is necessary. Another solution is adding a guiding element. A distinction is made between separate carts and a continuous rail.

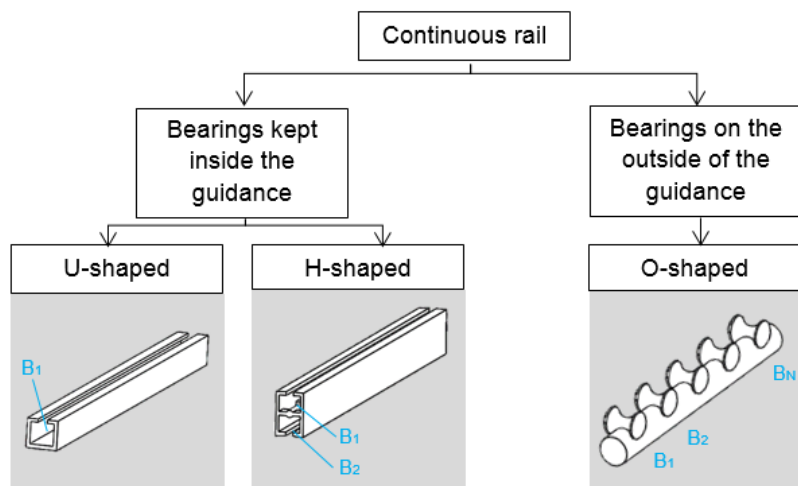


Figure 4.6: Solutions for the form of the continuous rail guidance. The U-beam and H-beam are designed to keep the bearings inside of the guiding element by the legs of the form. An O-shaped rail guides the bearings on its external surface. It requires hourglass-shaped rollers.

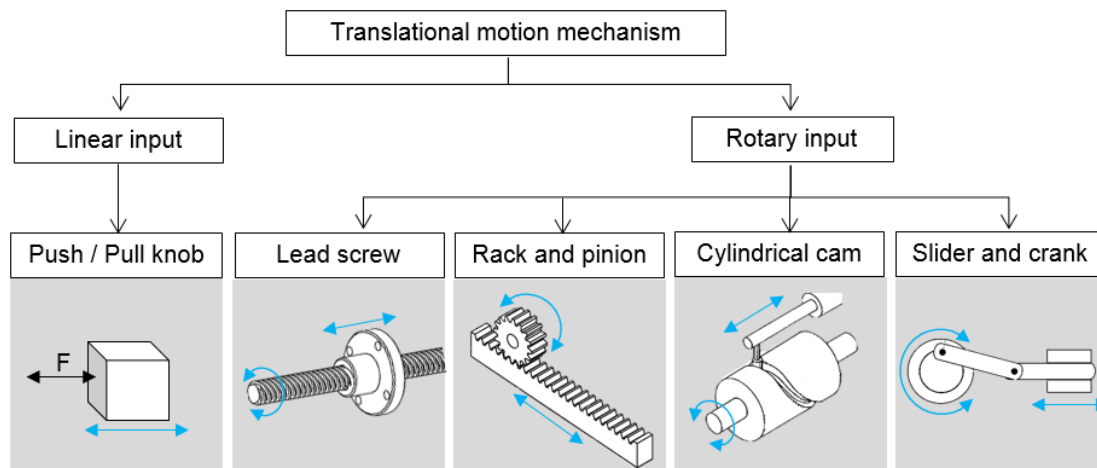


Figure 4.7: Solutions for the translational motion of the input elements. A distinction is made between linear input and rotary input.

4.3.4. Path insertion: translational motion

When the user has given the desired orientation to the input element, the input ring has to be slid towards the output rings to provide the path output. The motion in the opposite direction is also required: from the output position back to the input position to plan a new path. A component with the function "translational motion" is necessary to shift the memory element from present to past and the other way around, as described in requirement 2.6.

Translational motion can be accommodated by a linear input or a rotary input. Considering the requirement that the prototype is mechanically and manually actuated, there are several options available to translate the memory rings. The possible solutions for the function translational motion can be found in Figure 4.7. Firstly, by directly pushing and pulling the memory rings. This concept belongs to the first group: a linear input providing the translational motion output. The second group, converting a rotational input into a translational motion output includes multiple solutions. One solution is the implementation of a lead screw; turning the lead screw results in a linear motion of the lead nut or stage. This mechanism is used in linear stages for many different applications, such as a 3D printer. A similar mechanism is a rack and pinion mechanism: by rotating a pinion, the rack is moved back and forth. Instead of a rigid rack, a flexible belt with a teathed profile will also provide a translational motion if it is stretched between a pinion and pulley, like the caterpillar track of a tank. Another solution is the use of a cylindrical cam. A cylindrical cam is incorporated in, for example, the zoom mechanism of camera lenses. The cylinder contains a cam groove around its perimeter, which guides a roller attached to a follower element. Rotating the cylinder causes the follower to translate. Last, a slider and crank mechanism can be implemented to allow the user to shift the input rings with a rotary input. Out of these five possible solutions the linear input, the lead screw and cylindrical cam seem most suitable for this application. They are deemed to be more suitable, as they are easier to build in, into a design. For example, the slider and crank are not space efficient as the crank takes up a lot of space to create the translational motion.

Requirement 2.7 comprises the wish that the linear motion is stepwise with haptic feedback. To improve the ease of use, it is preferred to know when a memory element is positioned on the input axis or positioned on the output axis. Providing the translational motion mechanism with haptic feedback when a memory ring slides from one position to the other, will satisfy this wish. The potential feedback mechanism depends partially on the chosen translational motion mechanism. In Figure 4.8 a solution tree is shown, providing several possible solutions. The tree is divided into form fit and force fit mechanisms. The division in solutions is based on which input mechanism belongs to that specific solution. Only pushing (linear input), lead screw (rotary input) and cylindrical cam (rotary input) were taken into account, because these mechanisms were deemed to be most promising.

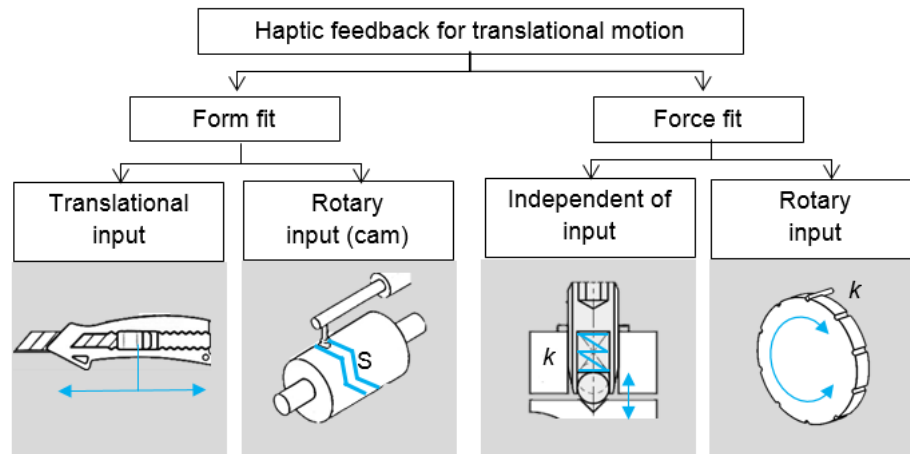


Figure 4.8: Solutions for haptic feedback while translating the memory elements from the input to the output shaft. The solutions are categorised based on form fit or force fit.

Translational motion with a linear input can be done stepwise by introducing a form fit mechanism to the push knob. For example, a method similar to the sliding mechanism used in Stanley knives. The extending and retracting of the blade in the Stanley knife is done in steps, so the user can adjust the length of the blade. Small slots in the handle are form fit with the push knob, causing the push knob to lock at certain positions. For a rotary input, used together with a cylindrical cam design, form fit stepwise motion is also possible. This can be done by introducing flat intervals in the cylindrical cam, instead of one smooth path. At those flat intervals, rotation of the input knob does not provide a translational motion. For lead screws, no solution is found based on form fit mechanisms. Results for force fit haptic feedback includes the implementation of springs. The use of a linear ball spring plunger is independent of the type of input mechanism; therefore it can be implemented in designs with both rotary as linear input. The mechanism contains a spring-loaded ball that can be compressed and will snap back to its desired position when it is given the space. By providing the translational motion mechanism with indents at the correct intervals, the spring-loaded ball snaps back to its preferred position when it is positioned above an indent. It will provide a click as haptic feedback. A similar force fit haptic feedback, that can only be implemented in combination with a rotary input, is the use of a small metal pin functioning as a leaf spring. The pin is connected to the rotary input knob and is desired to be straight, but can bend because of its material properties and design. This solution requires an additional part with indents along its perimeter. Knowing the lead of the screw or the lead of the path in the cylindrical cam (the amount of millimetre displacement per rotation), the indents can be placed at the precise locations, so the spring provides haptic feedback when one ring is slid from one axis to the other axis. The solution tree for haptic feedback can be found in Figure 4.8.

4.3.5. Cable guidance

The antagonist cables are attached to the reading rings. A small change in the length of the cables, produces an angular displacement of that specific shaft segment. The guidance of the cables towards the compliant shaft segments must be done while minimising friction and avoiding tangling of the cables (element design requirement 5.2). The prototypes of the MemoSlide and the MemoBox do not include a mechanism to guide the actuation cables towards a 3D printed shaft. The MemoFlex II has a funnel-shaped cable guidance. The cables are spread out over the perimeter of the funnel, separated with a consistent angle to avoid tangling. For the path-planning prototype, the cable guiding mechanism is not a part of the scope. However, having an idea about how the cables are directed from the path programming mechanism to the compliant shaft, can influence the design choices of for example the casing of the prototype. The solution tree for cable guidance is shown in Figure 4.9.

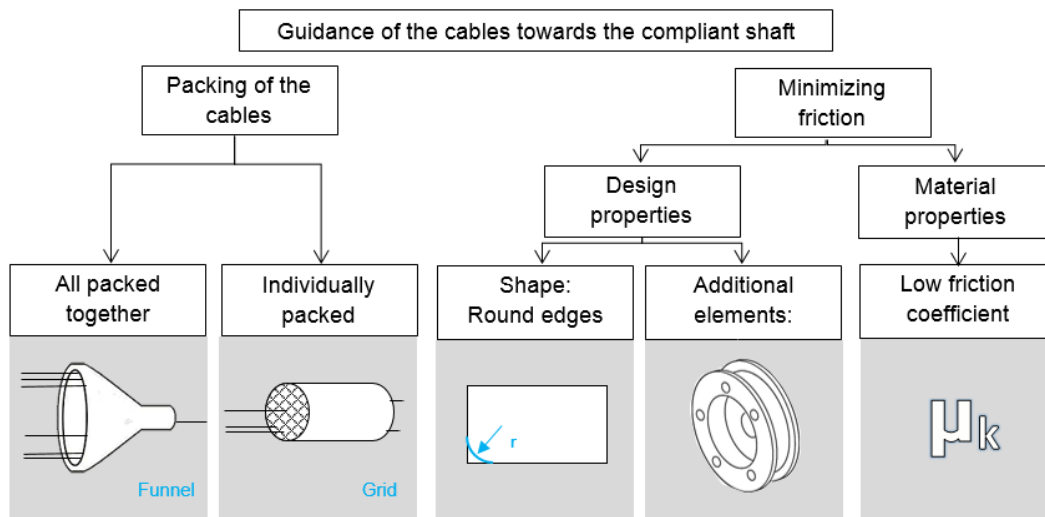


Figure 4.9: Solutions for guiding the cables from the programmable path mechanism to the compliant shaft.

A first division is made across the two main functions: minimal friction and avoiding tangling. The latter is determined by the manner the cables are packed. Packing the cables can be done by individually packing them or packing all the cables at once. Individually packing the cables requires a sort of grid, with separate pockets for each cable. Packing all the cables at once requires a funnel mechanism to convert the cables towards the small complaint shaft. To do so, the cables should be spread out over the perimeter of the funnel to avoid overlapping and tangling of the cables. This is similar to the MemoFlex II design. The division for minimising friction is based on design properties and material properties. Choosing a material with a low friction coefficient in combination with the material of the cable, is a relatively simple way to reduce friction. Design properties can be divided into the shape and form of the cable guiding element and the use of additional parts. Rounding off sharp edges at places where the cable is guided in an angle, is a measure based on shape. Additional rotating parts that move along with the cable translation, like small pulleys, will be the most effective method: the friction is reduced the most with this method. However, the design becomes more complex with extra parts, increasing the assembling time. To minimise friction, a combination of optimal design properties and material properties is desired. Depending on the path of the cables and what solution is chosen for the packing of the cables, it must be determined if round edges are sufficient or if pulleys are required.

4.3.6. Exclusion of solutions

In Appendix A the morphological chart is shown, providing an overview of all the results in the solution trees combined. Instead of creating multiple concepts using all the subsolutions per function, the subsolutions that were deemed insufficient are excluded from the conceptualisation. This selection is based on the main criteria, from most important to less important: feasibility, manufacturability, space efficiency, ergonomics and aesthetics, see Table 4.3. The feasibility is the likelihood of the mechanism to work. The feasibility of the solutions is determined by using technical knowledge and information from the previous designs. The ease of manufacturing is important to reduce manufacturing time and costs. The precision technicians from DEMO were consulted for the ease of manufacturing. Space efficiency reflects on the size of the path-planning mechanism. A smaller design is desired, so the actual surgical instrument is more compact. Ergonomics is the ease of handling the prototype. Last, aesthetics depends on, for example, the form and materials chosen. The criteria with a higher factor, have priority over the lower factors. Thus, feasibility and manufacturability are the most important criteria for this prototype. Per element and function, the selection is shortly elaborated below.

Table 4.3: Selection criteria

Criteria	Factor	Description
Feasibility	3	The likelihood the mechanism works. The practicality of the solution. Will it successfully accomplish the requirements. The feasibility is based on technical knowledge and the weaknesses and strengths of the previous designs.
Manufacturability	3	Ease of manufacturing. Aim to reduce manufacture time and costs. As the prototype is manufactured at DEMO TU Delft, the precision technicians are consulted during the design process.
Space efficiency	2	Minimising the size of the prototype is a wish. This would make the implementation step into an actual surgical instrument easier.
Ergonomics	2	Ease of handling the prototype. Factors like steering and holding the prototype are taken into account.
Aesthetics	1	The appearance of the prototype: form, materials et cetera.

Path input: shaft and memory rings

Six solutions have been proposed based on the type of locking mechanism and being force fit or form fit. From all solutions, the force fit solutions are assumed to be less feasible. The force fit solutions require a mechanism that supplies enough pushing force against the memory rings to lock them in position. Not only is this a more difficult design, with for example, the implementation of a stiff spring to provide the force. Also, the force against the input rings can damage the parts, because of friction and wear. A force fit design is more cumbersome than having a form fit mechanism that does not require a lot of force, but only the right placement. Therefore, the form fit solutions are more promising and the force fit solutions are excluded from the conceptualisation. Out of the three form fit solutions, the interlocking mechanism is excluded. An interlocking mechanism is more complex, as it requires components such as an additional wedge that could separate the memory rings and provide a rotational motion. Based on feasibility and manufacturability, internal steering with a form fit shaft is deemed to be the easiest. A form fit inner shaft can provide the rotational input when the memory rings are positioned on the shaft. It can also function as locking mechanism: by locking the rotation of the shaft when the rings are located on it, the motion of the rings is also locked. Thus, in the concepts created the internal form fit steering and locking mechanism is chosen.

Path output: reading rings

The functional requirements and design requirements limit the design freedom of the reading rings. The reading rings are required to be round, with bearings on the inside and cable attachment points on the outside. Consequently, the design of the path output is straight forward: a ring with bearings on its inside that are guided by the guiding element. A frame is necessary to keep the reading rings in place and let them rotate with minimal friction.

Path transmission: guidance

The guiding element is the most critical part of the design. It is the connection between the path input and the path output. Therefore, the design must be selected carefully. From the proposed solutions, the H-beam seems most promising for this purpose. No guidance, meaning a slot in the memory rings, is the easiest to manufacture, however it is not feasible. As can be seen in Figure 4.10A on the next page, the relative rotations of the memory rings would make the path irregular with sharp edges. If the width of the slot is the size of a bearing, the bearings of the reading rings would not be able to move through the path as their motion will be blocked by the edges. A wider slot can be a solution, however this will give the reading rings a lot of play, which is undesired. Separate cartridges, similar to the MemoBox, is a feasible solution. However it is time consuming to manufacture them. This also applies to a continuous rail with hinged connections. The manufacturability is low, because it is a difficult design and requires tiny hinges. A continuous compliant beam is 3D printable and therefore easy to manufacture. An advantage of the 3D printing method is that multiple beam designs can be printed and tested on their flexibility. The challenge of a continuous beam is that a curved path deforms the H-beam. In curves, the inner flank of the beam is compressed, while the outer flank is stretched and wants to elongate. As a result, the rail tends to become smaller in curves (shown in Figure 4.10 B). The H- or U-shape is deemed to be most feasible for the task, because the horizontal rib of the H- or U-beam makes sure that the width of the beam stays relatively consistent.

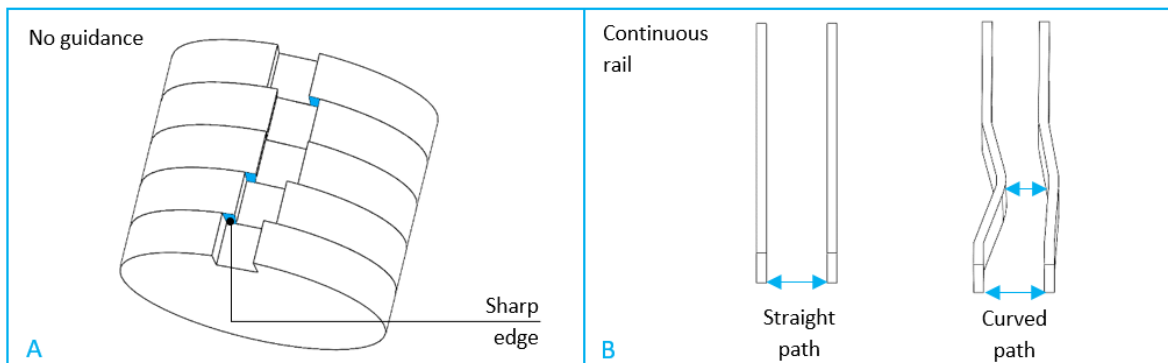


Figure 4.10: Challenges of the design of the guidance. Figure A shows an example of no additional guiding elements. The memory rings have a slot. The problem arises that irregular paths are created with sharp edges. Figure B shows the problem with a continuous rail. Curves in the continuous rail, reduce the width of the guidance. One flank is compressed while the other flank is stretched.

Translational motion mechanism

Five possible solutions can provide a translational motion of the memory rings. All mechanisms are feasible, however out of these solutions the linear input (push/pull knob), lead screw and cylindrical cam are most suitable for this application. They are deemed to be more suitable, as they are easier to build into the design. For example, the slider and crank is not space efficient, because the crank takes up a lot of space to create the translational motion. The rack and pinion solution and the slider and crank solution are excluded. Concepts are created for a linear input, lead screw and cylindrical cam. The solutions for the haptic feedback used in the translational motion of the memory rings were excluded based on ease of manufacturing and ease of use. The form fit mechanisms, for both the translational input and rotary input, are undesired as it makes the translational motion unsmooth. It is undesired for the ease of use. The force fit designs, depending on the stiffness of the spring, can be designed to be a simple click, rather than actually stopping the translational motion. The use of a spring plunger has as an advantage that it can be implemented in any design and it is a standard part that is commercially available. Thus, the ball plunger is chosen for the final design and the other subsolutions are excluded from the concept generation.

Cable guidance

The cable guidance is not part of the path-planning prototype yet. The selection of the most sufficient solution depends on how the path-planning mechanism is incorporated in the actual surgical instrument. The incorporated design and a proposed solution for cable guidance is elaborated in Chapter 8.

4.3.7. Basic idea of the concepts

With the exclusion of several solutions, one basic idea of the prototype is given in the sketch in Figure 4.11 on the next page. The rotational input is provided by an input shaft that is form fit with the memory rings (yellow). The input shaft and the memory rings have a geared profile, to make the input rotation stepwise. The system contains two shafts (green): one input shaft that is able to rotate and one fixed shaft that can be seen as fixed world. When the memory rings are positioned on the input shaft, they rotate along with the input. When the memory rings are positioned on the locked shaft, their given orientation is locked. The memory rings are contained inside an orange frame. The translational motion of the frame, moves the memory rings from one shaft to the other shaft. Attached to the memory rings is the guiding element, an H-beam (red). When the memory rings are translated from the input shaft to the fixed shaft, they enter the reading rings (blue). In this figure, only one reading ring is shown. The reading rings contain small ball bearings, that are guided by the path formed in the H-beam. A steering cable is attached on top of the reading ring. Its antagonist is attached on the bottom of the same reading ring. The sketch only shows the elements necessary in the prototype. How the elements move with respect to each other and how everything is kept in one assembly is yet to be determined.

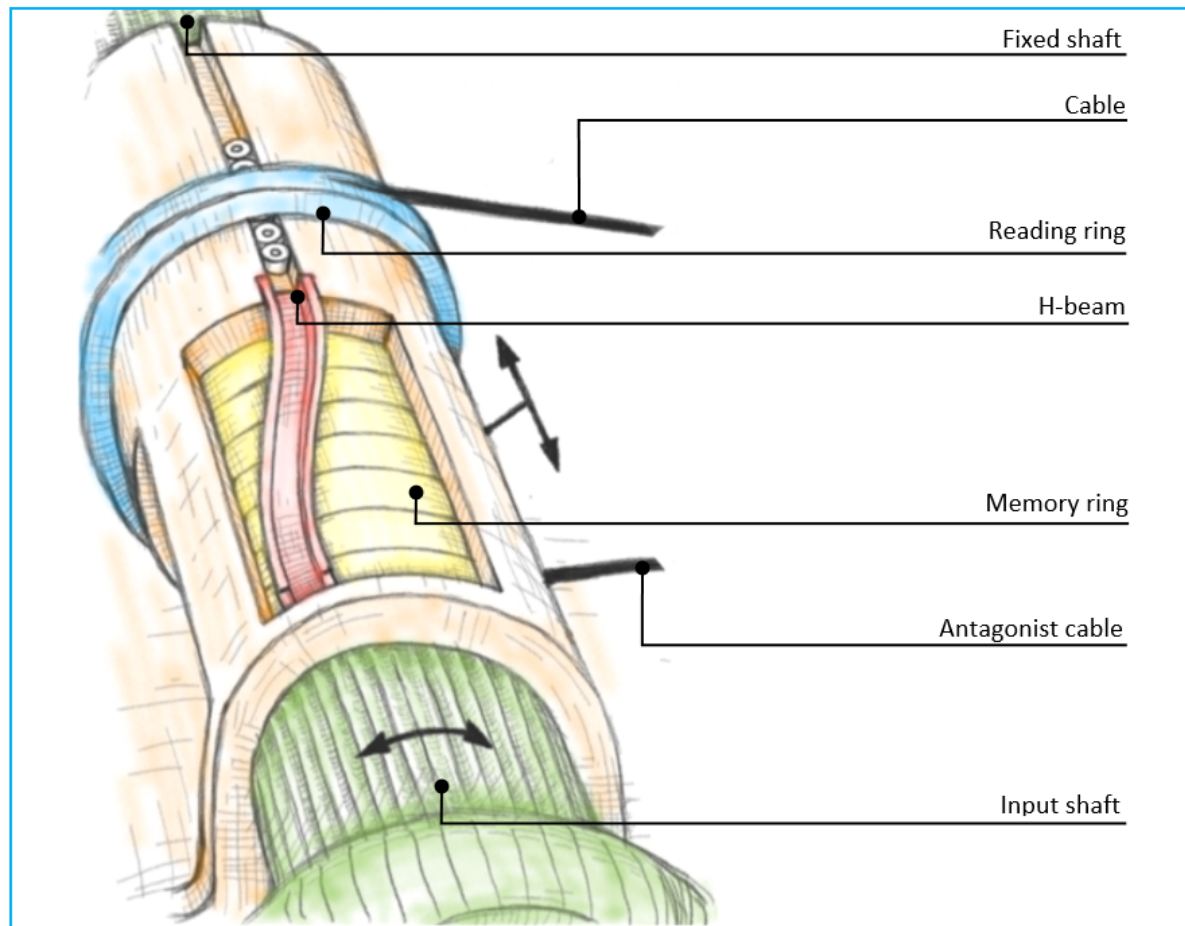


Figure 4.11: Basic idea of the concepts. Explanation is given in the text.

4.3.8. Concepts

Four concepts have been generated based on the sketch in Figure 4.2. All concepts contain the same designs for the shafts, memory rings, reading rings and H-beams. However, the mechanism used for the translational motion of the memory rings is different for each concept. The first concept is shown in Figure 4.12. In this design, the user directly pushes the translational motion mechanism by pushing and pulling the radial pins on the mechanism. The translational motion is in this case provided by a linear input. The second concept also includes a linear input. Here, the input knob rotates the input shaft, and also functions as input knob for the translational motion. Figure 4.13 shows the main parts of the second concept. The input knob has a geared profile on its inner perimeter, making it form fit with the shafts. Rotating the knob, would rotate the input shaft. The input knob and translational motion part are connected by small hooks. The hooks grasp in a slot in the translational motion part. The combination of the hooks with the slot enables the input knob to push and pull the translational motion part, without rotating it. Also, rotating the input knob only rotates the shaft and does not rotate the translational motion part. Concept 3 includes a cylindrical cam which converts a rotational input into a linear output, as shown in Figure 4.14. In this concept, the translational motion part also contains two radial pins, similar to concept 1. The pins are form fit with a slot in the cylindrical cam. Rotating the cylindrical cam would cause an axial advance of the pins, because the slot is designed with a certain lead. Consequently, rotating the cam causes the linear motion of the memory rings. Figure 4.15 shows the last concept, which consists out of a lead screw and lead screw nut that provide the sliding motion of the memory rings. The lead screw is incorporated in the shafts of the prototype. The distal side of the translational motion part includes a lead screw nut, that fits on the lead screw. It requires the fixed shaft to have slots along its length, so the translational motion part can be connected to the lead screw. The user controls two rotational knobs: one for the rotation of the input shaft and memory rings and the other for the translation of the memory rings.

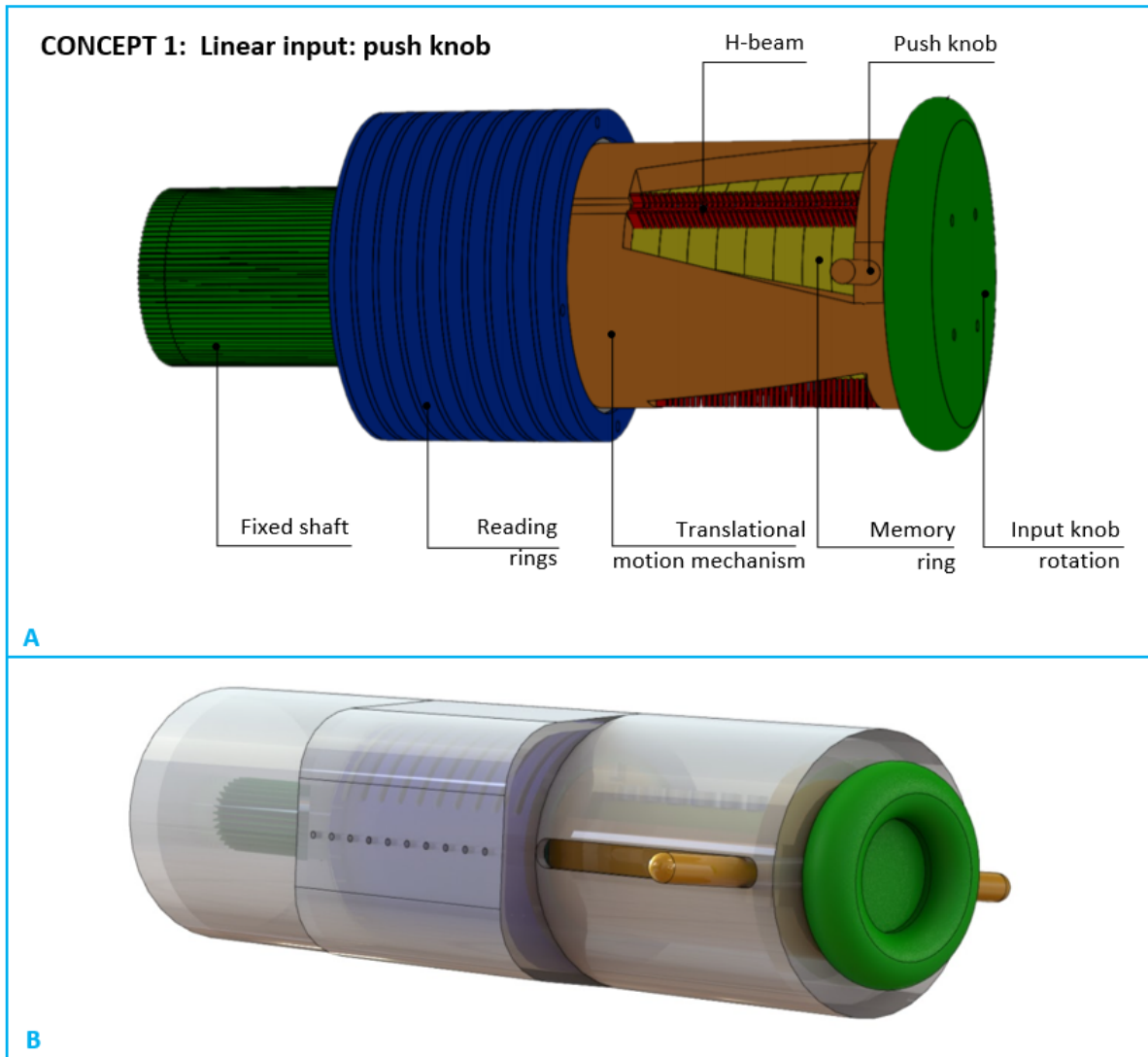


Figure 4.12: Concept 1: push knobs for a linear input. Figure A shows the main components of the design. The main components include the input shaft, input knob, fixed shaft, memory rings, reading rings, H-beams and the translational motion mechanism. In this design the user directly pushes the translational motion mechanism (orange), holding the pins on each side. The translational motion is in this case provided by a linear input. Figure B is a CAD drawing of how the design would look with a perspex casing around it.

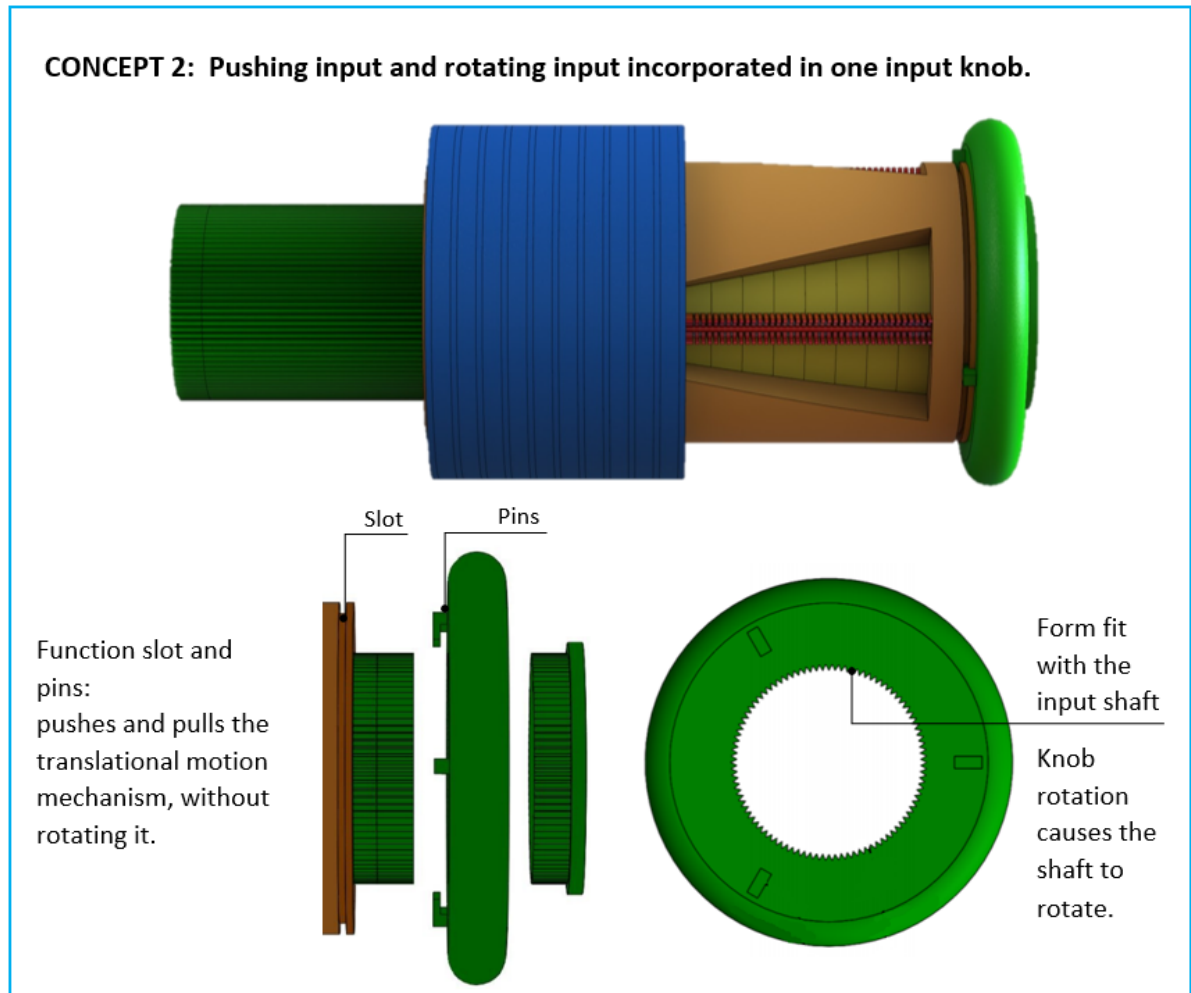


Figure 4.13: Concept 2: pushing and rotating input incorporated in one control knob. Concept 2 has a similar design as the first concept, consisting out of geared shafts (green), memory rings (yellow), guidance (red), reading rings (blue) and a translational motion mechanism (orange). The input knob has a geared profile on its inner perimeter, making it form fit with the shaft. Rotating the knob, would rotate the input shaft. The input knob and the translational motion part are connected by small hooks. The hooks grasp in a slot in the translational motion part. The hooks in combination with the slot disconnect the two functions of the input knob: it enables the input knob to push and pull the translational motion part, without rotating it. Also, when the input knob is rotated only the shaft moves along, while the translational motion component stays in place.

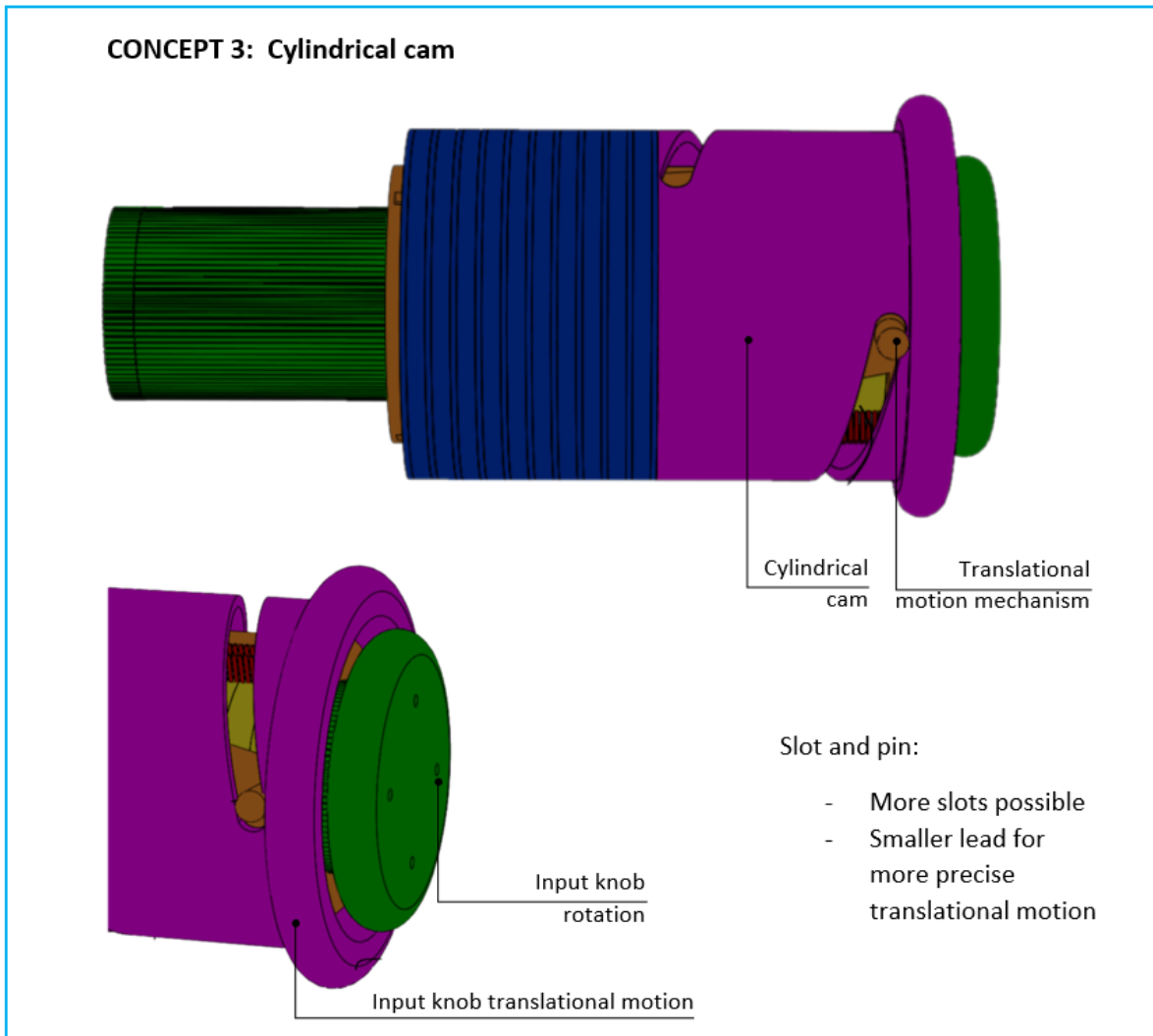


Figure 4.14: Concept 3: cylindrical cam. Concept 3 consists out of geared shafts (green), memory rings (yellow), guidance (red), reading ring (blue), a translational motion mechanism (orange) and a cam (purple). The translational motion part has the same shape as the one in concept 1, with two radial pins. The pins are form fit with the slot in the cylindrical cam. The slot is designed with a certain lead, which provides an axial advance during one complete turn. Thus, rotating the cylindrical cam would move the pins in a linear motion. This design requires a casing or an extra part that makes sure that the translational motion part (orange) can only translate, so it does not rotate along with the cam.

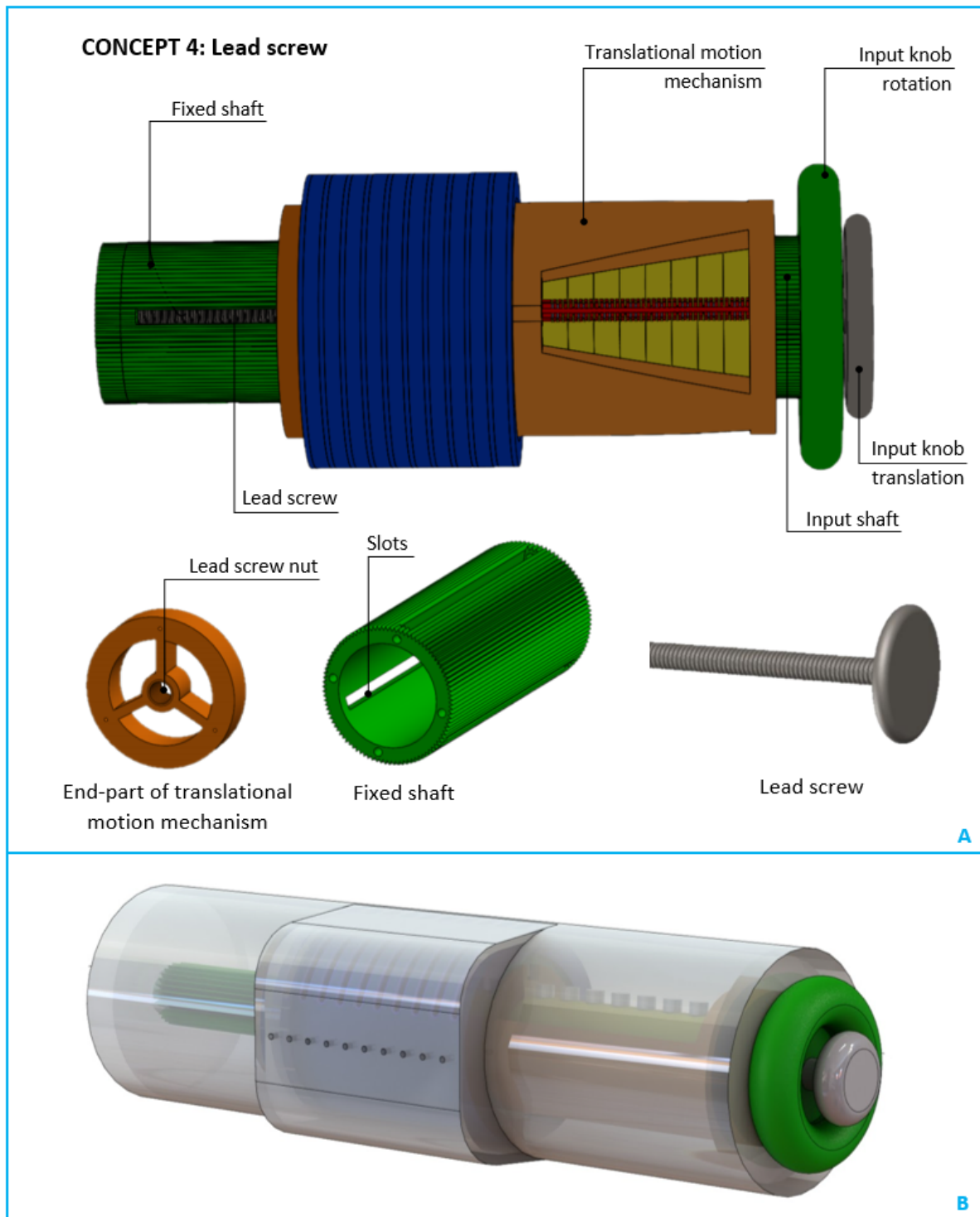


Figure 4.15: Concept 4: lead screw. Figure A shows the most important parts of this design. Figure B is a CAD drawing of how the design would look with a perspex casing around it. The lead screw is incorporated in the shafts of the prototype. The distal side of the translational motion part includes a lead screw nut, that fits on the lead screw. This requires the fixed shaft to have slots along its length, so the translational motion part can be connected to the lead screw. The user controls two rotational knobs: one for the rotation of the input shaft and memory rings and the other for the translation of the memory rings

4.4. Concept selection

Table 4.4: Concept selection

Criteria	Factor	Concept 1	Concept 2	Concept 3	Concept 4
Feasibility	3	3	2	2	1
Manufacturability	3	3	2	2	1
Space efficiency	2	2	3	1	2
Ergonomics	2	1	3	2	2
Aesthetics	1	2	2	1	2
Score		26	26	21	19

Concept selection is done based on the selection criteria previously shown in Table 4.3. The grading of the designs is provided above, in Table 4.4. For each criteria the concepts were given a grade from 1 to 3, in which 1 is the lowest score and 3 the highest score. The weight factor of that particular criteria is multiplied with the given the grade. Accumulating the scores for each criteria results in a final score of the concept. Concept 1 and 2 have the highest accumulated score and concept 4 scored the lowest.

The four concepts have a similar design: all main components are kept the same except for the translational motion of the memory rings. The translational motion of the memory rings is necessary to implement the path, but is not considered as a critical part. The mechanisms to provide the translational motion are existing mechanisms, used in many applications. For example, the cylindrical cam is used in the zoom mechanism of a camera and lead screws are used in linear stages. Consequently, all designs seem feasible. However, some concepts have an easier design, making them more suitable.

Concept 1 is the most straight forward design, containing relatively simple parts. The translational motion mechanism is directly pushed by the user and only requires two radial pins functioning as user interface. Thus, it is the most feasible design, and also the easiest to manufacture out of the four concepts. Therefore, concept 1 scores the highest for the criteria feasibility and manufacturability. The memory rings of concept 2 are also moved from shaft to shaft by a linear input. The combination of the rotational input and translational input in one knob is space efficient and also improves the ergonomics of the mechanism. However, the design of the input knob requires small features and is more difficult to manufacture. If there is friction between the slot and the pins, the uncoupling of the rotational and translational input will not function well. Therefore, concept 2 scores lower for feasibility and manufacturability. Concept 3 is a feasible concept. The cam can be made out of a plastic tube and the translational motion mechanism only requires two radial pins, similar to concept 1. However, the design is less space efficient. The translational motion requires a cam, but also an additional part to keep the translational motion mechanism in a linear path. This is necessary, to avoid the translational motion mechanism to rotate along with the rotational input given to the cam. Concept 4 is the most complex design. To provide the translational motion, the lead screw is incorporated inside the shafts. The translational motion mechanism should include a lead screw nut, which must be connected to the lead screw in the centre of the prototype. The design of the translational motion mechanism is difficult to manufacture and also the design of the shafts is altered with slots in it. Compared to the other concepts, concept 4 scores lowest for feasibility and manufacturability. Because the lead screw is implemented inside the shaft, the concept is space efficient. Based on aesthetics, all concepts look very similar. Concept 3 has been given a lower score, as it is difficult to make the cam and casing see-through. In the other designs, a perspex casing is optional and the user can see the orientation of the H-beam.

Concept 1 and 2 are both promising designs. Comparing those designs, the first concept scored higher on feasibility and manufacturability, which is more important. Therefore, concept 1 is selected as the final design. If desired, this design can still be transformed into the cylindrical cam design (concept 3). A more advanced version of concept 1 is given in Appendix A, Figure A.3. This version includes a Hirth coupling for haptic feedback for the rotary input.

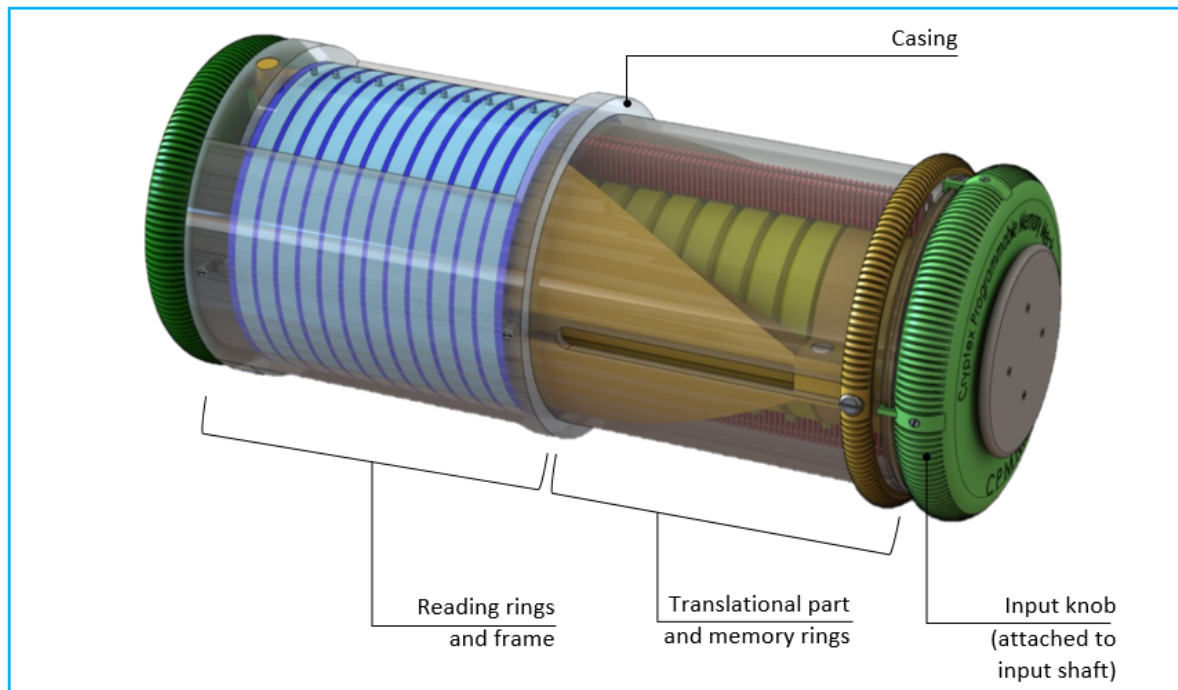


Figure 4.16: CAD drawings of the final design. The mechanism exists out of 4 major subassemblies. The shafts and end knobs (green), the translational motion part (orange) and memory rings (yellow), the reading rings (blue) and their frame (dark blue), the outer casing (see-through). The final design has 8 memory rings to input the path and 15 rings to provide the path output. Note: the design in this image still has 12 reading rings instead of the correct number 15. Instead of two radial pins, the translational motion mechanism is controlled by an input knob. The design is made symmetrical with two H-beams.

4.5. Final design

A CAD drawing of the final design is shown in Figure 4.16. Based on the aesthetics and its functions, the path-planning module is named *the Cryptex Programmable Memory Mechanism (the CPMM)*. The design can be separated into four major subassemblies:

1. Shafts
2. Memory rings and translational motion mechanism
3. Reading rings and frame
4. Outer casing

The final design consists out of 8 input rings and 15 output rings. A 3D printed H-beam transfers the orientation of the memory rings to the reading rings. In this section, first the key components parts are evaluated and after that the final design is shown with exploded views.

4.5.1. Design of possible critical parts

Some parts were deemed to be key components in this concept. Before manufacturing, the key components are evaluated. The main critical features are the teeth of the memory rings and shaft, the friction between the reading rings and the deformation of the H-beam. Firstly, the small teeth of the memory rings and shafts are subjected to normal forces, as a result from the applied torque by the user. Also, the H-beams exert forces on the memory rings. The teeth should be able to withstand those forces without breaking. Another critical subassembly is the reading rings: the reading rings should be able to rotate with minimal friction. The rotation of the reading rings is provided by the path formed in the H-beams. When the reading rings rotate with much friction, the flanges of the H-beams have to withstand much force to keep the bearings of the reading rings in its path. Last, the H-beams are subjected to both torsion and shear. The design of the H-beam should be flexible enough to form different paths, however it should also be stiff enough to guide the bearings of the reading rings.

Memory rings

The stepwise path input is provided by a gear profile of the shaft and memory rings. The teeth of the memory rings and the shaft are exposed to normal forces, which can be critical. The input torque of the user rotates the inner shaft. As a result, the teeth of the input shaft exert normal forces on the teeth of the memory rings, to rotate the memory rings. The H-beams work against the rotation of the memory rings, as they try to resist the deformation.

The dimensions of the teeth are based on the basic profile ratios given by the ISO 68-1 metric screw threads data. Figure 4.17A shows the chosen dimensions for the gear profile. The pitch (P) is 1.002 mm and the height of the fundamental triangle (H) is a result from the pitch and the top angle: $\cos(30^\circ) \cdot P$. Based on the functional requirements the pitch should be 1 mm, like the stepwise input of the *MemoSlide* and the *MemoBox*. However, because of the circular profile with the chosen diameter, 1.002 mm as pitch is the closest to 1 mm. The total number of teeth covering the inner perimeter of the memory ring is 94. The shaft, coloured in green in the figure, is the counterpart of the memory rings. Figure 4.17B provides a calculation to estimate the maximum total external force allowed. Some assumptions are made:

- The teeth contact area is equal to the multiplication of the width of a memory ring (excluding the sides that have a chamfered edge) and the total contact length.
- The pressure is equally spread over the complete contact area.
- All the teeth contribute to the input rotation.
- The memory ring is made out of brass, $E = 100$ GPa.
- The shaft is made out of aluminium, $E = 70$ GPa.
- Safety factor of 2.

The calculation shows that the maximum force allowed on the complete memory ring is 13.2E6 N. This external force is applied by the user by rotating the input knob which is attached to the shaft. The force is necessary to overcome the resistance of the H-beams and to make the memory rings move along with the shaft. This force is also required to overcome the friction between the past and present memory rings. The centre of the contact area is positioned at $r_t = 15$ mm away from the centreline of the shaft. Meaning that the maximum torque allowed to be applied by the user is the total force allowed (F_{tot}) multiplied by the radius (r_t). This results in $T = 19.9E4$ Nm. However, 19.9E4 Nm is a very high torque and will never be applied by the user's fingers. It is concluded that the forces on the teeth of the memory rings and the shaft will not be critical in this design. To improve the ease of manufacturing, the number of teeth of the memory ring is reduced to 8. A consequence of the reduction of the number of teeth is that the contact area between the memory ring and the shaft is less. As a result, the total force that can be applied is reduced to 1.13E6 N and the torque to 1.69E4 Nm. This is acceptable. Newton's third law, action is -reaction, applies to the memory rings and the shafts. The shafts are made from aluminium, which has a lower Young's Modulus than brass. The Young's modulus from aluminium is around 70 GPa [3], while the Young's modulus of brass is roughly 100 GPa, depending on the composition. The total force and torque are directly influenced by the Young's modulus, as could be seen in Figure 4.17B. Consequently, with a 30 percent decrease in Young's modulus, the maximum force and torque allowed on the shafts is respectively $0.70 \cdot 1.13E6$ N and $0.70 \cdot 1.69E4$ Nm. This is equal to 0.79E6 N and 1.18E4 Nm. These values are deemed to be acceptable.

Disk friction occurs between the present memory ring and the adjacent past memory ring. The other memory rings are at that moment not exposed to disk friction, because they do not rotate relative to each other. Thus, the disk friction only takes place between two rings and is therefore assumed to not be critical. The rings are form fitted on the shafts and the user can provide the necessary torque to rotate them. The maximum force allowed on the teeth is enough to overcome the disk friction. This is contrary to the reading rings, which is elaborated in the next subsection. While sliding the memory rings, there is also friction in the longitudinal direction between the shaft and the memory rings, which can cause wear and jamming. By choosing the right materials, as described in Section 6.1.1, the friction is minimised. Also, lubrication will minimise the friction between the shaft and the memory rings.

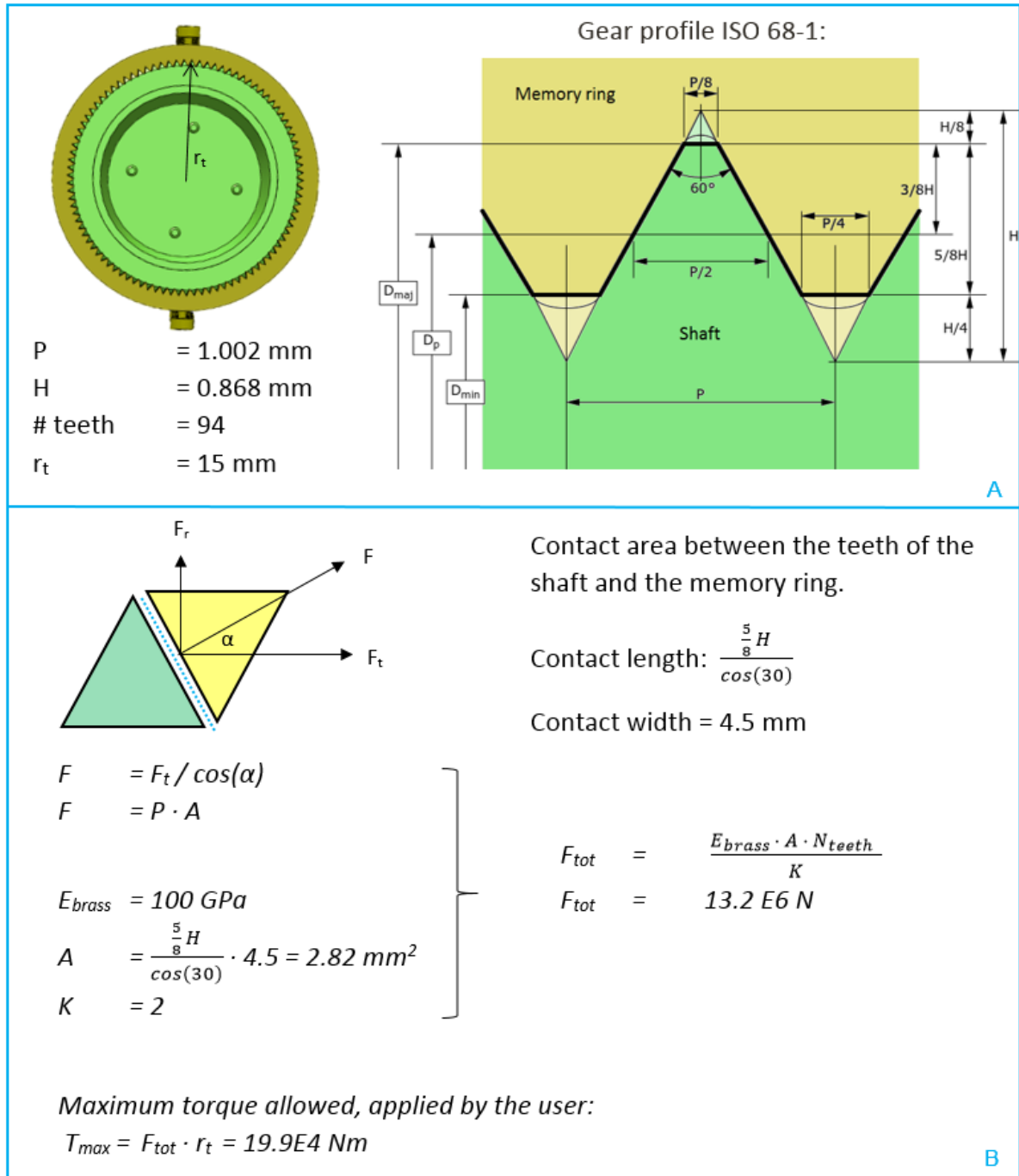


Figure 4.17: Forces on the gear teeth of the memory elements. Figure A shows a cross section of the input shaft and a memory ring. The gear profile is based on the ISO 68-1: the teeth have a pitch (P) close to 1 mm and a top angle of 60 degrees. In total there are 94 teeth placed at 15 mm (r_t) from the centre of the assembly to the tip of the tooth. Figure B provides a calculation of the maximal allowable force and torque applied by the user. It is assumed that the contact area of the force includes all 94 teeth ($A \cdot N_{teeth}$). The total force (F_{tot}) is calculated. The formula includes the multiplication of the Young's Modulus of brass (E_{brass}) in Pa, the contact area (A) in m^2 , the number of teeth (N), divided by the safety factor (K).

Reading rings

The reading rings have to form the path provided by the guiding element. As stated in element design requirement 3.4, the reading rings should rotate with minimal friction. Their input torque is provided by the normal forces of the guiding element on the bearings of the reading rings. Since the H-beams are flexible, they cannot provide an unlimited high normal force: the beam will deform or break. Therefore, it is necessary that the reading rings rotate with minimal friction, enabling the forces provided by the H-beam to overcome the friction torque. Disk friction can occur between the reading rings: the friction that exists between two or more bodies that do not rotate with the same speed or in the same direction. For example disk friction occurs between a rotating body and a stationary body. A moment is exerted on the bodies involved, because the disk friction tends to resist the relative rotation of the bodies. In this design, multiple reading rings are positioned next to each other and should rotate independently of each other. A risk of the reading rings placed next to each other is the accumulation of the normal forces and friction components. This can cause the friction to build up along the length of the reading ring assembly. Besides the wear of the reading rings, the reading rings can get locked in their position, causing the whole prototype to block.

Figure 4.18 provides the calculation of the frictional torque. The friction force is equal to the normal force at that specific point multiplied by the kinetic coefficient of friction. This normal force exists when the adjacent disks get in contact with each other. In the CPMM design the translational motion element or the H-beams can cause a normal force, pushing the disks together. The total friction moment on one reading ring is the sum of the individual moments over the entire contact area. It is assumed that the pressure and the coefficient of friction is uniform over the complete area of the reading ring. Therefore, the normal force pressure is integrated over the entire area of the disk: $2 \pi i (r_o - r_i)$, in which r_o is the outer radius of the reading ring and r_i the inner radius. The integration results in formula 4.1c, as can be seen in Figure 4.18. The guiding element should be able to provide enough force against the bearings of the reading rings, to overcome the frictional torque. Assuming the H-beam is stiff enough, the input rotation results in a normal force on the bearing of the reading ring. What must be noted is that the input torque (T_i) does not directly work on the H-beam. The torque input of the memory ring, results in a pushing force on the H-beam provided by the bearing of the memory ring (F_{N_m}). With two bearings attached to the reading ring, the input torque becomes: $T_i = 2 \cdot F_{N_r} \cdot r_{b_r}$, formula 4.1b.

$$\alpha = \frac{T_i - (\#rings \cdot T_f)}{I} \quad \text{Angular acceleration of the memory ring} \quad (4.1a)$$

$$T_i = 2 \cdot F_{N_r} \cdot r_{b_r} \quad \text{Input torque by guidance} \quad (4.1b)$$

$$T_f = \frac{2}{3} \cdot \mu_k \cdot F_n \cdot \frac{(r_o^3 - r_i^3)}{(r_o^2 - r_i^2)} \quad \text{Frictional torque} \quad (4.1c)$$

In which, α is the angular acceleration [$rad s^{-1}$], T_i the input torque [Nm], T_f the torque due to friction [Nm], I the moment of inertia [kgm^2], N_{b_r} the normal force on the reading ring [N], r_{b_r} the radius to the bearing of the reading ring [m], μ_k the coefficient of kinetic friction and r_o and r_i the outer and inner diameter of the reading rings respectively [mm].

The torque due to disk friction (T_f) can be minimised by reducing the normal force on the reading ring (F_n). The normal force accumulation is tried to be avoided by placing the reading rings in a fixed frame and separating them. Thin stationary rings in between the reading rings prevent the reading rings from directly touching each other. With a fixed frame, the only friction component is between the reading ring and the stationary separating ring. The reading rings are made from brass, as will be explained in section 6.2. Two brass surfaces contacting each other have a friction coefficient between 0.108 and 0.147 depending on the load [8]. The friction coefficient is circa 0.04 when a Teflon frame is added between the brass reading rings. Thus, with the same dimensions of the rings and the same normal force, adding a Teflon frame reduces the frictional torque with at least 63%. In Figure A.4 and Figure A.5 from Appendix A, different concepts of frames for the reading rings are shown. A division is made based on the size with respect to the memory rings. Firstly, the frame can be larger than the reading rings, completely encircling the reading rings. As an alternative, the separating rings can also be small and connected on the inside of the reading rings. The first concept results in a more sturdy design, while the latter solution is the most space efficient.

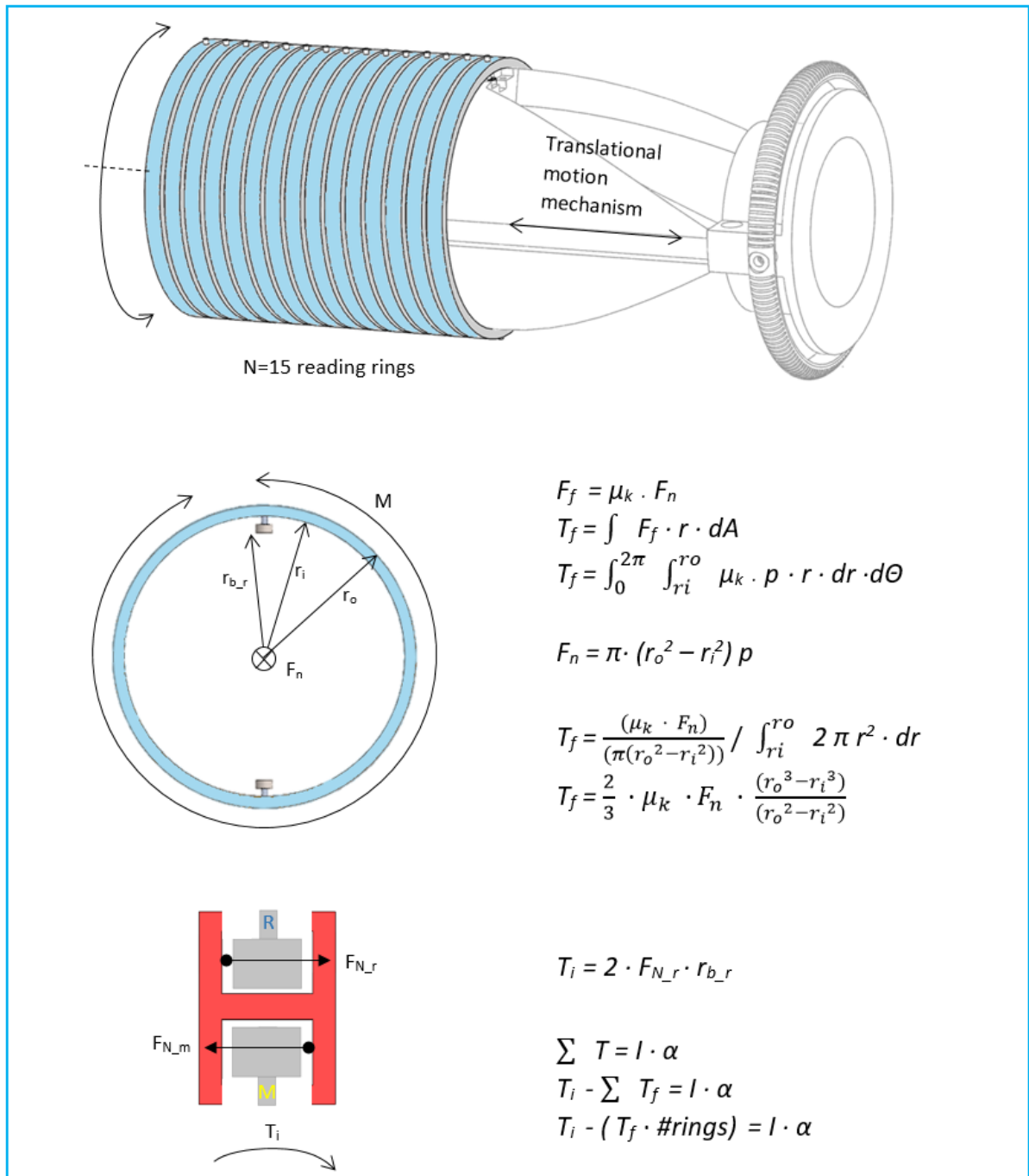


Figure 4.18: Disk friction between the reading rings. When the reading rings touch, the normal force results in a friction component between the rings. A torque (T_f) is exerted on the bodies involved, because the disk friction tends to resist the relative rotation of the bodies. Accumulation of the friction torques happens when multiple rings are in contact $\sum T_f = T_f \cdot \#rings$. The input torque (T_i) has to overcome the friction torque to be able to rotate the reading rings. What must be noted is that the input torque (T_i) does not directly work on the H-beam. The torque input of the memory ring, results in a pushing force on the H-beam provided by the bearing of the memory ring ($F_{N,m}$). Here, assuming the H-beam is stiff enough, the input rotation results in a normal force on the bearing of the reading ring. With two bearings attached to the reading ring, the input torque becomes: $T_i = 2 \cdot F_{N,r} \cdot r_{b,r}$.

Guiding element

As guiding element an H-beam has been chosen, because the horizontal rib of the H-beam can provide some rigidity in the width. The guidance should have two characteristics that conflict with each other. Firstly, it is desired to be flexible to enable the formation of multiple paths. On the other hand, it should also be stiff enough to hold the bearings inside the H-beam to guide them. The H-beam should provide a displacement of the reading rings, rather than plastic deformation of the H-beam or the derailment of the bearings out of the H-beam. The H-beam is deemed to be the most critical part of the assembly. The first challenge is the change in length. The second challenge is the loading of the H-beam.

A curved path requires a longer H-beam than a straight path. Stretching the H-beam is unwanted, as this would reduce the width of the beam and cause tension in the component. Thus, the H-beam should be given spare length, this is shown in Figure 4.19. The calculation is an approach based on geometry. Material properties and loading because of torsion are not taken into account. Also, in this approximation, the curved path is on a flat plane. In the actual design, the H-beam is also twisted. However, the calculation shows that indeed, to avoid stretching of the H-beam or the disconnection of the H-beam from the last memory rings, the H-beam must be given spare length.

$$L_s = N \cdot t_M \quad \text{Length straight beam [mm]} \quad (4.2a)$$

$$L_c \approx N \cdot \sqrt{(r \cdot w_t)^2 + t_M^2} \quad \text{Length curved beam [mm]} \quad (4.2b)$$

$$\frac{L_c}{L_s} \approx (r \cdot w_t)^2 \quad \text{Ratio curved / straight} \quad (4.2c)$$

In which t_M is the width of a memory ring [mm], N is the number of memory rings, r is the steering range (amount of steps as input) and w_t is the teeth size [mm] (width of one step). For a straight path, the length required is the width of the memory rings (t_m) multiplied by the number of rings (N), represented in formula 4.2a. For a curved path, the length is determined with Pythagoras, using the parameters: number of memory rings (N), width of a memory ring (t_m), steering range (r), width of one step (teeth size w_t). In which the steering range is equal to the number of input steps (formula 4.2b) Formula 4.2c shows that the change in length depends on the input given to the memory rings. Steering with the maximal range (amount of teeth), would require a longer H-beam. An H-beam as guiding element is sufficient in this situation: the H-beam is not fixed to the memory rings. The bearings of the reading rings enable the H-beam to translate. This is contrary to for example a U-beam, where the lower web of the U-beam should somehow be connected to the memory rings to form the path.

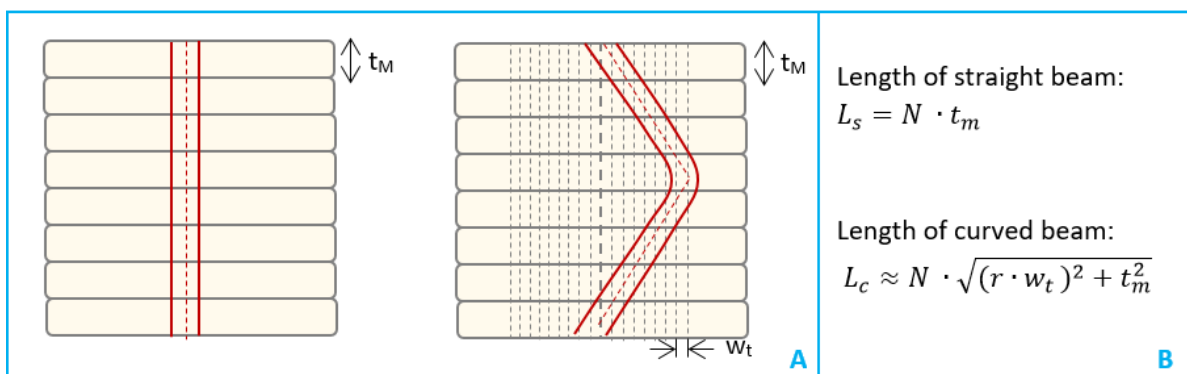


Figure 4.19: Approximation of H-beam change in length based on geometrics. Material properties are not taken into account in this calculation. Figure A shows a straight path and an example of a curved path. Figure B provides the formulas for the length of the beam. For a straight path, the length required is the width of the memory rings (t_m) multiplied by the number of rings (N). For a curved path, the length is determined with Pythagoras using the parameters number of memory rings (N), width of a memory ring (t_m), steering range (r), width of one step (teeth size w_t). In which the steering range is equal to the number of input steps. The steering range is limited to 2 steps to the right or 2 steps to the left.

The main challenge is the loading of the H-beam. The H-beam is subjected to both torsion and shear. The input torque is not along the midline of the H-beam itself, but around the centre of the concentric design. The normal forces provided by the bearings of the memory rings and the reading rings inside the H-beam, cause torsion around its own midline. In Figure 4.18, the image on the bottom, the forces from the bearings on the H-beam are shown. As a result of the input torque, the lower bearings push against the H-beam, and in return the H-beam pushes against the upper bearings. The thin members of the H-beam make the design more flexible, what is desired to form the paths. However, a torsional moment exerted on a thin walled cross section causes twisting and warping, rather than pure shear stresses. Warping is the phenomenon that the H-beam tends to displace axially, but twists because of the axial stresses. In this design, the warping is restricted by the bearing of the adjacent memory ring. Therefore, the warping deflections varies along the length of the H-beam. Thus, non-uniform torsion occurs: the rate of change of the twist angle varies along the length of the H-beam. Uniform torsion can be calculated with formula 4.2a, while non-uniform torsion is in formula 4.2b. The torsion can be approximated by an accumulation of the St. Venant torsion and warping torsion. St. Venant is referred to as pure torsion, which causes the twisting of the beam. The warping torsion is the bending moment in the flange as result of the shear stresses by the restraint of warping. The calculation is shown in Figure 4.20 and the main formulas are shown below [22].

$$T = \frac{\phi \cdot G \cdot J}{L} \quad \text{Uniform torque [Nm]} \quad (4.3a)$$

$$M_z = M_{sv} + M_w \quad \text{Torque with warping [Nm]} \quad (4.3b)$$

$$M_z = (G \cdot J \cdot \frac{d\phi}{dz}) - (E \cdot I_w \cdot \frac{d^3\phi}{dz^3}) \quad \text{Torque with warping [Nm]} \quad (4.3c)$$

In which T is the uniform torque [Nm], the ϕ is the twist angle [rad], G is the shear modulus [Pa], L the length of the beam [m] and J the polar moment of inertia [m⁴]. Non-uniform torsion is an accumulation of the St. Venant torsion (M_{sv}) and warping torsion (M_w) [22]. The E is the Young's modulus [Pa] and I_w is the warping constant. The formulas of the polar moment of inertia and warping constant are shown in Figure 4.20.

The term G times J is the torsional rigidity. The G is determined by the material choice and the J depends on the geometry of the guiding element. A higher value for J means that the H-beam has a higher resistance against torsion. The J should be low, to enable some elastic deformation to form paths. A low value for J can be accomplished by small thicknesses of the (t_x and t_y). A small H-beam with small dimensions b and h , also reduces the resistance against torsion. The stiffness of the guiding element is also influenced by other design parameters. Figure 4.20B shows a side view of the H-beam. Instead of having a solid beam, a segmented beam would increase the flexibility. A larger spacing between the ribs (t_g) relative to the width of the ribs (t_r) increases the flexibility for both torsion and shear. However, there is a trade-off: when the (t_g) is too large, the bearings can move through the flanges of the beam, limiting the guiding function of the H-beam.

The exact behaviour of the H-beam is unpredictable. Not only is the loading of the H-beam variable and non-linear, also the exact material properties are variable (such as the Young's modulus). The H-beam is 3D printed, thus even with the exact same design, the material properties are different per individual H-beam. Also within the same H-beam itself, the material properties can differ at separate locations. Factors like curing time, layer thickness, layer direction and cleanliness of the part all influence the physical properties of the 3D printed part. Also, the parts become stiffer because of oxygen in the air and ambient light. Therefore, the H-beam cures over time and becomes more brittle. Because of the unpredictable behaviour, different H-beams have been 3D printed and tested instead of calculating or modelling the optimal design. The choice of the H-beam has been a continuous process of testing and optimising the design. The H-beam design is further elaborated in section 6.3.

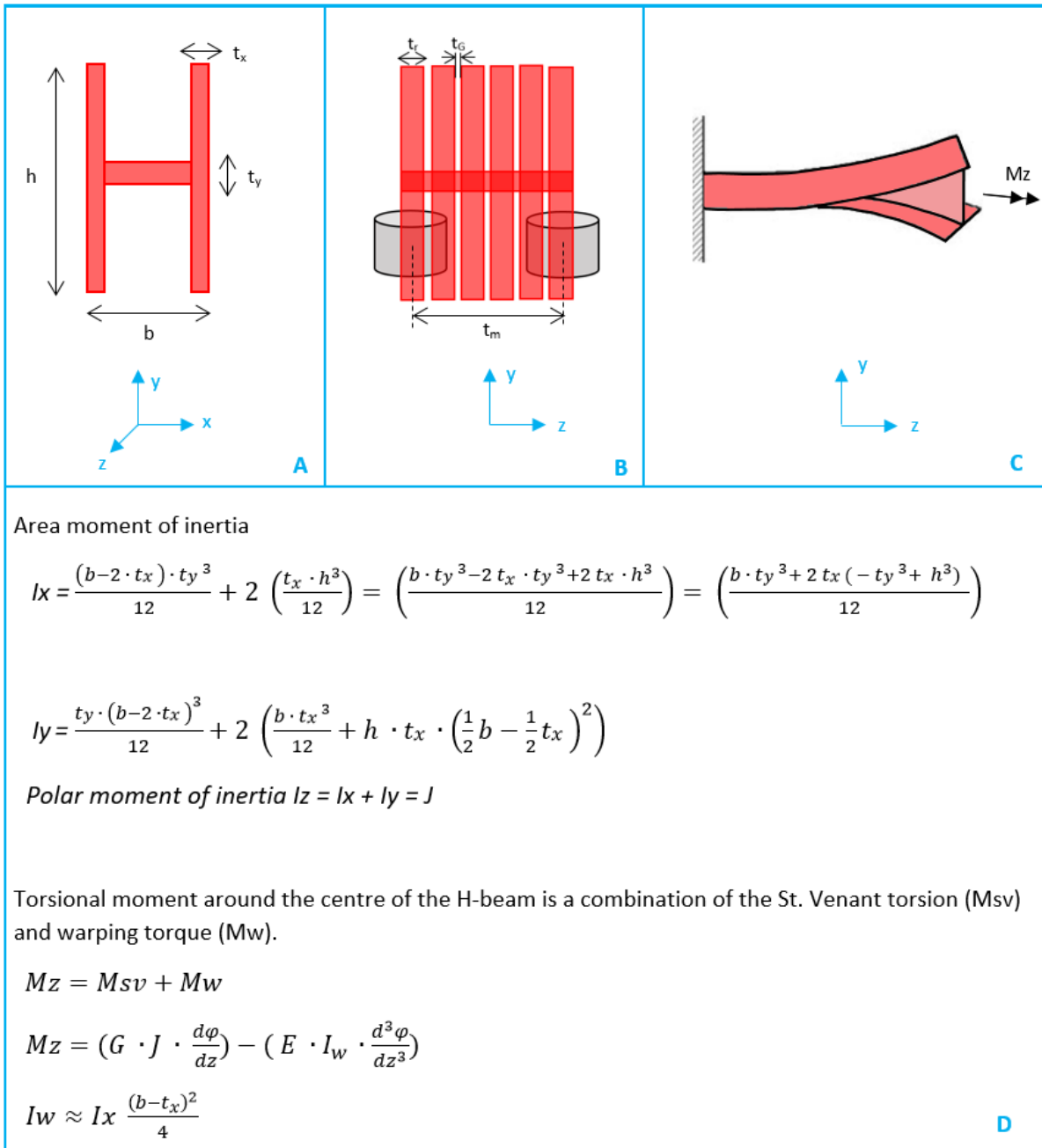


Figure 4.20: Loading of the H-beam. A cross section, the front view, of the H-beam is seen in Figure A. Height (h), width (b) and the thicknesses of the web (t_y) and flanges (t_x) are variable. Figure B is a side view of the H-beam. The bearings of the memory rings are shown in the lower part of the H-beam. The distance between two bearings is exactly the width of one memory ring (t_m). The thickness of the ribs (t_r) and the spacing between the ribs (t_g) are variable. Rotating one memory ring with respect to the adjacent ring, causes torsion and warping of the H-beam. However, the warping is restricted by the bearing of the adjacent ring. Figure C shows a beam restricted to warping, having a variable twist angle along the length of the beam. Therefore, the torsional moment around the centre of the H-beam is a combination of pure torsion and the warping torque. The calculation is shown in figure D.

4.5.2. Overview of the parts

The final design is shown at the beginning of this section in Figure 4.16. An exploded view of the design is provided in Figure 4.21. The prototype can be divided into four subassemblies: the shaft assembly, memory rings with the translational motion assembly, reading rings inside their frame and the casing assembly. The numbering in this subsection corresponds to the numbers in the images of the exploded views. A bill of materials is given in Figure 4.26. Fasteners are not included in the exploded views and the bill of materials.

An exploded view of the shaft assembly is provided in Figure 4.22. The mechanism contains a hollow inner shaft (1), functioning as the centre of the prototype and as fixed world. Two shafts with a teathed profile provide the rotational input and the locking of the memory rings. One shaft, the input shaft (6), is connected to the input knob (7), and therefore moves along with the user's input. The other shaft (5) is fixed against the casing end part (21), the end knob (8) and the inner tube (3). The path implementation is done with 8 memory rings (9), as can be seen in the exploded view in Figure 4.23. The rings have a geared profile on their inner perimeter, making them form fit with the shafts. The memory rings are limited in motion relative to each other. This is done with an adjustable pin on the side of the memory ring and a slot. The pin of one memory ring can move in the slot of the adjacent ring. In this version, the dimensions of the pin make sure that the memory rings can have a maximum relative input of 2 steps to the left or to the right. By changing the pin for a larger or smaller pin, the input range can be adjusted. Figure D.27 in Appendix D, is a picture of a machined memory ring, including the bearings and the pin. The memory rings are translated back and forth by the translational motion mechanism. The translational motion mechanism exists out of two parts (11 and 12), that push and pull the memory rings, but make sure the rings can rotate freely. Two H-beams (14) are fastened on the main part of the translational motion mechanism and are positioned over the bearings of the memory rings (10). The H-beams convert the discrete path input of the memory rings, into a continuous path.

The path output is provided by 15 reading rings (15) that are contained in a frame of Teflon rings (16). This can be seen in the exploded view in Figure 4.24. The reading rings have two bearings (17) on their inside, which are guided by the path formed in the H-beams. The Teflon rings are connected by two pins running through them (18). These pins are fastened inside the casing end part (21). The casing exists out of three parts: the front part (23), middle part (22) and the end part (21). The exploded view of the casing components is shown in Figure 4.25. The front part is positioned next to the input knob and prevents the H-beam from moving out of the assembly. A slot made in the complete perimeter in the front part, forms a slot and pin connection with four pins (24) that are attached to the input knob. Therefore, the input knob and casing are connected, but the input knob is free to rotate. On its sides, the casing front part has two longitudinal slots. Two pins (20), connecting the front part of the translational motion mechanism and the translational motion input knob (19), move in this slot. As a result, the translational motion mechanism is not able to rotate, only translate. The user can push and pull the translational motion knob (19) to slide the memory rings from one shaft to the other shaft. The middle part of the casing surrounds the reading rings. The reading rings are kept in place by the middle part and the end part of the casing. A spring plunger (25) is incorporated in the casing end part, as shown in Figure 4.21.

4.5.3. Dimensioning

The final design has the dimensions 60 x 155 mm (D x L). Two CPMM modules need to be incorporated into the handle of the surgical instrument. Minimising the size of the path programming modules, would reduce the size of the handle of the instrument. The current design of the path-planning module is relatively large. The purpose of this prototype is to show how a path can be planned and to test the follow-the-leader principle. The size is chosen by what is ergonomically nice to hold in the hand. As a result, an outer diameter of six centimetres has been chosen. Given the outer diameter of six centimetres, the dimensioning of the other parts is done consecutively from the outer parts to the inner parts. The construction drawings can be found in Appendix E. The SolidWorks parts are designed without additional spacing between the parts. Thus, in the assembly all the parts, even if they should rotate or translate relative to each other, are precisely fit. The precision technicians implemented the spacing between the parts while manufacturing. The spacing is kept at a minimal value for the most optional performance: no jamming or play.

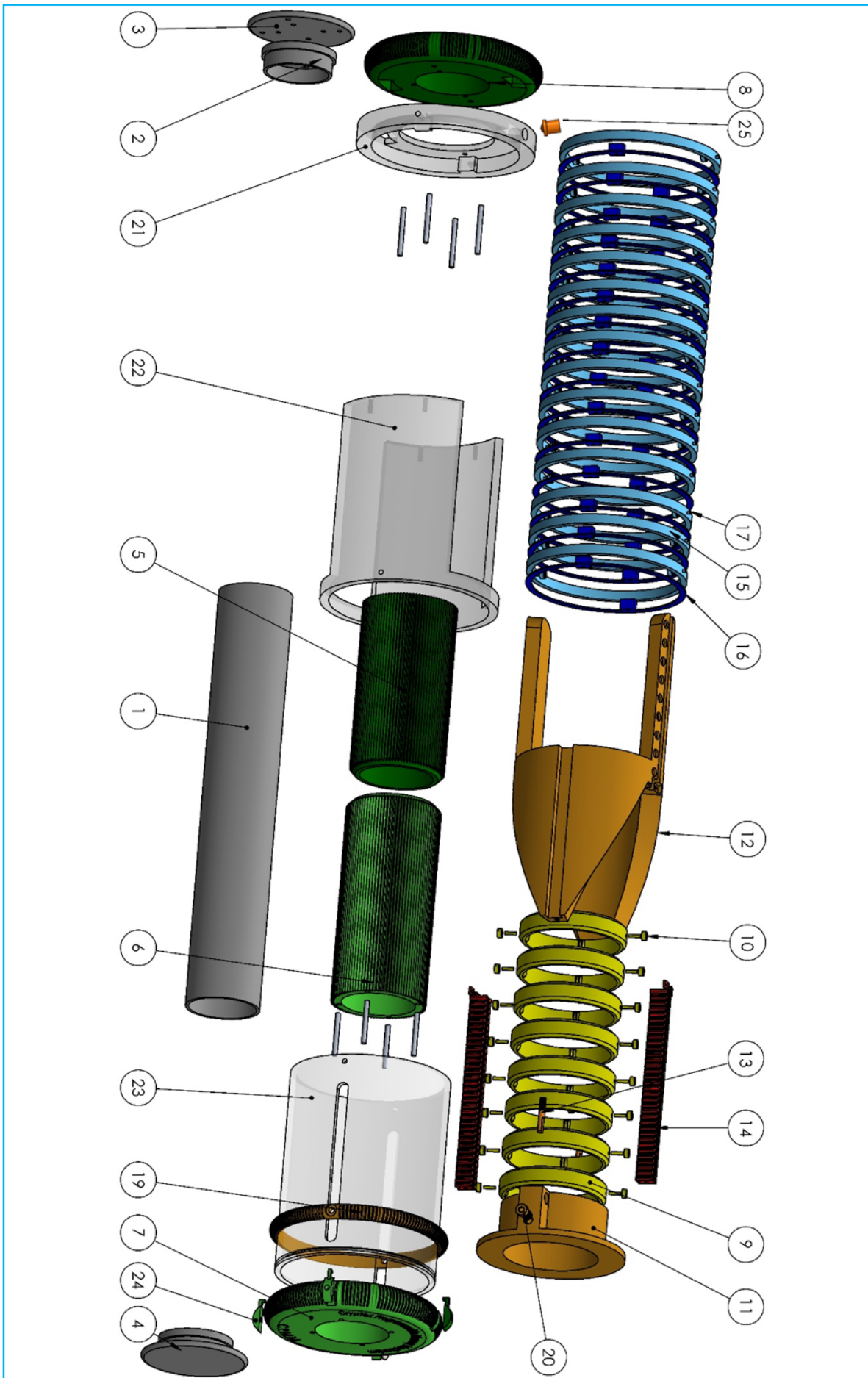


Figure 4.21: Exploded view of the complete design

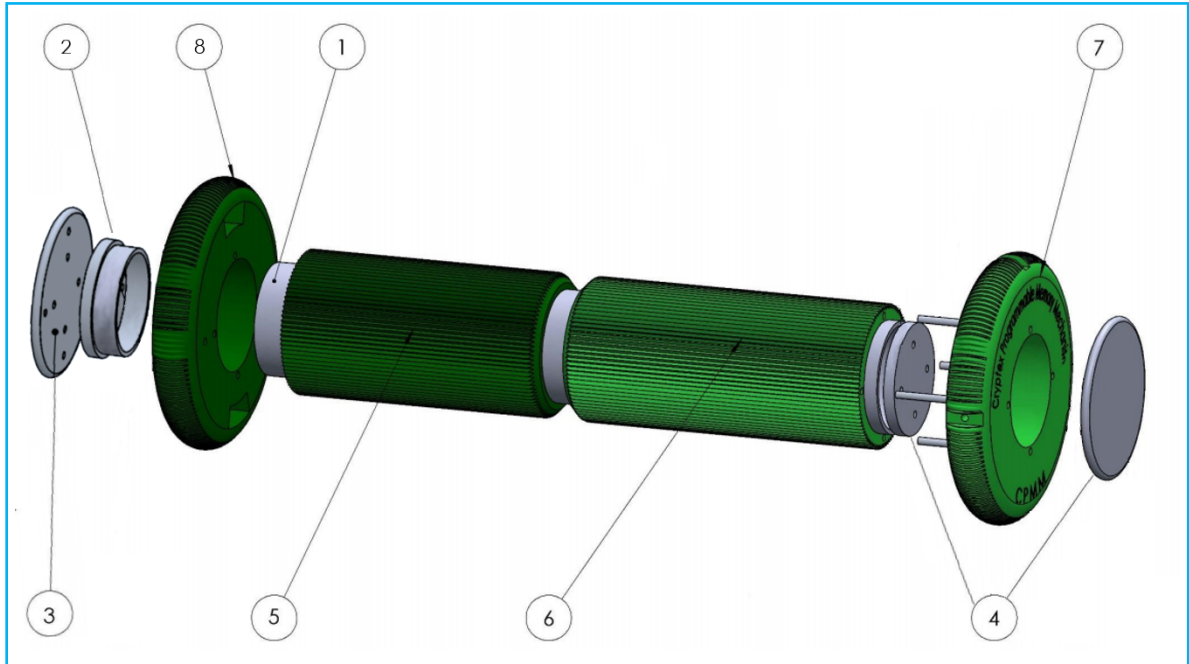


Figure 4.22: Exploded view of the shaft assembly

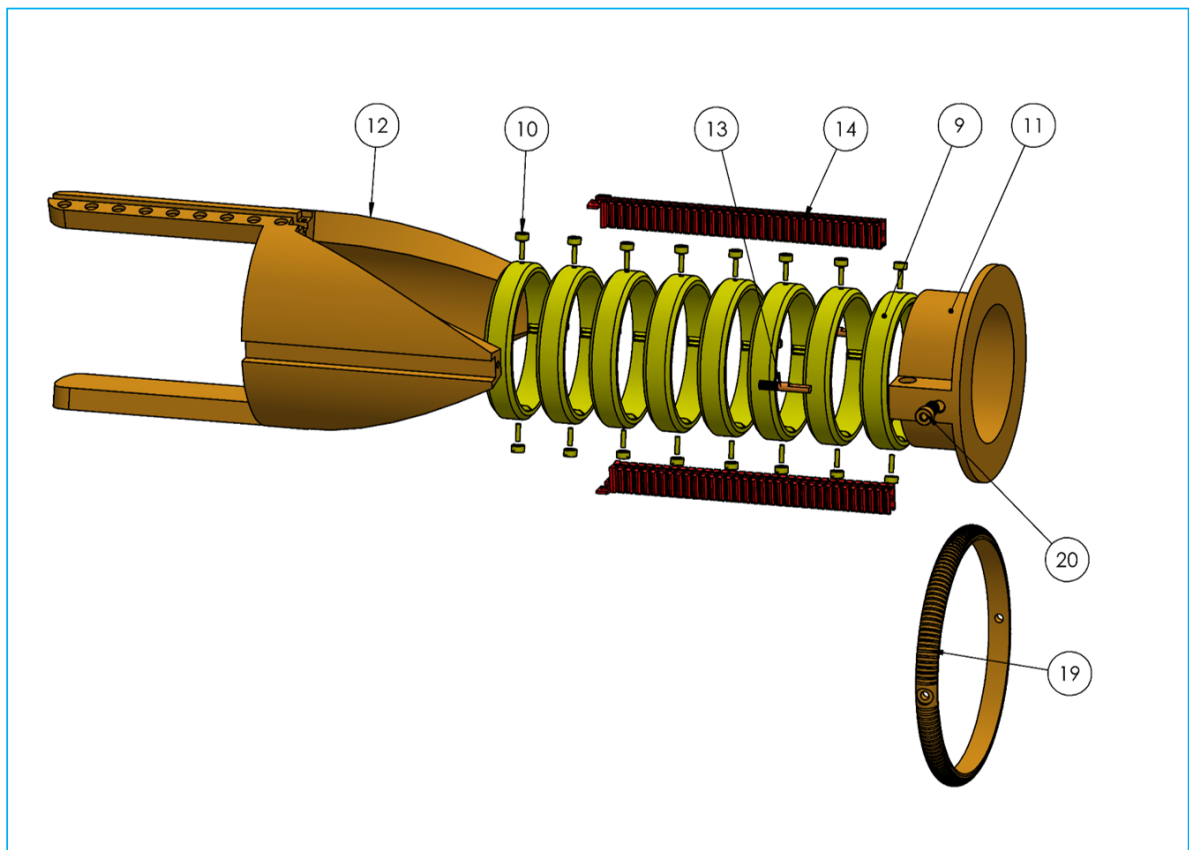


Figure 4.23: Exploded view of the memory rings with the translational motion mechanism

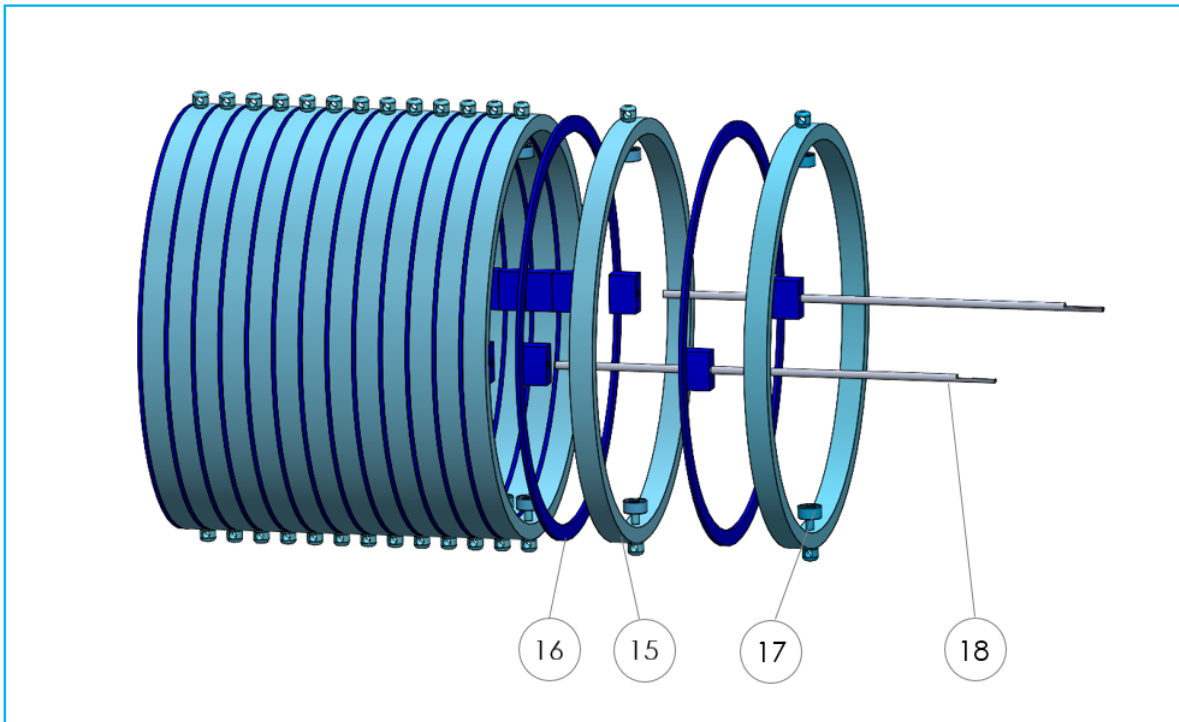


Figure 4.24: Exploded view of the reading rings and the frame

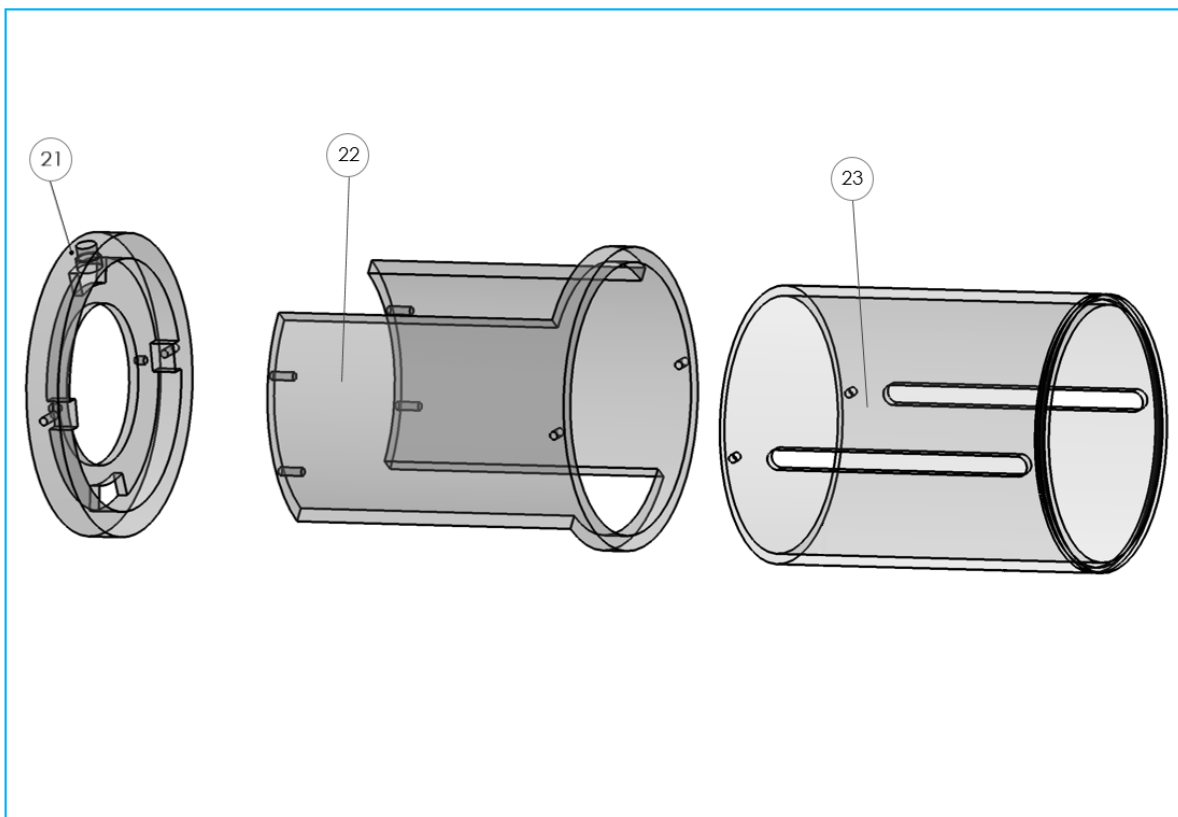


Figure 4.25: Exploded view of the casing components

Number	Component name	Quantity
1	Inner shaft part 1	1
2	Inner shaft part 2	1
3	Inner shaft part 3	1
4	Inner shaft part 4	1
5	Fixed shaft	1
6	Input shaft	1
7	Input knob	1
8	End knob	1
9	Memory ring	8
10	Ball bearing and pin memory ring	16
11	Translational motion front part	1
12	Translational motion main part	1
13	Translational motion connection pin	1
14	H-beam	2
15	Reading ring	15
16	Separator ring	16
17	Ball bearing and pin reading ring	30
18	Frame pin	2
19	Translational motion input knob	1
20	Translational motion knob connector	2
21	Casing end part	1
22	Casing middle part	1
23	Casing front part	1
24	Pin input knob	4
25	Spring plunger	1

Figure 4.26: Bill of materials

5

Integrated functioning: working principle

The complete prototype has two main functions: programmable path input by the user and a path output in the shaft of the surgical instrument. In this section the working mechanism of the CPMM is elaborated, explaining how the path is implemented and formed.

5.1. Path input

The path input exists out of 5 major components: the input shaft, the fixed shaft, the memory rings, the guiding elements and the translational motion part. The memory rings are the steering elements that form the programmable physical track. Both shafts have a gear profile and the memory rings have the counter profile on their inside, making them form fit with the shafts. When the memory rings are located on the input shaft, they rotate along with this shaft. The fixed shaft does not rotate and can be seen as the fixed world together with the casing. This means that when the memory rings are slid on the fixed shaft, their orientation is fixed and memorised. Sliding the memory rings from one shaft to the other shaft is done by an additional part: the translational motion mechanism. This assembly can be seen in Figure 5.1, coloured in orange. The user can control the translational motion with a knob that is attached to the front of the translational motion part. All memory rings are contained inside the translational motion mechanism, pushing the knob will push all memory rings at once. On the forks of the translational motion mechanism are small indents. In combination with a linear spring plunger, these indents contribute to the haptic feedback of the linear motion. The indents are spread over the forks with consistent intervals, having exactly the width of one memory ring. The spring plunger, located in the casing of the complete design, will snap back to its preferred position when it is positioned above an indent. As a result, it provides a small click when one memory ring is slid from one shaft to the other.

The steering elements can be divided into three groups: the past, the present and the future. The present (bright yellow in Figure 5.2) corresponds to the steering element for which the orientation is controlled at that specific moment. It is the leading element that controls the most distal segment of the compliant shaft, the tip of the instrument. The future (light yellow) represents the elements that are yet to be defined. Their orientations still have to be adjusted and implemented. The past (ocher) corresponds to the steering elements that are already rotated in position and implemented: they provide a path output on the compliant shaft. While inputting the path, one memory element shifts from future to future to past. The path input exists out of two steps, that are sequentially repeated, as can be seen in Figure 5.2:

1. **Steering:** by rotating the input knob, which is connected to the input shaft, all the memory rings positioned on the input shaft will rotate along. Therefore, the user provides input for the present memory ring. The future memory rings also rotate along.
2. **Advancing:** when the desired orientation is reached for the present memory ring, it is translated towards the fixed shaft. The input orientation of that memory ring is fixed and memorised. That ring has become part of the past.

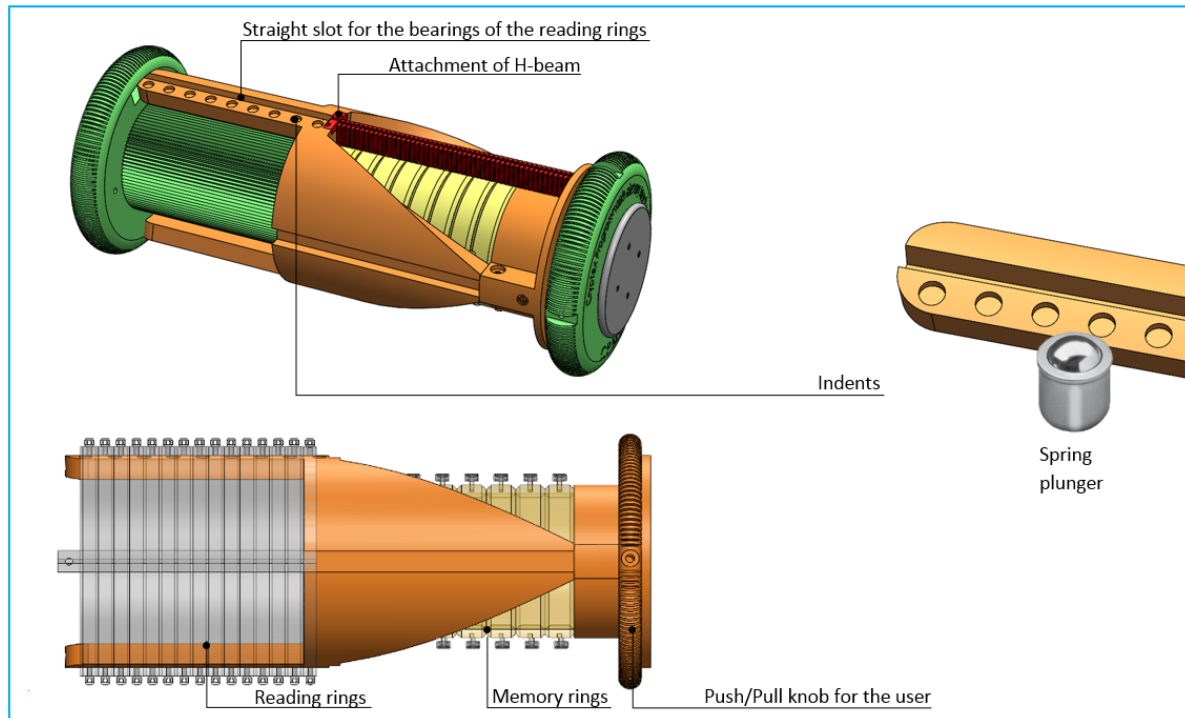


Figure 5.1: Schematic rendering of the translational motion mechanism. Coloured in orange is the additional part that is controlled by the user via an additional input knob. The mechanism is responsible for translating the memory rings from one shaft to the other shaft, shifting them from present to past and the other way around. Indents on this part in combination with a spring plunger, provide the user with haptic feedback while pushing or pulling the memory rings.

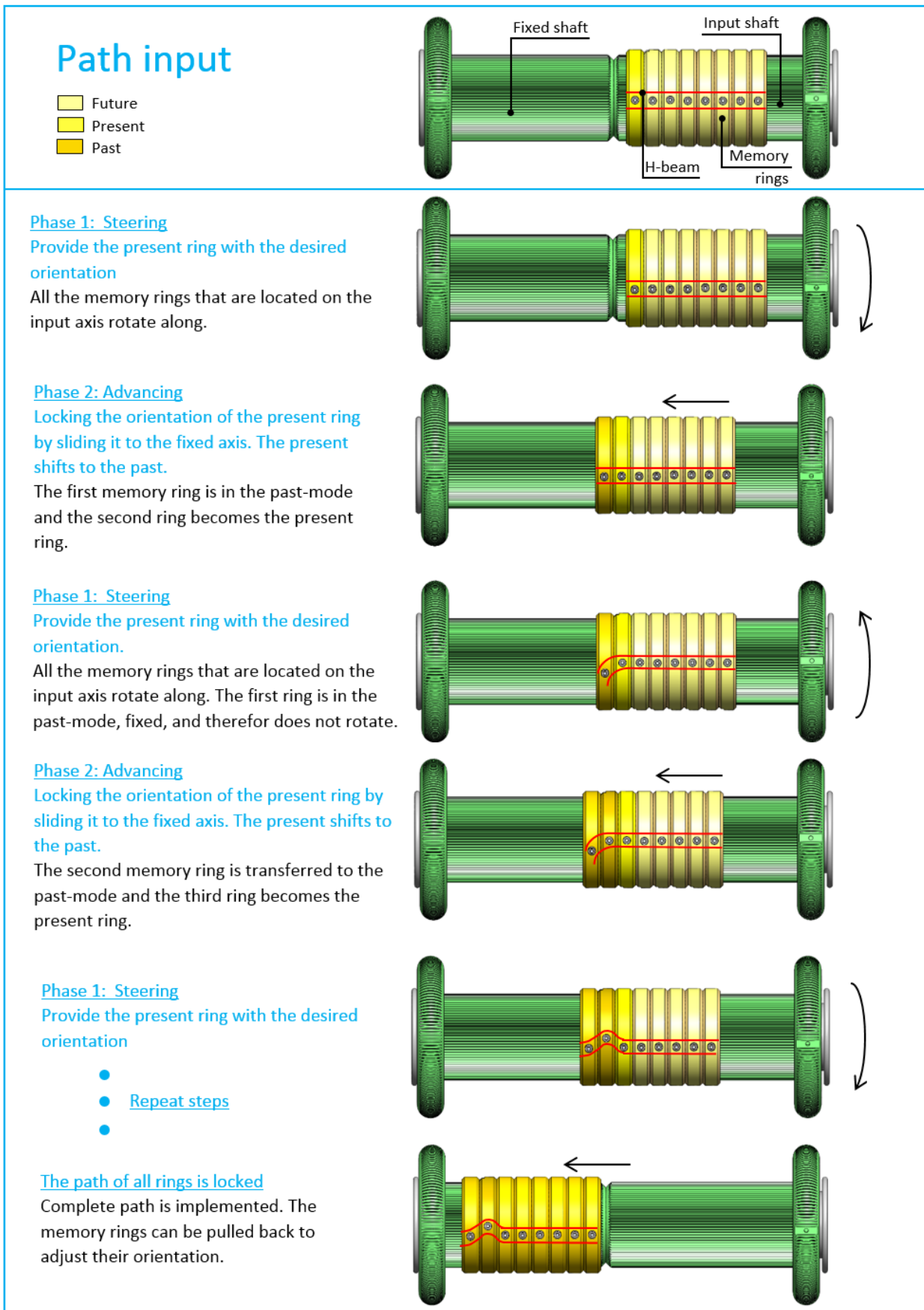
After steering and advancing the first memory ring, the sequence is repeated for the second memory ring, which now has become the present. The input rotation of this ring is a relative rotation to the previous present memory ring. This relative input rotation is limited to a maximum of two step sizes to the right or two step sizes to the left. The two steps of steering and advancing are repeated until all memory rings have the desired orientation and are locked on the fixed shaft. Pulling the translational motion mechanism back to the input shaft, will slide the memory ring from past to present. The user can change the orientation of that memory ring, enabling the user to adjust the shape the instrument's shaft makes. The future rings always rotate along with this adjustment of the present ring.

The path is formed in discrete steps, with as step size the size of one tooth of the inside profile of the memory ring. Attached on the opposite sides on the outer surface of a memory ring are two bearings. These bearings transmit the path to the guiding element and are able to translate inside the guiding element. Because the guiding element is H-shaped, the bearings are kept inside the two lower vertical ribs of the H. The compliant H-beam forms a continuous path from the discontinuous path input. It makes the path more smooth, and consequently the bearings of the reading rings are more easily guided, forming the path output on the compliant shaft of the surgical instrument. The positioning of the H-beam can be seen in Figure 5.3.

5.2. Path output

The main components contributing to the path output are the guiding elements, the reading rings and the cables. The reading rings contain two bearings on their inside separated with 180 degrees. The normal forces on these bearings cause the reading rings to rotate.

The reading rings are located around the fixed shaft. The casing of the reading rings is fixed to the outer casing of the complete prototype; therefore, the reading rings cannot translate but only rotate. Initially, the bearings are kept in a straight path, because of the design of the translational motion mechanism. The mechanism includes two long extruded forks with a straight slot. The slots form a rail for the bear-



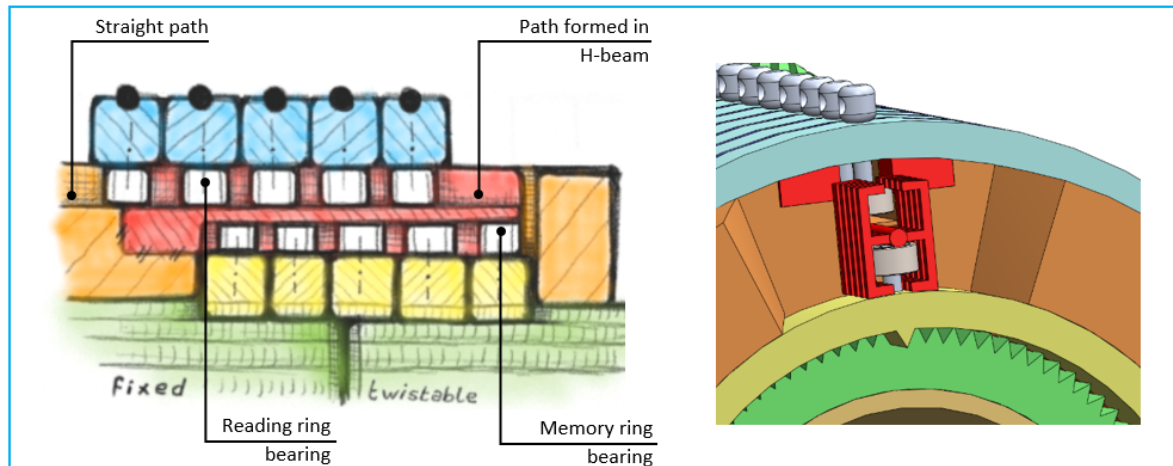


Figure 5.3: H-beam containing the bearings of the memory rings and the reading rings. The H-beam forms the path made by the memory rings and transmits this path to the reading rings.

ings. This can be seen in Figure 5.1, coloured in orange. When the bearings are located in this slot, they are kept in a straight line. This ensures that the shaft of the instrument is initially straight and rigid. After the first memory ring is steered to the position of the user's choice and advanced by pushing the translational motion mechanism, the bearings of the first reading rings are guided by the first part of the path formed in the H-beam. The two vertical ribs of the upper part of the H-beam enclose the bearings of the memory rings. The H-beam guides the bearings of the reading rings, forcing the rings to rotate. Figure 5.3 shows how the H-beam transfers the path formed by the memory rings to the reading rings.

The amount of reading rings is not equal to the amount of memory rings in this design. More reading rings means that more shaft segments can be controlled and that the inputted path is smoothed out over the segments. In this design, there are 8 memory rings and 15 reading rings. So advancing one memory ring to the fixed shaft provides a rotation in almost two reading rings. As can be seen in Figure 5.4, the second advancing image, advancing the second memory ring towards the fixed shaft means that the H-beam is inserted further into the reading ring assembly. Now, the third and fourth reading ring form the path from the first memory ring and the first and second reading ring form the path of the second memory ring. In other words, the path shifts distally over the reading rings. This output mechanism can be seen in Figure 5.4. Translating a memory ring from the present-mode to the past-mode immediately provides an output.

Attached to the reading rings are the antagonist cables. This is shown in Figure 5.5A. The bearings of the reading rings not only provide the rotation of the rings, their pins also function as control points. The control points are the attachment points of the antagonist cables. Rather than having one control point that is the attachment point of both antagonist cables, the CPMM has two control points separated with a 180 degrees angle. Each control point holds one of the antagonist cables. When the reading rings are rotated, one cable is pulled and the other cable is given more space: providing the angular displacement of a segment of the shaft of the instrument. This cable-driven actuation is elaborated in the next subsection (5.3) and shown in Figures 5.5B and 5.5C. For example, looking at Figure 5.5A, rotating the first reading ring counterclockwise makes sure that the lower control point moves away (thus, C1 is pulled), while the upper control point moves towards us with the same distance (thus, C2 is released). Each reading ring provides the control of one segment of the compliant shaft of the surgical instrument. In the configuration shown in Figure 5.4 and Figure 5.5A, the memory rings slide from the right to the left to input the path. Meaning, the most right reading ring is steered first. This reading ring is the control point of the leader element of the shaft. The other reading rings provide the motion of the follower segments.

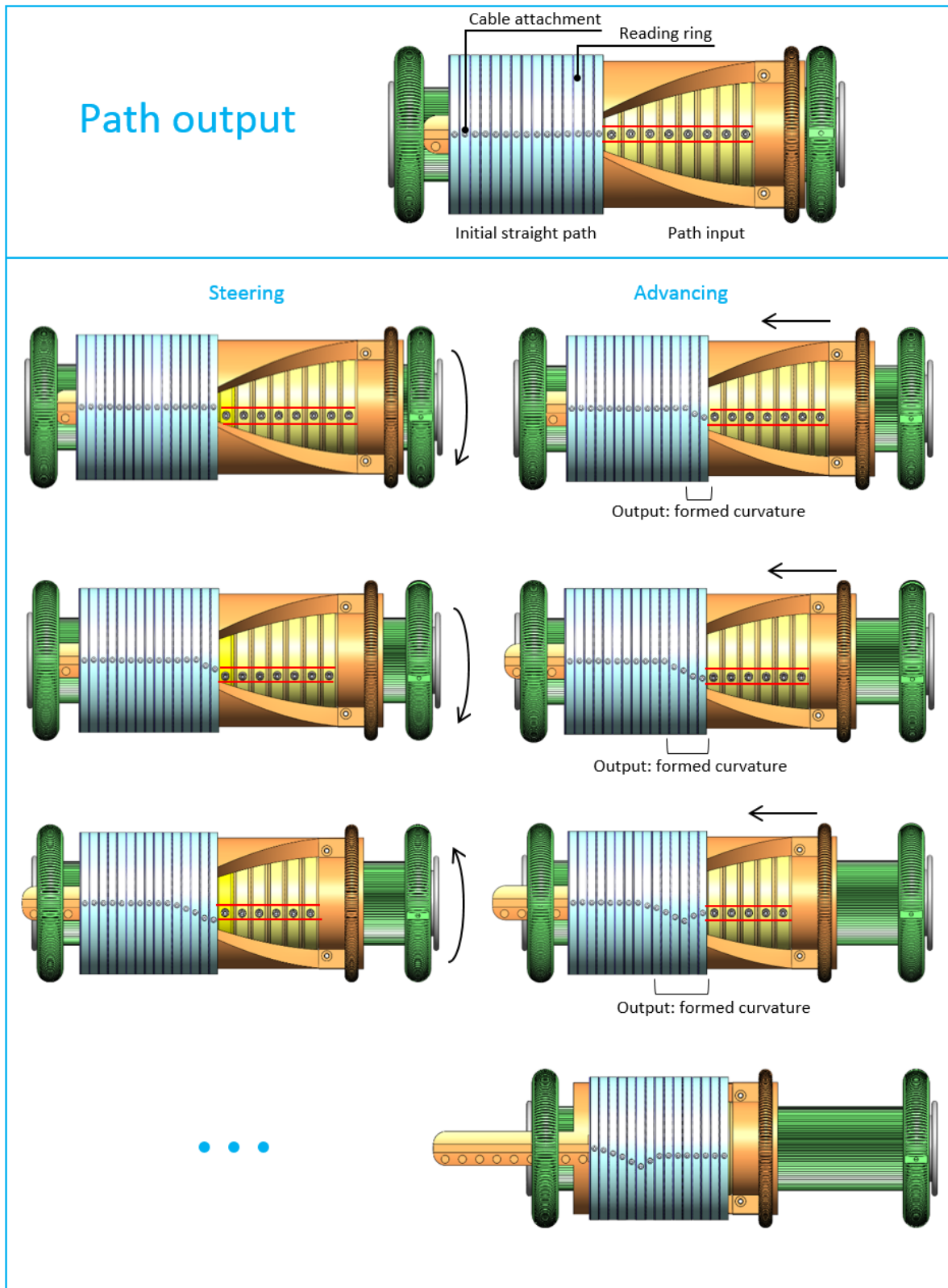


Figure 5.4: Working principle of creating a path output. Initially, the bearings of the reading rings are kept in a straight path by the translational motion mechanism. After steering and advancing the memory rings, the bearings of the reading rings are guided by the H-beam that forms the path of the memory rings.

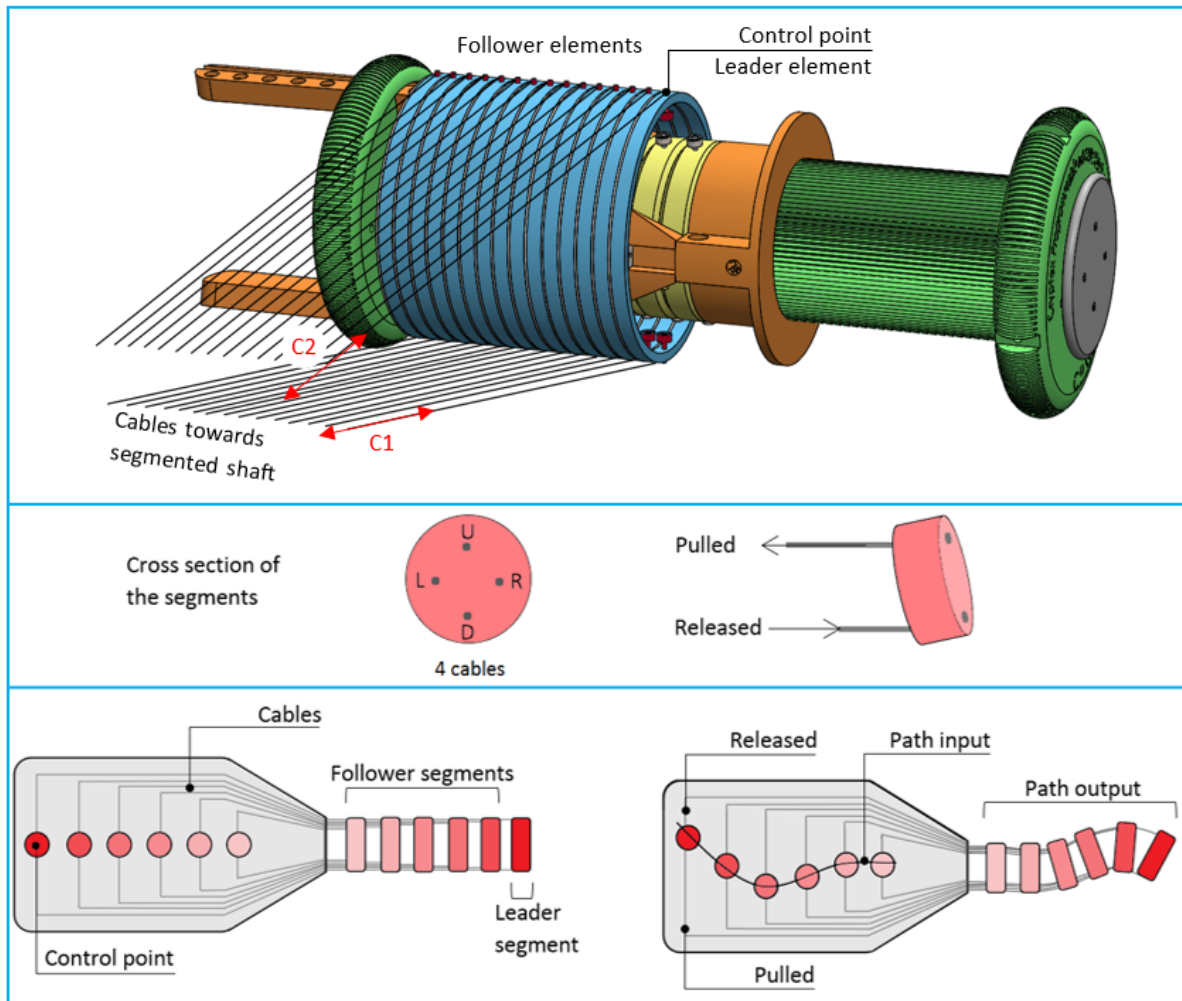


Figure 5.5: Working principle of the reading rings and antagonist cables. Figure A shows how the cables are attached to the reading rings. The guiding mechanism is not included in this drawing. Each reading ring steers two antagonist cables. Figure B shows how the cables provide the movement of the shaft segments. The upper (U) and lower (D) cable provide the motion in the vertical direction and the left (L) and right (R) cable provide the rotation of that segment in the horizontal direction. By pulling one cable and releasing its antagonist cable, the segment rotates in the pulling direction. Figure C is a schematic drawing how the displacement of a control point provides the pulling and release of cables. In the actual prototype, as shown in Figure A, the antagonist cables each have their own control point. The control points are connected to the reading rings. So, a rotation of the reading ring provides an equal displacement of both control points. One control point moves away (pulling the cable), while the other control point moves forward (releasing the cable).

In the next section, the relation between the user input and the output of the instrument is elaborated. Thus, what happens with the shaft of the surgical instrument (output) by rotating the memory rings (input).

5.3. User input and the instrument's shaft output relations

As described in the state of the art and the functional requirements, attached to the mechanical path planning mechanism is a 3D printed flexible shaft. The compliant shaft should allow forming paths with different curves, and therefore it is made out of multiple segments that are serially connected [20]. As can be seen in Figure 5.6A, each segment of the shaft is actuated by two sets of antagonist cables. One set of cables, U and D, provide the up and down movement of the instrument segments. The other set of cables, L and R, provide the left and right deflection of the shaft segments. The calculation in Figure 5.6B shows that the absolute change in cable length is equal for the left and right cable. This is the same for the upper and lower cable. Shortening the cable length of the left cable (L) by pulling the left cable, and elongating the right cable (R) with the same magnitude, provides a rotation of that specific segment towards the left side. One set of antagonist cables are attached to the reading ring of a single CPMM module. The rotation of the reading rings causes the change cable length, providing pull forces on the segments of the compliant shaft. Ultimately producing the angular displacement of the segments, resulting in a curved path. As one mechanical path planning mechanism provides the motion on a single plane, two path planning mechanisms are implemented to provide a three-dimensional motion of the shaft and tool attached.

The CPMM is designed with $N = 15$ output rings: the reading rings. Meaning, a shaft with 15 segments can be actuated with this design. Implementing two Cryptex mechanisms into the tool, results in 30 sets ($N = 60$) of antagonist cables running through the compliant shaft. As described in the design requirements, all cables are attached 3 mm away from the centreline of the shaft: $r_c = 3$ mm. To do so, the four cables that are fixed on a segment are twisted around its centreline over 6 degrees, compared to the previous segment to prevent the cables from overlapping and interfering. The memory rings of the mechanism function as input rings. The rotation of the memory rings is transmitted by the H-beam to the reading rings. The reading rings contain the attachment points of the cables, and thus directly provide the deflection of the shaft. Therefore, their rotation functions as the output of the complete mechanism. With a concentric design like this, the input is magnified. The rotation of the memory rings cause a greater rotation of the reading rings: they have the same angular displacement, but the reading rings have a greater radius. Given the position of the cables in the compliant shaft and the dimensions of the CPMM, the input-output ratios can be determined. Figure 5.6 provides the information that the angular displacement of the segment (α) depends on the change in cable length (ΔL) and the location of the cable with respect to the midline of the segment (r_c). Figure 5.7 shows the calculation of how that change in cable length can be introduced by rotating the input shaft. The change in cable length, ΔL , is the same as the arc length displacement of the reading ring, S_R . This is provided by an angular displacement of the memory ring, β , which is the same for the reading ring. The displacement in arc length depends on the radius, thus a ratio exist between the memory ring and reading ring. The input of one step in the memory rings, will create a larger output on the reading rings. Table 5.1 is generated by a MATLAB script including the formulas from Figure 5.7. The table shows the angle of the shaft segment (output) with the corresponding change in cable length and angular rotation of the rings (input). As can be seen in the table, a small angular displacement of the output rings (β), and thus a small change in cable length, provides a relative large change in the angular displacement of the shaft segment.

What must be noted is that this is only the case if the H-beam is stiff and does not deflect as result of the normal forces produced by the bearings of the reading rings. However, since the H-beam needs to be compliant to be able to form the implemented path, it is expected that the input-output ratio is closer to one.

$$r_c = 3mm \quad \text{Distance between cables and midline of the shaft} \quad (5.1a)$$

$$r_M = 18mm \quad \text{Outer radius of the memory ring (input)} \quad (5.1b)$$

$$r_R = 27mm \quad \text{Outer radius of the reading ring (output)} \quad (5.1c)$$

$$r_T = 15mm \quad \text{Location of the teeth (stepwise input)} \quad (5.1d)$$

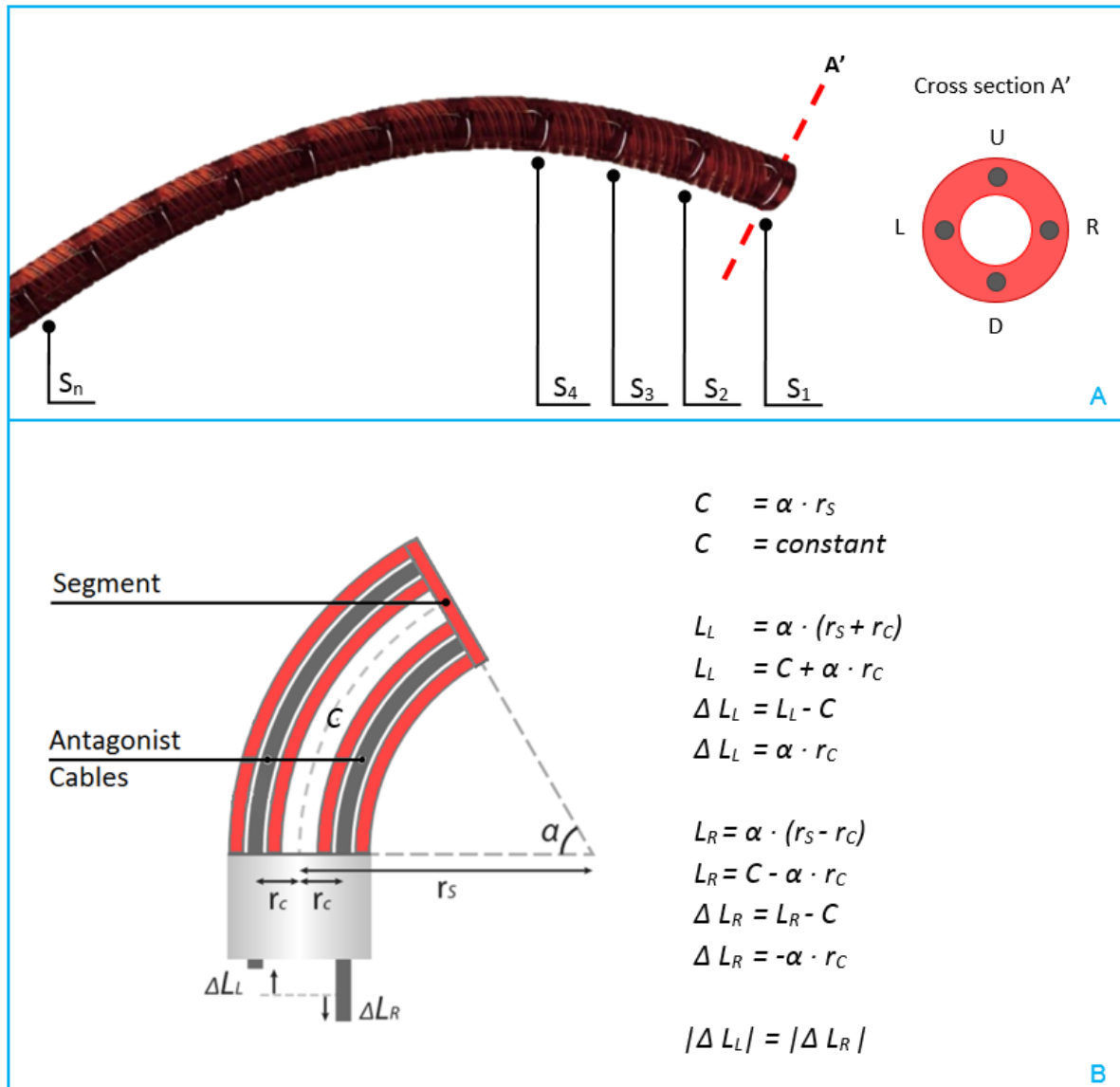


Figure 5.6: Shaft design with multiple segments that are steerable with four-cable control. Figure A includes a picture of the 3D printed shaft and a schematic cross-sectional view of the shaft. The silver lines on the shaft are the cables attached to that specific shaft element (S_n). A schematic view of cross section A' is shown in Figure A on the right, containing the two sets of antagonist cables: the left cable (L) and the right cable (R) form one set and the upper cable (U) and lower cable (D) form the other set. Figure B provides the calculation of the change in cable length. The drawing is a cross section of the shaft along its length. The cables coloured in grey are the left and right cables. The calculation concludes that the absolute change in cable length is equal for the left and right cable.

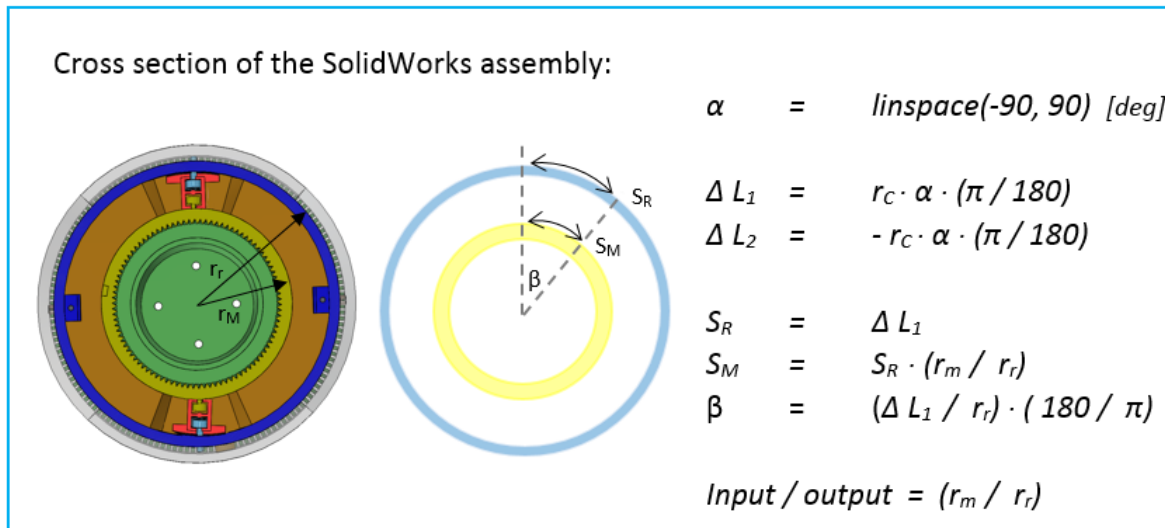


Figure 5.7: Cross section of the total assembly in SolidWorks, showing the multiple concentric layers. From the inner to the outer layer: green is the shaft, yellow is the memory ring (= input ring), orange is the translational motion mechanism, red is the guiding H-beam and blue is the reading ring (= output ring). The calculation shows that if one segment should be able to make angles in the range named α [deg], the change in cable length is dependent on the α and the location of the cable with respect to the midline of the shaft, r_C , which is the same as the arc length displacement of the reading (S_R) as the cables are attached to the reading rings. With a concentric design, the angular displacement (β) for the reading ring is the same for the memory ring, however the arc length displacement is dependent on the radii of the rings (r_R and r_M).

Table 5.1: Angle made by the shaft segment (output) with the corresponding angular displacement of the input rings (input)

Angle made by shaft segment α [deg]	Change in cable length [mm]	Angular displacement of the rings β [deg]
-90	-4.71	-10
-80	-4.19	-8.89
-70	-3.67	-7.78
-60	-3.14	-6.67
-50	-2.62	-5.56
-40	-2.09	-4.44
-30	-1.57	-3.33
-20	-1.05	-2.22
-10	-0.52	-1.11
0	0	0
10	0.52	1.11
20	1.05	2.22
30	1.57	3.33
40	2.09	4.44
50	2.62	5.56
60	3.14	6.67
70	3.67	7.78
80	4.19	8.89
90	4.71	10

Table 5.2: Angle made by the shaft segment (output) with the corresponding stepwise input (input)

Step input number of steps	Change in cable length [mm]	Angular displacement of the segment α [deg]
1	1.6909	32.293
2	3.3818	64.587
3	5.0726	96.880
4	6.7635	129.17

Another way to represent the input-output relations is shown in Table 5.2. In this table, the output as a result of one input step is shown. An input rotation of one step provides an output in the shaft of 32.3 degrees. Two steps to the left or right already provide a 64.6 degrees angular displacement of the shaft segment. Also here, it must be noted that this is only the case when the H-beam is stiff and the input-output ratio is solely determined by the radii of the memory ring (inner radius) and reading ring (outer radius). If the input-output ratio is one, the rotation of the segment is mostly dependent on the location of the cables in the segmented shaft. In that case, one step provides an output of 20 degrees, similar to the MemoBox. The MATLAB scripts resulting in Table 5.1 and Table 5.2, is given in Appendix F.

Rotating each memory ring with the maximum rotation to one side, would cause the shaft to form its maximum single curvature in one direction. This requires a total absolute displacement of 16 steps, namely the maximum steering range in one direction (2) times the amount of memory rings (8). Assuming the numbers in Table 5.2 are correct, one single input step causes an angular displacement of 32.3 degrees. Sixteen steps would provide a single curvature in the complete shaft of circa 516.8 degrees. Meaning, that for a single curvature, the shaft has a range between -516.8 and 516.8 degrees.

The maximum relative rotation of a memory ring with respect to the adjacent memory ring is set to be two teeth to the left or right. This limitation is done with a slot and a pin, as described in the section Mechanism Design. Comparable with the MemoBox, the limitation in relative rotation is done to avoid creating irregular paths. Now, the steering range of the prototype is equal to five steering positions: one in the middle, two to the right and two to the left. The CPMM prototype can create many different paths, namely 390625 paths. The number of different paths is calculated using the number of memory rings and the steering range:

$$\#Paths = sr^N \quad \text{Number of paths the tool can make} \quad (5.2a)$$

$$sr = 5 \quad \text{Steering range} \quad (5.2b)$$

$$N = 8 \quad \text{Number of memory rings} \quad (5.2c)$$

The design and its input limits are adjustable: changing the limiting-pin for a smaller pin provides the memory rings with a larger input range. A more difficult and time consuming approach is to make the slot in the memory rings longer by milling. This will also provide a larger range to the input. The pin can also be replaced by a larger pin. By doing so, the input can be limited to only one step to the left or right with respect to the adjacent memory ring.

5.4. Ergonomics

Figure 5.8, on the next page, shows the ergonomics of one CPMM module. The CPMM prototype can be controlled by holding it in one hand and steering the input knobs with the other hand. The user only has two actions, controlling two individual input knobs. The first input knob is rotated by the user to provide the rotation of the memory rings. The second input knob is translated by the user, to translate the memory rings forwards and backwards. The ratio of the hand-size and prototype-size in the images in Figure 5.8 are true to the actual proportions.

An alternative solution is shown in Appendix B Figure B.1. This would require a small adaptation to the prototype. In that concept, instead of attaching a translational motion knob to the front of the translational motion mechanism, a knob is attached to the "forks" of the translational motion part. Consequently, rather than pushing the rings towards the reading rings, the user pulls them. For the current prototype, the design of Figure 5.8 is chosen, with the advantage of having one hand supporting the prototype, and steering with the other hand.

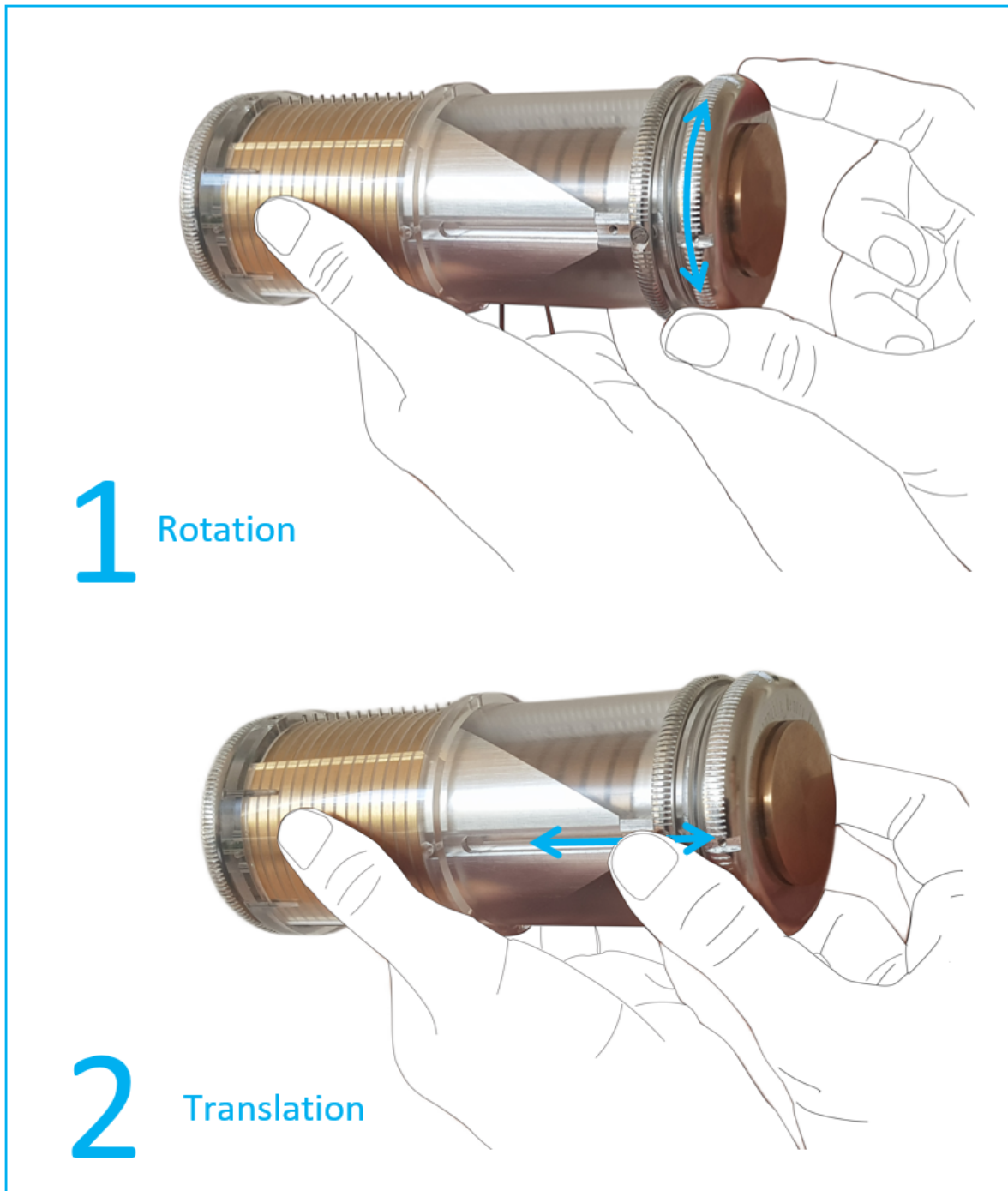


Figure 5.8: Ergonomics of the prototype. The user has two actions, using two input knobs. With one hand, the prototype is held. With the other hand the user rotates the first input knob, to provide the rotation of the memory rings. The second input knob is translated by the user, to translate the memory rings forwards and backwards. The ratio of the hand-size and prototype-size in the images is true to the actual proportions.

Proof of concept: Machined prototype

6.1. Introduction

The prototype is developed at DEMO with subtractive manufacturing methods by precision technicians D. Jager and R. van Starckenburg. During the design process, both technicians were consulted about the design concepts with the aim to improve the ease of manufacturing. Figure 6.1 shows the CPMM prototype, and in Appendix D, pictures of subassemblies are shown.



Figure 6.1: Pictures of the machined prototype. The upper picture is the complete prototype. The picture in the left corner shows the 8 memory rings, contained within the translational motion mechanism. In the bottom right, the output is shown: the reading rings and Teflon frame are contained in a perspex casing.

Table 6.1: Overview of the parts, the materials and manufacturing methods used for the prototype.

Part	Material	Manufacturing method
Inner shaft	Brass	Turning
Inner shaft end-parts	Brass	Turning, milling
Input shaft	Aluminium	Turning, milling
Input knob	Aluminium	Turning, milling
Fixed shaft	Aluminium	Turning, milling
End knob	Aluminium	Turning, milling
Memory rings	Brass	Turning, EDM
H-beam	Durable resin	Stereolithography
Translational motion main part	Aluminium	Turning, milling, EDM
Translational motion front part	Aluminium	Milling
Translational motion knob	Aluminium	Turning, milling
Reading rings	Brass	Turning
Reading ring frame	Teflon	Milling
Casing	Perspex	Turning, milling

6.2. Materials

The choice of materials is based on limiting the friction between moving parts and enhancing the ease of machinability. Therefore, materials with a low friction coefficient were chosen, which are also easy to manipulate by milling, turning and other machining methods. The majority of the parts are made from brass or aluminium. Brass is an alloy of copper and zinc. The alloy is a low-friction, non-ferrous metal [3]. Brass is easy to machine due to its high stability and relatively low strength, compared to metals such as steel. Other advantageous properties of brass are high heat conduction and resistance to corrosion. Brass is often used in small gears and bearings, because of the low-friction properties. Aluminium also has many beneficial properties, including being lightweight, non-magnetic, non-corrosive and a good heat conductor. Consequently, aluminium is used widely for a lot of applications. The metal is relatively easily machined and cast. In this prototype, the materials brass and aluminium are applied in an alternating manner. For example, the inner shaft is made from brass; the input shaft should be able to rotate around the inner shaft, thus is made from aluminium. On the input shaft and the fixed shaft, the memory rings should be able to translate with minimal friction. Because both shafts are made from aluminium, the memory rings are made from brass. The memory rings are translated by the translational motion parts, but should be able to rotate with minimal friction inside those parts. Consequently, the translational motion mechanism is made from aluminium. At last, the reading rings are made from brass, because the translational motion parts translate inside the reading rings. For several parts a polymer is used as material, instead of metal. The frame in between the reading rings is made from Teflon. As described previously in Section 4.5.1, Teflon has a very low friction coefficient. Adding a Teflon frame is done with the purpose to limit the friction between the reading rings when they rotate. The H-beams are 3D printed by stereolithography, as they require to be flexible to form paths without plastic deformation. Two resins were used and tested: the R5 liquid polymer (EnvisionTEC) and Durable resin (Formlabs). The types of 3D printers are elaborated in section 7.3. At last, the outer casing is made from perspex. A transparent design is desired, so the user can see what kind of path is being made and implemented. The list of the parts, the material of choice and the machining method is provided in Table 6.1. The manufacturing methods mostly included turning and milling. Some components were also manipulated by electrical discharge machining (EDM).

6.3. Testing the key component: H-beam

The H-beam is the key component of the design. For this prototype, the design of the H-beam was deemed to be sufficient if it is able to make straight and curved paths, such as diagonal and S-shaped paths. The design of the H-beam was an iterative process, in which multiple H-beams were tested, optimised and tested again. As described above, all H-beams were manufactured with stereolithography (SLA). Two stereolithography printers were available during this project: Formlabs Form 3 (Formlabs, Somerville, MA, United States of America) and EnvisionTEC Perfactory 4 Mini XL (EnvisionTEC, Gladbeck, Germany). The 3D printers are further elaborated in section 7.3.

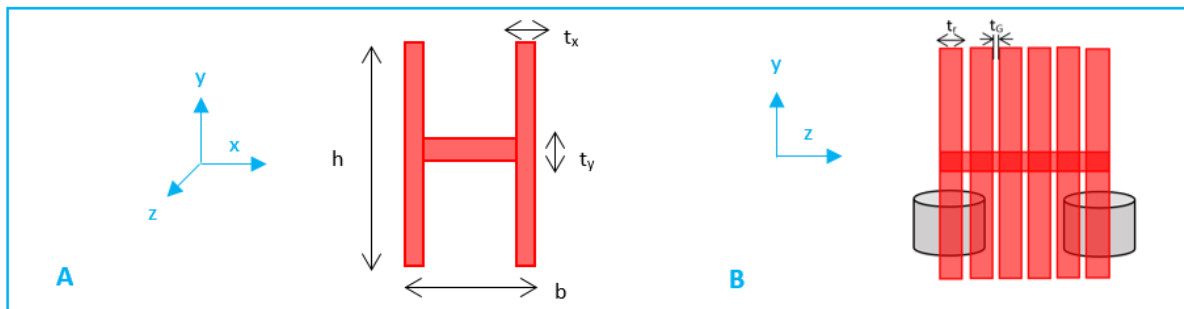


Figure 6.2: The dimension variables of the H-beam. h is the height, b the base and therefore width. Thicknesses of the web and flanges are indicated with t_y and t_x respectively. A side view is given in Figure B. The H-beam can be made solid or segmented. If it is a solid beam, the length of a rib t_r is the same as the complete length of the beam and the gap size is equal to zero. If it is segmented, the width of a rib (t_r) and the gap size (t_g) are variable.

6.3.1. Testing different H-beams

In this subsection, the dimensions and their symbols refer to the dimensions indicated in Figure 6.2. The h is the height of the H-beam and b the base, width. The thicknesses of the web and flanges are indicated with t_y and t_x respectively. In a segmented design, the width of a rib is described by t_r and the gap size by t_g .

To gain knowledge about the influence of the geometry on the stiffness of the H-beam, the first H-beams were printed as one solid beam with different widths and thicknesses for the web and flanges. Thus, the t_g was set to zero in these designs. The width without flanges ($b-2t_x$) varied between 1, 2 and 3 mm. Three different thicknesses of the web (t_y) and flanges (t_x) were applied to the designs: 0.5, 0.75 and 1 mm. Thus, in total 9 beams were printed. All H-beams were given a five millimetres height (h). In this first test, the beams were printed with the R5 material on the EnvisionTEC. The designs were evaluated on their flexibility by bending and twisting them manually. The characteristics of the H-beams and the corresponding test results are shown in Table C.1 in Appendix C and are represented by H1A - H1I. The H-beams with a low t_x and t_y were the most flexible. They were able to twist around the z -axis and to bend around the y -axis. An increasing width (b), reduced the ability of the H-beam to bend around the x -axis and y -axis. This is consistent with the findings in section 4.5.1. Over time, the H-beams cured further and became more stiff. Consequently, the H-beams with 1 mm thicknesses t_x and t_y , could hardly bend and twist anymore. Only the H-beams with 0.5 mm thickness still showed some flexibility, but was not able to make multi-curved paths without plastically deforming. Therefore, all solid beams were deemed to be insufficient to function as guiding mechanism.

The flexibility of the H-beams was enhanced by making them segmented, in which t_g is nonzero and variable. The segmented H-beam could be printed as one part, with a small central rod connecting all segments. The first tested segmented H-beam (H2) was made with a width of 3 mm, t_x and $t_y = 0.75$ mm, $t_r = 0.5$ mm and $t_g = 0.5$ mm. The results were improved compared to the solid beams: the H-beam was flexible and could twist, bend and form multiple paths. Therefore, beam H2 served as basis for the succeeding H-beam designs. Tests have been conducted to see the guiding capabilities of the H-beam. The H-beam was placed over the bearings of the memory rings, and manually a path was implemented by the relative rotation of the memory rings. Three types of paths have been tested: a diagonal, S-shaped and an alternating pattern. The H-beam was deemed sufficient, if it could form the implemented path without failure. A beam would fail as guidance, when the path input was deformed and unsmooth. This could be caused by for example, warping of the H-beam or derailment of the bearings. If the H-beam showed promising results, thus could form multiple paths without failure, a reading ring was manually moved through the guidance to see if it would translate smoothly. It was done to test the guiding capabilities of the H-beam. This can be seen in Figure C.1 in Appendix C. The first segmented H-beam (H2) could form many paths, however the H-beam was not strong enough to consistently keep the bearings of the memory rings inside its track. The bearings of the memory rings moved through the ribs by deforming or breaking them. As a result, the guiding capability of the H-beam was insufficient. Adjustments were made to H2 for an optimised design.

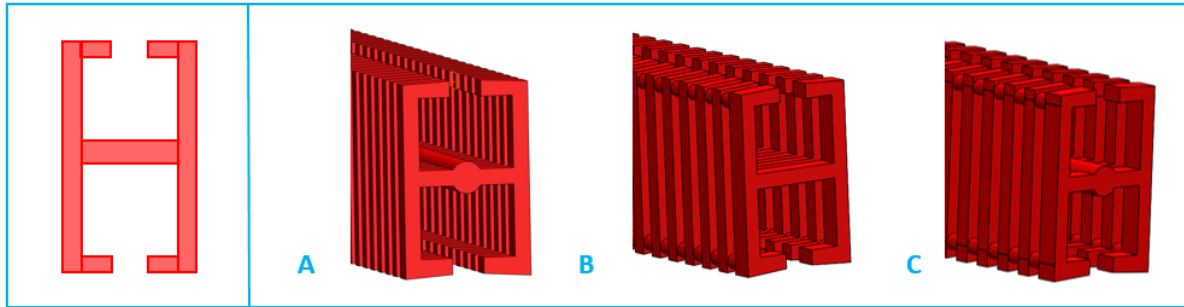


Figure 6.3: Tested H-beams, including additional hooks on both sides of the flanges to capture the ball bearings. Figure A shows version 1 (H3A), in which the ribs are connected through the middle of the H-beam. In the second version (H3B), shown in Figure B, the ribs of the H-beam are connected in the four corners of the flanges. Figure C shows the third version (H3C), here the ribs are connected in the middle and in every corner.

The refined versions, H3A - H3C, can be seen in Figure 6.3. All new H-beams had horizontal hooks on top of their flanges. The horizontal hooks captured the bearings of the memory rings, with the aim to prevent derailment of the bearings. The first version (H3A) was similar to the previous beam H2, but included the additional hooks. H3A is shown in Figure 6.3A. The ribs were connected by a rod through the middle of the H-beam. In the second design (H3B), the ribs of the H-beam were connected by four rods, located in the corners of the flanges, as can be seen in Figure 6.3B. The rods in the corners should keep the ribs at a fixed distance from each other, preventing the bearings from moving out of the H-beam. It was expected that this implementation would make the H-beam stiffer. The last design (H3C) is shown in Figure 6.3C. H3C was the most rigid design, because the ribs were connected in both the midline of the H-beam and all four corners. The dimensions of the three H-beams were based on the previous H-beam: $t_y = 0.75$ mm, $t_r = 0.5$ mm and $t_g = 0.5$ mm. For each design, a version with $t_x = 0.5$ mm and $t_x = 0.75$ mm were printed. Similar to the previous design, the H-beams were tested by placing them on the memory rings and implementing different paths. The characteristics and the results are shown in Table C.1 in Appendix C. Figure C.2 in Appendix C shows pictures of the tests. The first design, H3A, was very flexible and performed well under torsion. However, the ribs of the first design were still not strong enough. Consequently, the bearings moved through the H-beam when a curved path was implemented. An alternating path could also not be achieved with this design. The failure mode can be seen in 6.4A. H3B showed promising results. The H-beam was stiffer than the first design. It was able to make small diagonal and small S-shapes. However, deformation occurred when a larger curve or an alternating pattern was implemented. The deformations were small, but the bearing of the reading ring was not able to move through the guidance. Due to the deformation, the width of the H-beam varied along its length, blocking the motion of the reading rings. H3C was much stiffer than both versions. The H-beam was able to keep the bearings of the memory rings in place, however S-shaped and alternating paths caused the H-beam to deform majorly. As a result, the path was not smooth anymore and could not guide the bearings of the reading rings. The failure mode is shown in Figure 6.4B.

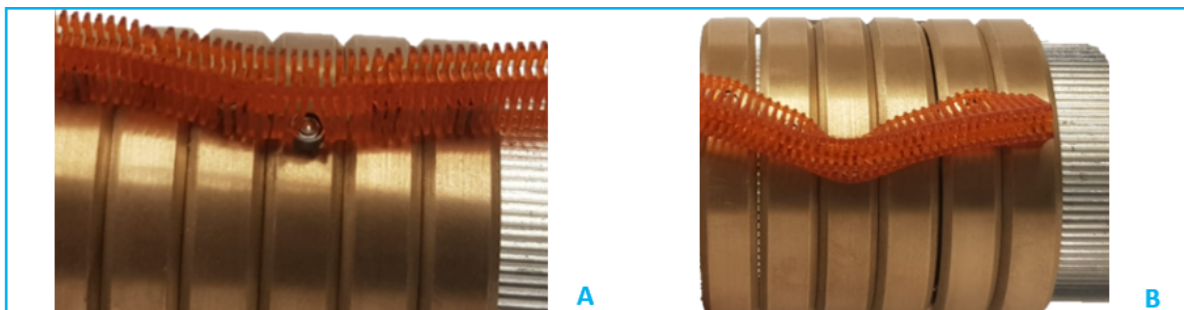


Figure 6.4: Failure modes of the H-beams. Figure A is test H3A, with a small single curvature. The ribs of the bearing are not strong enough. Consequently, the bearing moves through the H-beam. Figure B is test H3C, testing a single curve. The H-beam is deformed majorly. Therefore, the path is not smooth, blocking the translational motion of the reading rings.

From these tests, it was concluded that when the segments were connected in the corners, the H-beam deformed under bending and torsion. The problem arose that while bending, one side of the H-beam was loaded under tension while the other side was compressed. The rods in the corners were not compliant and could not elongate or shorten. Consequently, the tension in the H-beam deformed the H-beam. Connecting the corners of the H-beam was a good solution to keep the bearings of the input rings inside the track. However, the rods should be disconnected from the H-beam segments, so that they could translate freely. A disadvantage of that solution is that the manufacturing would be time-consuming, because all segments have to be printed separately. A continuous beam seemed most promising with version H3A, in which the segments were connected in the midline of the H-beam. However, the design needed to be optimised to avoid the bearings from moving out of the guidance.

With the aim to make the flanges of the H-beam stronger, three new H-beams were designed and tested. Contrary to the previous H-beams, which were printed with the EnvisionTEC, these new designs were printed with durable resin on the Formlabs Form 3 printer. The designs are shown in Figure 6.5. The first version was the same H-beam as the previous design, but specific dimensions were enlarged: $t_x = 1$ mm, $t_y = 0.75$ mm, $t_r = 1.5$ mm and $t_g = 0.5$ mm. Thus, the ribs of the H-beam were larger and thicker, as could be seen in Figure 6.5A. The second version, H4B, is shown in Figure 6.5B. The design was similar to the H-beam shown in Figure 6.3A with thin ribs, but to increase the stiffness of the H-beam, some ribs were given broad flanges. Version C was different than the previous H-beams. The connection of the ribs of the H-beams had an S-shape. This is shown in Figure 6.5C; the bottom image represents the top view of the H-beam. The ribs were made longer and were located in an alternating fashion. Meaning, the bearing would always be supported by at least one side of the H-beam. The dimensions of this design were: $t_x = 0.75$ mm, $t_y = 0.75$ mm, $t_r = 3$ mm and $t_g = 0.75$ mm. Pictures of the results are shown in Appendix C Figure C.3. H4A showed promising results: the design was able to make small and large diagonal and S-shaped paths. An alternating path was difficult, as the bearings deformed the ribs of the H-beam. However, the H-beam was able to keep the bearings inside the guidance. The second version, H4B also had good results. The H-beam could make diagonal and curved shapes, but was not able to make an alternating shape. The results for H4C varied per test. The H-beam could achieve a diagonal shape, but the beam showed inconsistencies for curved shapes. For some tests, the path formed was smooth without failures. Other tests, the bearings moved out of the H-beam. Looking at the design, the bearings of the memory rings always provide force on the outside of the curve. The outside of the curve stretches, as the length is longer than the inner curve, making the gaps t_g larger. When a bearing is located at the position of a gap, it moves out of the beam. Therefore, beam H4C was deemed to be insufficient as guiding element. Out of these three versions, H4A functioned the best and was chosen as the final design. A limitation of this H-beam was the formation of alternating patterns.

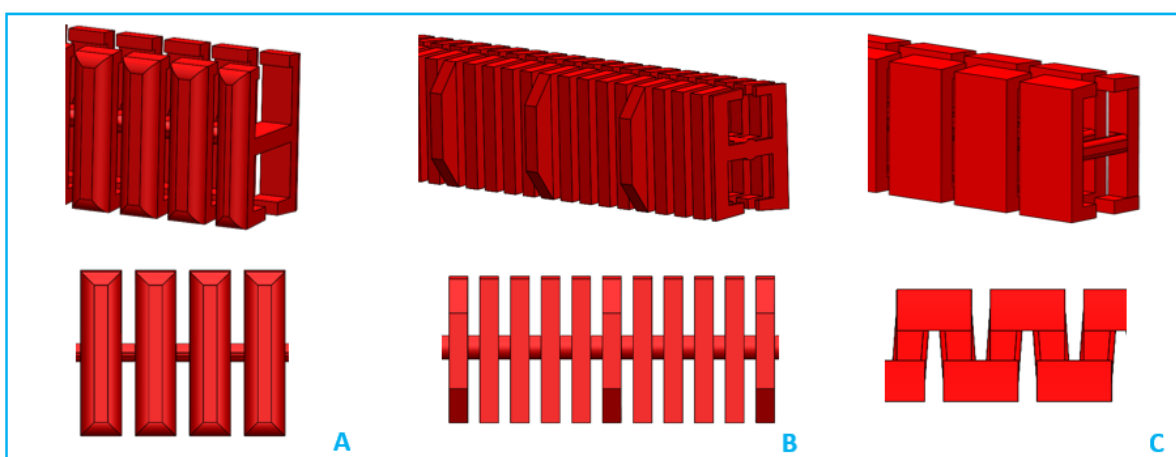


Figure 6.5: Optimised and tested H-beams. Figure A shows a typical H-beam in which the ribs are connected through the midline, this is version H4A. t_r and t_x are made larger with respect to previous designs. Figure B shows the second design (H4B). To increase the stiffness of the H-beam, some ribs have broad flanges. The third design (H4C) is different from the previous designs. As can be seen in Figure C, the t_r is increased a lot and the ribs are located in an alternating fashion. The bottom images of Figure A and B show a side view of the H-beam, while Figure C is a top view.

6.3.2. H-beam evaluation

A table of all the results described above is provided in Table C.1 in Appendix C. H4A was selected as H-beam design to function as guiding element. The segmented design, with the attachment point in the middle of the H-beam, made the H-beam very flexible. By increasing the thickness of the ribs (t_g) and width of the flanges (t_x), the ribs were enhanced in strength. This reduced the flexibility, but it was required to keep the bearings inside the guiding element. Concluding, the H-beam design was a trade-off between flexibility and strength. Version H4A could make diagonal shapes and curved paths. The design limitation was alternating patterns, in which the input given to the memory rings was alternated from the most right orientation to the most left orientation, respectively. Further optimisation will be necessary for future research to improve the performance of the H-beam. As described above, the H4-versions were printed with durable resin instead of the R5 resin. The H-beams printed by the EnvisionTEC cured more over time and became brittle. For example, the solid beams (H1) were relatively flexible in the beginning: all beams could twist under pure torsion, and bending was possible to a certain extend. Two weeks later, they were unable to bend, and only the H-beams with the small thicknesses of 0.5 mm could still twist. This also applied to the H2 and H3 versions: the ribs of the H-beam became more brittle over time. Durable resin resulted in more flexible H-beams. The beams printed with durable resin cured over time as well, but remained flexible. Therefore, the durable resin of the Formlabs printer was more suited for the H-beams than the R5 material of the EnvisionTEC.

6.4. Testing the prototype

6.4.1. Test method

The machined prototype was tested in four main phases, starting with individual parts and ending with the complete design:

1. Individual parts and subassemblies
2. Prototype without H-beam
3. Path input: H-beam
4. Path input and output: complete prototype

The components and subassemblies had been tested simultaneously with the manufacturing process of the prototype. The machining of the components was done in order, starting with the innermost components and working towards the outside. This gave the opportunity to adjust or redesign parts before the remainder of the components were manufactured. In the first test phase, individual parts and subassemblies were examined. In the second phase of testing, the complete prototype was tested without the H-beams. This test functioned as verification to see if the main components moved without friction and jamming. Since the H-beam was expected to be the most critical part, the other components should be able to function properly when the H-beam is not present. The memory rings were examined on their sliding motion and their shifting motion from the rotating axis to the fixed axis. The rotation and translation of the memory rings should be done with minimal friction, to minimise wear and to reduce the input force required from the user. Also, the reading rings should be able to rotate with minimal force required. In general, all moving components should have minimal friction and play, to avoid blockage of the prototype. The third phase of the testing procedure included the examination of the path input. In this test, the H-beam performance in combination with the memory rings and translational motion mechanism was evaluated. The ability to form diagonal, curved and alternating paths was tested, in combination with the rotating, sliding and locking capabilities of the memory rings. Phase 3 is shortly discussed in section 6.4.4., and overlaps with section 6.3. The last test was conducted with the complete prototype. The function of the H-beam as guiding mechanism was examined. This step tested what type of paths could be formed as output with this path-planning module. During the testing procedure, small malfunctions in certain parts and subassemblies needed to be resolved. In section 6.4.6 the changes made to the parts to improve the performance of the design are elaborated.

Testing individual parts and subassemblies	Desired behaviour	
H-beam	<ul style="list-style-type: none"> - Flexible design - Keep the bearings inside the track - Smooth path for guidance 	<ul style="list-style-type: none"> ✓ ✓ ~ ✓ ~
Memory rings and shafts	<ul style="list-style-type: none"> - Input shaft rotates with minimal friction - Memory rings slide with minimal friction - Smooth transition from one shaft to the other shaft 	<ul style="list-style-type: none"> ✓ ✓ ✓
Memory rings and translational motion mechanism	<ul style="list-style-type: none"> - Translational motion mechanism slides with minimal friction over the shafts - Translational motion mechanism moves the memory rings from shaft to shaft - Memory rings can rotate freely inside the translational motion mechanism 	<ul style="list-style-type: none"> ✓ ✓ ✓
Reading rings and Teflon frame	<ul style="list-style-type: none"> - Reading rings rotate with minimal friction 	<ul style="list-style-type: none"> ✓
Reading rings and translational motion mechanism	<ul style="list-style-type: none"> - Reading rings rotate with minimal friction around the translational motion mechanism - Translational motion and reading ring frame do not touch while translating 	<ul style="list-style-type: none"> ✓ ✓

Figure 6.6: Testing individual parts and subassemblies. The functionalities have been tested manually, to see if optimisation is required before the complete prototype is assembled. A check-mark means that the desired behaviour is accomplished. An orange tilde means that optimisation is required for further research.

6.4.2. Test phase 1: individual parts and subassemblies

The machining of the components was done in order, starting with the innermost components and working towards the outside. Individual parts and subassemblies were tested in this sequence:

1. H-beams
2. Memory rings and shafts
3. H-beams on memory rings
4. Memory rings and the translational motion mechanism
5. Reading rings and Teflon frame
6. Reading rings and translational motion mechanism

A summary of the results for the first test phase is provided in Figure 6.6. First, the flexibility of multiple solid H-beams (H1A - H1I) and a segmented H-beam (H2) were examined, as described in section 6.3. Because the segmented H-beam showed promising results for path formation, the precision technicians started with the fabrication of the path-planning module. The innermost components were manufactured first; consequently, the memory rings and the shafts were tested first. The desired behaviour of this subassembly included: the input shaft must rotate with minimal friction around the inner shaft, the memory rings must translate with minimal friction, and the transition from one shaft to the other shaft must be done smoothly. After some small adjustments, all functionalities performed satisfactorily. For example, the outer diameter of the inner shaft was reduced, so the input shaft could rotate better around the inner shaft. The adjustments are elaborated in section 6.4.6. After that, the translational motion mechanism, the reading rings and the reading ring casing were manufactured and examined. Simultaneously, different H-beam designs were tested on the memory rings, which is elaborated in section 6.3. The chosen H-beam design (H4A) was flexible and could make multiple paths, but the limitation of this design was forming alternating patterns. The motion of the memory rings in combination with the translational motion components was tested next. The memory rings must rotate freely within the translational motion mechanism. Also, the sliding motion of the translational motion mechanism over the input and fixed shaft must be done without jamming and with minimal input force needed. Both working principles functioned well. The inner diameter of the translational motion mechanism was enlarged, to provide more space for the memory rings. Due to this adjustment, the memory rings could

rotate freely inside the translational motion components. The desired behaviour of the reading rings included that they should rotate inside the Teflon frame requiring minimal force. This behaviour of the subassembly was deemed sufficient. At last, the translational motion mechanism was tested in combination with the reading ring assembly. The translational motion mechanism should be able to translate without jamming against the reading rings or the Teflon frame. Therefore, the outer diameter of the translational motion mechanism had to be reduced, to create more spacing between the reading rings and translational motion mechanism. The adjustment improved the performance, and the reading ring assembly functioned well. Figure 6.6 shows the results of test phase 1, with the optimised components. All subassemblies worked well; only the function of the H-beam was limited to diagonal and curved paths. The H-beam could not make alternating patterns.

6.4.3. Test phase 2: prototype without H-beam

The H-beam was expected to be the most critical part of the path-planning mechanism. Therefore, the prototype should be able to function properly when the H-beams are not present. Phase 2 functioned as verification to see if all components could move without friction and jamming. The path formation exists out of two steps: rotational input and a translational input. Therefore, the rotational motion and translational motion of the components were examined in the integrated design. The desired behaviour of the prototype without H-beam is shown in Figure 6.7, in the middle column. The memory rings should be able to translate and rotate with minimal friction. Also, when a memory ring is slid from one shaft to the other, the user must be provided with haptic feedback. The translational motion of the memory rings is influenced by the performance of the translational motion mechanism. This mechanism must slide with minimal input force. Therefore, the mechanism should not jam against the casing, reading rings or the shafts. The output functioning of the prototype depends on the rotational motion of the reading rings: the reading rings should rotate with minimal friction inside their Teflon frame.

Testing prototype without H-beam	Desired behaviour	
Rotational motion	- Memory rings rotate along with the input shaft	✓
	- Memory rings rotate with minimal friction	✓
	- Reading rings rotate freely inside the Teflon rings	~
	- The casing prevents the translational motion mechanism from rotating	✓
Translational motion	- Memory rings translate with minimal friction	✓
	- Memory rings can slide smoothly from one shaft to the other shaft	✓ ~
	- Translational motion mechanism does not jam against the reading rings	✓
	- Translational motion mechanism does not jam against the casing	✓
	- Bearings of the reading rings are guided by the slot of the translational motion mechanism	✓
	- Haptic feedback when a memory ring is slid from one shaft to the other shaft	✓

Figure 6.7: Testing the prototype without the H-beam. Phase 2 functions as verification to see if all components move without friction and jamming. A check-mark means that the desired behaviour is accomplished. An orange tilde means that optimisation is required for further research.

In Figure 6.7, a summary of the results for test phase 2 is shown. The input rotational and translational motion of the memory rings functioned very well, after some small adjustments. The adjustments made, are elaborated in section 6.4.6. The memory rings could rotate freely inside the translational motion mechanism. The translational motion of the memory rings did not require a high input force. The transition from the rotating shaft to the fixed shaft worked well, when the shafts were aligned. Since no haptic feedback mechanism for the rotational input was incorporated in this design, the user had to find the right position to align the shafts. For future research, haptic feedback for the rotational motion will enhance the ease of use.

The haptic feedback mechanism for the translational motion of the memory rings worked sufficiently; the spring element provided a small click and resistance when one ring was moved from one shaft to the other shaft. However, in the first tests, the spring plunger applied too much force on the translational motion mechanism. Hence, the resisting force was higher than desired. To improve the performance, the indents in the forks of the translational motion component were made deeper. As a result of this adjustment, the spring element had some play. When the spring element is located above an indent in the translational motion mechanism, the translational motion mechanism could move 0.5 mm back and forth. However, this play did not limit the functionalities of the complete prototype. The translational motion knob also had some play, causing it to rotate around its fastening points. For ergonomics, this was undesired, however it did not limit the working principle of the mechanism. The reading rings were able to rotate smoothly, but some rings required more torque to rotate them than others. The reading rings should rotate with minimal friction, otherwise the H-beam would not be able to guide the bearings of the reading rings in the formed path. As result, the mechanism will block. Some adjustments can be made to improve the performance, this is discussed in Chapter 9. For the proof of principle, it was concluded that the machined prototype worked acceptably without the H-beam.

6.4.4. Test phase 3: path input

In the third test phase, the chosen H-beam was tested on the memory rings, including the translational motion mechanism. The H-beam was fastened on top of the translational motion part and captured the bearings of the memory rings. The rotation and translation of the memory rings were tested, while inserting different paths:

1. Diagonal shape
2. Single-curved shape
3. Multi-curved shape
4. Alternating shape

Test phase 3 overlaps with the results elaborated in section 6.3. The results are shown in Figure 6.9. The tests showed that the connection of the H-beam with the translational motion mechanism was weak. Rotating the first memory ring with the maximum range, damaged the H-beam. The H-beam tried to rotate around its fasteners, but was limited. When the first memory ring was rotated a lot, the first couple of ribs of the H-beam broke, decoupling the remainder of the H-beam from the translational motion part. A refined H-beam was introduced, in which the first two ribs of the H-beam were printed as one rib. As a result, the first part of the H-beam was stiffer and the first memory ring was limited in its rotation. The first memory ring had a range of one step to the right or left. An input of two steps required more force, because the H-beam resisted it. This alteration had a positive effect, because the connection of the H-beam with the translational motion mechanism did not break or deform anymore. The test results shown in Figure 6.9 include the refined H-beam. As can be seen in Figure 6.9, this H-beam design was able to make straight, diagonal and curved paths. An alternating pattern, shown in the bottom row, caused deformation in the ribs of the H-beam. This was a design limitation of the prototype. An overview of test phase 3 is provided in Figure 6.8.

Testing the path input: H-beam	Desired behaviour	
Path formation	The H-beam can form different types of paths, without deformation or derailment of the bearings: <ul style="list-style-type: none"> - Diagonal path - Single-curved path - Multi-curved path - Alternating path 	✓ ✓ ✓ ✗

Figure 6.8: Testing the path input: the performance of the H-beam. The H-beam must be able to form diagonal, curved and alternating paths. A check-mark means that the desired behaviour is accomplished. A red cross means that the H-beam did not meet the requirement.

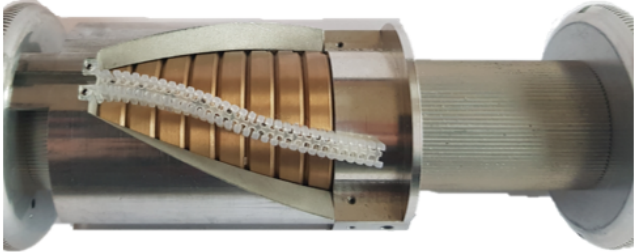
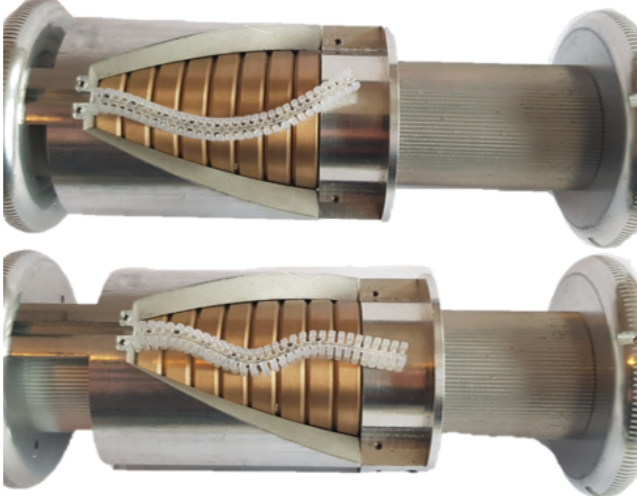
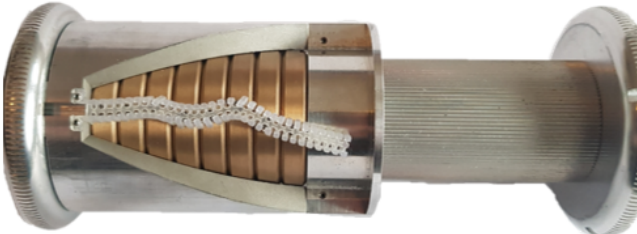
Path input	Picture	Prototype abilities
Diagonal shape		Yes
Curved shape		Yes, single curved and multi curved paths are possible
Alternating		Inconsistent, the ribs of the H-beams deform. The path is not smooth anymore

Figure 6.9: Test results: input function of the machined prototype. The H-beam is connected to the translational motion part and captures the bearings of the memory rings. The rotation and translation of the memory rings have been tested, while inserting different paths. The machined prototype in combination with this H-beam design is able to make straight, diagonal and curved paths. An alternating pattern, shown in the bottom row, causes deformation in the ribs of the H-beam.

6.4.5. Test phase 4: complete prototype

The complete prototype was tested for different types of paths. To be able to form a large single curvature in the compliant shaft, the reading rings must provide a diagonal path. The compliant shaft should also be capable to make multi-curved paths. An alternating path was not tested, because test phase 3 concluded that alternating patterns were not achievable as path input. Thus, in total three types of paths were examined:

1. Diagonal shape
2. Single-curved shape
3. Multi-curved shape

The prototype could create a diagonal and curved path as output. Figure 6.11 shows the formation of a diagonal path in the reading rings. The pictures in Figure 6.12 and Figure 6.13, show the formation of two different curved paths. The front part of the casing is knowingly excluded in these tests, to make the H-beam more visible. In addition, without casing the failure mode could be inspected better, if present.

Even though the prototype was capable of making diagonal and curved paths, the performance of the integrated design was not sufficient. In all figures, the most distal reading elements have a straight configuration. This is because the first ribs of the H-beam were printed as one rib, limiting the input of the first memory ring. The translational motion of the memory rings required a lot of force compared to test phase 2. The further the path was inserted, the more force was necessary. One possible cause could be the accumulation of normal forces in the reading rings. The reading rings were compressed together when the H-beam moved distally. High normal forces on the reading rings would require more force provided by the H-beams to overcome the friction. However, it was noticed that the increase in input force was also required when a straight path was inserted. It was expected that for a straight path, the accumulation of normal forces would not limit the translational motion of the memory rings, as the reading rings did not have to rotate. Therefore, it was presumed that the H-beam was the critical part rather than the reading rings. The H-beam jammed against the reading rings or the bearings of the reading rings. Possibly, the force exerted on the H-beam caused the guidance to deform. The movement of the memory rings back from the fixed axis towards the input axis seemed to be the most critical loading of the H-beam: it required the most input force. Compression occurred and the path became irregular due to buckling. In the worst case, the bearing moved out of the H-beam, which can be seen in Figure 6.14. The derailment of bearings blocked the complete working mechanism of the prototype: the prototype needed to be disassembled to place the bearing back into the track. In case of serious damage, the H-beam needed to be replaced.

With the aim to reduce the jamming of the H-beam against the bearings of the reading rings, a refined H-beam was implemented. The horizontal hooks on top of the flanges of the H-beam were removed. The alteration did not completely solve the problem: the translational motion of the memory rings still required a lot of force provided by the user. Figure 6.10 shows the test results. The design limitation and the failure of the H-beam are discussed in Chapter 9.

Testing the complete prototype	Desired behaviour	
Path formation	The reading rings can form different types of paths, without deformation or derailment of the bearings: <ul style="list-style-type: none"> - Diagonal path - Single-curved path - Multi-curved path - Alternating path 	~ ~ ~ x

Figure 6.10: Testing the path output: the performance of the integrated prototype. The prototype should be able to provide diagonal, curved and alternating paths. An orange tilde means that the prototype was able to make that path, but further optimisation is required to improve the performance of the prototype. A red cross means that the prototype was not able to form that path.

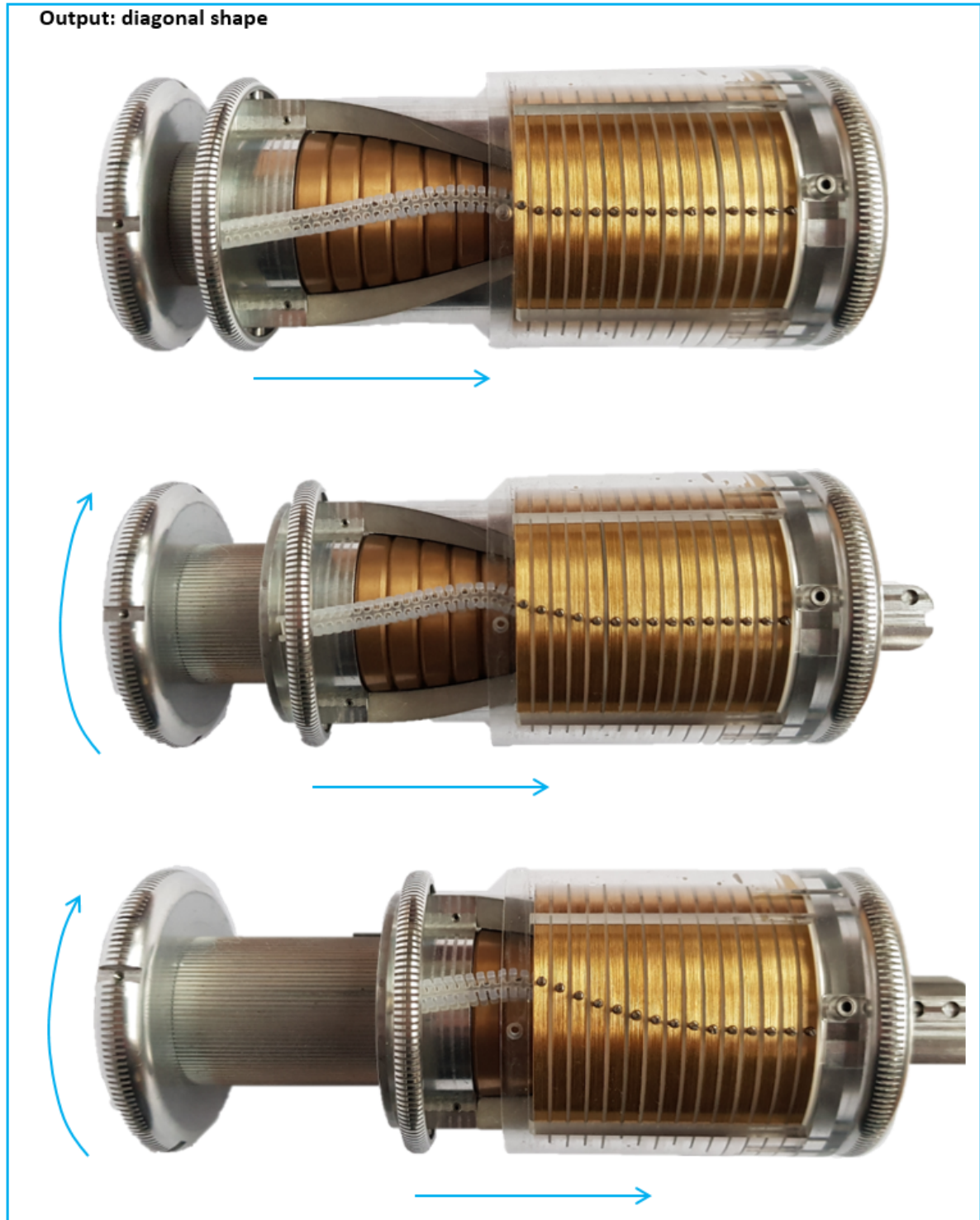


Figure 6.11: Test results for the diagonal shape.

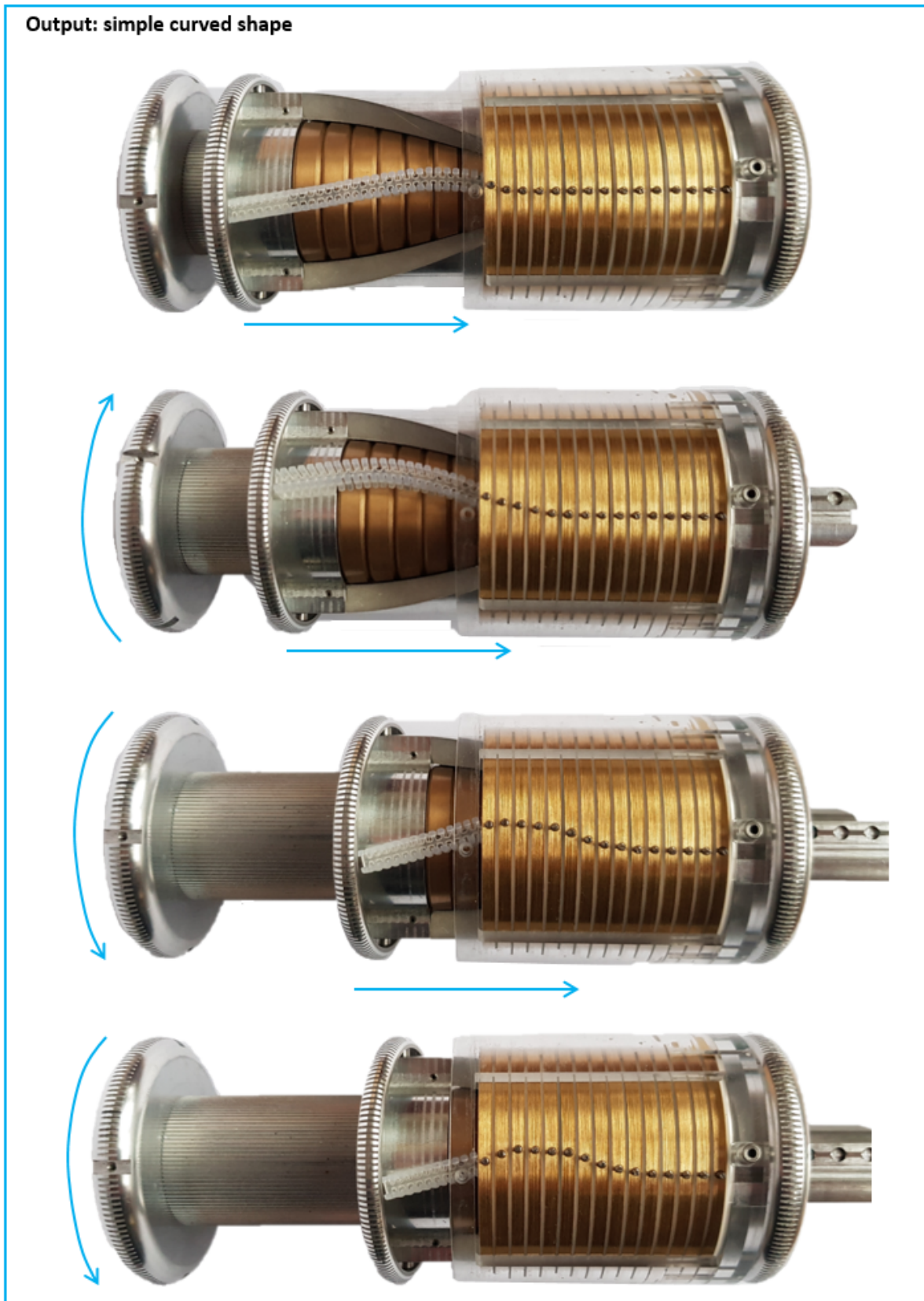


Figure 6.12: Test results for a curved shape.

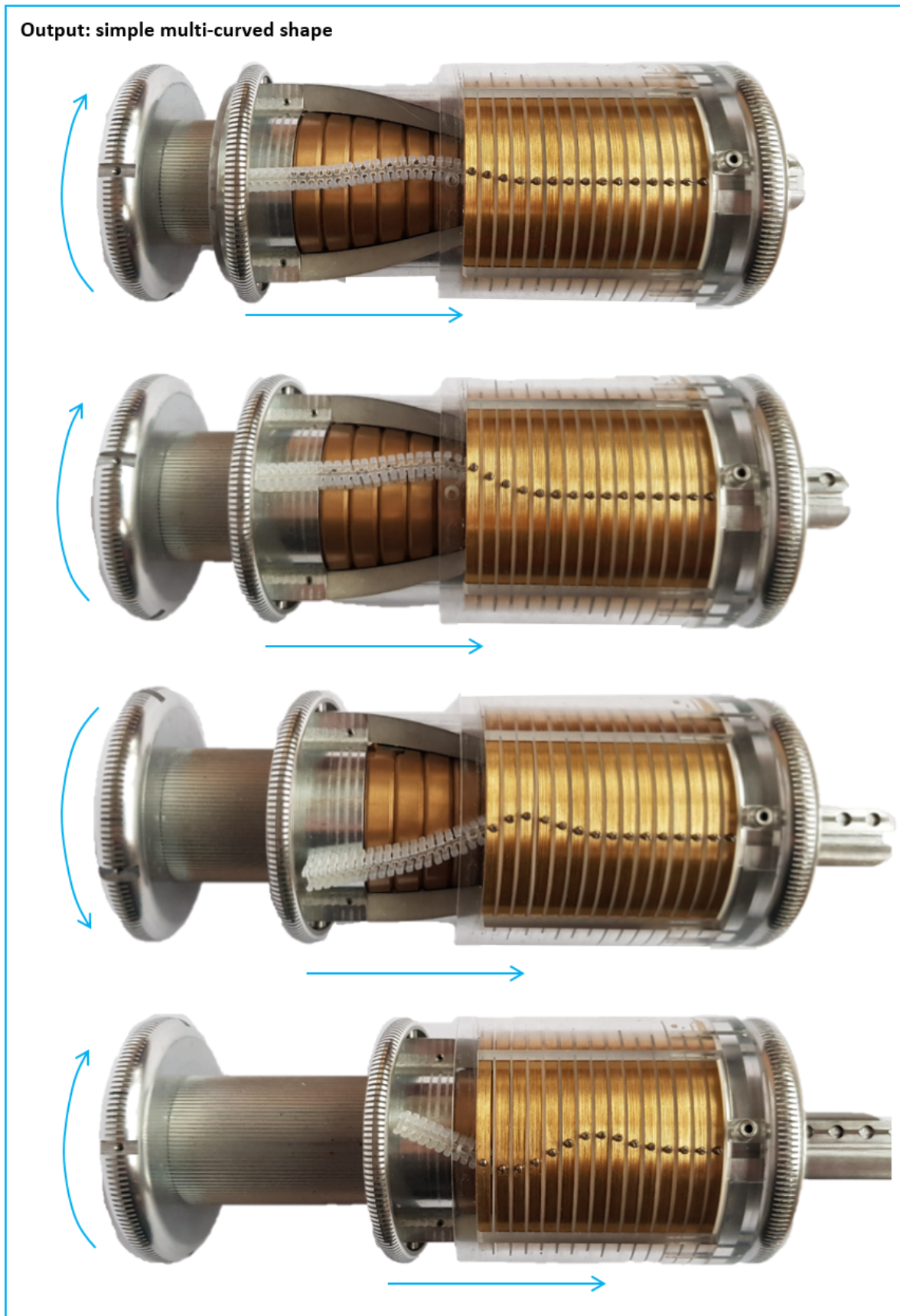


Figure 6.13: Test results for a multi-curved shape.

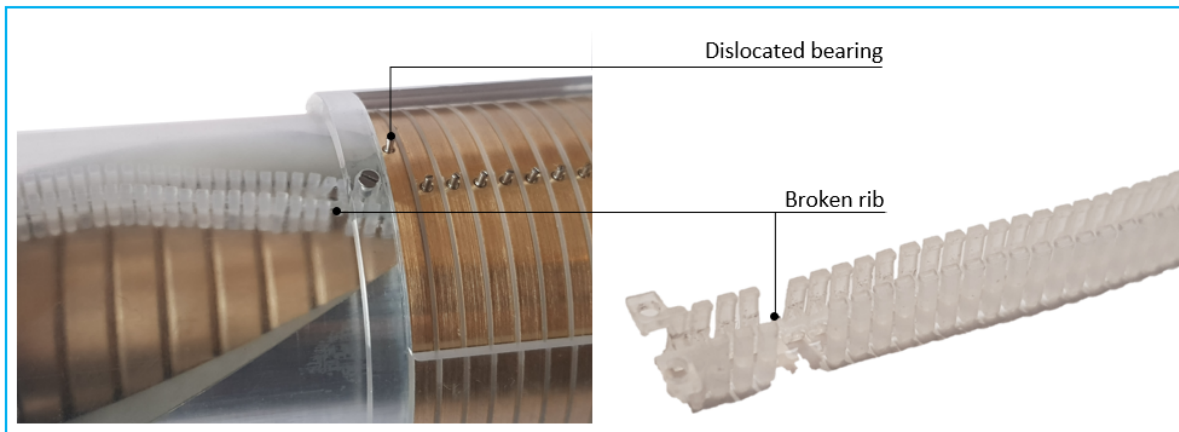


Figure 6.14: H-beam failure in test phase 3. While moving the memory back from the fixed shaft to the input shaft, the H-beam is exposed to compression forces by the bearings of the reading rings. In the worst case, the bearings break the ribs of the H-beam and move out of the guiding element.

6.4.6. Changes made during the test phases

During the test phases, some small malfunctions have been adjusted to optimise the design. In the first phase, the adjustments mainly included creating more space between moving components. The individual components and subassemblies were evaluated based on their fitting and motion capabilities. The alterations included for example, turning a small layer off the outer surface of the inner shaft, so the input shaft and input knob could rotate better around the inner shaft. The translational motion components also needed size adjustments: the inner diameter was enlarged so that the memory rings could rotate freely, and the outer diameter was reduced for the motion of the reading rings. To enhance the motion of the memory rings on the input and output shaft, the shafts required to be cleaned, removing small aluminium chips. Also, shape-correction of the memory rings was required. The rings got an oval shape, after pressing the ball bearings into the memory rings. The shape had to be corrected, so the linear motion on the shafts would be smooth again in any configuration.

In the second phase, the prototype was tested without the H-beam. This is the first time that all components were assembled, including the outer casing. Especially, the translational motion mechanism needed adjustments, because the sliding motion of the memory rings required more input force than desired. The first alteration was made to increase the spacing between the casing and the translational motion mechanism. The components seemed to have friction, because you could hear the scrubbing sound of the aluminium part against the perspex casing. Therefore, the outer diameter of the translational motion front part was reduced, and a small layer was removed from the inside of the perspex tube. The casing end part required alterations as well, to provide more spacing for the forks of the translational motion mechanism. The forks should move through the casing, without jamming. During the tests the forks fitted well, but with a very small misalignment they moved against the casing, resulting in a lot of friction. A significant adjustment was done to the mechanism of the ball-spring plunger. The spring plungers exerted a lot of force on the forks of the translational motion component. By making the indents deeper, the force from the ball plunger was reduced. All modifications combined completed the second test phase: the performance of the prototype without the H-beams was deemed sufficient.

The only change made in phase 3 included the reinforcement of the first section of the H-beam. The attachment point of the H-beam to the translational motion mechanism was made more stiff, by printing the first two ribs of the H-beam as one large rib. This minimised the deformation at the beginning of the H-beam, with as trade-off the limiting rotation of the first memory ring.

In the last phase, more specific alterations were made to improve the integrated prototype. For example, fastening methods were replaced and H-beam optimisation was required. A high input force was required for the translational motion, due to the jamming of the H-beam. A refined H-beam was tested, in which the upper horizontal hooks of the H-beam that capture the bearings of the reading rings, were removed. Still, a high input force was needed for the linear motion of the memory rings. As a result, the pin connection between the two translational motion parts broke, when it was tried to pull the memory rings back to the input shaft. Originally, two pins coupled the two translational motion parts. One side of the pin had an M1.6 tapped profile, and the other side had a flat area to fix the pin with a set screw. The pin was secured in the main part with the tapped side and locked in the front part with one set screw. While testing the prototype, the pin broke exactly where the tapped area ended. The pin was replaced by a solid pin, with a 2 mm diameter and a flat side on one end. The solid end was glued into the main part and the flat end was fixed with a set screw in the front part. New tests were performed, which concluded that the coupling was still not sufficient: the set screws could not keep the pins in place. To improve the design, two more tapped holes were machined in the front part, and two additional set screws were introduced on each side. Thus, each pin is now fixed with three set screws: from the side (the original set screw), from above and from underneath. This adjustment worked well. At last, to reduce the friction between all moving parts, the parts have been lubricated. This included the shafts and memory rings, the ball plunger and the forks of the translational motion mechanism and the reading rings in their frame.

6.5. Design evaluation

The evaluation of the prototype is summarised in Figure 6.15. After multiple adjustments to the prototype to optimise the performance, it is concluded that the prototype works sufficiently without the H-beams incorporated in the design. Except for the reading rings, all parts do not require much input force to rotate or translate. The reading rings move smoothly, but some rings need more torque to rotate them than others. This is undesired and should be optimised for the prototype to perform better. The third test phase showed that the input function of the prototype works adequately. The input mechanism can implement diagonal and curved paths. A limitation of the input is the implementation of alternating patterns. The H-beam deforms or damages, resulting in an irregular path. The deformed H-beam is not capable of guiding the bearings of the reading rings. With this prototype, the follow-the-leader working principle is proved. The prototype, with the incorporated H-beam, is able to make diagonal, straight and simple curved paths and s-shapes. However, multi-curved or alternating paths can not be achieved with this mechanism. The H-beam design is not optimal and limits the performance of the prototype. A high input force is necessary to translate the formed path into the reading rings. The guidance is weak, and the H-beam breaks with complex paths. Compression forces exerted on the H-beam due to jamming, cause the guiding element to buckle. As a result, failure modes occur such as deformation, damage to the ribs and the derailment of bearings. Therefore, it can be concluded that the H-beam is the critical part in this design. The machined prototype is promising, but optimisation of the H-beam is required to improve the performance of the prototype. The discussion and recommendations for these results are given in Chapter 9.

Performance of the machined prototype	
Functionalities of the design	<ul style="list-style-type: none"> + Proves the follow-the-leader working principle + Path input works well + Complete prototype without H-beam works well + Diagonal paths can be formed as output + Simple curved paths can be formed as output
Limitations of the design	<ul style="list-style-type: none"> - No alternating patterns possible as input and output - The further the memory rings are translated into the reading rings, the more input force necessary - H-beam is weak: deformation of the H-beam and derailment of the bearings are occurring failure modes - Friction in the reading rings

Figure 6.15: Summary of the machined prototype evaluation.

Proof of concept: 3D printed prototype

7.1. Purpose

Simultaneous to the machining of the original prototype, a 3D printed prototype has been developed. 3D printing has many benefits compared to machining a prototype, mainly based on time and cost reduction. Making this mechanism 3D printable, would immensely reduce the costs of the prototype and therefore the complete surgical instrument. Also, the production only requires 3D printers and existing CAD-files. In contrary to machining, for which precision technicians with hard skills are necessary to manufacture the components, 3D printing is a simple manufacturing method. The components can be printed in batches. Consequently, 3D printing enhances the affordability and accessibility for poorer countries as well. However, the CPMM design is complex with many components moving relative to each other, including small features such as the gear profiles. The 3D printed version is made to determine if 3D printing is a manufacturing option for this design.



Figure 7.1: Picture of the 3D printed prototype.

7.2. Parts and differences with the machined prototype

Figure 7.1 shows a picture of the 3D printed prototype. Additional pictures of parts and subassemblies are provided in Appendix E. The prototype is similar to the machined prototype and has almost the same dimensions. Small adjustments were made compared to the original prototype, to improve the ease of manufacturing and adapt to the 3D print limitations. The exploded view and bill of materials are provided in Figure E.1 and Figure E.2 in the appendix. An overview of the differences between the machined prototype and the 3D printed prototype is shown in Appendix E. The main adjustments are elaborated in this section. The changes are based on what was achievable with the available 3D printers and the corresponding material properties. The available 3D printers are elaborated in the next section.

An advantage of the 3D printing technique is that it enables printing multiple parts as one component, rather than having several parts that are connected by fasteners. Machining methods are based on removing material from a solid or hollow bar or rod. Thus, machining is a subtractive manufacturing method. The methods are limited to the size of the tools and also the motion and steering range of the machines. Accessibility is the main limitation of subtractive manufacturing. Consequently, on occasions it is necessary to divide one part into two or more separate parts. 3D printing on the other hand, is a method based on additive manufacturing. The layer-by-layer build up during 3D printing, enables the production of more complex shapes. Therefore, in this 3D printed prototype the input knob and input shaft were printed as one part. The same applied to the fixed shaft and the end knob. Also, the inner shaft of the prototype was made out of two parts instead of four. Thus, less assembling was required. The adjustments can be seen in Figure E.3, Appendix E.

Downsides of 3D printing are related to the lower accuracy, the material properties, the weakness of layers and their printing direction. Metals such as aluminium are stronger than plastics: the Young's modulus of aluminium (~70 GPa) is higher than polymers like ABS (~ 1 - 3 GPa) and PLA (~3.5 GPa) [3]. Therefore, some components required adjustments to their design to avoid weak features. For example, the memory rings in the 3D printed design contained teeth along the complete inner perimeter. This is contrary to the machined prototype, in which the number of teeth was reduced to 8 for the ease of manufacturing. Due to the lower strength of plastic, the amount of teeth was necessary so that the normal forces are lower per gear tooth. Furthermore, the connection between the front and main translational motion part was adjusted as well, because the coupling pins in the original design were relatively small. Printing the coupling pins resulted in a weak connection that broke during assembling. Thus, an alternative coupling was implemented, that included a larger overlapping area. Also, the separating rings between the reading rings were made thicker in the 3D printed version. The Teflon frame in the original design included rings with a thickness of 0.5 mm. This was not sufficient for a 3D printed part: the component would exist out of a few layers only, and be very weak and bendable. In the 3D printed prototype, the reading ring frame was modified to make it more sturdy. Two additional parts were printed that hold the separating rings together. A pin going through the holders and separating rings, connected the frame components. The amount of reading rings was reduced from 15 to 12. Meaning, the 3D printed prototype was designed to control a compliant shaft with 12 segments. The table in Figure E.4 in the appendix shows CAD drawings of the machined and 3D printed memory rings, reading rings and casing.

The 3D printed prototype is a simplified version of the machined prototype. Therefore, the spring plunger had not been incorporated in the design yet. Also, instead of 3 mm ball bearings, M1 screws were used as pins that are guided by the H-beam. This required the H-beam to have a smaller width, and a reduced spacing in between the ribs (t_g). Otherwise, the M1 screws would easily move out of the H-beam rather than being guided in the formed path. Furthermore, the casing was 3D printed as well, instead of made from transparent perspex tubes. The memory rings should be visible for the user, so the user can see the path input. As a solution, additional holes were made in the casing to create an open structure. This can be seen in Figure E.5 in the appendix. Not only is the accuracy of 3D printed parts lower than the accuracy of machined parts. Also, plastic on plastic generally causes a lot of friction. The surface finish of metals is better than 3D printed plastics. To avoid blockage of the complete mechanism, all parts were given extra spacing. Holes for pins and screws were also enlarged. This is elaborated in subsection 7.0.4. Dimensioning.

7.3. 3D printers and materials

Three types of 3D printers were available for this project. An Ultimaker 3 (Ultimaker, Geldermalsen, The Netherlands), a Formlabs Form 3 printer (Somerville, MA, United States of America) and EnvisionTEC Perfactory 4 Mini XL (EnvisionTEC, Gladbeck, Germany). The Ultimaker is a 3D printer based on Fused Deposition Modeling (FDM), capable of printing with plastics such as ABS and PLA. The Formlabs and EnvisionTEC printers are both stereolithography (SLA) printers. In other words, they are liquid bed printers, in which the layers are formed by solidifying the liquid with an ultraviolet-laser. The printers and their main characteristics are shown in Figure 7.2.

The resolution of the parts printed by SLA printers is higher than FDM-printed parts. For FDM, the resolution of the component is defined by the size of the extruder nozzle. A common nozzle diameter is 0.4 mm, but nozzles with size 0.25 mm also exist. The Ultimaker is not capable of printing small extrudes. Generally, layers are visible on the surface of FDM printed components. Stereolithography is based on highly precise and small lasers, enabling the printer to achieve fine details. Another factor that influences the quality of the parts is that FDM is based on temperature and SLA on light. The Ultimaker melts the plastic in order to extrude it. Consequently, the layers of the part are subjected to thermal stresses. This is not the case in SLA printed parts. The bond between FDM layers is weaker than layers printed with SLA. This can cause layer delamination, making the component weak along the line of the layers. However, the Ultimaker is a much cheaper method. The liquid resin of the EnvisionTEC and Formlabs is costly compared to FDM filament.

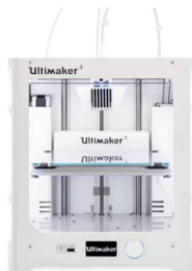
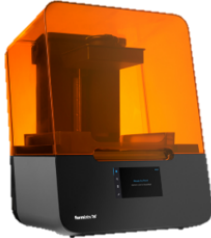

Printer	Ultimaker 3	Formlabs Form 3	EnvisionTEC
			
Type	FDM	SLA	SLA
Material	PLA, ABS	Durable, Dental	R5 liquid polymer
Print volume	215 x 215 x 200mm	145 x 145 x 185 mm	115 x 72 x 220 mm
XY resolution	12.5 μ m	25 μ m	22 – 30 μ m
Layer height	20 - 200 μ m	25 – 300 μ m	15 – 150 μ m

Figure 7.2: 3D printers available for this project and their specifications. Specifications retrieved from the factsheets provided on the websites of the companies. The pictures are adapted from the original websites of the companies. [38][17][14]

The majority of the parts were printed with the Ultimaker, because the Formlabs and EnvisionTEC are expensive methods. An advantage of the cheaper FDM method was that the components could be printed multiple times, to find the right spacing. Only parts that required small extruded sections, which were not achievable with the Ultimaker, were printed with the SLA printers. This included the shafts with the geared profile, the memory rings and the H-beams. The reading rings, reading ring frame, inner shaft, translational motion parts and the casing were printed with the Ultimaker. The stereolithography methods produced very flexible components. Additional curing of the components was necessary to finalise the process. After printing the components, they were cleaned in an alcohol tank to remove all residual resin. After that, they were cured in an oven, in which the parts were simultaneously heated up and exposed to UV-light. A high temperature and curing time, made the components stiffer. The temperature and curing time determined the stiffness of the SLA components. Over time, the parts cured more because of ambient light and oxygen in the air. In the 3D printed prototype the shafts and memory rings must be hard: the geared profile should be able to remain stiff without breaking. Therefore, dental resin was used, which has a higher tensile strength than durable resin. Besides that,

Table 7.1: 3D printed prototype parts, printing technique and materials

Part	3D print method	Printer	Material	Curing temperature (degrees)	Curing time (min)
Inner shaft	Fused Deposition Modeling	Ultimaker 3	PLA	-	-
Inner shaft end-part	Fused Deposition Modeling	Ultimaker 3	PLA	-	-
Input shaft	Stereolithography	Formlabs Form 3	Dental resin	60	60
Fixed shaft	Stereolithography	Formlabs Form 3	Dental resin	60	60
Memory rings	Stereolithography	Formlabs Form 3	Dental resin	60	60
H-beam	Stereolithography	Formlabs Form 3	Durable resin	60	2
Translational motion main part	Fused Deposition Modeling	Ultimaker 3	PLA	-	-
Translational motion front part	Fused Deposition Modeling	Ultimaker 3	PLA	-	-
Translational motion knob	Stereolithography	Formlabs Form 3	Dental resin	60	60
Reading rings	Fused Deposition Modeling	Ultimaker 3	PLA	-	-
Reading ring frame	Fused Deposition Modeling	Ultimaker 3	PLA	-	-
Casing	Fused Deposition Modeling	Ultimaker 3	PLA	-	-

the shafts and memory rings were fully cured. The H-beam, on the other hand, was required to be more flexible. The durable resin was used, and the H-beams were not fully cured to provide the flexibility. Some H-beams were printed with the EnvisionTEC, this is elaborated in the previous chapter. Table 7.1 shows the printing technique, materials and if applicable, the curing temperature and time.

7.4. Dimensioning

The 3D printed prototype has the same dimensions as the machined prototype. However, some dimensioning changes were required in terms of additional spacing between parts. This was done to avoid blockage and jamming of the complete mechanism. The surface roughness of 3D printed parts is relatively high, and the accuracy is lower compared to machined parts. Plastic on plastic generally results in a lot of friction.

The most challenging parts to 3D print were the memory rings and the shafts. These parts include the smallest extruded areas. The geared profile should be sufficiently form fit, to provide the rotational input. On the other hand, there must be some spacing to make sure the rings can translate along the shafts with low friction. See Figure 7.3. If the spacing is too small, the memory rings would not fit around the shafts. Or, they do fit, but the friction for the linear motion of the rings is too high, which is undesired. Making the spacing too large would cause play. For example, if dimension A (Figure 7.3) is too large, the rings can rotate relative to the shaft (around the roll-axis). When dimension B is significantly large, the memory rings can rotate around the pitch axis. Pitch can cause jamming of the memory rings on the shaft, possibly blocking the translational motion. Jamming is presumed to be limited, because the eight memory rings are placed in series and the translational motion mechanism packs them together.

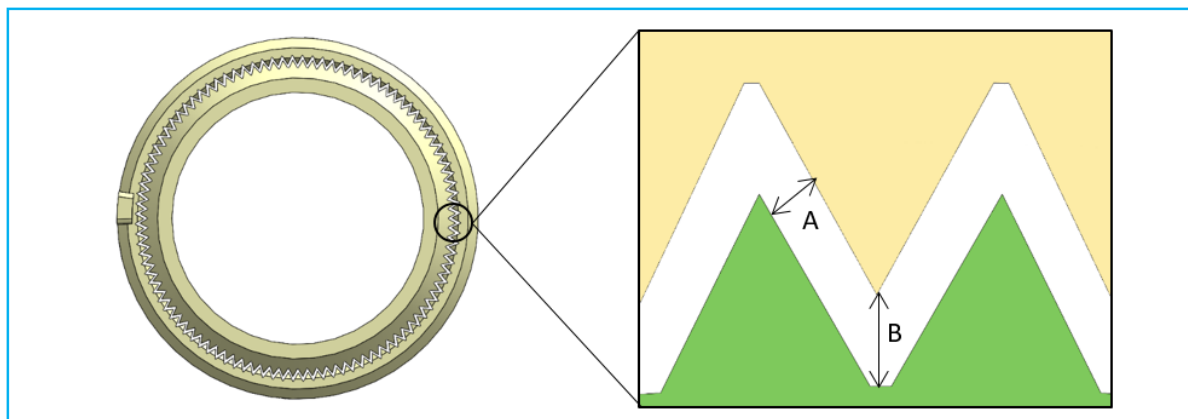


Figure 7.3: Spacing for the geared profile in the 3D printed prototype. In the zoomed-in image, the green teeth are from the shaft and the yellow from the memory rings.

Table 7.2: Spacing used for the printed shaft and memory rings. Three versions have been tested. Version 1 with little play, Version 2 with a lot of play and Version 3 with a little less play compared to Version 2. Dimensions A and B correspond to the dimensions in Figure 7.3.

Version	Dimension A [mm]	Dimension B [mm]
1	0,077	0,10
2	0,33	0,55
3	0,22	0,38

Three versions of the memory ring were printed subsequently. The dimensions are shown in Table 7.2. The spacing of version 1 turned out to be too small. A lot of force was necessary to place the memory ring on the shaft: translating the ring was not possible. A second version was designed with more spacing. The spacing was enlarged significantly, because the previous test showed that the printed shaft and the memory rings contained inconsistencies, such as left-over plastic between the teeth that had cured. The second version moved smoothly on the shafts. However, as expected, the ring had a lot of play. The spacing was reduced for the third version. Simultaneously with the third version, a section of a shaft and one ring with rectangular teeth were printed as well. The design can be found in Figure E.24 in Appendix E. Both provided an acceptable result. The design with the geared teeth was chosen, because this resembled the original prototype more. The memory rings of the third version could slide over the axis smoothly. Also, the transition from the input shaft to the fixed shaft performed well. The rings could still rotate around the pitch axis, however it was deemed to be acceptable for the proof of principle. The translational motion mechanism would help to avoid jamming by packing eight memory rings together.

The prototype is a concentric design, including many parts that have to rotate or translate with respect to each other. Initially, all FDM-parts were given a fixed spacing of 0.15 mm on each side, thus 0.4 mm difference in diameter. For some parts, this was not sufficient. Table 7.3 shows the inner and outer diameters of the main parts. The table shows the components and their position relative to other parts. For example, the translational motion mechanism is located around the memory rings and moves inside casing 1 and the reading rings. This means that the inner diameter of the translational motion mechanism should be larger than the outer diameter of the memory rings. It also means that the outer diameter of the translational motion part should be smaller than the inner diameter of the casing and reading rings. As can be seen in Table 7.3, in many parts the spacing was between 0,4 and 0,6 mm in the final design. The construction drawings of all the parts are provided in Appendix E. Most parts needed to be sanded or manipulated with a file, to remove the rough surfaces and edges. Especially the translational motion parts seemed to be blocking with the reading rings and their frame, due to its rough surface.

The holes for fasteners were modelled with the exact diameter of the fastener. Printing a small hole with an inner thread was not possible. Thus, by making the diameter of the hole exactly the size of the screw, inserting the screw would plastically deform the hole and cut away a threaded profile. This fastened the screw in the hole. Naturally, after inserting and removing the screw multiple times, the hole was widened because of wear. This was a limitation of the 3D printed design: fastening components to each other was challenging.

The H-beam was modified as well. Replacing the ball bearings of the memory rings and reading rings with M1 screws, required the H-beam to have a smaller width and smaller spacing in between the ribs. If the gaps between the ribs of the H-beam (t_g) were designed too large, the M1 screw would not be guided by the H-beam but slip out of the H-beam through the gaps. On the other hand, the gaps could not be made very small. Partly, because the part was limited by the printing accuracy. The printer could not achieve very small gaps: some gaps cured, resulting in a very stiff H-beam. Also, an H-beam with small ribs could not make sharp angles, as the ribs on the inner side of the curve were compressed together and blocked the bending motion. Thus, giving dimensions to the H-beam was a trade-off between being able to keep the screws in place and being flexible. The H-beam used in the prototype had ribs with 1 mm thickness and gaps of 0.35 mm.

Table 7.3: Spacing between the 3D printed parts in millimetre. The parts and their inner and outer diameter are shown. The last two columns show the part's location with respect to other parts. One column showing what is on the inside, the other column what part should fit around it. For the shaft and memory ring, the dimensioning of the gear profile is provided in the text.

Part	Inner Diameter [mm]	Outer diameter [mm]	Around	Inside
Inner shaft	20	24.7	-	Shaft
Shaft	25.1	Teeth profile	Inner shaft	Memory rings
Memory ring	Teeth profile	36.0	Shaft	Translational motion mechanism
Translational motion mechanism	37	50.0	Memory ring	Casing front, Reading rings
Reading ring	50.45	54.0	Translational motion mechanism	Casing middle
Casing front	50.5	54.0	Translational motion mechanism	Casing middle
Casing middle	54.4	60.5	Reading rings	-

7.5. Testing the prototype

7.5.1. Test method

Testing the prototype was done simultaneously with the manufacturing of the prototype. Each printed component was tested, with the intention to see if the component fitted or needed additional spacing to function properly. Similar to the machined prototype, the 3D printed prototype was tested in four main steps:

1. Individual parts and subassemblies
2. Prototype without H-beam
3. Path input: H-beam
4. Path input and output: complete prototype

In the first step, individual parts and subassemblies were tested. This step was necessary to determine the right spacing between parts. In the second phase, the complete prototype was tested without the H-beams. This phase functioned as verification to see if the main components would move without friction and jamming. Also in the 3D printed design, the H-beam was expected to be the key component. Therefore, the complete prototype should function well without the H-beam. The third phase included the testing of the path input. The results for the path input were expected to be different from the machined prototype, because the H-beams used have different dimensions. In this test phase, the H-beams in combination with the memory rings and translational motion mechanism were examined. The ability to form diagonal, curved and alternating paths were tested, in combination with the rotating, sliding and locking of the memory rings. The last phase was conducted with the completely integrated prototype. The function of the H-beam as guiding mechanism was examined. This step tested what type of paths can be created as output with the 3D printed prototype.

7.5.2. Test phase 1: individual parts and subassemblies

Similar to the machined prototype, the memory rings and shafts were manufactured and tested first. After that, the other parts were printed, starting with the inner components and ending with the casing. The desired behaviour of the 3D printed prototype is the same as for the machined prototype. The results are shown in Figure 7.4. All parts needed optimisation based on dimensions, as described in section 7.4. The chosen dimensions for the memory rings resulted in a good working linear motion of the memory rings. The translational motion mechanism in combination with the shafts and memory rings worked acceptably: the rings slid with minimal force over the shafts. The transition from the input shaft to the fixed shaft worked well when the shafts were aligned. The 3D printed prototype was a simplified version of the machined prototype. Therefore, the 3D printed mechanism did not include haptic feedback mechanisms for the rotational or translational motion. Shifting the memory element from one shaft to the other, required the user to try and find the right position to align the shafts. Also, due to the lack of haptic feedback, the user did not know when a ring was slid from one shaft to the other. The user must find the right position by rotating the input shaft. If a ring was positioned at the transition

Testing individual parts and subassemblies	Desired behaviour	
Memory rings and shafts	<ul style="list-style-type: none"> - Input shaft rotates with minimal friction - Memory rings slide with minimal friction - Smooth transition from one shaft to the other shaft 	<ul style="list-style-type: none"> ✓ ✓ ~
Memory rings and translational motion mechanism	<ul style="list-style-type: none"> - Translational motion mechanism slides with minimal friction over the shafts - Translational motion mechanism moves the memory rings from shaft to shaft - Memory rings can rotate freely inside the translational motion mechanism 	<ul style="list-style-type: none"> ✓ ✓ ✓
Reading rings and Teflon frame	<ul style="list-style-type: none"> - Reading rings rotate with minimal friction 	<ul style="list-style-type: none"> ✓
Reading rings and translational motion mechanism	<ul style="list-style-type: none"> - Reading rings rotate with minimal friction around the translational motion mechanism - Translational motion and reading ring frame do not touch while translating 	<ul style="list-style-type: none"> ~ ✗

Figure 7.4: Testing individual parts and subassemblies of the 3D printed prototype. The functionalities have been tested manually, to see if optimisation is required before the complete prototype is assembled. A green check-mark means that the desired behaviour is accomplished. An orange tilde means that it is required for further research. A red cross means that the desired behaviour is not met and optimisation is required.

point, exactly at the ends of the two shafts, the input shaft could not be rotated. Ergonomically, this was not desired, but for a proof of principle it was considered sufficient. Therefore, the smooth transition function was given an orange tilde in Figure 7.4. The reading rings rotated freely inside their frame: the rotation did not require much force. However, they had a lot of play and could translate inside the frame: the reading rings could move up and down inside their frame. The consequences of the play were further examined and evaluated in test phase 2.

7.5.3. Test phase 2: prototype without H-beam

The 3D printed prototype must function properly when no H-beams are present. The H-beams are expected to be the critical parts of the design, because this was concluded from the test results of the machined prototype. Phase 2 functioned as verification to see if all components moved without friction and jamming. Therefore, the rotational motion and translational motion of components in the integrated design were examined. The desired behaviour included that the memory rings should rotate and translate with minimal friction. Also, the translational motion mechanism must be prevented from rotating and should only provide a linear motion. The reading rings should rotate freely inside the reading ring frame and their pins must be guided by the slot in the translational motion mechanism. When parts are moved relatively to each other, jamming should not occur. The desired behaviour of the prototype without H-beam and the test results are shown in Figure 7.5.

The motion of the components functioned properly: both the reading rings and memory rings rotated with minimal input force required. The memory rings combined with the translational motion assembly performed well. The linear motion of the memory rings did not require a lot of input force from the user. However, as evaluated in test phase 1, the incorporation of haptic feedback for translational and rotational motion would enhance the ease of use. The input knob for the linear motion had too much play causing it to rotate around its fasteners. This limited the ease of use, but did not influence the performance of the prototype. The reading rings were able to rotate very easily, because they were given a lot of space with respect to the translational motion mechanism. A downside of this spacing was that the reading rings had too much play. Consequently, the reading rings could move up and down inside their frame. The weak and uneven design of the frame elements was not capable of keeping the reading rings in place. This effect can be seen in Figure 7.6, in which the reading rings are shown in their casing. The reading rings were not aligned: some moved up, other rings were positioned lower. The difference in position is represented by the blue line in Figure 7.6. The amount of play is undesired, because the reading rings would lean on the translational motion mechanism, resulting in much friction or jamming. Optimisation of the reading rings and their frame is required for a refined design.

Testing prototype without H-beam	Desired behaviour	
Rotational motion	- Memory rings rotate along with the input shaft	✓
	- Memory rings rotate with minimal friction	✓
	- Reading rings rotate freely inside the Teflon rings	✓
	- The casing prevents the translational motion mechanism from rotating	✓
Translational motion	- Memory rings translate with minimal friction	✓
	- Memory rings can slide smoothly from one shaft to the other shaft	~
	- Translational motion mechanism does not jam against the reading rings	✗
	- Translational motion mechanism does not jam against the casing	✓
	- Pins of the reading rings are guided by the slot of the translational motion mechanism	~
	- Haptic feedback when a memory ring is slid from one shaft to the other shaft	✗

Figure 7.5: Testing the prototype without the H-beam. Phase 2 functions as verification to see if all components move without friction and jamming. A check-mark means that the desired behaviour is accomplished. An orange tilde means that optimisation is required for further research. A red cross means that the desired behaviour is not met with the current prototype.

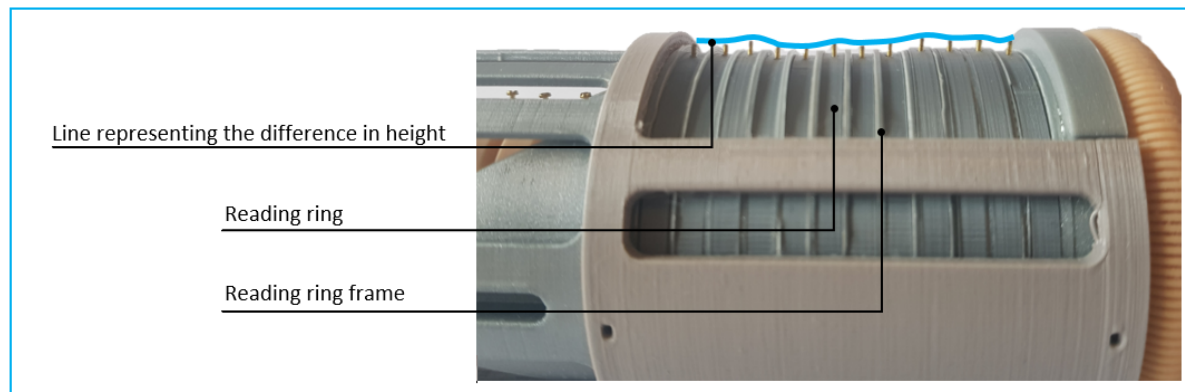


Figure 7.6: 3D printed prototype: play in reading rings. Due to too much spacing, the reading rings can move up and down in their frame.

In general, the complete mechanism did have a lot of friction: translating and rotating parts relative to each other made noise. This was expected, due to the material properties and printing accuracy of the components. All FDM components had a rough and inconsistent surface. It is concluded that even with this friction, the 3D printed prototype worked acceptably without the H-beam, to function as a simplified version of the machined prototype. The reading ring frame has to be adjusted to improve the performance, this is discussed in Chapter 9.

7.5.4. Test phase 3: path input

In the third test phase, the H-beam was tested on the memory rings including the translational motion mechanism. Compared to the machined prototype, the H-beam was made smaller with smaller gaps to guide the M1 screws instead of ball bearings. The smaller dimension t_g made the H-beam stiffer than the H-beam used in the machined prototype. Therefore, additional tests needed to be done to determine the performance of this H-beam.

The rotation and translation of the memory rings had been tested, while inserting different paths:

1. Diagonal shape
2. Single-curved shape
3. Multi-curved shape
4. Alternating shape

Figure 7.7 shows pictures of the results for the path input mechanism. In these tests, the H-beam was not fastened to the translational motion part. The connection of the H-beam to the translational motion part was not adequate. The holes for the screws in the translational motion mechanism did not form properly, making the fixation of the H-beam difficult. In the tests, the lower flanges of the H-beam captured the bearings of the memory rings. The 3D printed prototype in combination with the H-beams was able to make straight and diagonal paths. Some small curved paths could be formed, similar to the curve shown in the second row of Figure 7.7. The H-beam was not able to form larger curves and S-shapes, as the H-beam started to deform and the screws tended to move out of the H-beam. Consequently, an alternating pattern was also not achievable, because it caused major deformations in the ribs of the H-beam. As can be seen in the picture shown in the bottom row, a pin moved out of the H-beam. This is a design limitation of this prototype. The results showed that the H-beam design was not sufficient. The smaller design with a small gap between the segments, was more stiff, which limited the path formation in the H-beam. It did not perform as well as the input of the machined prototype. A summary of the results is provided in Figure 7.8.

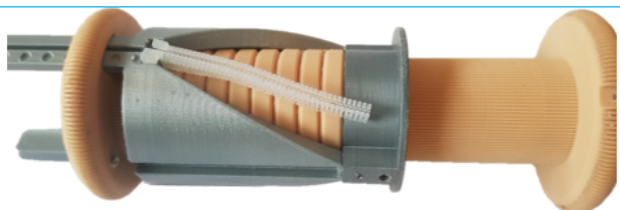
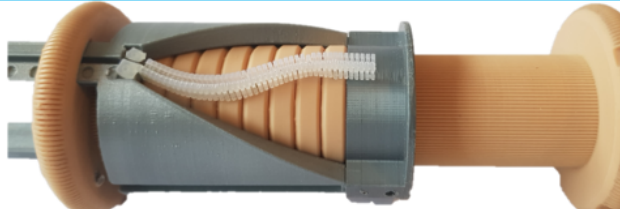

Path input	Picture	Prototype abilities
Diagonal shape		Yes.
Curved shape		Inconsistent. A small single curve is possible (picture on the left). Bigger S-shapes are not possible
Alternating		No. The M1 screws move out of the H-beam. Causing plastic deformation of the H-beam

Figure 7.7: Test phase 3: the input function of the 3D printed prototype. The H-beam is placed over the M1 screws of the memory rings. The flanges of the H-beam capture the screws of the memory rings. The rotation and translation of the memory rings have been tested, while inserting different paths. The 3D printed prototype in combination with this H-beam design is able to make straight, diagonal and simple curved paths. The performance of the design for curved paths is inconsistent. An alternating pattern, shown in the bottom row, causes deformation in the ribs of the H-beam. The H-beam is plastically deformed and derailment occurs.

Testing the path input: H-beam	Desired behaviour	
Path formation	The H-beam can form different types of paths, without deformation or derailment of the bearings: <ul style="list-style-type: none"> - Diagonal path - Single-curved path - Multi-curved path - Alternating path 	 ✓ ~ ✗ ✗

Figure 7.8: Testing the path input: the performance of the H-beam. The H-beam must be able to form diagonal, curved and alternating paths. A check-mark means that the desired behaviour is accomplished. An orange tilde means that optimisation is required for further research. A red cross means that the H-beam did not meet the requirement.

7.5.5. Test phase 4: complete prototype

The compliant shaft of the instrument should be able to make single-curved and multi-curved forms. A single curvature is achieved by a diagonal path in the reading rings. Other paths require curved or alternating patterns in the reading rings. Therefore, the integrated prototype should be able to form a diagonal, curved and alternating shape in the reading rings. Test phase 3 concluded that S-shapes and alternating patterns could not be provided with the current guiding element. Consequently, the integrated prototype was not tested on the ability to form multi-curved and an alternating. Two types of paths were examined:

1. Diagonal shape
2. Single-curved shape

The fourth test had negative results: the 3D printed prototype was unable to form any path as output. The test evaluation is presented in Figure 7.9. The main problem was that the translational motion jammed when the H-beams are incorporated in the design. Multiple factors contributed to this problem: the H-beam design, the H-beam connection and the play of the reading rings. The connection of the H-beam to the translational motion part was not adequate. The holes for the screws in the translational motion mechanism did not form properly, therefore, the fixation of the H-beam is not secured sufficiently. The H-beam could rotate around its fastening points, blocking the translational motion. As a result, the pins of the reading rings jammed against the H-beam. The play of the reading rings contributed to the blocked translational motion: the reading rings leaned on the H-beam causing additional loading on the H-beam. A lot of force was required to force the path into the reading rings. Consequently, the fragile design of the guiding element deformed. During the tests, the H-beams broke multiple times at their connection points due to fatigue. Optimisation of the H-beam, the H-beam connection and reading rings is required to test the prototype properly.

Testing the complete prototype	Desired behaviour	
Path formation	The reading rings can form different types of paths, without deformation or derailment of the bearings: <ul style="list-style-type: none"> - Diagonal path - Single-curved path - Multi-curved path - Alternating path 	 ✗ ✗ ✗ ✗

Figure 7.9: Testing the path output of the 3D printed prototype: the performance of the integrated prototype. The prototype should be able to provide diagonal, curved and alternating paths as output. The red cross means that the prototype was not able to form that path.

7.6. Design evaluation

7.6.1. Functionalities of the 3D printed prototype

The first two test phases showed promising results. There was friction present in the prototype, however the motion of the components relative to each other did not require much force and was deemed to be acceptable. A point of concern was the spacing of the reading rings: the reading rings had too much play, causing them to move up and down in their frame. The third and fourth test phases revealed the malfunctions of the 3D printed design. The H-beam did not function sufficiently. The adjusted design was stiffer than the H-beam used in the machined prototype. The guiding element deformed majorly in curved and alternating paths, due to lack of flexibility. This limited the guiding functionality of the H-beam. Only a straight or diagonal path could be formed. A common failure mode was that an M1 screw moved out of the H-beam, while deforming or breaking the ribs of the H-beam. In the integrated design, the translational motion was blocked and no path could be formed. The H-beam jammed with the pins of the reading rings, but also with the reading rings themselves as they could translate inside the reading ring frame. It is concluded that the 3D printed prototype could not provide the follow-the-leader motion in its current state. Optimisation of the H-beam and its connection points is required to test the prototype properly. This is further discussed in Chapter 9.

7.6.2. Benefits and downsides of 3D printing

The 3D printing manufacturing method implies advantages and disadvantages. 3D printing is a cheap and relatively fast method compared to machining methods. Therefore, if a component needs to be adjusted and improved, the component can be printed again. For example, during the production of the 3D printed prototype, the translational motion mechanism had been printed four times with the Ultimaker to minimise its friction and replace broken parts. Another benefit of the 3D printing method is that some assemblies could be simplified by printing them as one part. For example, the shaft was printed in combination with the input knob as one part. It was expected that the shaft and memory rings would be the most challenging to print, because of the geared profile. Against expectations, the shaft and memory rings turned out well. The SLA printing technique showed good results. Components printed with fused deposition modelling required more attention, which will be elaborated below. A significant benefit of the 3D printing technique is that the manufacturing method does not require many hard skills. The machine prints the components for you, the only actions required are the removal, cleaning and, if applicable, the curing of the part.

However, 3D printing the prototype did bring drawbacks and challenges in different forms. The challenges are mainly based on the material properties and printing accuracy. The layer-by-layer build-up of the parts, resulted in surface roughness. Especially the parts printed with the Ultimaker (FDM), had uneven surfaces. The printing layers were clearly visible. The right picture in Figure 7.10, shows the surface roughness of the translational motion part. The problem of the surface roughness and uneven layers is that it causes friction between moving parts. To limit the friction, the parts had to be sanded or given more spacing. The surface roughness of parts printed with stereolithography is less. However, residual resin that could not be removed with alcohol, resulted in uneven areas. The resin located at undesired areas, cured and became hard. For example, the printed shafts contained some inconsistencies between the geared profile. Consequently, these inconsistencies had to be removed with a file, because the linear motion of the memory rings jammed at certain locations. Another example is that the support of the input knob could not be removed properly, causing an uneven surface. Besides surface roughness, the layer-by-layer build-up of the components makes components weak. Loading the layers under tension, pulls the layers apart. This is called delamination. Therefore, parts with only a couple of layers width or thickness are weak. For example, the blocks that form the connection between the main and front part of the translational motion mechanism, delaminated and broke. This failure mode is shown in Figure 7.10. Only FDM printed components of this prototype broke, SLA printed parts were strong enough to fulfil their function.

Due to the low accuracy of printers compared to machining methods, small features such as holes for fasteners, did not form. This was a problem for both the FDM and SLA printed parts. In FDM printed parts, the holes turned out too small, oval or did not form at all. For SLA printed parts, the resin stayed inside small features. Consequently, the holes cured along with the rest of the component. Sometimes,

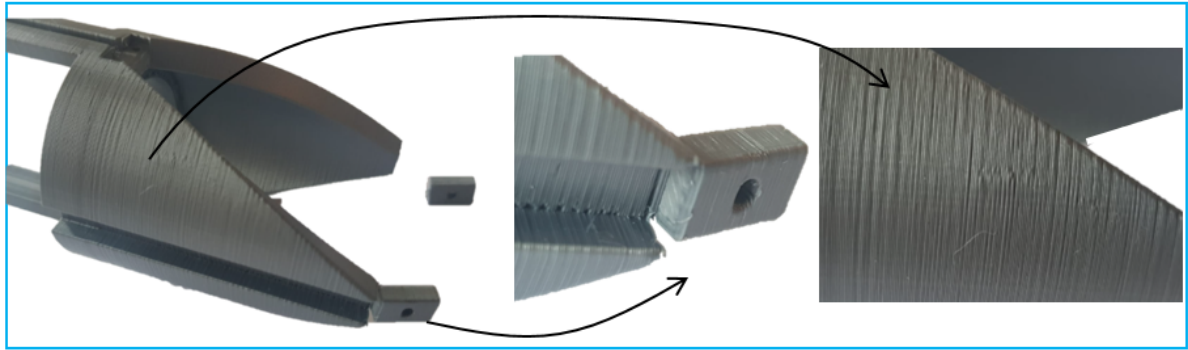
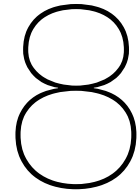


Figure 7.10: Common downsides in 3D printed components: breaking and surface roughness. This is the translational motion mechanism. The first failure mode is the breaking of parts. Polymers have a lower strength than metals. Also, the layer-by-layer design, makes the component weak if the layers do not completely stick together. Loaded the layers with tension, can pull the layers apart. The image in the middle shows dilamination, causing the part to break off. The other downside of 3D printing is the surface roughness. The layer-by-layer build-up can result in uneven surfaces. The most right image shows the surface roughness of the translational motion mechanism. The layers are clearly visible. The surface roughness causes undesired friction.

the hole was already partly cured during the printing process: the laser moving around the hole cured the resin partially. Most parts required to be manipulated with a file afterwards, to be able to fit the fasteners. The same problem arose while printing the H-beam. Because M1 screws are used to replace the 3 mm ball bearings, the H-beam needed to be reduced in size, with smaller spacing in between the ribs (t_g). The possible reduction in t_g is limited, as the ribs of the beam will stick together and cure as one solid beam if t_g is too small. Because of the lower accuracy of the printers, much more spacing between moving parts was required. The downside of this much spacing is the occurrence of jamming, due to play. For example, the reading rings had too much play and could move up and down in their frame. So, there was a trade-off between moving smoothly and having too much play. Finding the right spacing was an iterative process, in which some parts had to be printed multiple times.

Thus, 3D printing is a relatively fast and cheap manufacturing method. However, the downside of the 3D printed prototype is that the design requires continuous remodeling, sanding and filing the components, which is still a time consuming task. Also, the components are weaker than machined metal components. Thus, machining gives better results when the manufacturing job includes a complex design with many moving components and a difficult loading of the components. This also reflects on the performance of the 3D printed prototype compared to the machined prototype, which will be further elaborated in the discussion.



Design implementation

8.1. CPMM in a surgical instrument

The CPMM prototype can provide the path planning on one plane. To produce a 3D motion in the shaft, two CPMM modules are necessary. One module is responsible for the motion in the horizontal plane, and a second module manages the motion in the vertical plane. A combination of these planar motions results in a 3D motion. In the first sketch, shown in the chapter Mechanism Design, the CPMM modules were positioned in each other's length, resulting in a T-shape. This arrangement is not space efficient. Two other configurations are proposed for the incorporation of the CPMM modules in the tool. Drawings of the concepts are given in Figure 8.1. In the first concept, the modules are placed next to each other with their length along the horizontal plane, as can be seen in Figure 8.1A. An alternative is shown in Figure 8.1B, in which the modules are placed next to each other, with the input knobs facing upward. Both configurations have advantages and disadvantages. Looking at the drawings, concept A is more space efficient. Concept B will result in a square-like instrument, while concept A will be a long cylindrical tool with a small height. Therefore, concept A is more space efficient and aesthetically more pleasing. However, the guidance of the cables from the modules towards the compliant shaft is more simple in design B compared to design A. In design B, the cables have a straight path towards the funnel-shaped casing. Guiding the cables can be done with an open or closed structure. Additional parts, such as pulleys are not necessary. The cables in design A make a 90 degrees angle towards the compliant shaft of the instrument. To make sure the cables are not tangled and move with limited friction, a closed structure is required. Pulleys and rounded-off edges are needed to guide the cables towards the funnel. Consequently, design B is easier to manufacture, but design A is ergonomically and aesthetically better. Concept A is chosen as final design for the implementation of two CPMM modules in the complete surgical tool. Some additional components are introduced to pack the two modules in one instrument and guide the cables towards the shaft: a cable guiding mechanism, a funnel that converges the cables towards the shaft, a casing around the two modules and a stable base.

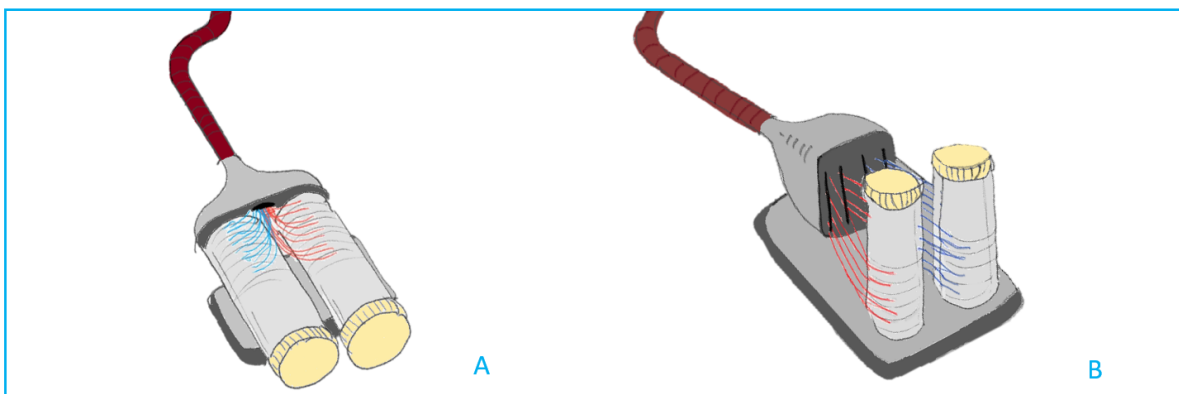


Figure 8.1: Concepts for CPMM incorporated in surgical instrument

8.2. Incorporated design

Figure 8.2, shows CAD-drawings of the surgical tool. The presented design is not a final and definite design of the complete mechanism, however it is a suggestion for how the path programming mechanisms can be incorporated into a surgical instrument. In this design, the CPMM modules are placed next to each other and are fixed in an outer casing.

The outer casing is made from perspex, making the instrument see-through. The user can see the path that is given as input. A metal frame supports the casing and is connected to a base. A slot in the metal frame guides the translational motion of the memory rings. This can be seen in Figure 8.2B, the side view of the instrument. Input knobs, here made from brass, are attached to the translational motion mechanisms of the CPMM modules. It is required that the linear motion of the right module and left module is done simultaneously. In other words, the memory rings for the up and down movement and the memory rings for the left and right movement of the compliant shaft, should slide at the exact same moment. Otherwise, the corresponding segment moves in one plane first and then in the other plane, instead of one smooth movement. Therefore, the two translational motion mechanisms are joined. Here, the input knobs are incorporated on both sides of the instrument, to make it a symmetrical design. The user controls the sliding of the memory rings by pushing and pulling the knobs. Instead of pushing and pulling, the design can also be modified into a rotational input. A rack and pinion mechanism is an alternative design. If the slot is given a gear profile, it will function as the rack. The knob and translational motion mechanism are attached to a pinion. The knob is directly attached to the pinion, while the translational motion mechanism should not rotate along with the pinion. In this way, rotating the knob would cause a linear motion of the memory rings. The design presented in Figure 8.2 has a stationary base. In reality, the whole tool itself should translate while it is being inserted in the patient's body. The insertion of the path has to be done simultaneously with the insertion of the tool into the body. Therefore, in the final design the base is not stationary but is able to slide back and forth. An additional transmission is required to couple the forward motion of the base with the pushing of the memory rings, and the backward motion of the base with the pulling of the memory rings.

The cable guidance can be done with a closed structure containing pulleys and a funnel. In this design, it is presented as an hourglass-shaped block, that is form fit with the path-planning modules. Each cable is packed individually, to avoid tangling of the cables. The cable guiding component contains small curved passages, with entry points directly next to the reading rings, a path turning roughly 90 degrees, and exit points directed to the compliant shaft. The use of small pulleys inside the component, makes sure that the cables make the 90 degree turn with minimal friction. The guidance part is complex with small passages, consequently it needs to be divided into a couple separate parts to machine it and to be able to build in the pulleys. When the cables leave the guiding mechanism, a funnel converges the cables towards the compliant shaft with an outer diameter of 8 mm. Implementing two Cryptex mechanisms into the tool, results in 30 sets ($N = 60$) of antagonist cables running through the compliant shaft. To do so, the four cables that are fixed on a segment are twisted around its centreline over 6 degrees compared to the previous segment to prevent the cables from overlapping and interfering.

The dimensions of the proposed medical instrument, including the base and excluding the compliant shaft, are 230x150x135 mm (l x w x h). If a smaller instrument is preferred, the base can be reduced in size. The length and width of the tool mainly depend on the size of the path-planning mechanisms. The current design of the CPMM module has an outer diameter of 60 mm and a length of 150 mm. This is relatively large, as it functions as a proof of principle. Minimising the size of the path-programming modules, would reduce the size of the complete instrument. The prototype was developed for validating the functionality of the proposed concept. The mechanism is not designed for direct use in a medical setting. In order to implement the path-planning module in an actual medical instrument, it should meet all current medical instrument regulations and protocols. Chapter 9 shortly elaborates on the CPMM in a medical setting.

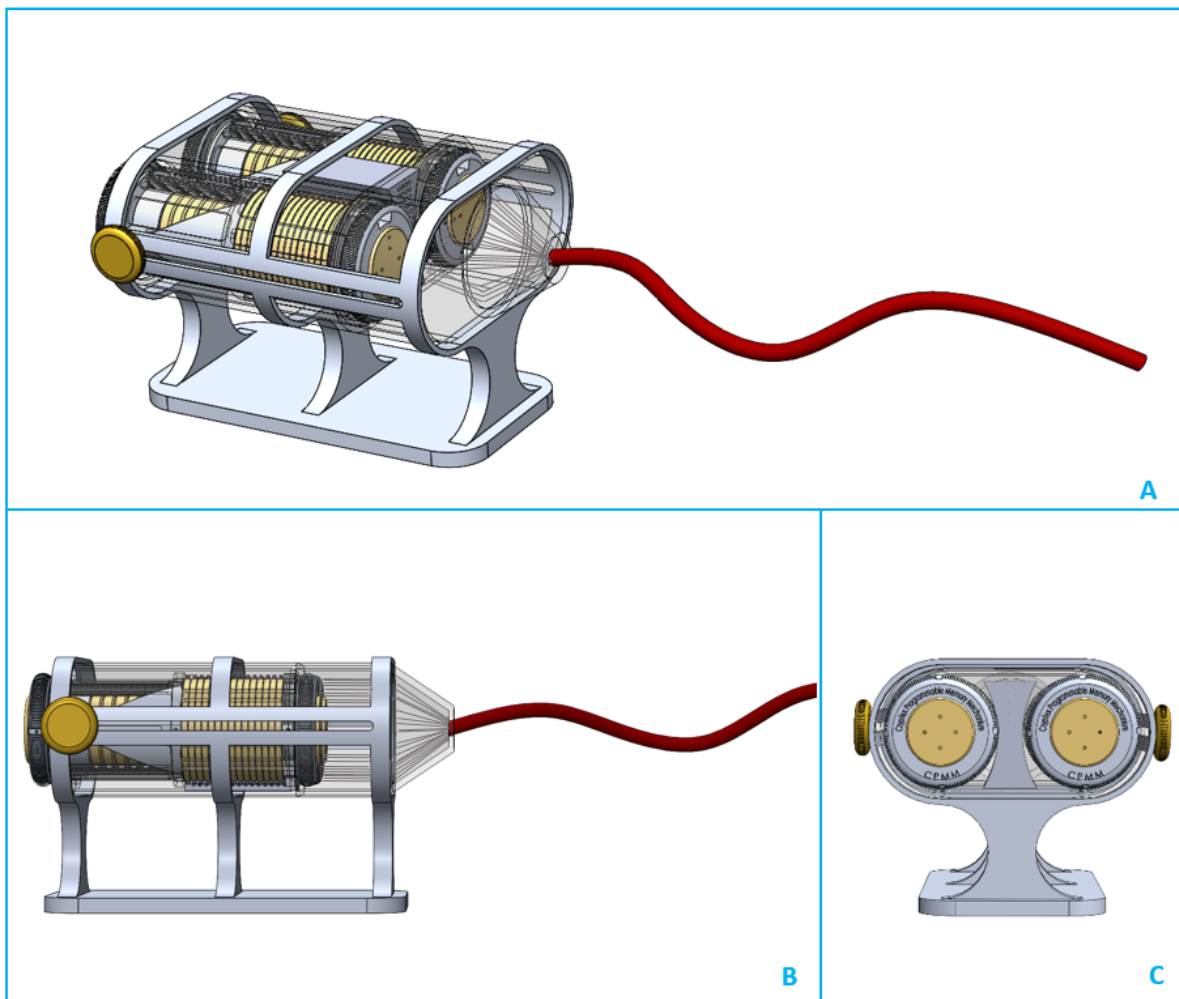


Figure 8.2: CAD drawings of the surgical instrument, including the Cryptex path-planning modules. Figure A shows the three-dimensional view of the model. Figure B is the side view and Figure C the back view. This model does not include the actual tools yet, such as graspers and clipping devices. An entry point is necessary in the casing.

9

Discussion

9.1. Machined prototype

9.1.1. Performance of the prototype

The path-planning mechanism is designed to enable the user to insert and repeatedly change the path that is formed by the shaft of the minimally invasive surgery instrument. In theory, the CPMM module should be able to form 390625 different paths, because there are 8 memory rings and each ring has a steering range of 5 positions: the middle position and two steps to the left and right. Based on the calculations, one step input will result in an angular displacement between 20 and 32.3 degrees with a compliant H-beam and stiff H-beam respectively. Since the CPMM module is a concentric design, the angular displacement (β) for the memory rings is the same as the angular displacement of the reading rings, however the arc length displacement is dependent on the radii of the rings (r_M and r_r). Thus, a ratio exists between the memory ring input and reading ring output. With an infinite stiff H-beam that does not provide any play, the ratio completely depends on the ratio of the input and output radii. The input-output ratio comes closer to one when a compliant beam is used. The latter is the case in this prototype, because the durable material and the segmented design of the H-beam make the component flexible. Additional tests should be performed to quantify the input-output relations and to determine if the functional requirements are met. Assuming one step input results in a 25 degree angular displacement, each input ring can provide a maximum output angular displacement of 50 degrees, namely two input steps. Also, theoretically, the CPMM design should be able to form one single curvature with a maximum angle of 400 degrees, which is equal to the amount of memory rings times the maximum output angular displacement.

In Figure 9.1, the performance of the prototype is compared to the functional requirements set at the beginning of the design process. A green check means that the prototype meets the requirements well. An orange tilde is given when the performance of the prototype partially meets the requirements, but some optimisation is necessary. The requirements assigned with a red cross were not achieved with this prototype. The functional requirements focus on the overall working mechanism of the prototype. The introduced CPMM prototype is fully mechanically actuated and designed to control shaft segments by the pulling and releasing motion of cables. One path-planning module can control the motion on one plane, thus provides the control of one cable and its antagonist. The path planning is done by the user, in discrete steps of 1 mm. The teethed profiles of the input elements ensured the stepwise input. The CPMM design gives the user the opportunity to continuously insert and adjust the path. Thus, functional requirements 1 and 2 are met with the CPMM prototype. The path formation in the compliant shaft is the output of the mechanism. Functional requirements 3.1 - 3.5 cover the desired behaviour of the path output in the compliant shaft. The CPMM is the controller only, which excludes the cables and the compliant shaft. Therefore, functional requirement 3.2 is not met. However, the design includes 15 reading rings, which means that a compliant shaft with 15 segments can be coupled to the controller.

Functional requirement	Performance of the prototype
1. Actuation of the total design	
1.1 Mechanically actuated	✓
1.2 Four cable control of the compliant shaft	✓
2. Path planning by the user (input)	
2.1 Path planning existing out of 3 modes: past, present, future	✓
2.2 Step wise path input	✓
3. Path formation in the compliant shaft (output)	
3.1 Control a compliant shaft with at least 11 segments	✓
3.2 Cable guidance from CPMM to compliant shaft	✗
3.3 Improving cable guidance by making the prototype cylindrical	✓
3.4 Multi curvature with 40 degree angle per segment	~
3.5 Single curvature of 170 degrees	✓

Figure 9.1: Performance of the prototype compared to the functional requirements. A green check means that the prototype meets the requirements well. An orange tilde is given when the performance of the prototype partially meets the requirements, but some optimisation is necessary. The requirements assigned with a red cross were not achieved with this prototype. See text for explanation.

The tests performed with the prototype showed that the prototype was able to provide the follow-the-leader motion. The path was transferred distally over the reading rings. The results are elaborated in sections 6.4. and 6.5. The prototype could form diagonal, single-curved and simple multi-curved paths in the reading rings. A diagonal shape in the reading rings provides one large single curvature in the shaft. The path formation has not been measured and quantified yet, but theoretically one step input would result in an angular displacement of minimally 20 degrees. A small diagonal shape, in which each memory ring is rotated with only one step relative to the previous ring, would already result in a 160 degrees rotation. A larger diagonal shape, in which each memory ring has been given an input of 2 steps, results in a single curvature of 320 degrees. Thus, it is expected that functional requirement 3.5 is met, but quantification is necessary to substantiate this. The prototype could form simple curved paths, but the formation of alternating patterns and sharp multi-curved paths was not achieved with the current design. For this reason, functional requirement 3.4 is assigned with a tilde.

Figure 9.2 on page 106 compares the performance of the prototype to the element design requirements. The element design requirements are more component-specific, and therefore evaluate the path input performance separate from the path output. Assessing individual parts and subassemblies separate from the integrated design, is important in order to see which functions work well and which components are actually critical. The prototype was tested in four phases, described in section 6.4. Test phase 1 focused on the individual components and subassemblies, and test phase 2 examined the complete prototype without the H-beam. These test results are compared to the design requirements for the memory elements and for the reading elements. In test phase 3 the H-beam was evaluated solely, because this gave insights to what types of paths could be formed with the guiding element. The last phase, test phase 4, examined the completely integrated design including the H-beam. Comparing the test results of the integrated design without the H-beams with the test results from phase 4, shows how the H-beam functions as guiding element. This is necessary to evaluate requirements 4.1 and 4.2.

The memory rings meet most requirements. In the conceptual design phase, the memory rings were expected to be critical, due to the loading on the teethed profile of the memory rings. Fortunately, the memory rings functioned well as input elements. The machined CPMM prototype contains 8 memory rings, which provided the path input in steps of 1 mm. The teethed profile of the input elements ensured this stepwise input. The performance of the memory rings in combination with the shafts and translational motion mechanism was very good. The rings rotated along with the input shaft and were locked when they were positioned on the fixed shaft. The rotational motion did not require much input force, because the memory rings could rotate freely inside the translational motion mechanism. The

translational motion of the memory rings on the shafts also required little input force from the user: the memory rings slid smoothly over the shafts. The haptic feedback for the translational motion of the memory rings worked sufficiently, providing a force and sound feedback when one ring was slid from one shaft to the other. To transfer the memory ring from one shaft to the other shaft, the shafts had to be perfectly aligned. Requirement 2.4 is the only design requirement for the memory rings that is not met. Haptic feedback for the rotational input was a wish to improve the ergonomics. In this prototype, no haptic feedback mechanism is incorporated in the design for the stepwise input. Proposed designs, such as the Hirth coupling, could be a solution. In the current design, the user had to try and find the right orientation to align the shafts. This limited the ease of use, but did not limit the functionality of the path input by the memory ring. Thus, the path input works acceptably.

Fifteen reading rings are incorporated in this design. Small pins were manufactured on opposite sides of the reading rings, which represent the attachment points for the antagonist cables. The reading rings function as path output, because their rotational motion provides the pulling and releasing of the antagonist cables. In test phase 1, it was concluded that the reading rings could rotate well, however some rings required more force than others, despite the Teflon frame between the reading rings. Less friction is desired for an optimal design. Therefore, design requirement 3.4 is assigned with an orange tilde. The other design requirements are met. The design limitation of the reading rings will be further elaborated in the next subsection. The guidance of the cables from the reading rings towards the compliant shaft is not implemented in the final design. The pins in the reading rings are screwed into the reading rings. Therefore, they can easily be replaced with another design. Design requirement 5.1 and 5.2 are not met, but can be implemented with minimal effort. In Chapter 8, a suggestion was given on how the CPMM modules can be implemented in the surgery tool.

Design requirements 4.1 and 4.2 focus on the guiding element. The guidance couples the input with the output, and therefore must provide smooth paths with minimal play. A deformed rail is not able to guide the bearings of the reading rings. In test phase 3, solely the H-beam was tested. It was concluded that the H-beam could form diagonal paths and simple multi-curved paths. More complex paths, such as an alternating pattern, were not achieved as path input. Common failure modes included the warping of the H-beam or the derailment of the bearings. The integrated design from test phase 4 was able to output diagonal shapes and simple single- or multi-curved paths, but required a lot of input force. More complex patterns could not be achieved. The path implementation deformed the H-beam plastically, resulting in an unsmooth path. Consequently, the translational motion jammed. In design phase 1 and 2 it was concluded that the prototype functioned properly without H-beam. In comparison with test phase 4, it can be concluded that the H-beam is indeed the most critical part of the design and needs to be refined for the prototype to function properly. This is discussed in the next subsection. Thus, design requirements 4.1 and 4.2 are not met with the current guiding element.

9.1.2. Design limitations and recommendations for improvements

In the conceptual design phase, the memory rings, reading rings and guiding elements were expected to be the key components: possibly critical parts. The memory rings and the shaft contain a geared profile with very small teeth. The loading of the teeth was a point of concern: the memory rings should rotate along with the input rotation of the input shaft, but the H-beam will try to oppose this rotation. Therefore, the teethed profile is exposed to forces. After calculations to estimate the maximum normal force allowed, provided in Figure 4.17 in Chapter 4, it was expected that brass and aluminium are strong enough to withstand high loading. The test results showed that indeed the memory rings worked acceptably: the rotational motion functioned well, requiring little force, and without damaging the components. The reading rings were expected to be potentially critical due to disk friction. To avoid this problem, the Teflon frame was introduced. The test results from test phase 1 indicated that the reading rings could rotate well, however some rings required more force than others. Thus, the Teflon frame was not completely sufficient. The guiding element was assumed to be the most challenging part, and the test results agreed with that assumption. The complex loading in combination with the small dimensions and the material properties, made the H-beam the weakest component in the design. The reading rings and the H-beam are discussed in the next subsection. Table 9.1 on page 107 shows the possible issues the mechanism can have and summarises which issues occur and which not.

Design requirement	Performance of the prototype
1. Shape of the mechanism	
1.1 Round or cylindrical shape	✓
1.2 Four cable control of the compliant shaft	✓
2. Memory elements	
2.1 At least 8 elements	✓
2.2 Path input existing out of 3 modes: past, present and future	✓
2.3 Path input in steps of 1 mm	✓
2.4 Haptic feedback for rotational input	✗
2.5 Future memory elements rotate along with present	✓
2.6 Translational motion of the memory elements	✓
2.7 Haptic feedback for translational motion	✓
2.8 Rotation and translation with minimal friction	✓
2.9 Locking and unlocking of the memory elements	✓
3. Reading elements	
3.1 Function as path output	✓
3.2 At least 11 elements	✓
3.3 Include attachment points for the actuation cables	✓
3.4 Rotate with minimal friction	~
4. Guidance	
4.1 Smooth path by guiding elements	✗
4.2 Minimal play	✗
5. Transmission from controller to shaft of the surgery tool	
5.1 Cables attached to the reading elements	✗
5.2 Cables guiding, avoiding friction and tangling	✗
6. Ease of manufacturing	
6.1 Standard parts	~
6.2 Number of parts	~
6.3 3D printable	~

Figure 9.2: Performance of the prototype compared to the design requirements. A green check means that the prototype meets the requirements well. An orange tilde is given when the performance of the prototype partially meets the requirements, but some optimisation is necessary. The requirements assigned with a red cross were not achieved with this prototype. See text for explanation.

Table 9.1: Possible failure modes of the CPMM prototype and their occurrence in the machined prototype

Main function	Component / Assembly	Possible failure mode	Failure present?
Path input			
1. Rotational motion of the memory rings	Memory rings	1. Too much friction between memory ring and translational motion mechanism	No
		2. H-beam too stiff, requiring much input torque for rotational motion	No
		3. Loading damages the teeth of the memory rings and shafts	No
2. Path formation	Guiding element	1. Warping of the H-beam (too stiff)	No
		2. Dislocated bearings (too weak)	Yes
		3. Buckling due to compression	Yes
		4. Stretch due to tension	Yes
		5. Plastic deformation / breaking	Yes
3. Translational motion of the memory rings	Memory rings	1. Too much friction between shaft and memory rings	No
		2. Too much play causing jamming on the shafts: rotation around pitch axis	No
		3. Transfer from one shaft to other shaft impossible	No
	Translational motion mechanism	1. Too much friction with the shafts	No
		2. Too much friction with the outer casing	No
		3. Jamming against the reading rings	No
		4. Ability too rotate, while it should only translate	No
		5. Improper haptic feedback: at the wrong moment or requiring too much force	No
	Guiding element	1. Irregular path formation due to deformation: jamming with bearings of the reading rings	Yes
Path output			
1. Rotational motion of the reading rings	Reading rings and frame	1. Teflon frame not stiff enough	Yes
		2. Accumulation of the normal force: disk friction	Yes
		3. Too much friction between reading rings and translational motion mechanism	No
		4. Too much friction between reading rings and outer casing	No
		5. Too much play around the translational motion mechanism and inside the casing: jamming due to up and down movement	No
	Guiding element	1. Irregular path formation due to deformation: jamming with bearings of the reading rings	Yes

The design of the guiding element is the main issue in the CPMM design. It is assumed that the H-beam jams with the bearings of the reading rings. As a result, the linear movement of the H-beam relative to the reading rings causes compression in the H-beam. In Figure 9.3 two scenarios are shown. The first scenario takes place when the path is inserted. Here, the H-beam moves distally towards the reading rings. The H-beam is kept in position by its attachment to the translational motion part, and also by the flanges that capture the bearings of the memory rings. Due to jamming, the bearings of the reading rings exert a normal force on the H-beam (F_{br}). This force, in combination with the forces applied by the bearings of the memory rings (F_{bm}) results in compression areas in the H-beam. With further insertion more readings engage to the H-beam, consequently more jamming takes place. The second scenario is shown in the bottom image, in which the memory rings move back to the input axis. The H-beam is kept in place by the translational motion mechanism (F_t). Due to jamming of the bearings of the reading rings, an opposite force is exerted on the H-beam (F_{br}). The area in between is compressed. This also happens in areas where the bearings of the memory rings exert an opposite force to the H-beam. When the H-beam is compressed, the H-beam can not move away. It is either pushed against the translational motion part or fixed on the memory rings. Moving up is also not an option, this motion is avoided by the reading rings or by the perspex casing. Consequently, the H-beam starts to buckle and deforms. The deformation of the H-beam makes the path irregular, and the guidance of bearings even more difficult. Thus, the buckling amplifies the jamming of the reading ring bearings against the H-beam, which in turn causes more compression. As a consequence, the complete path can block, dislocation of bearings happens or the H-beam breaks.

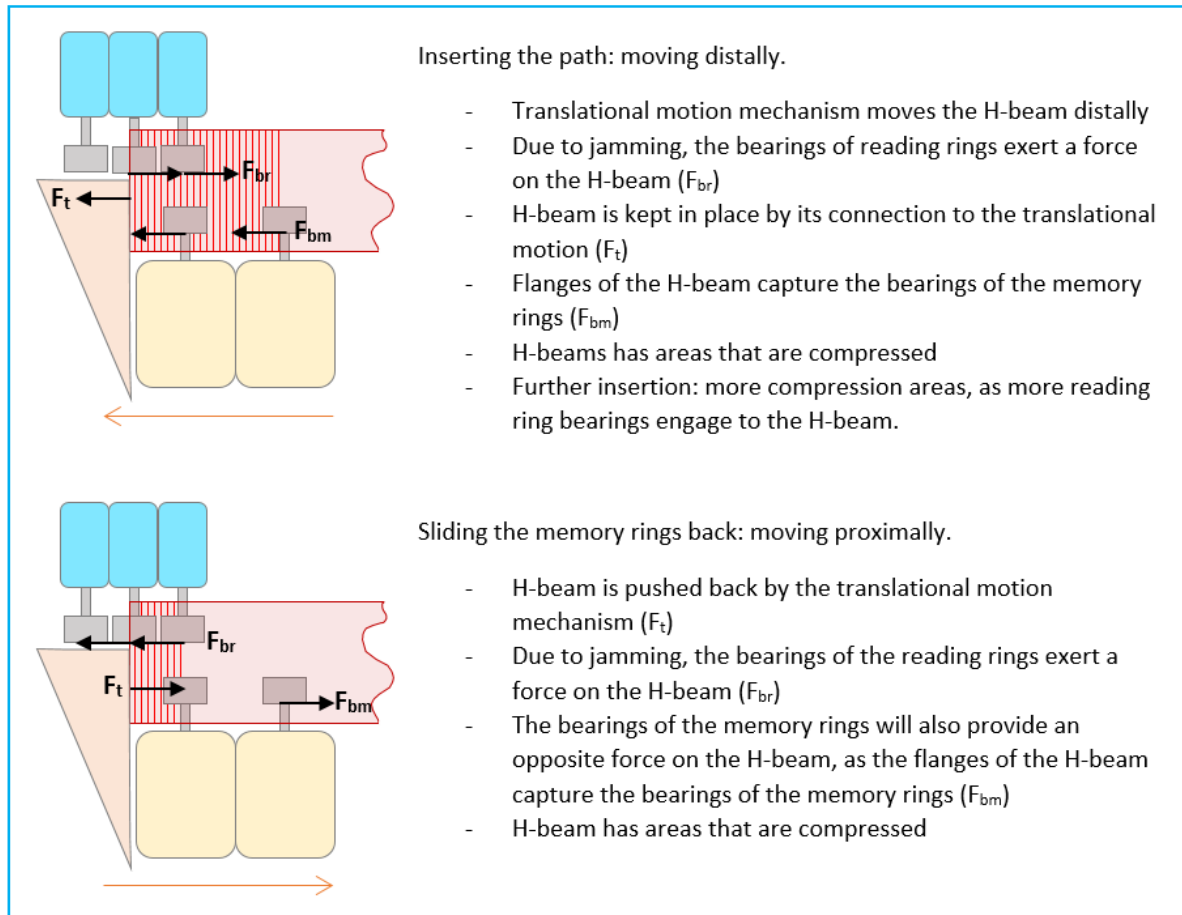


Figure 9.3: The assumed failure mode of the H-beam due to compression and buckling. The upper image shows the situation in which the path is inserted and the memory rings are moved distally. The lower image shows the movement backwards from the fixed shaft to the input shaft. The schematic drawings are colour coordinated, similar to the exploded views in Chapter 4. Forces exerted by the bearings of the reading and memory ring are represented with F_{br} and F_{bm} respectively. The force exerted by the translational motion part is indicated with F_t .

The jamming of the bearings against the H-beam can possibly be solved by redesigning the geometry of the H-beam. The H-beam should be made wider (b) and the web (t_y) should be thinner. By doing this, the path is more broad, giving the bearings of the reading rings more space to move and thus reducing the chance of jamming. As downside, widening the beam gives the complete prototype more play, which is undesired because the formed path in the compliant shaft will be less stable. The derailment of the bearings out of the H-beam can be limited by reinforcing the H-beam. For example, adding thin metal leaf springs on each side of the H-beam. The implementation is challenging, because the leaf springs can not be attached to the H-beam. Their continuous solid design, limits the ability to stretch or compress when the beam is bent. Further research is required to determine how the H-beam can be reinforced.

It is debatable if a 3D printed guiding element is acceptable for this design, even with a modified and improved version. The main advantages of the 3D printed design include that it can be printed as one part and the material is flexible. Therefore, the manufacturing is quick and produces a highly compliant component. However, a significant disadvantage is that the 3D printed H-beam is weak. There is a trade-off in being flexible to form different paths and being stiff to guide the bearings. If the H-beam is not stiff enough, the reading ring bearings deform the H-beam or move out of the H-beam. This means that the reading rings have play and can still rotate a bit. As a result, the segments of the compliant shaft have play as well and are not fixed in their planned orientation. Besides that, the plastic deformation of the H-beam reduces its guiding capabilities: blockage occurs. Another disadvantage of the 3D printed guiding element is that the H-beam cures over time. The H-beam becomes more brittle, which

increases the chance of breaking. As a consequence, the H-beam has to be replaced regularly. Thus, many additional tests need to be done to see if a refined 3D printed H-beam works sufficiently. These test should for example include the quantification of the possible paths that can be formed. Also, the amount of loading the compliant shaft can withstand in certain positions and the corresponding play should be measured. An estimation of the mechanical failure modes, fatigue and service life-time is useful information to determine the performance of the guiding element. If the 3D printed H-beam still performs below par, another guiding element should be incorporated in the CPMM mechanism.

A metal guidance is expected to perform better than a 3D printed guiding element, because metal is stronger than a polymer. Failure modes, such as plastic deformation or the dislocation of bearings will be limited. However, the manufacturing of a metal guiding element is more time consuming, because the guiding element should be made with subtracting manufacturing methods. A flexible metal guiding element cannot be made from one part. Therefore, the design must either include separate carts, or a continuous beam made from segments that are connected by hinges. Figure 9.4 shows two alternative guiding element designs, made from metal. One possible alternative is implementing separate carts as guiding element, similar to the MemoBox. In the MemoBox, each input element has its own cart. The carts are connected to the corresponding input element via a pin, enabling them to rotate. They are v-shaped and include thin-walled flexible lateral flaps. These flaps form a continuous path as the flaps of one guiding element and the body of the next guiding element overlap. The only change necessary to the existing components of the CPMM mechanism, is that the bearings of the memory rings are replaced by pins to fasten the cart on the memory ring. A challenge of this design compared to the MemoBox is that the carts do not move planar, but around the perimeter of the memory rings. To make sure the carts stay overlapped, they can be connected. The connection should be able to move, to allow the guiding element to change in length while forming a different path. An example is shown in Figure 9.4A. Another proposed guiding element design is shown in Figure 9.4B. It is a continuous H-beam, made from hinged rigid bodies. The H-segments can be made from a metal sheet by lasercutting. The segments are connected by five wires running through the length of the guiding element. One wire is located in the centre of the H-beam and the other four wires are located in the corners of the H-beam. The additional wires in the corners avoid the bearings from slipping out of the H-beam. It is important that the wires are free to translate and rotate in the segments. Otherwise, the same will happen as the 3D printed testbeam H3C: the beam deforms majorly under bending and torsion. The segments should stay at a fixed distances from each other, otherwise gaps would appear in the H-beam. Therefore, separators or small bearings need to be incorporated in the beam. For further research, it is recommended to replace the 3D printed H-beam with a metal H-beam. The designs proposed above are examples, further brainstorm and testing are required to find the optimal design.

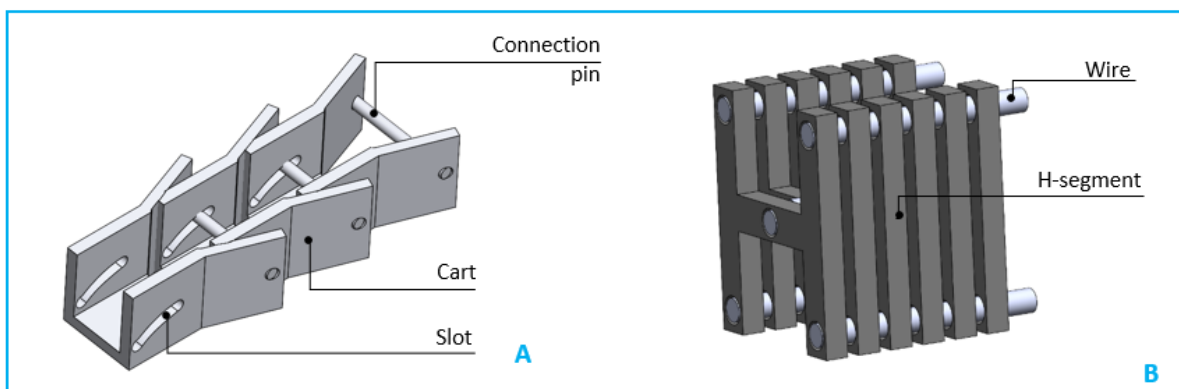


Figure 9.4: Alternatives for the guiding elements. Figure A shows a separate guiding elements, small carts. The carts overlap and are connected by a pin that is able to move in a slot. Figure B shows a continuous H-beam, made from hinged rigid bodies. The segments are connected by five wires running through the length of the guiding element.

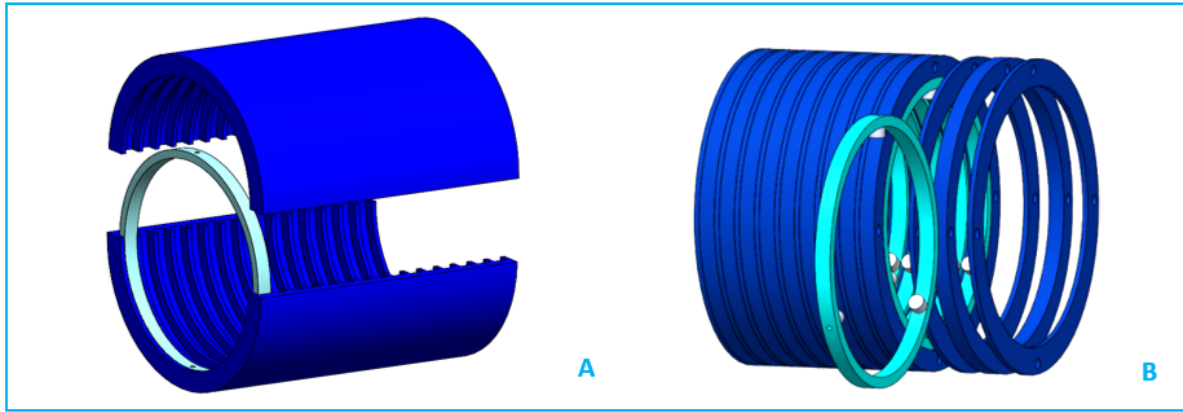


Figure 9.5: Reading ring frame design recommendation. The frame is larger than the reading rings: the rings are completely enveloped. Making the casing thicker and from aluminium would result in a rigid casing, which is therefore more suitable. Figure A is an example in which the frame is made from two parts. Figure B the frame is separated into disks that are connected by pins running through them. Note, in Figure B, the design of the reading ring has 3 bearings, as it is an old design.

Table 9.1, implies that another design limitation of the prototype was the movement of the reading rings. The reading rings must rotate with minimal friction, so the guiding element does not need to overcome a high friction torque to rotate the reading rings. The friction present in the current design was an expected issue, but the Teflon frame in between the reading rings were supposed to function as stationary separators that limit disk friction. The tests performed with H-beam influenced the rotational motion of the reading rings more. As discussed above, the bearings of the reading rings jammed with the H-beam. Presumably when a path was inserted, the reaction force of the H-beam on the bearing pushed the reading ring distally. The Teflon rings, with 0.5 mm thickness, acted as separators but could not keep the reading rings in place. The Teflon separators were not stiff enough: the normal forces bent the Teflon rings. Consequently, the reading rings were squished together against the perspex casing end part, when the memory rings were moved from the input shaft to the fixed shaft. This also happened when the memory rings are slid back to the input shaft: in this case, the reading rings were compressed against casing front part. The problem is partly solved when the H-beam does not jam with the bearings of the reading rings anymore. In that case, the reading rings are compressed together to a lesser extent. However, to optimise the design, it is recommended to change the frame of the reading rings. The frame should be more rigid for example, thicker separators made out of aluminium. Each reading ring should have its own compartment, in which it can rotate with minimal friction. Therefore, when the reading rings are translated due to undesired normal forces, they are compressed against the stiff frame. The accumulation of the normal forces is avoided. Alternative designs for the reading ring frame were mentioned in subsection 4.5.1 and shown in Figure A.4 in Appendix A. These designs are also shown in Figure 9.5. The frame is larger than the reading rings; the rings are completely enveloped. Making the casing thicker and from aluminium would result in a rigid casing, which can be a solution for the problem. A more advanced prototype could incorporate three small ball bearings in each separator ring, so the reading rings rotate with very limited friction.

The other components and subassemblies are deemed to perform sufficiently. The CPMM prototype is a promising design to function as follow-the-leader path-planning mechanism. Therefore, it is recommended to refine the guiding element and the frame of the reading rings as further research.

9.1.3. Overview of recommendations for further research

In the previous subsections the design issues, limitations and possible solutions were elaborated. The current design is promising, but requires optimisation. From most important to less important, the recommended adjustments for further research are:

- Replace guiding element by a metal guiding element
- Replace the Teflon reading ring frame with a thicker aluminium frame
- Add haptic feedback mechanism for rotational input

The evaluation of the prototype is limited to what functions are achieved and which components form issues in the current design. The results are not measured and quantified. Also, the steering functionality of the CPMM has not been examined yet, because the prototype has not been tested with a compliant shaft attached to it. For further research it is required to quantify the performance of the controller by using an experimental set-up with measuring equipment such as force sensors, for example:

- Measure the force required to slide the memory rings over the shafts to determine the friction
- Measure the resistance force for the rotational motion of the guiding element
- Measure the force required to rotate the reading rings inside their frame to determine the friction
- Quantify all paths the H-beam can make
- Quantify all paths the compliant shaft makes
- Determine the input/output ratio of the prototype
- Measure which loading the complaint shaft can withstand and the corresponding play

9.2. 3D printed prototype

9.2.1. Performance of the prototype

The aim of this prototype was to determine whether or not 3D printing is an option as manufacturing method for the CPMM module. 3D printing has many benefits compared to machining a prototype, mainly based on time and cost reduction. The path-planning module is the most complex and time consuming component to manufacture in comparison to the other components of the surgical instrument: the compliant shaft of the instrument can be 3D printed and the casing can be simplified as well. Thus, making the path-planning mechanism 3D printable would immensely reduce the costs of the surgical instrument. Also, the production only requires 3D printers and existing CAD-files. No precision technicians are necessary to machine the mechanism. Consequently, 3D printing enhances the affordability and accessibility across the globe.

The path-planning module is a complex design with many components moving relative to each other. It also includes some very small features, such as the geared profile on the shafts and memory rings. Despite the fact that 3D printing is a cheap and relatively fast method, 3D printing the prototype had drawbacks. As described in section 7.6.2., the prototype outcome is limited by the printing accuracy and material properties. Especially the FDM printed parts had rough surfaces, in which the print layers were clearly visible. The components had to be sanded or redesigned with more spacing to limit the friction. The FDM printed components were weak and required altered designs with thicker areas to function better. The shaft and memory rings were printed with dental resin by stereolithography. These components had a better surface finish and were stronger. Therefore, for future research it is recommended to print all parts with SLA. Due to the low accuracy of both printing techniques, small features such as holes for fasteners, did not form completely or did not form at all. Most parts required to be manipulated with a file afterwards, to be able to insert the fasteners. Thus, the downside of the 3D printed prototype is that the design required continuous remodelling, sanding and filing the components, which is a time consuming task.

In Figure 9.6 the performance of the 3D printed prototype is compared to the functional requirements. The 3D printed prototype has the same working principle as the machined prototype. Some simplifications were made to facilitate the 3D printing process, but the main components were the same. Consequently, functional requirements 1 and 2 are met. Functional requirement 3 includes subrequirements about the path formation in the compliant shaft. The model contains 12 reading rings that can control a compliant shaft with 12 segments. Similar to the machined prototype, the prototype only exists out of the path-planning controller and does not include the cables and a compliant shaft. The current design is unable to provide any path output on the reading rings and cannot prove the follow-the-leader working principle. Test phase 4 showed that the path implementation is blocked by the H-beam and reading rings. As a consequence, requirements 3.4 and 3.5 are not met.

Functional requirement	Performance of the prototype
1. Actuation of the total design	
1.1 Mechanically actuated	✓
1.2 Four cable control of the compliant shaft	✓
2. Path planning by the user (input)	
2.1 Path planning existing out of 3 modes: past, present, future	✓
2.2 Step wise path input	✓
3. Path formation in the compliant shaft (output)	
3.1 Control a compliant shaft with at least 11 segments	✓
3.2 Cable guidance from CPMM to compliant shaft	✗
3.3 Improving cable guidance by making the prototype cylindrical	✓
3.4 Multi curvature with 40 degree angle per segment	✗
3.5 Single curvature of 170 degrees	✗

Figure 9.6: Performance of the 3D printed prototype compared to the functional requirements. A green check means that the prototype meets the requirements well. An orange tilde is given when the performance of the prototype partially meets the requirements, but some optimisation is necessary. The requirements assigned with a red cross were not achieved with this prototype. See text for explanation.

Despite the insufficient performance of the complete prototype, some individual components and sub-assemblies did show promising results. In Figure 9.7, the performance of the 3D printed prototype is compared to the element design requirements, which focus more on separate components and their functionalities. Test phase 1 and 2 implied that the memory rings functioned acceptably: they slid with minimal friction over the shafts and were able to rotate freely inside the translational motion mechanism. The 3D printed prototype did not include haptic feedback for the translational and rotational motion. This reduced the ease of use, but did not limit the performance of the memory rings in combination with the shafts and translational motion mechanism. Thus, except for design requirement 2.4 and 2.7, the 3D printed memory rings meet all requirements. The reading rings showed more complications. Due to the low accuracy of the FDM printed parts, the reading rings of the 3D printed prototype had excessive play. Consequently, the rings were able to rotate easily, but could also translate inside their frame. The reading rings moved up and down in the frame. In test phase 2 in which the prototype is tested without the H-beam, the reading rings made contact with the translational motion mechanism, causing friction and jamming. Thus, element design requirement 3.4 is not met. Optimisation of the reading rings and their frame is required for better performance. The guiding element did not function sufficiently. The results from test phase 3 concluded that the H-beam could only make simple diagonal paths or a single simple curve. More complex curves, such as S-shapes and other multi-curved paths could not be achieved: the guiding element deformed majorly, resulting in an irregular path. The deformed H-beam was not able to function as a guidance for the pins of the reading rings. Therefore, subrequirements 4.1 and 4.2 are not met. The malfunction of the reading rings in combination with the poorly functioning H-beam, caused the complete prototype to block when a path is implemented.

9.2.2. Limitations of the prototype

Table 9.2 is an overview of all the possible issues the mechanism can have, and summarises which issues occur and which do not. In the conceptual design phase, the memory rings, reading rings and guiding elements were expected to be the potential critical parts of the assembly. Especially in the 3D printed model, the memory rings and reading rings were expected to function less, due to the weaker material properties and rough surface finish. The teathed profile of the memory rings must be able to withstand the normal forces to rotate the rings. The table shows that the memory rings and translational motion mechanism functioned well. The rings translated and rotated smoothly, and the teeth of the rings and shaft stayed undamaged. However, every action that included the H-beam or reading rings showed certain failure modes while performing. These components are limitations of the prototype, which require optimisation for further research.

Design requirement	Performance of the prototype
1. Shape of the mechanism	
1.1 Round or cylindrical shape	✓
1.2 Four cable control of the compliant shaft	✓
2. Memory elements	
2.1 At least 8 elements	✓
2.2 Path input existing out of 3 modes: past, present and future	✓
2.3 Path input in steps of 1 mm	✓
2.4 Haptic feedback for rotational input	✗
2.5 Future memory elements rotate along with present	✓
2.6 Translational motion of the memory elements	✓
2.7 Haptic feedback for translational motion	✗
2.8 Rotation and translation with minimal friction	✓
2.9 Locking and unlocking of the memory elements	✓
3. Reading elements	
3.1 Function as path output	~
3.2 At least 11 elements	✓
3.3 Include attachment points for the actuation cables	✓
3.4 Rotate with minimal friction	✗
4. Guidance	
4.1 Smooth path by guiding elements	✗
4.2 Minimal play	✗
5. Transmission from controller to shaft of the surgery tool	
5.1 Cables attached to the reading elements	✗
5.2 Cables guiding, avoiding friction and tangling	✗
6. Ease of manufacturing	
6.1 Standard parts	✓
6.2 Number of parts	~
6.3 3D printable	✓

Figure 9.7: Performance of the 3D printed prototype compared to the design requirements. A green check means that the prototype meets the requirements well. An orange tilde is given when the performance of the prototype partially meets the requirements, but some optimisation is necessary. The requirements assigned with a red cross were not achieved with this prototype. See text for explanation.

Table 9.2: Possible failure modes of the 3D printed CPMM prototype and their occurrence

Main function	Component / Assembly	Possible failure mode	Failure present?
Path input			
1. Rotational motion of the memory rings	Memory rings	1. Too much friction between memory ring and translational motion mechanism	No
		2. H-beam too stiff, requiring much input torque for rotational motion	No
		3. Loading damages the teeth of the memory rings and shafts	No
2. Path formation	Guiding element	1. Warping of the H-beam (too stiff)	Yes
		2. Dislocated bearings (too weak)	Yes
		3. Buckling due to compression	Yes
		4. Stretch due to tension	Yes
		5. Plastic deformation / breaking	Yes
3. Translational motion of the memory rings	Memory rings	1. Too much friction between shaft and memory rings	No
		2. Too much play causing jamming on the shafts: rotation around pitch axis	No
		3. Transfer from one shaft to other shaft impossible	No
	Translational motion mechanism	1. Too much friction with the shafts	No
		2. Too much friction with the outer casing	No
		3. Jamming against the reading rings	Yes
		4. Ability too rotate, while it should only translate	No
		5. Inproper haptic feedback: at the wrong moment or requiring too much force	N/A
		1. Irregular path formation due to deformation: jamming with bearings of the reading rings	Yes
Path output			
1. Rotational motion of the reading rings	Reading rings and frame	1. Frame not stiff enough	Yes
		2. Accumulation of the normal force: disk friction	Yes
		3. Too much friction between reading rings and translational motion mechanism	No
		4. Too much friction between reading rings and outer casing	No
		5. Too much play around the translational motion mechanism and inside the casing: jamming due to up and down movement	Yes
	Guiding element	1. Irregular path formation due to deformation: jamming with bearings of the reading rings	Yes

Table 9.2, shows that the path formation is limited by the H-beam. The H-beam tends to warp, buckle or stretch, depending on the load. Often it resulted in a plastically deformed H-beam, that had broken ribs and was not able to guide the pins of the reading rings. These issues are due to the dimensions of the H-beam. As described in Chapter 7, the width of the H-beam and the gaps between the segments had to be reduced because M1 screws were used instead of 3 mm ball bearings. As a result, the H-beam design was too stiff, causing enhanced deformations when a curved path was inserted. Another critical area of the H-beam was the connection point with the translational motion part. The holes did not form properly in the translational motion part, making the fixation very weak. When a path was inserted, the H-beam tried to rotate around its fastening points, blocking the path for the reading rings. The H-beam is an essential part, that should convert the discrete path input into a continuous path for the output. An malfunction in the H-beam directly influences the path output. Therefore, with the current H-beam design the follow-the-leader function of the prototype can not be proved. Optimisation of the H-beam is required to test the prototype properly. Similar to the machined prototype, a metal guidance can be a possible solution.

The H-beam jammed against the pins of the reading rings. In addition, the reading rings leaned on the H-beam and translational motion mechanism, due to too much play. This issue increased friction between the reading rings and translational motion mechanism, and caused more jamming with the H-beam. The path output is limited by the current reading rings and their casing, as can be seen in Table 9.2. Components such as the reading rings require a refined version with less play and less surface roughness. The frame and reading rings can be improved by using dental resin instead of PLA. Also, a refined design such as the designs proposed in Figure 9.5, should be examined for further research.

9.2.3. Comparison of the two prototypes

In Figure 9.8, the 3D printed prototype is compared to the machined prototype. This table is a summary for both prototypes, showing their performance. The machined prototype functions better than the 3D printed prototype. The difference in performance is due to the accuracy of the manufacturing methods and the properties of the materials used. The machined components have a better surface finish and could be machined very precise. Consequently, both the friction and the play are minimised in the machined prototype. This is in contrast to the 3D printed prototype. Thus, the machined prototype performed better in test phase 1 and 2. Another important influence is the simplification of the 3D printed prototype. The use of a 1 mm screw instead of miniature ball bearings, required the H-beam to be modified. The altered H-beam, which has a smaller width (b) and a lower value for t_g , is much stiffer than the H-beam used in the machined prototype. As a result, the H-beam is not able to form curved paths and alternating paths. Except for a straight or diagonal path, the H-beam tends to deform or break loose from the bearings of the memory rings. Therefore, the 3D printed prototype performed worse than the machined prototype in test phase 3. This can be seen in Figure 9.8, underneath "path input with H-beam". For this reason, as expected, the complete 3D printed prototype in test phase 4 performs worse as well. The stiff H-beam design, in combination with the bad fixation of the H-beam and the play in the reading rings, blocks the path input and output. Therefore, the 3D printed prototype has not been tested on its path output. The H-beam and its connection to the translational motion part have to be modified first, before tests can be performed. The machined prototype functioned better in test phase 4 and is able to provide the follow-the-leader motion in the readings for diagonal and simple-curved paths. A fair comparison between the machined prototype and 3D prototype can only be made if the 3D printed prototype also includes bearings.

	Machined prototype	3D printed prototype
Ergonomics		
Size (DxL)	60 x 155 mm	60.5 x 155 mm
Haptic feedback	Translational motion	Not present
Performance of subassemblies		
Path input without H-beam (test phase 1 & 2)	Good	Medium
Path input with H-beam (test phase 3)	Good	Limited
Straight path	✓	✓
Diagonal path	✓	✓
Simple curved path	✓	~
Multi-curved path	✓	✗
Alternating path	✗	✗
Performance of complete prototype		
FTL motion proof of principle	✓	✗
Path output (test phase 4)	Promising	Insufficient
Straight path	~	✗
Diagonal path	~	✗
Simple curved path	~	✗
Multi-curved path	✗	✗
Alternating path	✗	✗
Failure mode	H-beam deformation	H-beam deformation

Figure 9.8: Comparison of the machined prototype and the 3D printed prototype. A green check means that the prototype meets the requirements well. An orange tilde is given when the performance of the prototype partially meets the requirements, but some optimisation is necessary. The requirements assigned with a red cross were not achieved with this prototype.

9.2.4. Overview of recommendations for further research

The current 3D printed prototype requires a lot of optimisation to enable a fair comparison between the machined prototype and the 3D printed prototype. Like the machined prototype, optimisation is required for the guidance and reading ring frame. However, the 3D printed prototype needs additional alterations based on the printing accuracy and material properties. From most important to less important, the recommended adjustments for future research are:

- Replace guiding element by a metal guiding element
- Replace M1 screws with ball bearings
- Replace FDM printed parts with SLA printed parts
- Adjust the reading ring frame design
- Optimise the spacing between components
- Optimise fastening methods of the components
- Add haptic feedback for translational input
- Add haptic feedback for rotational input

Similar to the metal prototype, the evaluation of the 3D printed prototype does not include quantification of its performance. With quantified results, it is easier to compare the functionalities of both prototypes. Thus, for further research it is required to quantify the performance of the controller by using an experimental set-up with measuring equipment such as force sensors, for example:

- Measure the force required to slide the memory rings over the shafts to determine the friction
- Measure the resistance force for the rotational motion of the guiding element
- Measure the force required to rotate the reading rings inside their frame to determine the friction
- Quantify all paths the H-beam can make
- Quantify all paths the compliant shaft makes
- Determine the input/output ratio of the prototype
- Measure which loading the complaint shaft can withstand and the corresponding play

9.3. CPMM in a medical instrument

9.3.1. Incorporated design

The CPMM module can steer a shaft with 15 segments in one plane. Two path planning mechanisms are necessary to provide a three-dimensional motion. The required length and controllability of the compliant shaft depend on the surgical task. The steerability of the shaft is increased with an increasing amount of steerable segments. More complex paths, require more shaft segments. Thus for the final medical instrument, more memory elements and steering elements may be necessary.

The current size of the cylindrical prototype is 60 x 155 mm. Incorporating two mechanisms in the surgical instrument would result in a large medical instrument, compared to hand-held surgical devices. The incorporated design proposed in Chapter 8, including the base and excluding the compliant shaft, is 230 x 150 x 135 mm (l x w x h). On one hand, the size of the path-planning mechanism is not crucial. Only the size of the compliant shaft is limited. The compliant shaft should be able to enter the patient's body via natural orifices and travel through confined surroundings to reach the area of interest. The controller of the instrument is placed outside the body, on a fixed base. The surgeon does not need to support the instrument. This is similar to the Da Vinci Surgical System (Intuitive Surgical, Sunnyvale, CA, United States of America): the medical robot is large, only the tools that are inserted into the body are minimised in size. On the other hand, for aesthetics and aspects such as transportation of the instrument, a smaller design can be desired. The machined prototype can be reduced in size. To do

so, all components have to be scaled down. For the casing, reading rings, and translational motion mechanism this is not a problem. However, the size reduction of the shafts and the memory rings is more challenging. To retain the same pitch of the gear profile and keep the 1 mm stepwise input, the amount of teeth is reduced. Consequently, with the same stepwise input, the angular displacement of the H-beam becomes larger. As a result, the H-beam is loaded with more torsion and shear, which is undesired because the beam tends to warp. Thus, the size reduction of the machined prototype depends on the guiding element used. The 3D printed prototype can hardly be reduced in size: the dimensions of the components are dependent of what is achievable with 3D printers.

The prototype was developed for validating the functionality of the proposed concept. The mechanism is not designed for direct use in a medical setting. In order to implement the path-planning module in an actual medical instrument, it should meet all current medical instrument regulations and protocols. Requirements such as mechanical safety, risk management, biocompatibility and sterilisability should be inspected. Safety and sterilisability are shortly elaborated below.

9.3.2. Safety

Safety is an important requirement for medical devices. Medical devices should be designed and manufactured in such a way that the clinical condition or the safety of patients is not compromised. Also, the safety of the user is taken into account. Absolute safety cannot be guaranteed in any system, thus the design of an instrument or tool is a risk management issue [7]. A medical device is called safe, if any risk associated to the use of that medical device is deemed to be acceptable and the benefits of the procedure outweighs the risks involved. Many regulations exist for the design of a medical instrument. For example, ISO 14971 provides the risk management framework for medical devices on how to identify, evaluate and control risks [36]. ISO 13485 describes the quality management system of a medical device [7]. Three important components of risk management include electrical safety, mechanical safety and thermal safety. The main concern for electrical safety is the risk of electrical shock and the hazards associated with this shock. A minimally invasive instrument comes into close contact with internal organs. A shock can do much harm in these situations. The risk of an injury caused by moving components in a medical device is assessed with mechanical safety. Thermal safety focuses on the hazards associated with the heat of the medical instruments. Regulations are made for temperature limits for the parts that touch the patient and the components that are in contact with the operator. Generally overheating is caused by electrical components, in mechanical systems heat is a less significant risk.

The proposed path-planning mechanism is mechanically driven. Consequently, risks based on electrical safety and thermal safety do not play a role and are not further discussed in this section. Mechanical safety is an important factor for this design, because the CPMM module contains many moving components. Moving components and mechanisms are associated with hazards such as squeezing or cutting tissue. The path-planning mechanism itself is placed at a safe distance from the patient on a stable base. The external perspex cover proposed in Chapter 8 is an additional safety measure that prevents the patient and the operator to be exposed to harm. However, the compliant shaft is inserted in the patient's body. Therefore, the main concern of this prototype is when the path-planning mechanism breaks or blocks during the procedure. In this situation, the mechanism should be removed without damaging tissue. The critical component in the CPMM design is the guiding element. Two critical situations can occur:

- The H-beam blocks the mechanism due to plastic deformation: the shaft is locked in its position and cannot return to its initial shape.
- The H-beam breaks or derailment of the reading rings: the motion of the reading rings and therefore also the shaft segments cannot be controlled anymore.

The first situation means that the formed curvature is fixed and the compliant shaft cannot be retrieved from the patient. If the compliant shaft is pulled out of the body, the shaft will press against surrounding tissue and damage it. Depending on the location inside the body and the curvatures of the paths formed, the injury can be very hazardous: cutting tissue or internal organs. A mechanism is necessary to uncouple the cables from the path planning modules. The compliant shaft will be flexible, but uncontrollable. In the second scenario the reading rings have play and the compliant shaft of the instrument

will not maintain its given shape. If the path output is completely disconnected from the path input, the flexible shaft cannot be controlled anymore. The instrument should be pulled back out of the patient's body. Uncoupling the path output from the path input by accident or on purpose, is not optimal, because the compliant shaft will use internal tissue as support to guide itself back.

Thus, any cable-driven mechanism should have a safety system for when the controller fails. In the current design, an improved H-beam will already reduce the risks for both situations. Still, the risk of controller failure is present. A mechanism that can easily uncouple and re-couple the compliant shaft from the controller should be examined for future research. Overall, it is important to define all possible risks and find solutions to avoid the risks or reduce the risks.

9.3.3. Sterilisability

All medical instruments that are in contact with body tissue or fluid need to be sterile. Sterile instruments are free from viable microorganisms. When the instrument is not sterile, any microbial contamination could result in an infection. To use the proposed minimally invasive surgery mechanism in a medical setting, it should be disposable or sterilisable after every procedure. The disposable solution is only profitable when the path-planning module is 3D printed. The machined prototype takes a relatively long time to manufacture and is expensive. Thus, disposing the instrument after every operation is not cost efficient. An advantage of the path-planning mechanism is that it is located outside the patient's body, on a fixed base. The controller itself does not touch the patient. The compliant shaft of the instrument is the only component that comes in contact with the patient's body. Therefore, the incorporated instrument should be partly re-usable and partly disposable. The controller of the instrument is made sterile, while the shaft of the instrument should be disposed after each procedure. This is similar to the Da Vinci Surgical system (Intuitive Surgical, Sunnyvale, CA, United States of America): the robotic arms are re-usable, while the instruments are disposed. The path-planning module contains many movable components, which makes cleaning laborious. The outer casing proposed in Chapter 8 functions as a protector, avoiding microorganisms to enter the CPMM modules. It also protects the mechanism from moisture and dust. The casing and the input knobs can be sterilised after each procedure. If necessary, an additional disposable cover sleeve can be provided. After every procedure, the compliant shaft should be disposed. A 3D printed shaft, such as the HelicoFlex [10], is cheap to manufacture and a suitable disposable solution. However, when the shaft is made disposable and the controller is re-usable, the main challenge is to couple and uncouple a shaft to the controller. The 60 steering cables need to be reattached, which is a precise and time consuming task. The compliant shaft is not inside the scope of this thesis, but the replacement of the compliant shaft should be part of future research.

9.3.4. Recommendations for the CPMM in a medical instrument

The current prototype is developed for validating the functionality of the proposed concept. In order to implement the path-planning module in an actual medical instrument, it should follow all current medical instrument protocols. Requirements such as risk management and sterilisability should be inspected for further research. For both safety and sterilisability, it is recommended to improve the connection of the compliant shaft to the controllers. So that the compliant shaft can be coupled and uncoupled in case of failure or to dispose the shaft after the procedure.

10

Conclusion

In this thesis, a cylindrical, mechanically controlled follow-the-leader mechanism is introduced, that can be used for natural orifice transluminal endoscopic surgery: **the Cryptex Programmable Memory Mechanism (CPMM)**. Natural orifice transluminal endoscopic surgery (NOTES) is a new development in surgery methods, which includes flexible instruments that are inserted via natural orifices such as the mouth, nose, anus or vagina. The instrument then passes transluminally towards the areas of interest [5]. Benefits of this method compared to conventional open surgery include, among others: the reduction in tissue trauma, no external scar tissue, less blood loss and a shorter recovery period [1][37]. However, the procedure requires highly advanced medical devices that are slender and able to form different paths to reach the area of interest without the support of the surrounding tissue. Bio-inspired by the movement and the propulsion of a snake, new instruments are being developed that provide a follow-the-leader motion. In a follow-the-leader mechanism, the user steers the tip of the instrument. The position given to the tip is stored and passed along proximally from segment to segment. Existing mechanically driven prototypes, such as the MemoSlide and MemoBox showed promising results for path-planning mechanisms. However, their rectangular form requires optimization for cable guidance and cable control to incorporate it in a medical instrument. The cylindrical shape of the proposed CPMM module is a solution for improved cable control in an FTL-mechanism.

A machined prototype and a 3D printed prototype have been developed as part of this research. The 3D printed prototype is a simplified version of the machined prototype. Except for spacing and some fastening methods, the main components and working mechanism are the same for each prototype. The mechanism contains 8 memory rings for path input, 2 H-beams for path guidance, and 15 reading rings for path output. The 3D printed prototype only has 12 reading rings. The user implements a path by rotating the memory rings and locking their given orientation (*input*). The given orientation of the memory rings relative to each other form a path. The stepwise input is converted into a continuous path by the H-beams. While inserting the path, the reading rings are guided through the H-beams and copy the orientation of the input. Each reading ring includes one set of antagonist cables, which are connected to one segment of the compliant shaft. The rotation of the reading rings causes the pulling and releasing of those cables and steers the shaft segments (*output*). The CPMM module controls the motion of the shaft on one plane. Two CPMM modules have to be combined to enable a three-dimensional motion. The prototype is developed for validating the functionality of the proposed concept. The mechanism is not designed for direct use in a medical setting. In order to implement the path-planning module in an actual medical instrument, it should meet all current medical instrument regulations and protocols. Requirements such as mechanical safety, biocompatibility and sterilisability should be inspected.

In theory, this design should be able to form 390625 different paths based on the steering range of each memory ring. Each step input results in an angular displacement between 20 and 32.3 degrees, which depends on the stiffness of the guiding element. Assuming one step input results in a 25 degrees angular displacement, a memory ring can provide a maximum output angular displacement of 50 degrees; namely two input steps. Thus, theoretically, the path-planning design is able to form one single

curvature with a maximum angle of 400 degrees. This is equal to the amount of memory rings times the maximum output angular displacement. It should also be able to make multi-curved paths, in which each segment can make a rotation of 25 degrees or 50 degrees relative to its adjacent segments. Both prototypes have been manually tested in four phases: 1. the individual parts and subassemblies, 2. the integrated design without H-beam, 3. the H-beam performance and 4. the complete prototype.

The machined prototype shows promising results, as it is able to prove the follow-the-leader principle. The integrated prototype is able to make straight, diagonal and simple curved paths. Steep multi-curved and alternating patterns cannot be achieved with this mechanism. The path formation requires more force than desired; this is due to the jamming of the H-beam. While inserting the path, the bearings of the reading rings jam against the H-beam instead of being guided by the H-beams. Consequently, the H-beam deforms and the path output is limited or blocked. The tests of the prototype without the H-beam are sufficient, because all subassemblies function properly. Thus, it can be concluded that the H-beam is the most critical part of the prototype. Optimization of the H-beam is required to improve the performance of the path planning module.

The 3D printed prototype is deemed to be insufficient in the current state: the design cannot provide the follow-the-leader motion. The prototype is limited by the printing techniques and the corresponding material properties. Issues included the spacing between parts, rough surfaces, weak features and brittle components. For example, the reading rings have too much play inside the fixed frame, causing them to move up and down in the frame. The main issue of the 3D printed prototype is that instead of ball bearings, M1 screws are used for the path transfer. The redesigned H-beam, in combination with the M1 screws, does not work sufficiently as a guiding element. Common failure modes are the derailment of the screws out of the H-beam and significant plastic deformation. As a result, the path input and path output are blocked. Other subassemblies, such as the movement of the memory rings over the shafts, work well. Thus, for the 3D printed prototype, optimization for spacing between parts is required, and the H-beam must be refined. A 3D printed design is an advantage over a machined design, because it is a cheap and quick manufacturing method. Therefore, improving the prototype is necessary to see if an acceptable 3D printed version is achievable.

For further research, it is recommended to improve the performance of both prototypes by refining the guiding element and changing the reading ring frame. Instead of a 3D printed H-beam, it is recommended to design a new guiding mechanism made out of metal. For example, separate metal carts or a continuous H-beam made from hinged metal sheets. A metal guiding mechanism will deform less than the 3D printed H-beam, which will avoid the jamming of the path insertion. Also, changing the frame of the reading rings will reduce the friction between the reading rings. Limiting the friction between the reading rings is desired, because the force required to rotate them is minimised, which reduces the loading on the guiding elements. In the 3D printed prototype, the spacing between parts should be optimised and FDM printed parts should be replaced by SLA printed parts. Components such as the reading rings require a refined version with less play and less surface roughness. Also, besides replacing the H-beam with a metal version, a fair comparison between the machined prototype and 3D prototype can only be made if the 3D printed prototype also includes ball bearings. Further research can investigate a prototype that is a combination of 3D printed parts and machined parts. This will reduce the costs and manufacturing time of the final design.

Future research should also include quantification of the functionalities. The current prototypes have been tested manually. For further research it is required to quantify the performance of the controller by using an experimental set-up with measuring equipment such as force sensors. Quantified results substantiate the design evaluation and make it easier to compare the functionalities of both prototypes. The tests should include the cables and compliant shaft to measure the path output. The performance can be tested by quantifying all paths the H-beam can make and the corresponding paths the compliant shaft makes. Also, the forces that can be applied to the compliant shaft of the instrument and their corresponding play, is a measurement necessary to evaluate the quality of the mechanism.

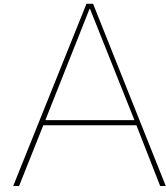
It is concluded that the CPMM module is capable of providing a follow-the-leader motion, however adjustments need to be made to improve the performance of the design.

Bibliography

- [1] Riaz Agha and Gordon Muir. Does laparoscopic surgery spell the end of the open surgeon? *Journal of the Royal Society of Medicine*, 96:544–6, 12 2003. doi: 10.1258/jrsm.96.11.544.
- [2] Homa Alemzadeh, Jaishankar Raman, Nancy Leveson, Zbigniew Kalbarczyk, and Ravishankar K Iyer. Adverse events in robotic surgery: a retrospective study of 14 years of fda data. *PloS one*, 11(4):e0151470, 2016.
- [3] Michael F Ashby, Hugh Shercliff, and David Cebon. *Materials: Engineering, Science, Processing and Design*. Butterworth-Heinemann, 2013.
- [4] Sergio Jose Bardaro and Lee Swanström. Development of advanced endoscopes for natural orifice transluminal endoscopic surgery. *Minimally Invasive Therapy & Allied Technologies*, 15(6): 378–383, 2006.
- [5] TH Baron. Natural orifice transluminal endoscopic surgery. *British journal of surgery*, 94(1):1–2, 2007.
- [6] Paul Breedveld. Memoflex 1 – mechanical surgical snake. URL <https://www.bitegroup.nl/maneuverable-devices/memoflex-1-mechanical-surgical-snake/>. (accessed: 10.11.2020).
- [7] Michael Cheng. *Medical device regulations: global overview and guiding principles*. World Health Organization, 2003.
- [8] MA Chowdhury, DM Nuruzzaman, AH Mia, and ML Rahaman. Friction coefficient of different material pairs under different normal loads and sliding velocities. *Tribology in Industry*, 34(1): 18–23, 2012.
- [9] Medrobotics Corp. Flex robotic system: Expanding the reach of surgery. URL <https://medrobotics.com/gateway/flex-system-int/>. (accessed: 07.09.2020).
- [10] Costanza Culmone, Paul WJ Henselmans, Remi IB van Starckenburg, and Paul Breedveld. Exploring non-assembly 3d printing for novel compliant surgical devices. *Plos one*, 15(5):e0232952, 2020.
- [11] Costanza Culmone, David J. Jager, and Paul Breedveld. Memobox: A mechanical follow-the-leader system for minimally invasive surgery. not published yet.
- [12] Cambridge dictionary. Meaning of surgery in english. URL <https://dictionary.cambridge.org/dictionary/english/surgery>. (accessed: 01.05.2020).
- [13] George Ellwood Dieter, Linda C Schmidt, et al. *Engineering design*. McGraw-Hill Higher Education Boston, 2009.
- [14] EnvisionTEC. Perfactory p4k series. URL <https://envisiontec.com/3d-printers/perfactory-family/perfactory-p4k-series/>. (accessed: 02.09.2020).
- [15] Andrew J Epstein, Peter W Groeneveld, Michael O Harhay, Feifei Yang, and Daniel Polsky. Impact of minimally invasive surgery on medical spending and employee absenteeism. *JAMA surgery*, 148(7):641–647, 2013.
- [16] International Organization for Standardization. Iso-13485 medical devices. URL <https://www.iso.org/iso-13485-medical-devices.html>. (accessed: 15.11.2020).
- [17] Formlabs. Form 3. URL <https://formlabs.com/eu/3d-printers/form-3/>. (accessed: 02.09.2020).

- [18] Giada Gerboni, Paul WJ Henselmans, Ewout A Arkenbout, Wouter R van Furth, and Paul Breedveld. Helixflex: bioinspired maneuverable instrument for skull base surgery. *Bioinspiration & biomimetics*, 10(6):066013, 2015.
- [19] Paul Henselmans. Mechanical snakes: Path-following instruments for minimally invasive surgery. 2020.
- [20] Paul Henselmans, Stefan Gottenbos, Gerwin Smit, and Paul Breedveld. The memoslides: An explorative study into a novel mechanical follow-the-leader mechanism. *Proceedings of the Institution of Mechanical Engineers, Part H: Journal of Engineering in Medicine*, 231:095441191774038, 11 2017. doi: 10.1177/0954411917740388.
- [21] Paul Henselmans, Gerwin Smit, and Paul Breedveld. Mechanical follow-the-leader motion of a hyper-redundant surgical instrument: Proof-of-concept prototype and first tests. *Proceedings of the Institution of Mechanical Engineers, Part H: Journal of Engineering in Medicine*, 233:095441191987646, 09 2019. doi: 10.1177/0954411919876466.
- [22] AF Hughes, DC Iles, and AS Malik. Design of steel beams under torsion. URL https://www.steelconstruction.info/images/6/6f/Sci_p385.pdf. (accessed: 20.04.2020).
- [23] Gül Kremer and Shafin Tauhid. Concept selection methods - a literature review from 1980 to 2008. *International Journal of Design Engineering*, 1, 01 2008. doi: 10.1504/IJDE.2008.023764.
- [24] Damian McKay and Geoffrey Blake. Optimum incision length for port insertion in laparoscopic surgery. *The Annals of The Royal College of Surgeons of England*, 88(1):78–78, 2006.
- [25] John Hopkins Medicine. Arthroscopy. URL <https://www.hopkinsmedicine.org/health/conditions-and-diseases/arthroscopy>. (accessed: 01.05.2020).
- [26] P.N. Nesargikar and S.S. Jaunoo. Natural orifice transluminal endoscopic surgery (n.o.t.e.s). *International Journal of Surgery*, 7(3):232 – 236, 2009. ISSN 1743-9191. doi: <https://doi.org/10.1016/j.ijssu.2009.04.001>. URL <http://www.sciencedirect.com/science/article/pii/S1743919109000508>.
- [27] Maria Neumann and Jessica Burgner-Kahrs. Considerations for follow-the-leader motion of extensible tendon-driven continuum robots. pages 917–923, 05 2016. doi: 10.1109/ICRA.2016.7487223.
- [28] Maria Neumann and Jessica Burgner-Kahrs. Considerations for follow-the-leader motion of extensible tendon-driven continuum robots. In *2016 IEEE international conference on robotics and automation (ICRA)*, pages 917–923. IEEE, 2016.
- [29] Takeyoshi Ota, Amir Degani, David Schwartzman, Brett Zubiate, Jeremy McGarvey, Howie Choset, and Marco A Zenati. A highly articulated robotic surgical system for minimally invasive surgery. *The Annals of thoracic surgery*, 87(4):1253–1256, 2009.
- [30] Education Transfer Plan and Seyyed Khandani. Engineering design process. 2005.
- [31] Jay D Raman, Jeffrey A Cadeddu, Pradeep Rao, and Abhay Rane. Single-incision laparoscopic surgery: initial urological experience and comparison with natural-orifice transluminal endoscopic surgery. *BJU international*, 101(12):1493–1496, 2008.
- [32] John R Romanelli and David B Earle. Single-port laparoscopic surgery: an overview. *Surgical endoscopy*, 23(7):1419–1427, 2009.
- [33] Chad J. Smith, Raj Rane, and Luis Melendez. 89 - operating room. In Joseph F Dyro, editor, *Clinical Engineering Handbook*, Biomedical Engineering, pages 376 – 384. Academic Press, Burlington, 2004. ISBN 978-0-12-226570-9. doi: <https://doi.org/10.1016/B978-012226570-9/50098-3>. URL <http://www.sciencedirect.com/science/article/pii/B9780122265709500983>.

- [34] Shelley Jane Spaner and Garth Loren Warnock. A brief history of endoscopy, laparoscopy, and laparoscopic surgery. *Journal of Laparoendoscopic & Advanced Surgical Techniques*, 7(6):369–373, 1997.
- [35] S. Tappe, J. Pohlmann, J. Kotlarski, and T. Ortmaier. Towards a follow-the-leader control for a binary actuated hyper-redundant manipulator. In *2015 IEEE/RSJ International Conference on Intelligent Robots and Systems (IROS)*, pages 3195–3201, 2015. doi: 10.1109/IROS.2015.7353820.
- [36] Meseret N Teferra. Iso 14971-medical device risk management standard. *International Journal of Latest Research in Engineering and Technology (IJLRET)*, 3(3):83–87, 2017.
- [37] John J. Tiedeken and Anthony J. LaPorta. Chapter 80 - laparoscopic surgery. In Peter R. McNally, editor, *GI/Liver Secrets (Fourth Edition)*, pages 589 – 594. Mosby, Philadelphia, fourth edition edition, 2010. ISBN 978-0-323-06397-5. doi: <https://doi.org/10.1016/B978-0-323-06397-5.00080-0>. URL <http://www.sciencedirect.com/science/article/pii/B9780323063975000800>.
- [38] Ultimaker. Ultimaker 3d printers. URL <https://ultimaker.com/3d-printers>. (accessed: 02.09.2020).
- [39] Robert J Webster III, Joseph M Romano, and Noah J Cowan. Mechanics of precurved-tube continuum robots. *IEEE Transactions on Robotics*, 25(1):67–78, 2008.
- [40] Julian Whitman, Nico Zevallos, Matt Travers, and Howie Choset. Snake robot urban search after the 2017 mexico city earthquake. In *2018 IEEE international symposium on safety, security, and rescue robotics (SSRR)*, pages 1–6. IEEE, 2018.



Design process

Solution space

The complete solution space is shown in Figure A.1 and Figure A.2. Figure A.1 shows all the solutions for the functions of the mechanism and Figure A.2 shows the solutions for haptic feedback.

Concept 1 version 2

An alternative concept for the final design, in which the translational motion mechanism is based on a linear input. In addition to the current final design, this concept includes a Hirth coupling, providing haptic feedback for the stepwise input. The concept is provided in Figure A.3.

Reading ring frame concepts

Concepts for the reading ring frames are given in Figure A.4 and Figure A.5. Two concept groups are introduced. The first group shows concepts in which the frames are bigger than the reading rings. Thus, the reading rings are packed inside a frame. The second group shows two concepts in which the frame is small and incorporated between and inside the reading rings. Description is given in the figures.

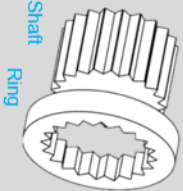
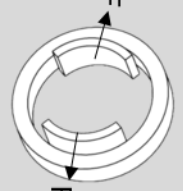
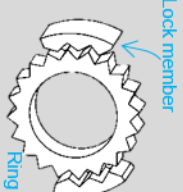
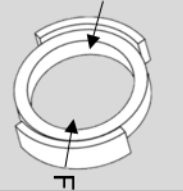
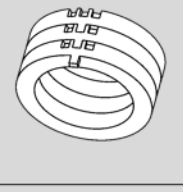
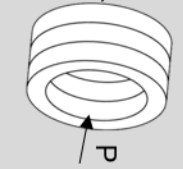
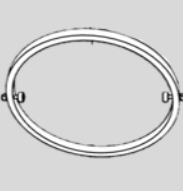

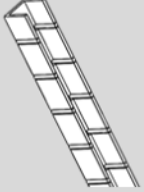

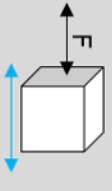
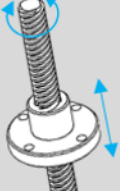
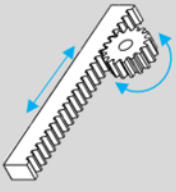
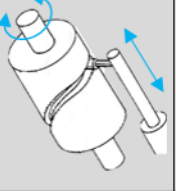
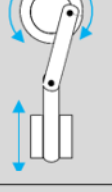


Solution	Solution 1	Solution 2	Solution 3	Solution 4	Solution 5	Solution 6
Function Path input Guidance Path output Translational motion Cable guidance						
						
						
						

Figure A. 1: Solution space of the main functions

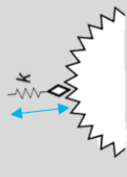



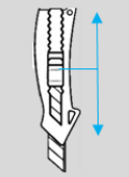

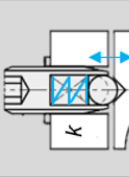

Solution Wish	Solution 1	Solution 2	Solution 3	Solution 4
Haptic feedback step input				
Haptic feedback Translational motion				

Figure A.2: Solution space of the haptic feedback mechanisms

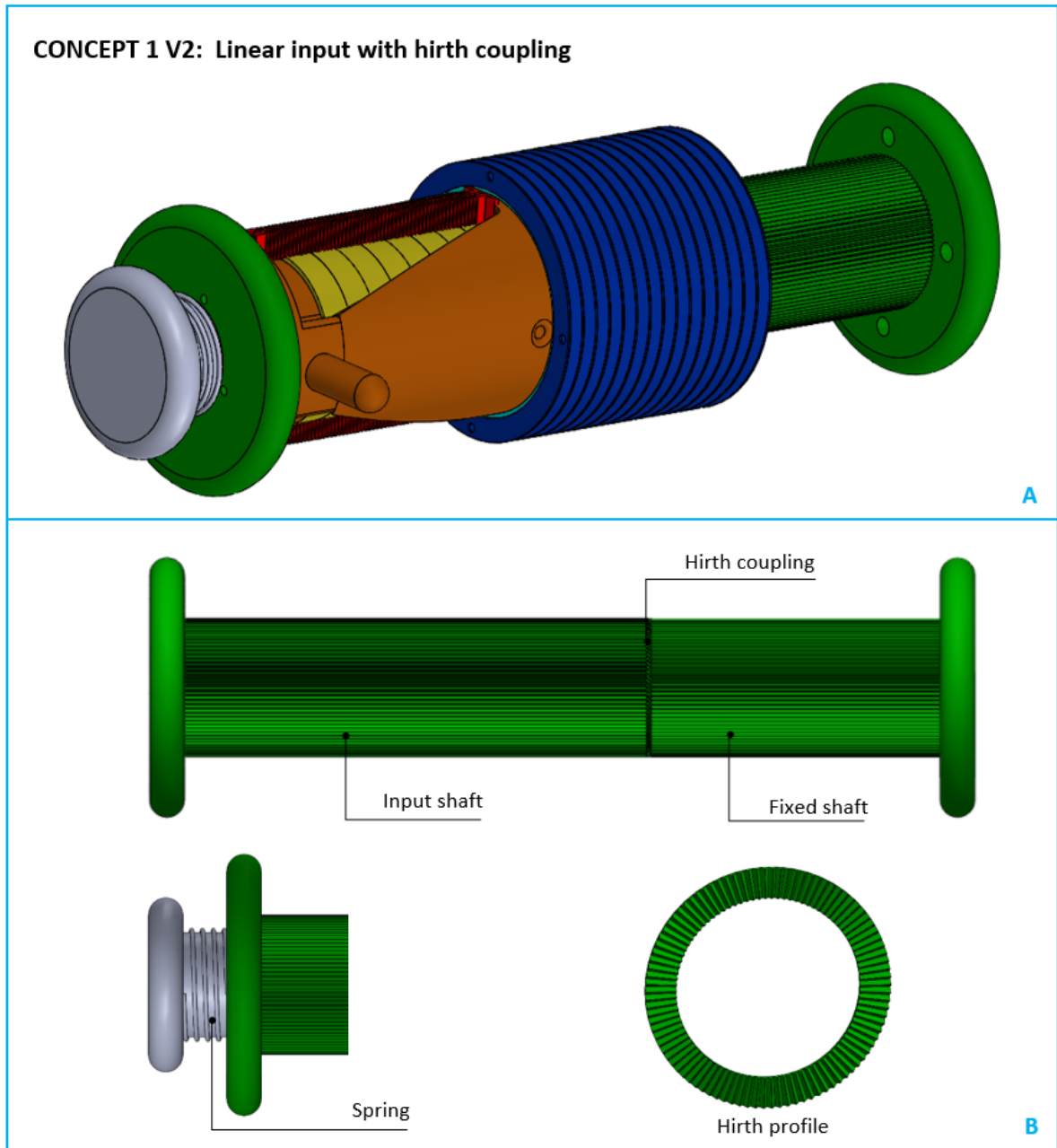
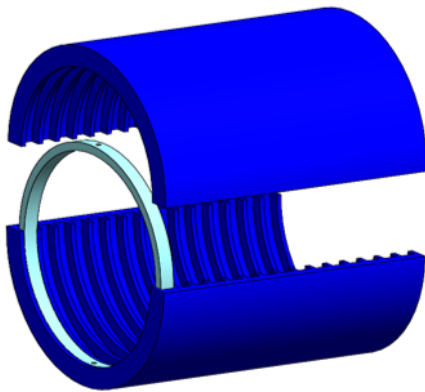


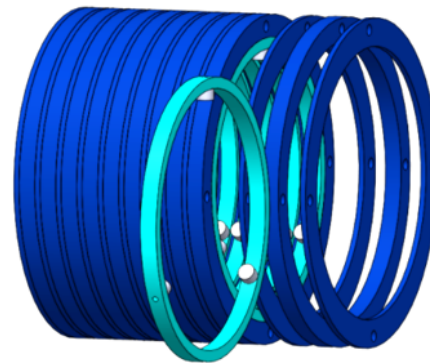
Figure A.3: Concept 1 version 2. Linear input with a Hirth coupling.

Frame bigger than the reading rings:



A

Rigid casing made out of two parts with concavities for the reading rings.
Needs to have a slot in it for the cables.



B

Casing made out of separate rings, 2 types:
- Thin (1mm) with smaller inner diameter than the reading rings (separator rings)
- Thick (3mm) with inner diameter the same as the outer diameter of reading rings. Needs to have a slot in it for the cables

Rings are kept together with pins going through the assembly

Figure A.4: Concepts for a frame holding the reading rings. In this figure, the frames are bigger than the reading rings: the rings are completely enveloped. Two concepts are shown, description is given in the figure.

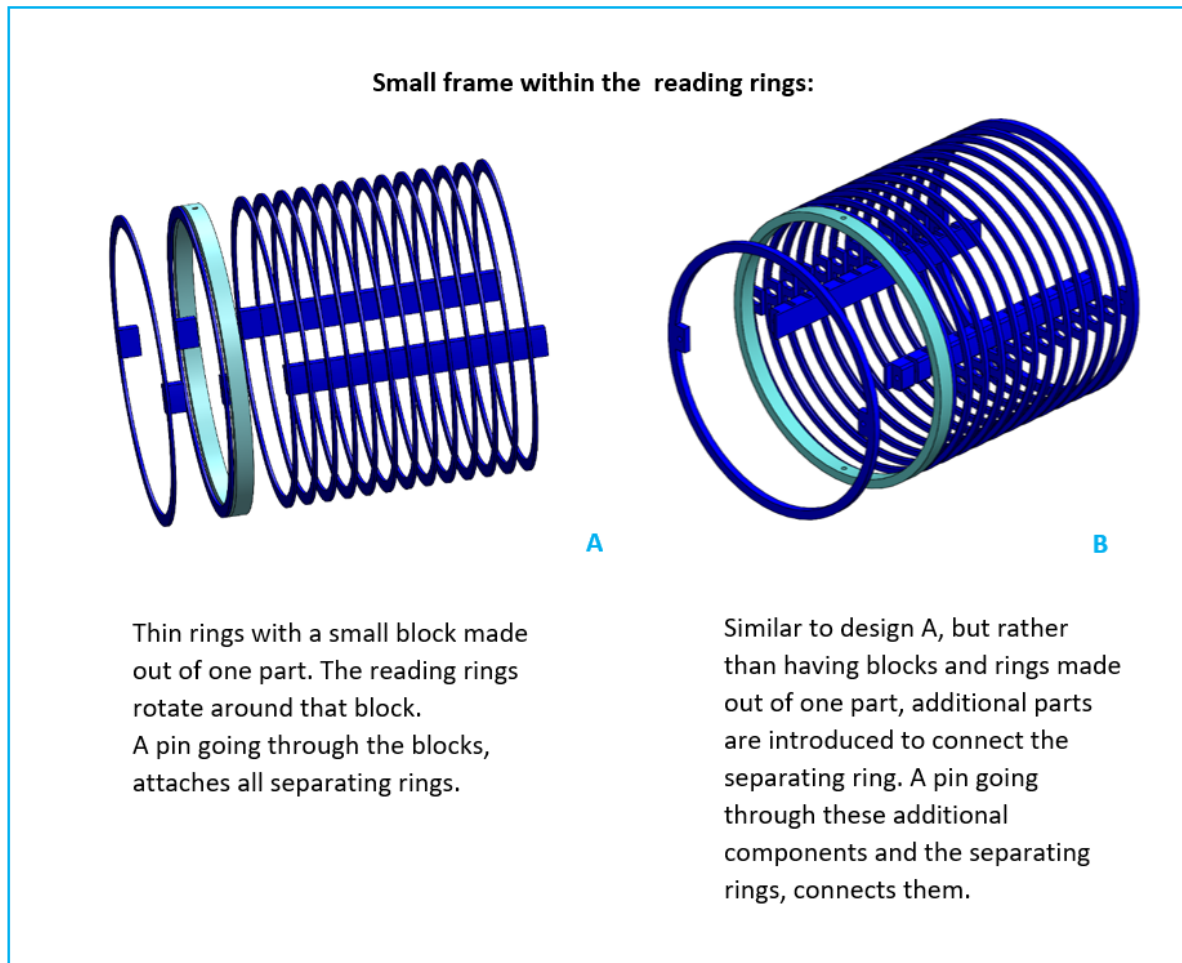


Figure A.5: Concepts for a frame holding the reading rings. In this figure, the frames are the same size as the reading rings: the separating rings are connected to each other on the inside of the reading rings. Two concepts are shown, description is given in the figure.

B

Integrated functioning

Ergonomics concept

An alternative concept for holding and steering the prototype is shown in Figure B.1. In this design, instead of attaching an translational motion knob to the front of the translational motion mechanism, a knob is attached to the "forks" of the translational motion part.

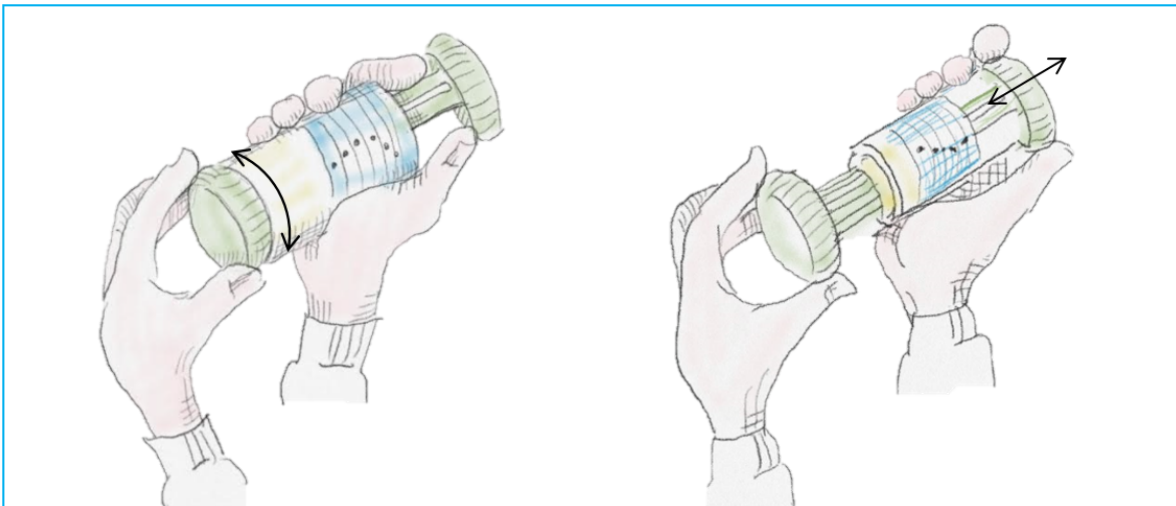
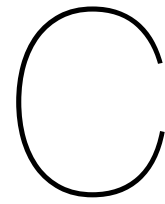


Figure B.1: Alternative solution for steering the prototype. In this design, instead of attaching an translational motion knob to the front of the translational motion mechanism, a knob is attached to the "forks" of the translational motion part.



H-beam

Tested H-beams

Table C.1 is a summary of the different types of H-beams tested. The dimensions and test results are given. Figure C.1 is a picture of the H-beam test method. The H-beam has been tested on its abilities to make a diagonal, S-shaped and alternating path. If the H-beam showed promising results, a reading ring was moved distally to test if the path is smooth and able to guide the bearings of the reading rings. Figure C.2 and Figure C.3 provide pictures of the performance of different H-beams.

Table C.1: Test results and characteristics of H-beams

H-beam number	width [mm] ($b-2t_x$)	height [mm]	t_x [mm]	t_y [mm]	t_r [mm]	t_g [mm]	Solid / Segmented	Connection of segments	Flexibility (feeling)	Diagonal shape	Curved S-shape	Alternating shape	Failure	Sufficient?
H1A	1	5	0.5	0.5	65	0	Solid	-	Pure torsion and bending possible, multiaxial paths not possible	-	-	-	Too stiff, no path forming possible	No
H1B	1	5	0.75	0.75	65	0	Solid	-	Pure torsion possible	-	-	-	Too stiff, no path forming possible	No
H1C	1	5	1	1	65	0	Solid	-	Not flexible	-	-	-	Too stiff, no path forming possible	No
H1D	2	5	0.5	0.5	65	0	Solid	-	Pure torsion possible, not bending	-	-	-	Too stiff, no path forming possible	No
H1E	2	5	0.75	0.75	65	0	Solid	-	Pure torsion possible	-	-	-	Too stiff, no path forming possible	No
H1F	2	5	1	1	65	0	Solid	-	Not flexible	-	-	-	Too stiff, no path forming possible	No
H1G	3	5	0.5	0.5	65	0	Solid	-	Pure torsion possible, not bending	-	-	-	Too stiff, no path forming possible	No
H1H	3	5	0.75	0.75	65	0	Solid	-	Not flexible	-	-	-	Too stiff, no path forming possible	No
H1I	3	5	1	1	65	0	Solid	-	Not flexible	-	-	-	Too stiff, no path forming possible	No
H2	3	5	0.75	0.75	0.5	0.5	Segmented	Midline	Very flexible	Able	Fail	Fail	Bearings move through the ribs	No
H3A	3	6	0.5, 0.75	0.75	0.5	0.5	Segmented	Midline	Very flexible	Able	Fail	Fail	Bearings move through the ribs	No
H3B	3	6	0.5, 0.75	0.75	0.5	0.5	Segmented	Corners	Flexible, but bending more difficult	Able	Able	No	Deformation	No
H3C	3	6	0.5, 0.75	0.75	0.5	0.5	Segmented	Corners, midline	Flexible, but bending more difficult	Able	Fail	Fail	Deformation	No
H4A	3	6	1	0.75	1.5	0.5	Segmented	Midline	Very flexible	Able	Able	Fail	Bearings move through the ribs	Promising
H4B	3	6	0.75	0.75	0.75	0.5	Segmented	Midline	Very flexible	Able	Able	Fail	Bearings move through the ribs	No
H4C	3	6	0.75	0.75	3	0.75	Segmented	Midline (s-shape)	Very flexible	Able	Fail	Fail	Bearings move through the ribs	No

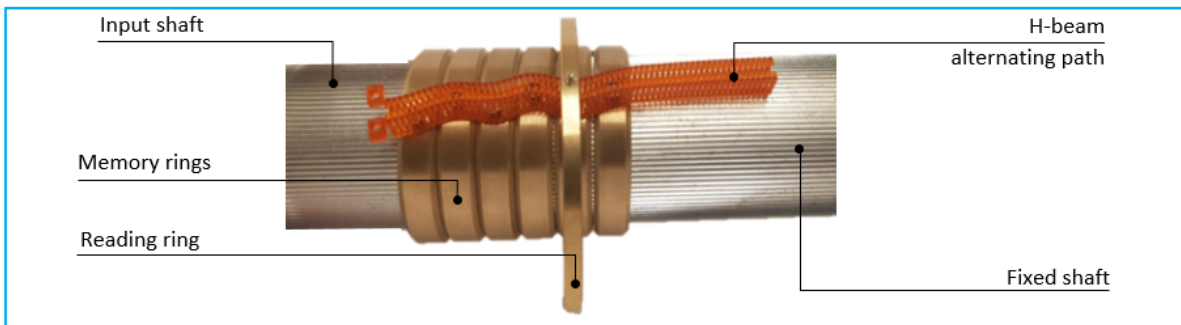


Figure C.1: H-beam test method. The H-beam has been tested on its abilities to make a diagonal, S-shaped and alternating path. If the H-beam showed promising results, a reading ring was moved distally to test if the path is smooth.

H-beam	Diagonal shape	Curved path	Alternating path
H3A			
H3B			
H3C			

Figure C.2: Test results H-beam test 3

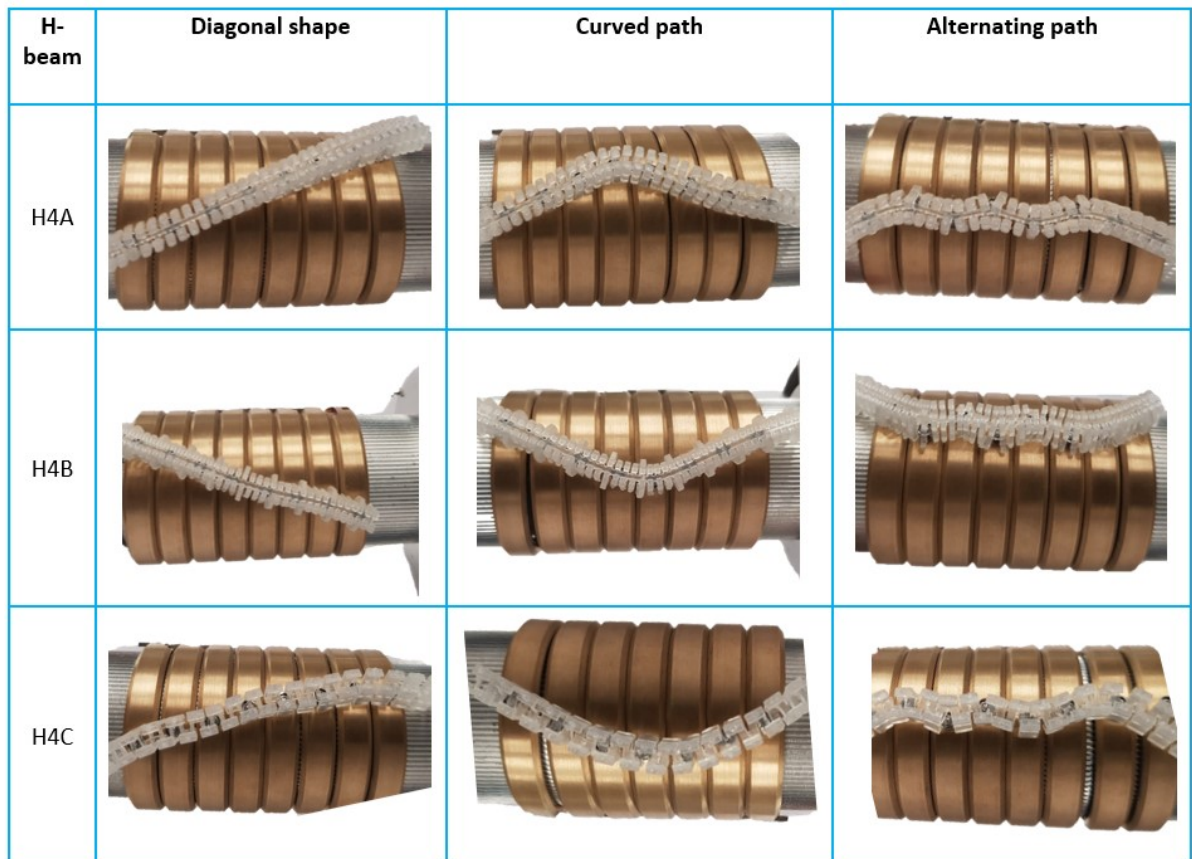
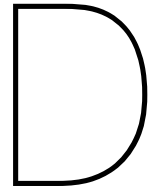


Figure C.3: Test results H-beam test 4. Note: an alternating path with H3A is not provided in the figure. The curved path already resulted in derailment of bearings, an alternating pattern was not achievable.



Machined prototype

Construction drawings

Construction drawings of the components are provided in from Figure D.1 to Figure D.23. What must be noted is that the drawings do not have the same scale.

Pictures of the prototype

Figure D.24 to D.29 include pictures of components or subassemblies from the machined prototype. Figure D.24, shows the three main assemblies. Figure D.25 is a picture of the input knob connected to the input shaft. Figure D.26 shows the 8 memory rings, located inside the translational motion mechanism. In Figure D.27, a close-up picture of a memory ring is shown. The memory ring includes two bearings, a pin and a slot. The pin of this memory ring moves inside the slot of an adjacent ring. Therefore, it functions as a rotation limiter. The reading ring assembly is shown in Figure D.28. Teflon rings function as separator rings in between the reading rings. The reading ring assembly is located inside the middle part of the casing. The casing assembly is shown in Figure D.29.

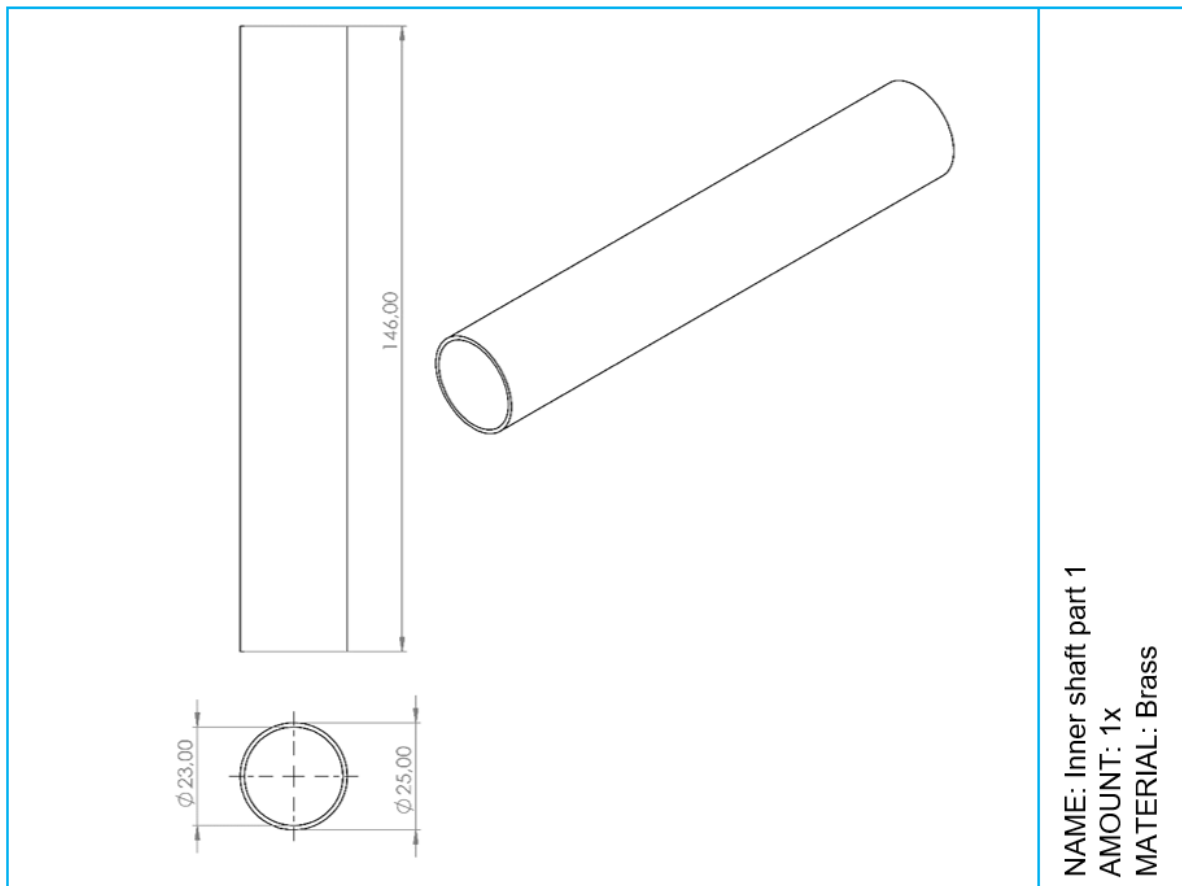


Figure D.1: Construction drawings of the inner shaft - Machined prototype

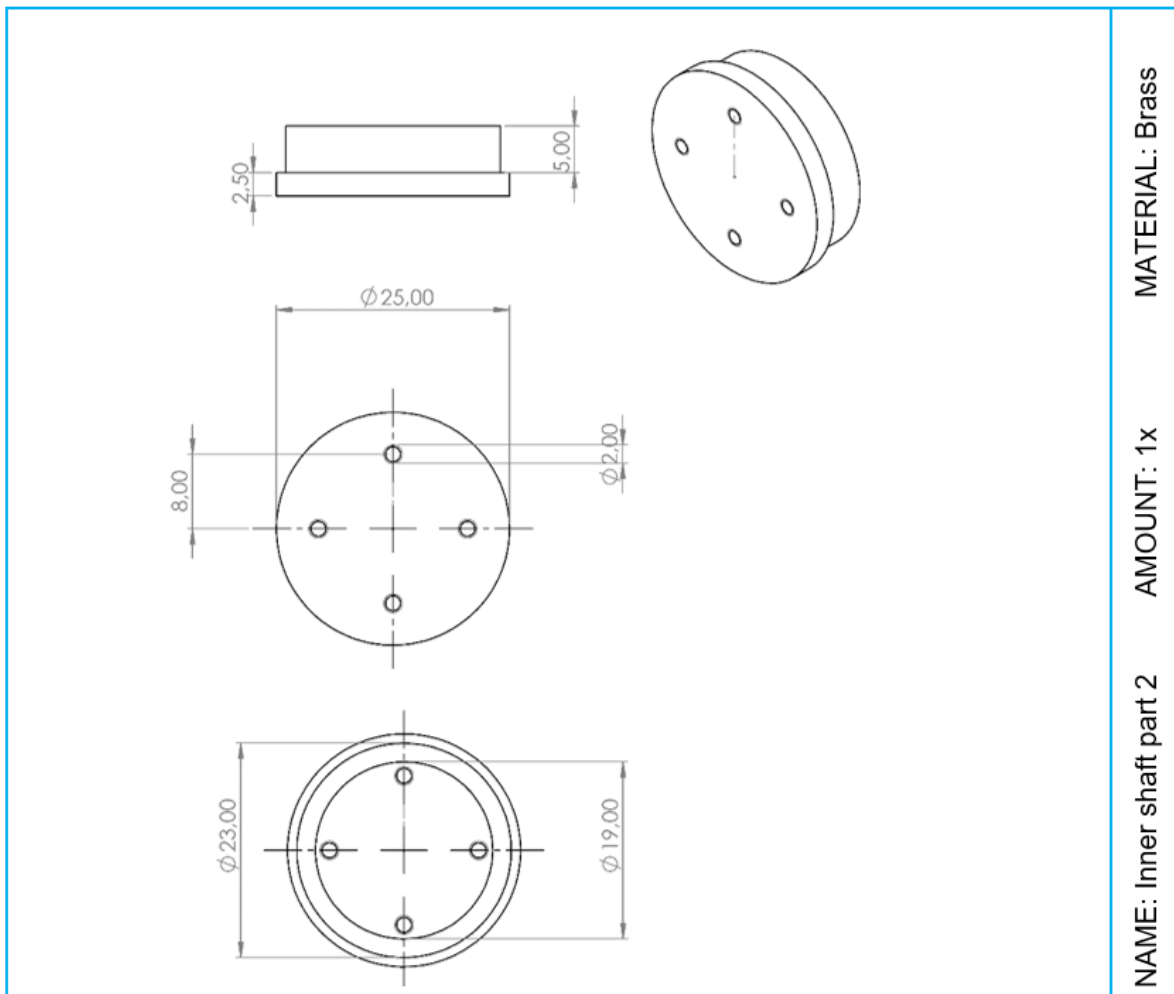


Figure D.2: Construction drawings of the inner shaft part 2 - Machined prototype

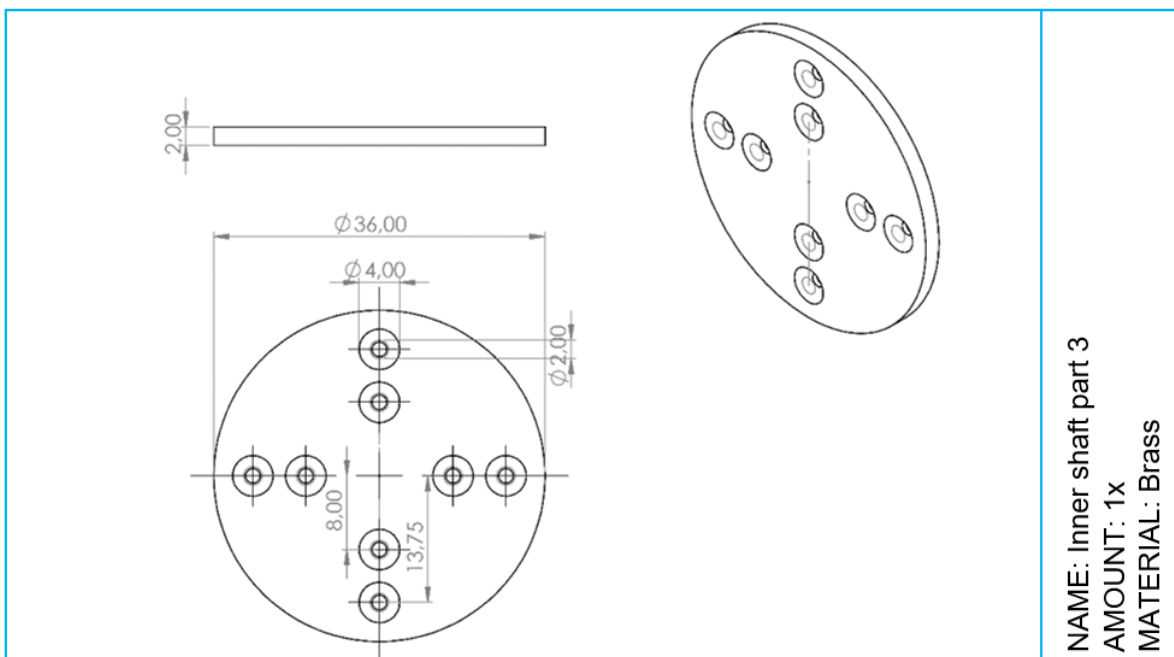


Figure D.3: Construction drawings of the inner shaft part 3 - Machined prototype

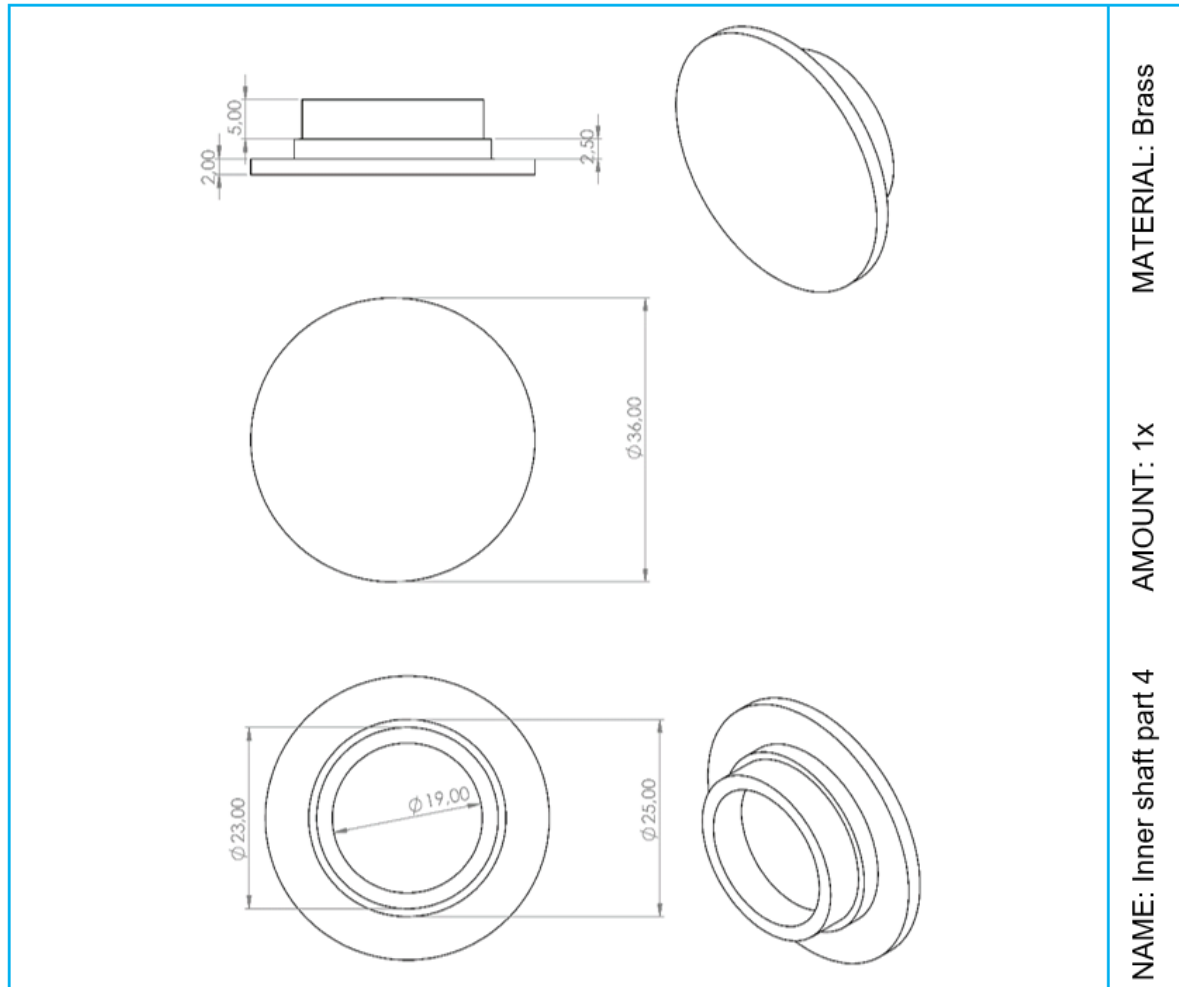


Figure D.4: Construction drawings of the inner shaft part 4 - Machined prototype

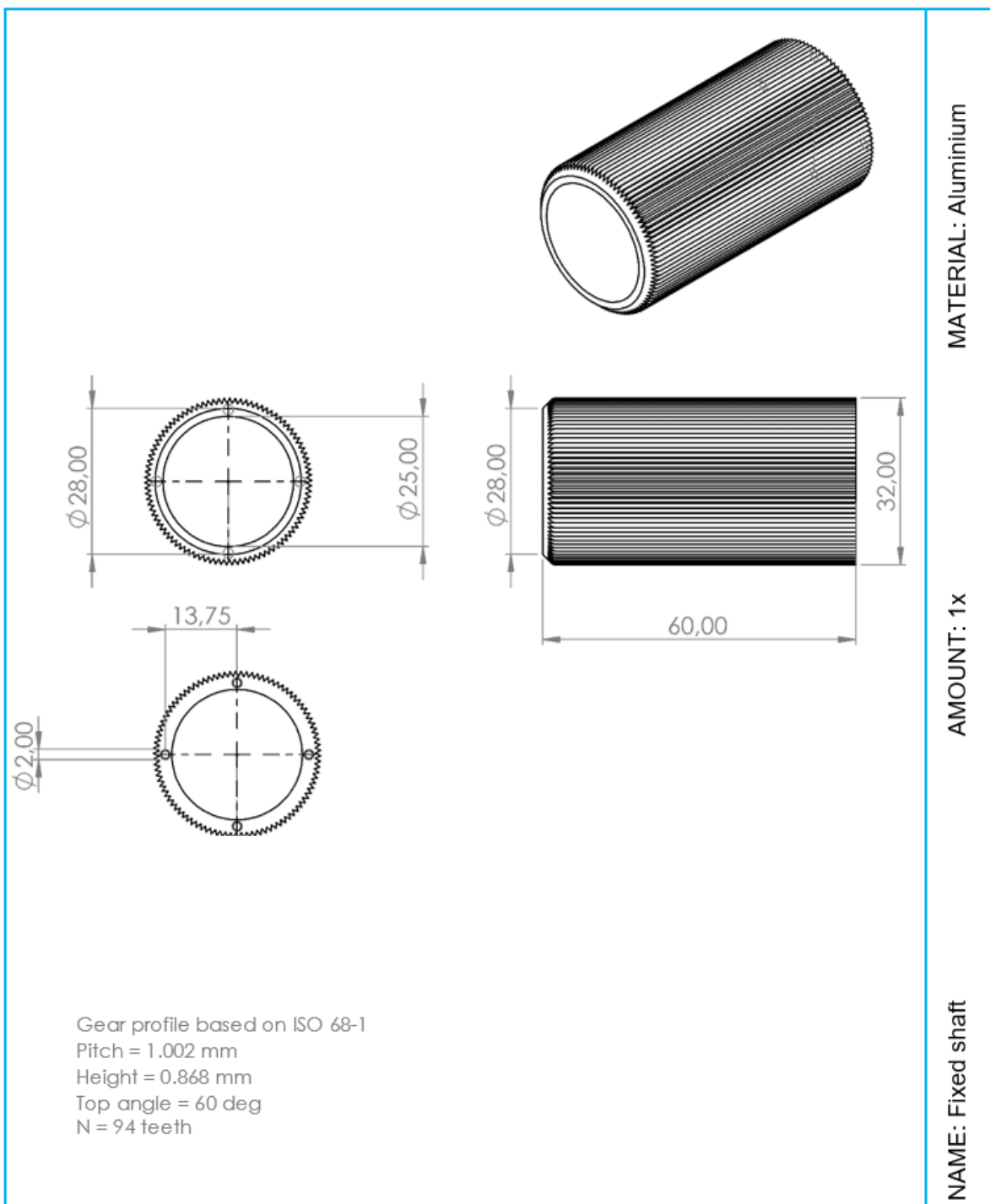


Figure D.5: Construction drawings of the fixed shaft - Machined prototype

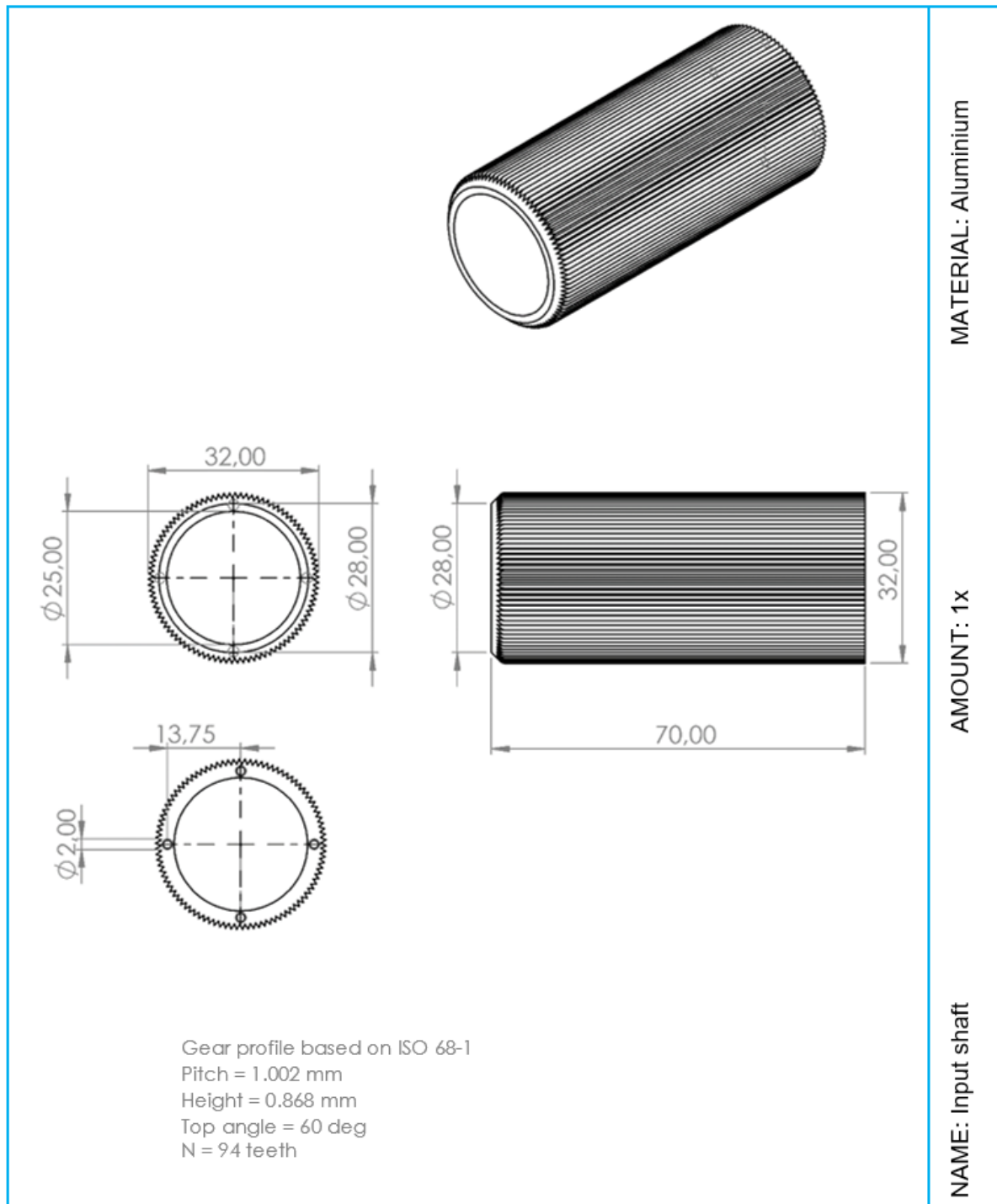


Figure D.6: Construction drawings of the input shaft - Machined prototype

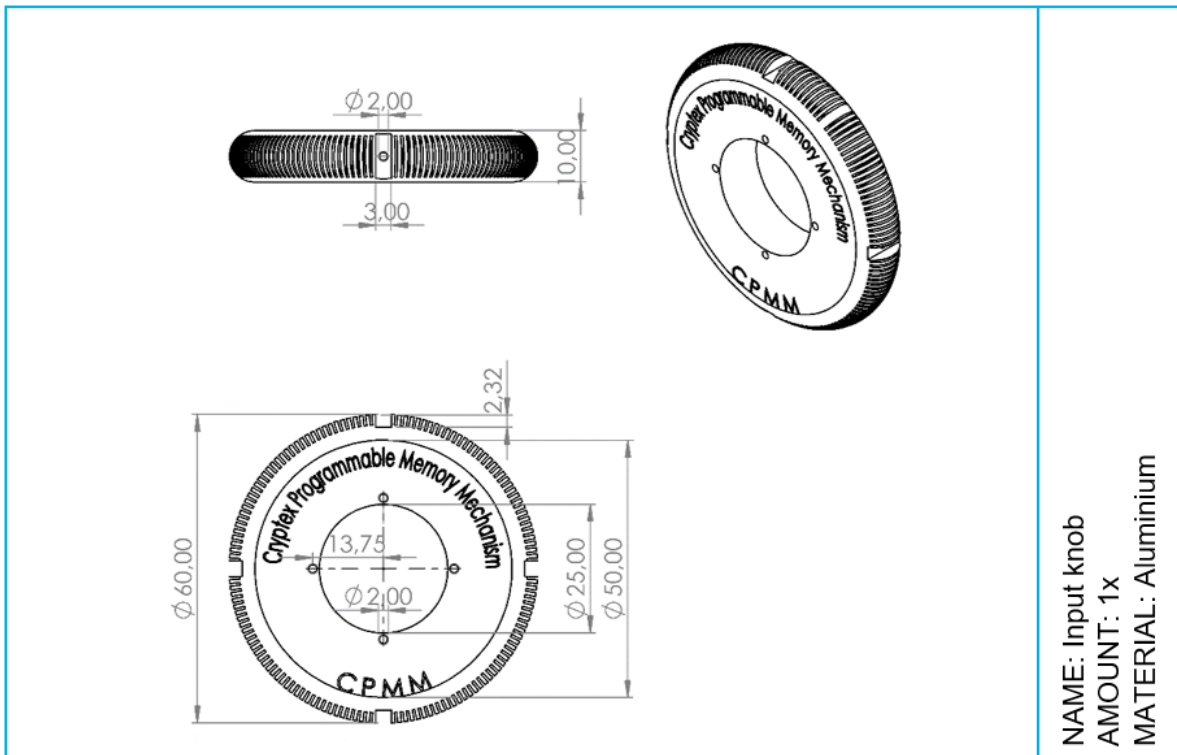


Figure D.7: Construction drawings of the input knob - Machined prototype

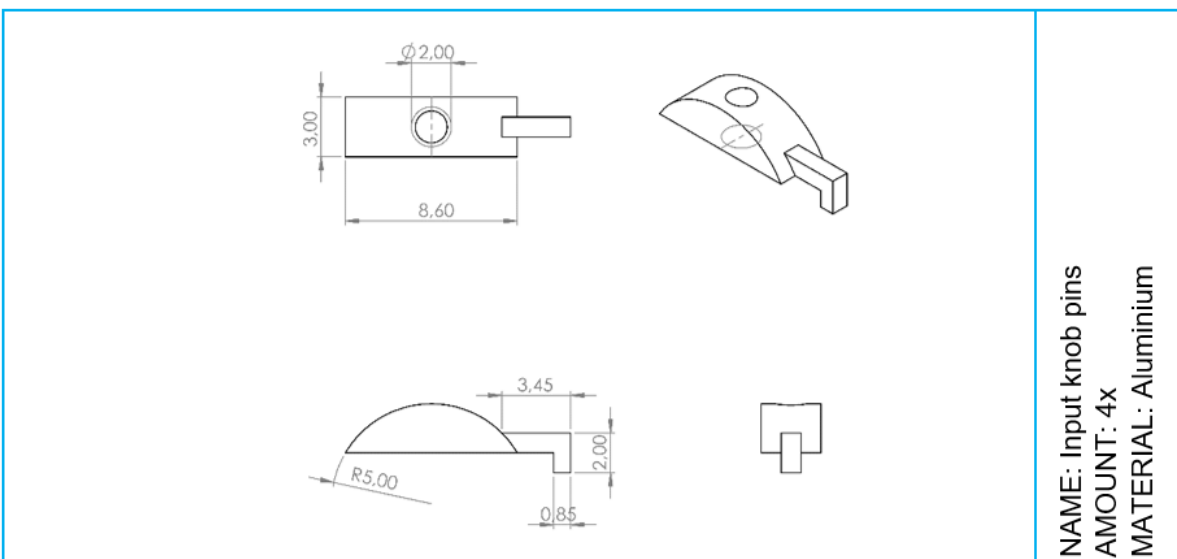


Figure D.8: Construction drawings of the input knob pins - Machined prototype

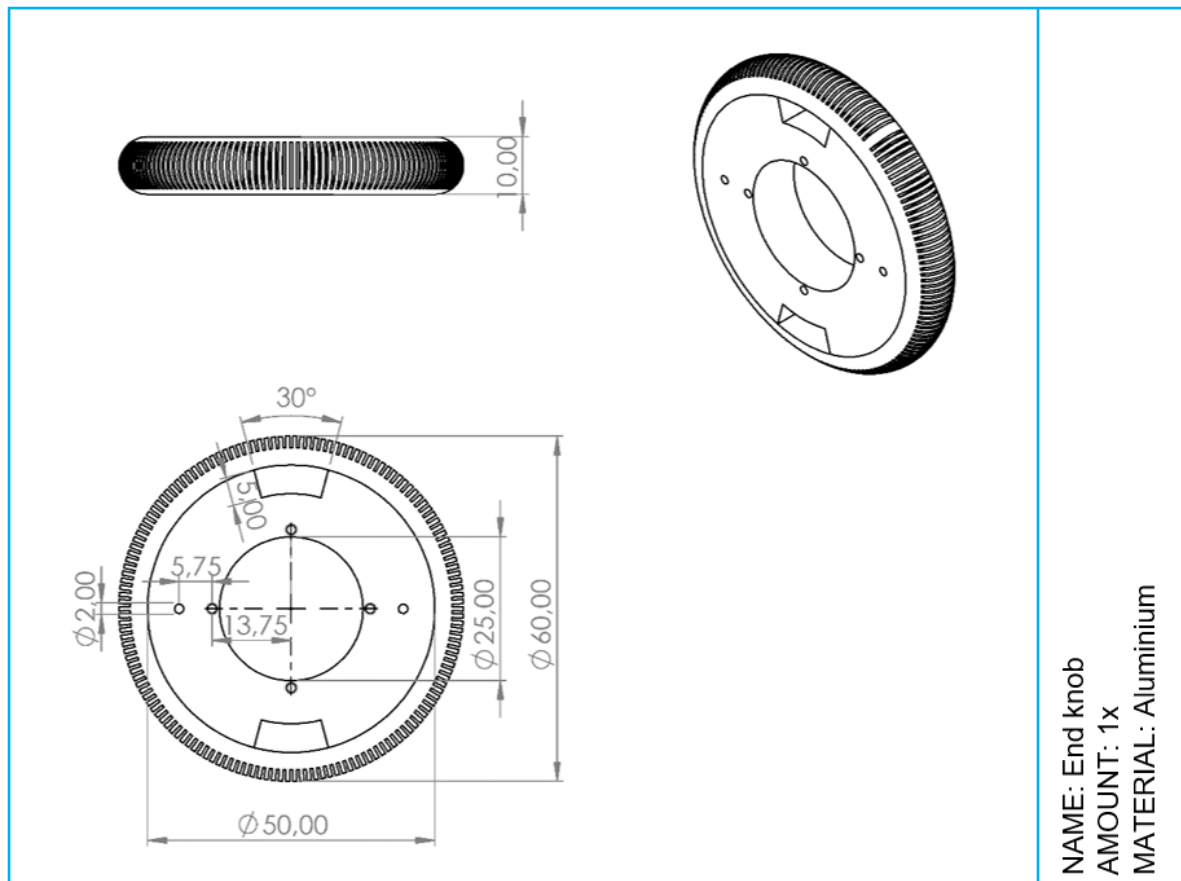


Figure D.9: Construction drawings of the end knob - Machined prototype

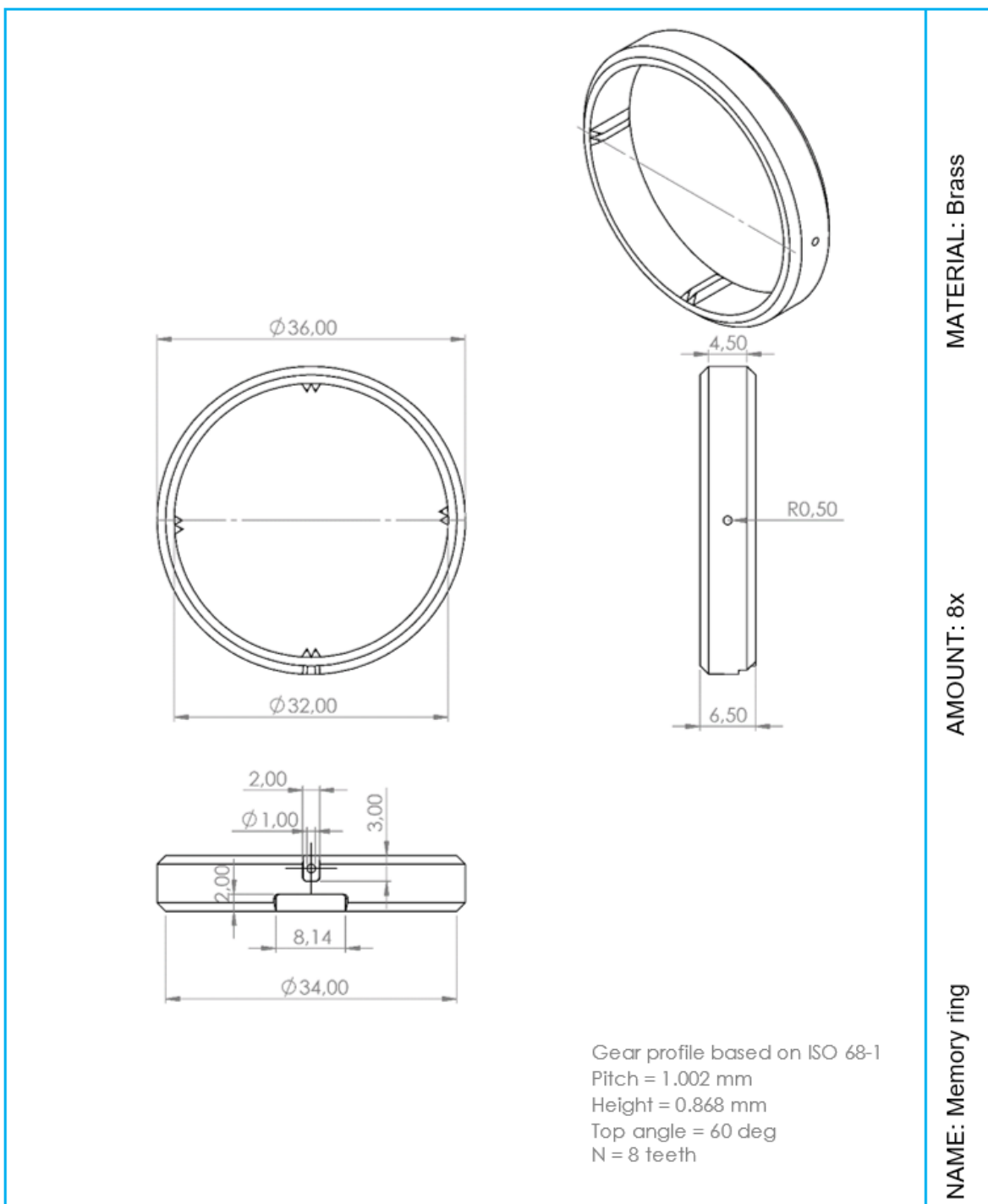


Figure D.10: Construction drawings of a memory ring - Machined prototype

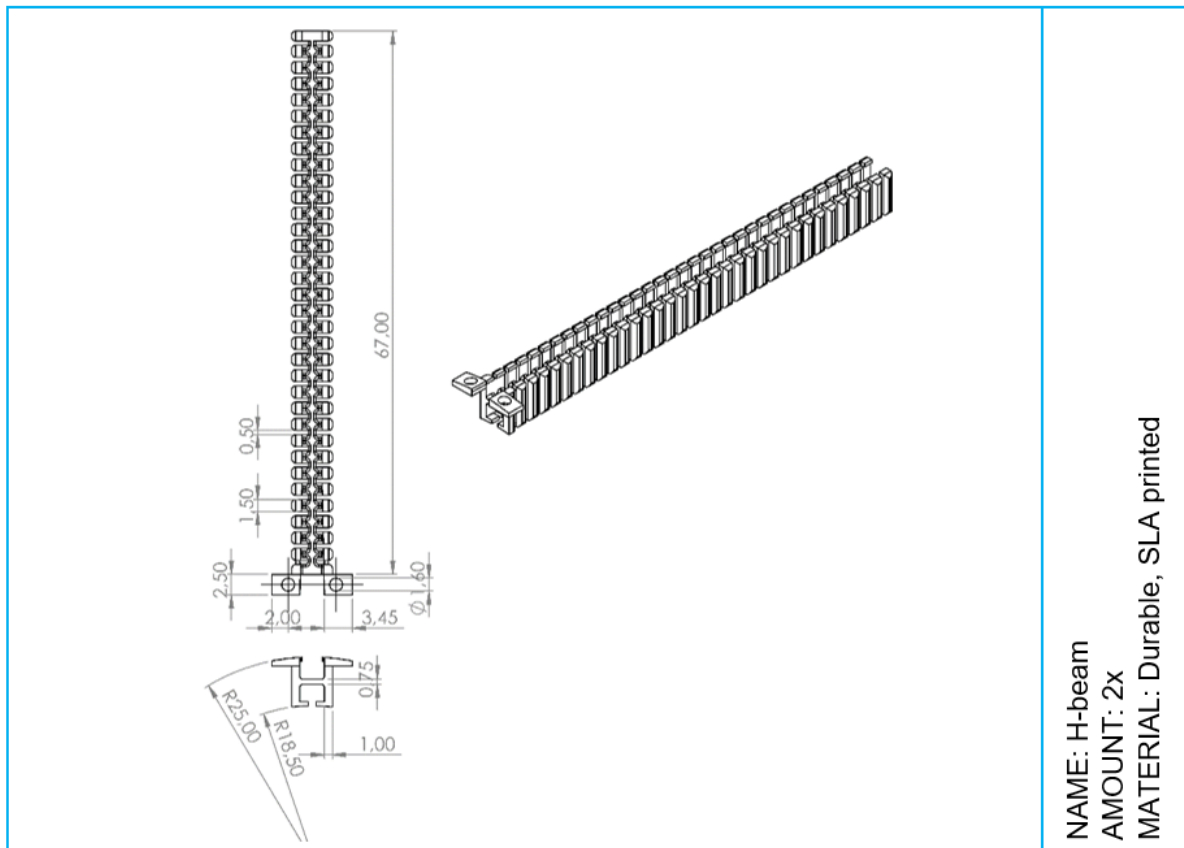


Figure D.11: Construction drawings of the H-beam - Machined prototype

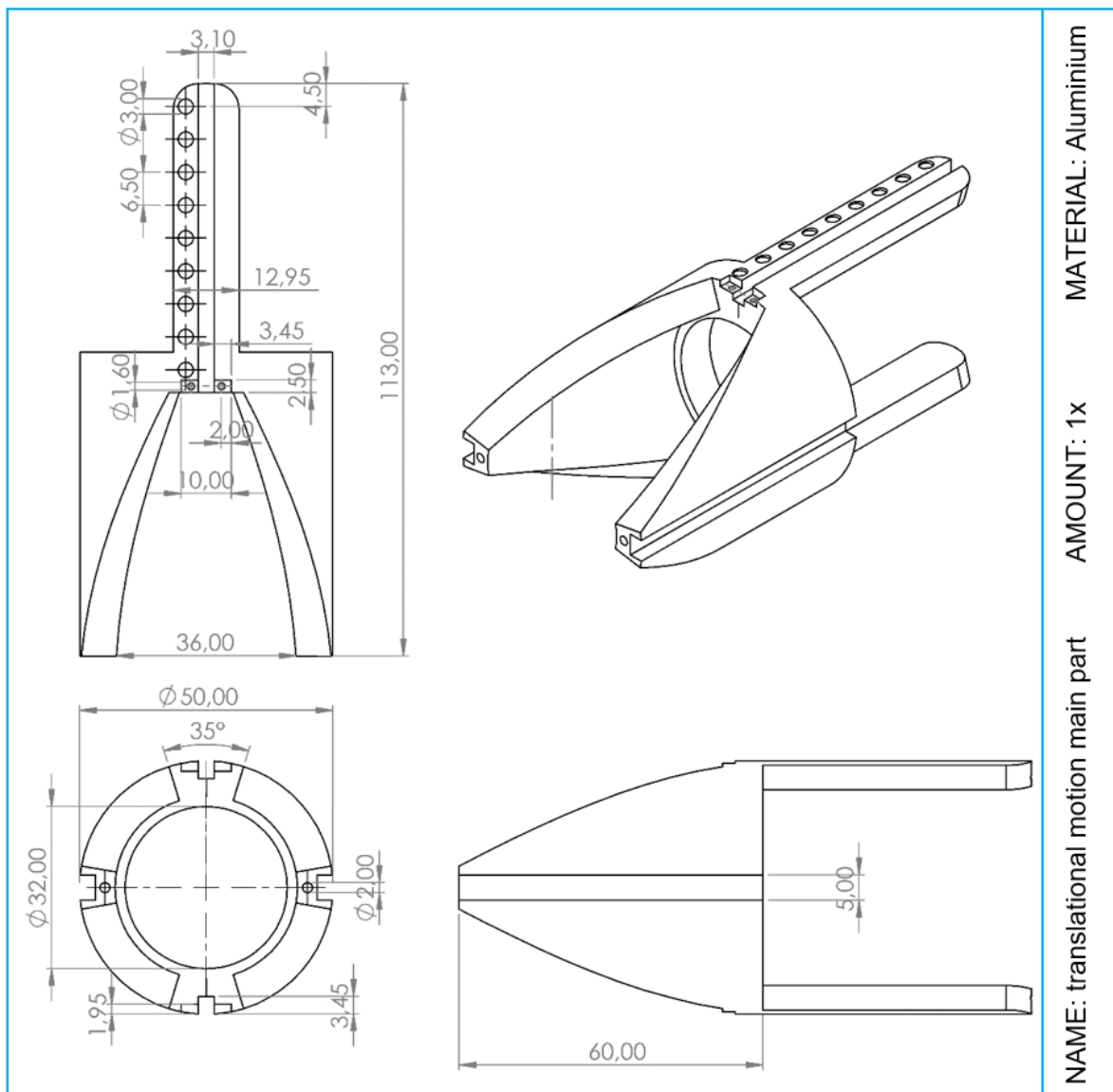


Figure D.12: Construction drawings of the translational motion main part - Machined prototype

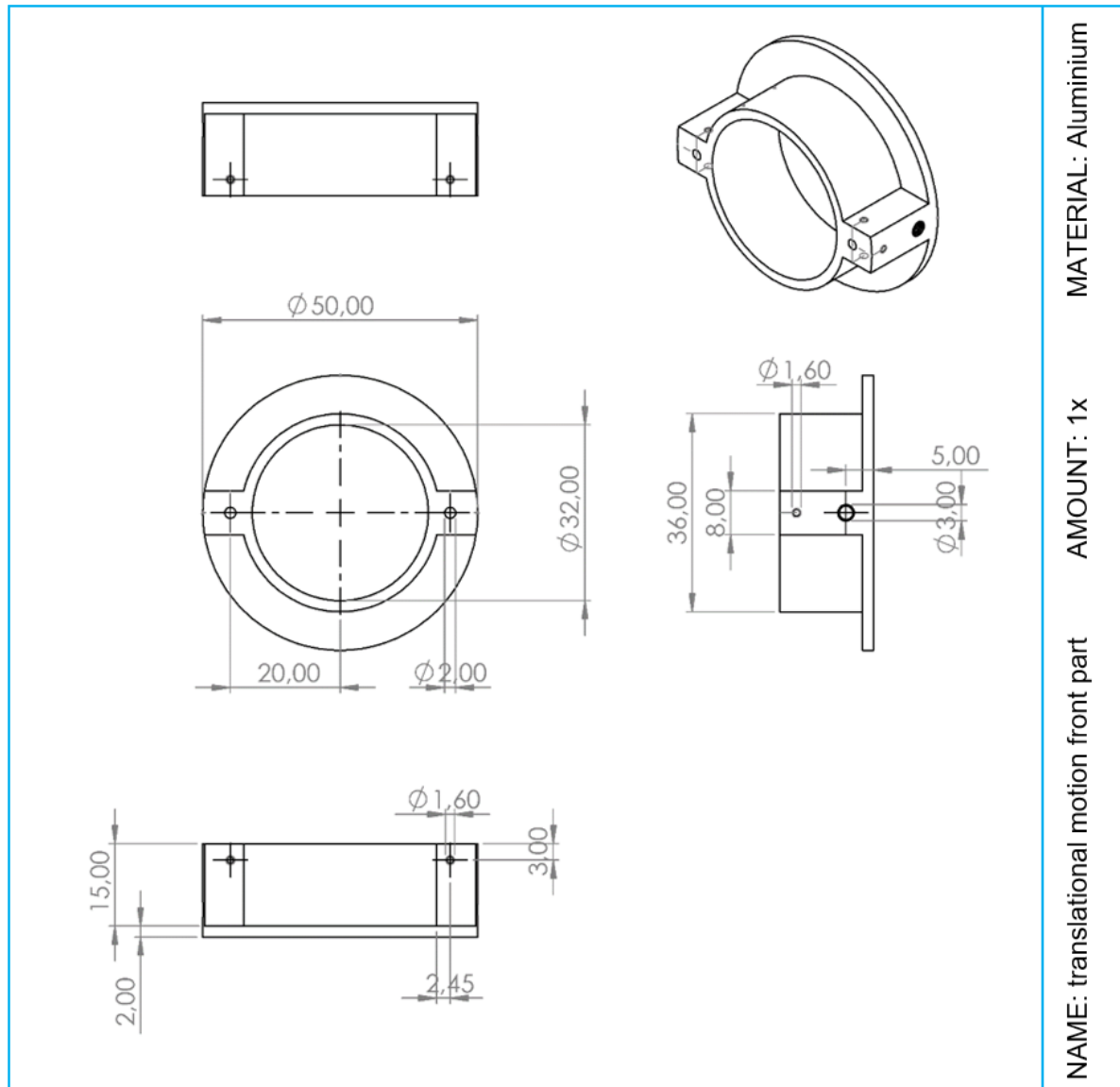


Figure D.13: Construction drawings of the translational motion front part - Machined prototype

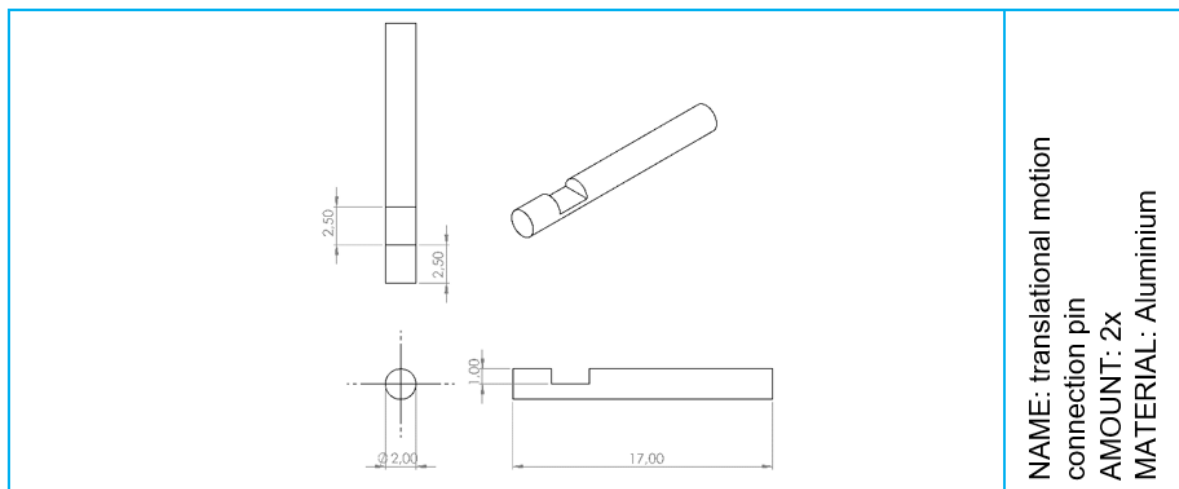


Figure D.14: Construction drawings of the connection pin connecting the two translational motion parts - Machined prototype

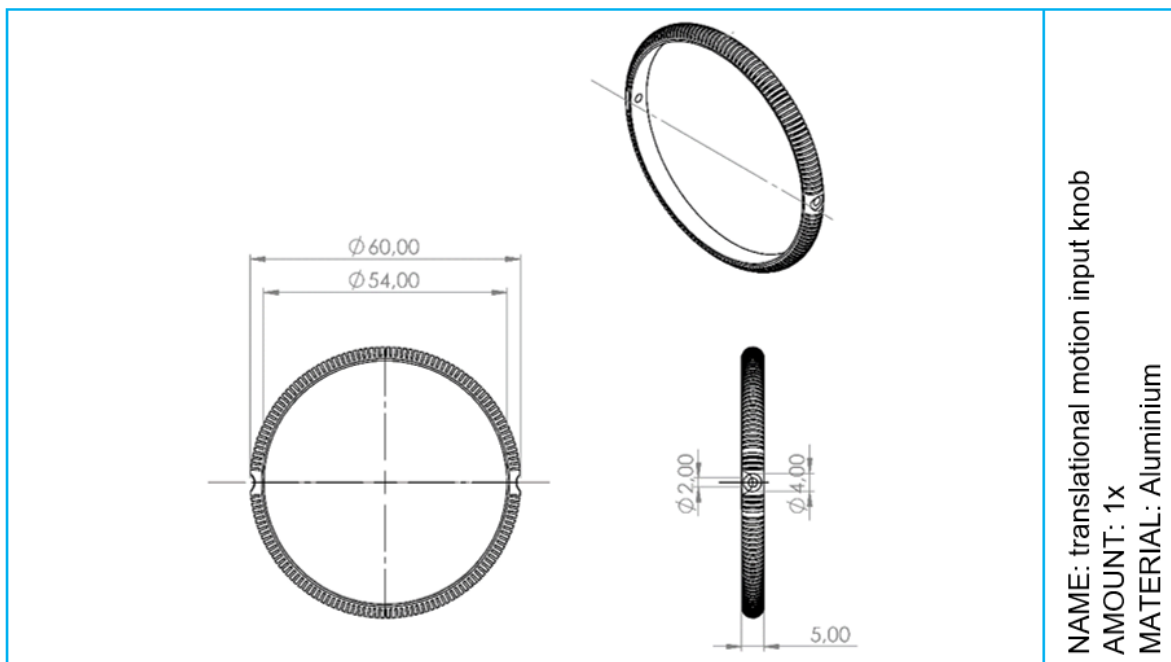


Figure D.15: Construction drawings of the translational motion input knob - Machined prototype

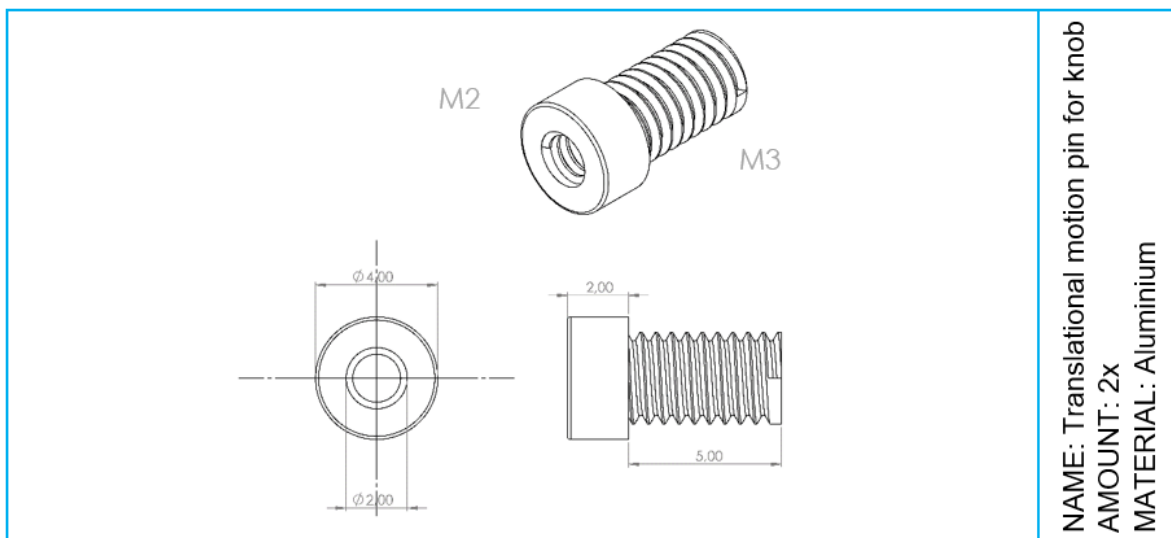


Figure D.16: Construction drawings of the pin connecting the translational motion mechanism to the translational motion input knob - Machined prototype

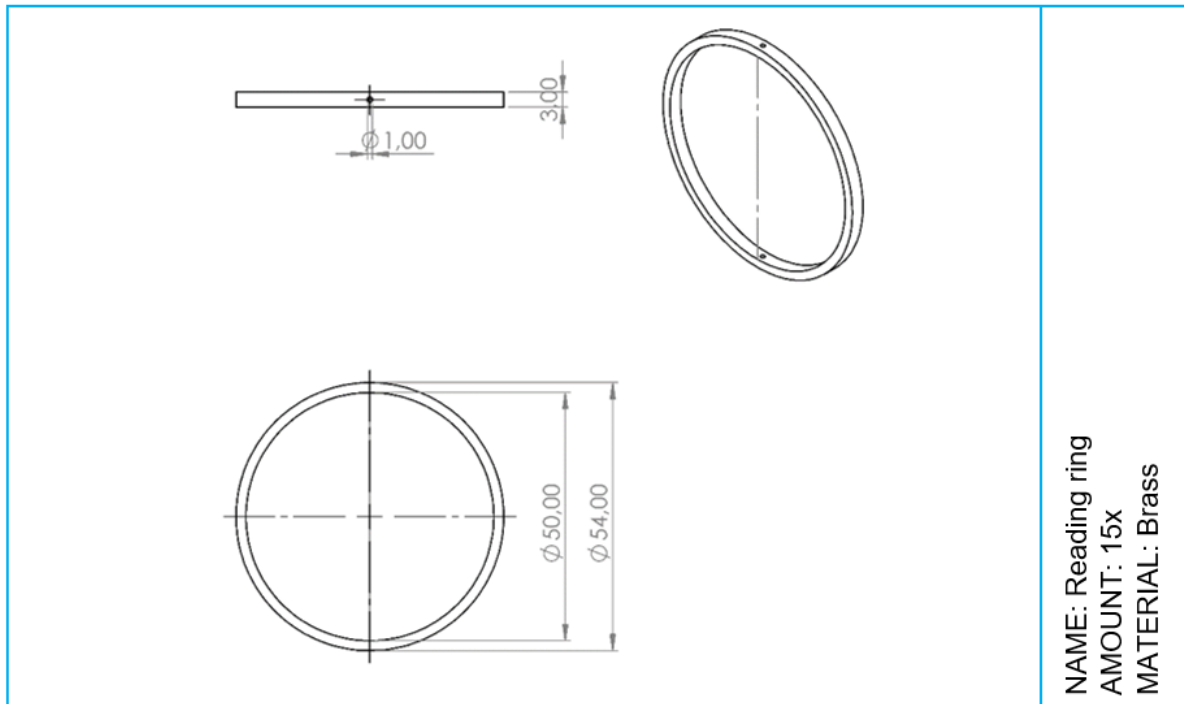


Figure D.17: Construction drawings of the reading ring - Machined prototype

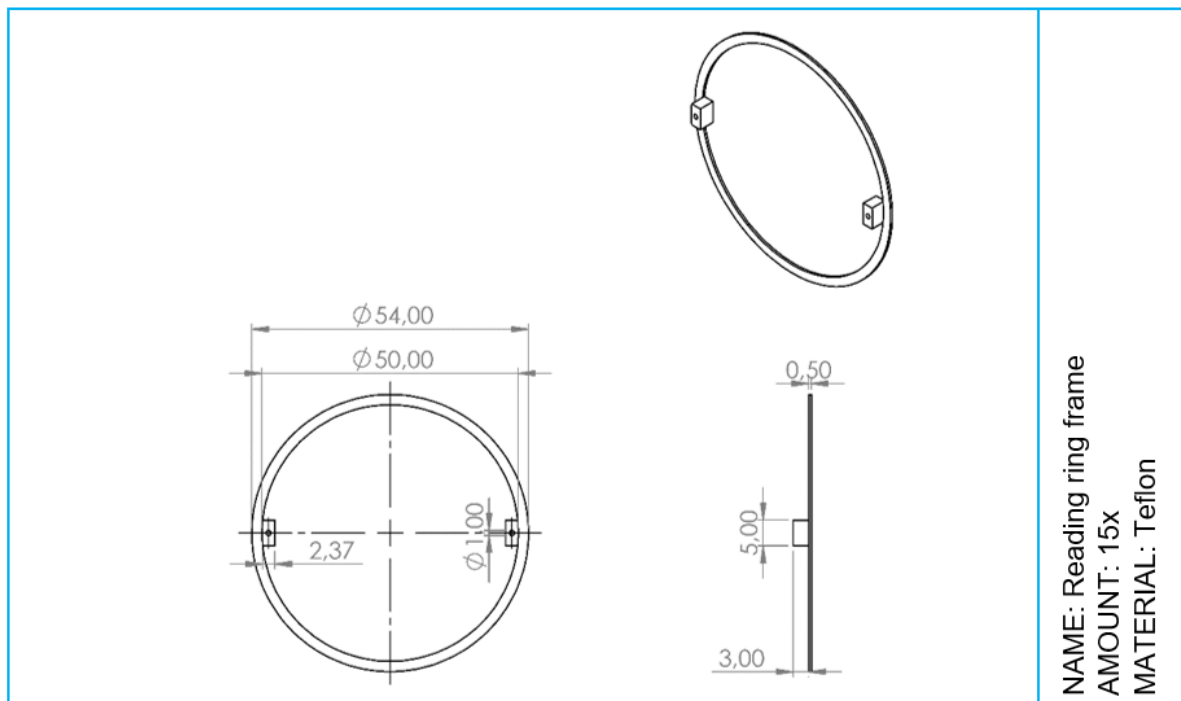


Figure D.18: Construction drawings of the reading ring frame rings in between - Machined prototype

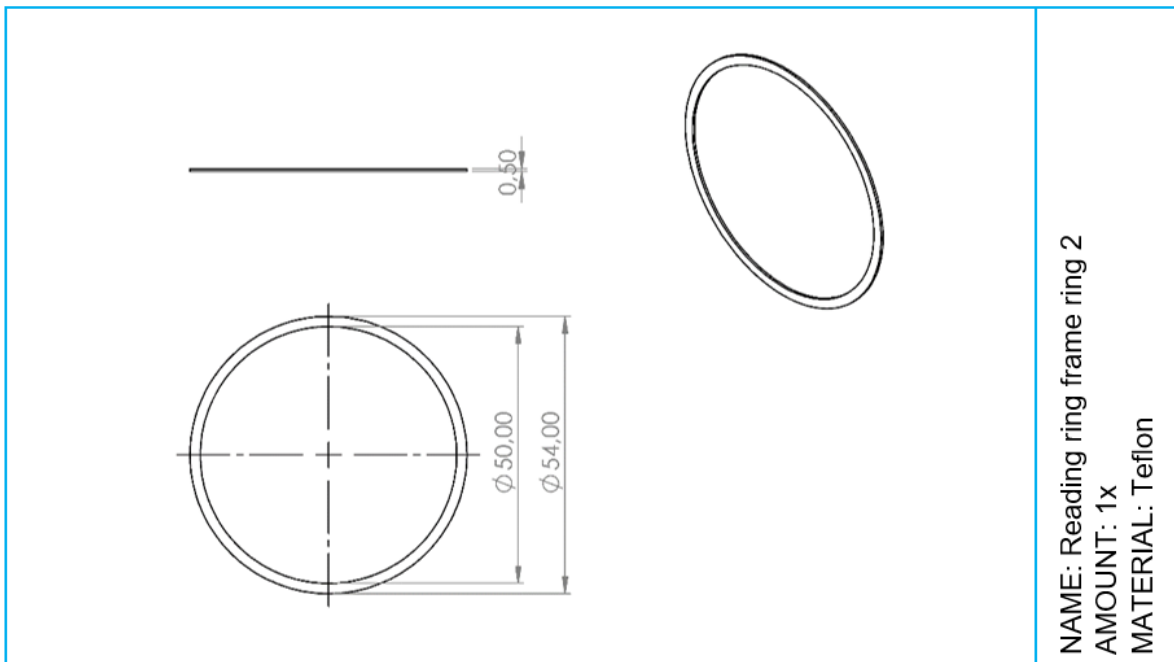


Figure D.19: Construction drawings of the reading ring frame outside ring- Machined prototype

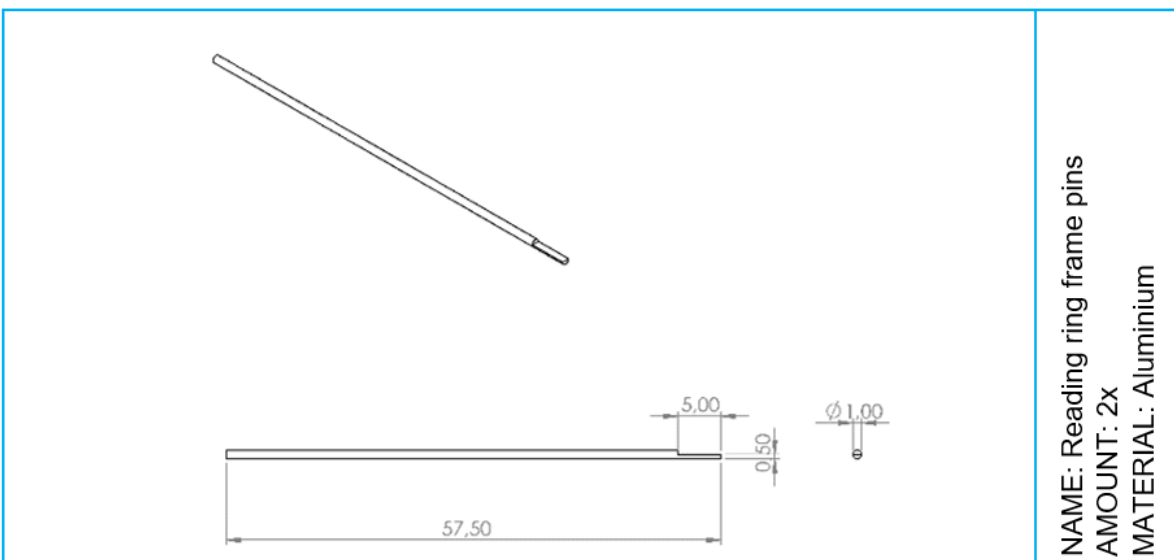


Figure D.20: Construction drawings of the reading ring frame pin - Machined prototype

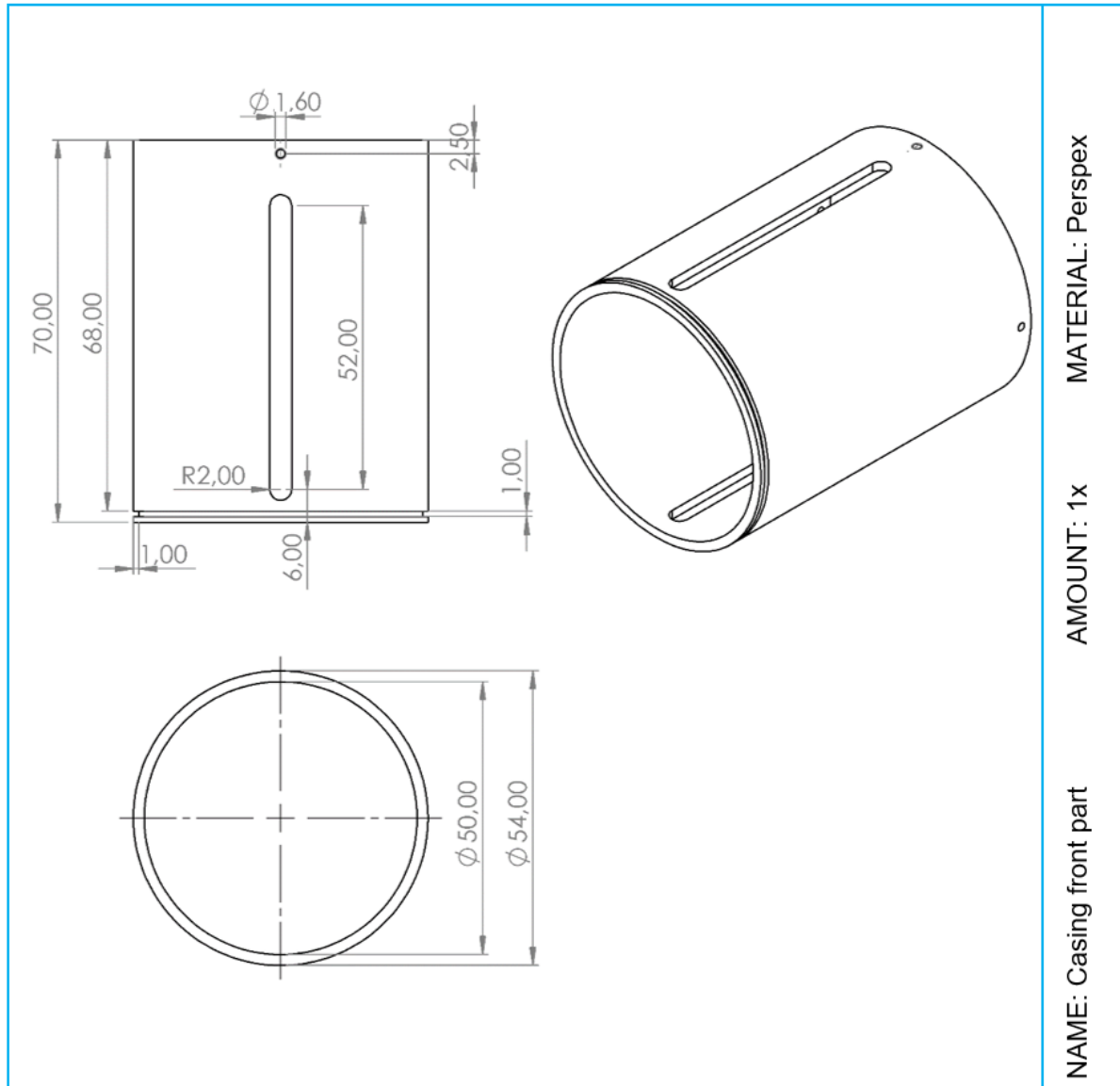


Figure D.21: Construction drawings of the casing front part - Machined prototype

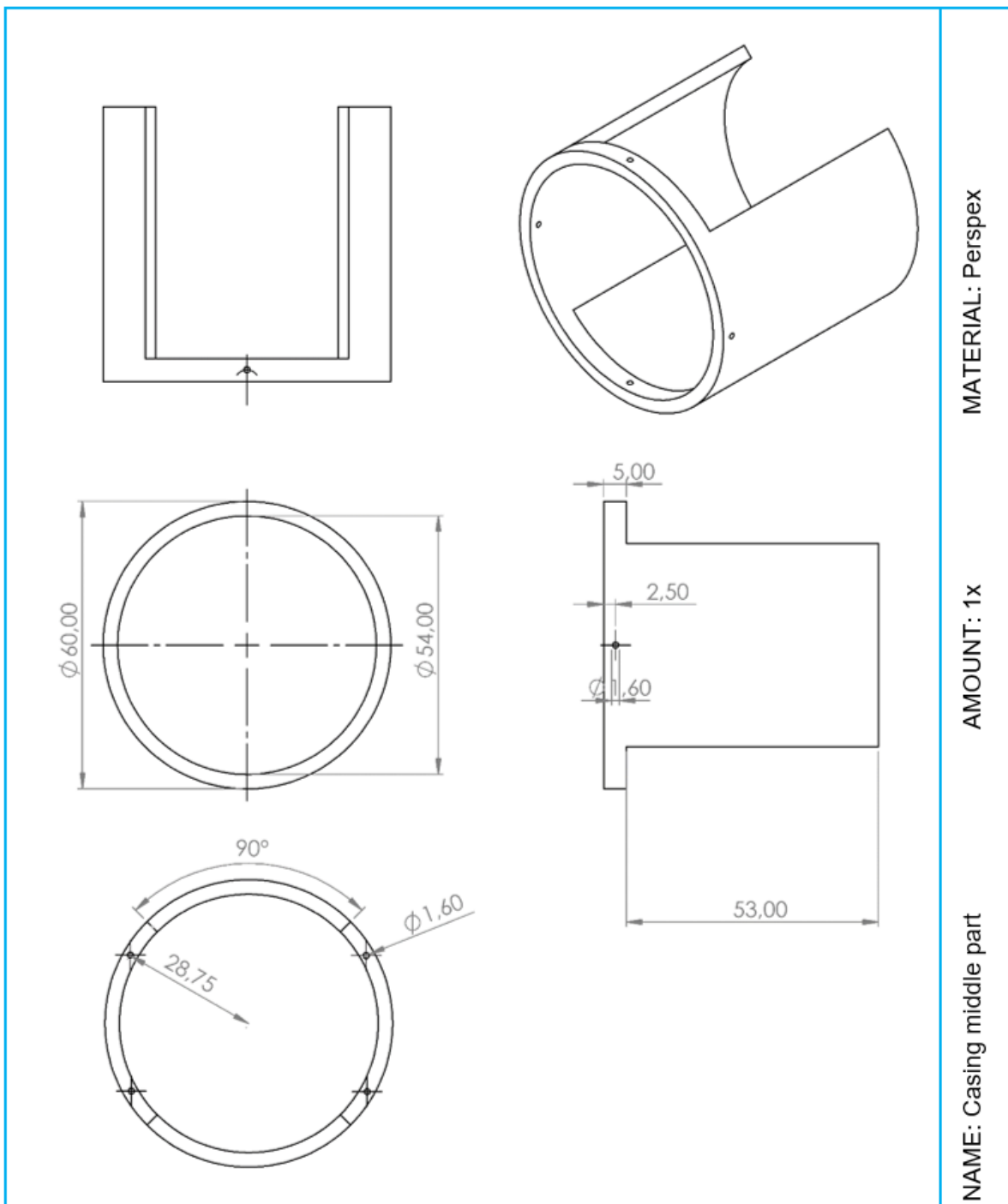


Figure D.22: Construction drawings of the casing middle part - Machined prototype

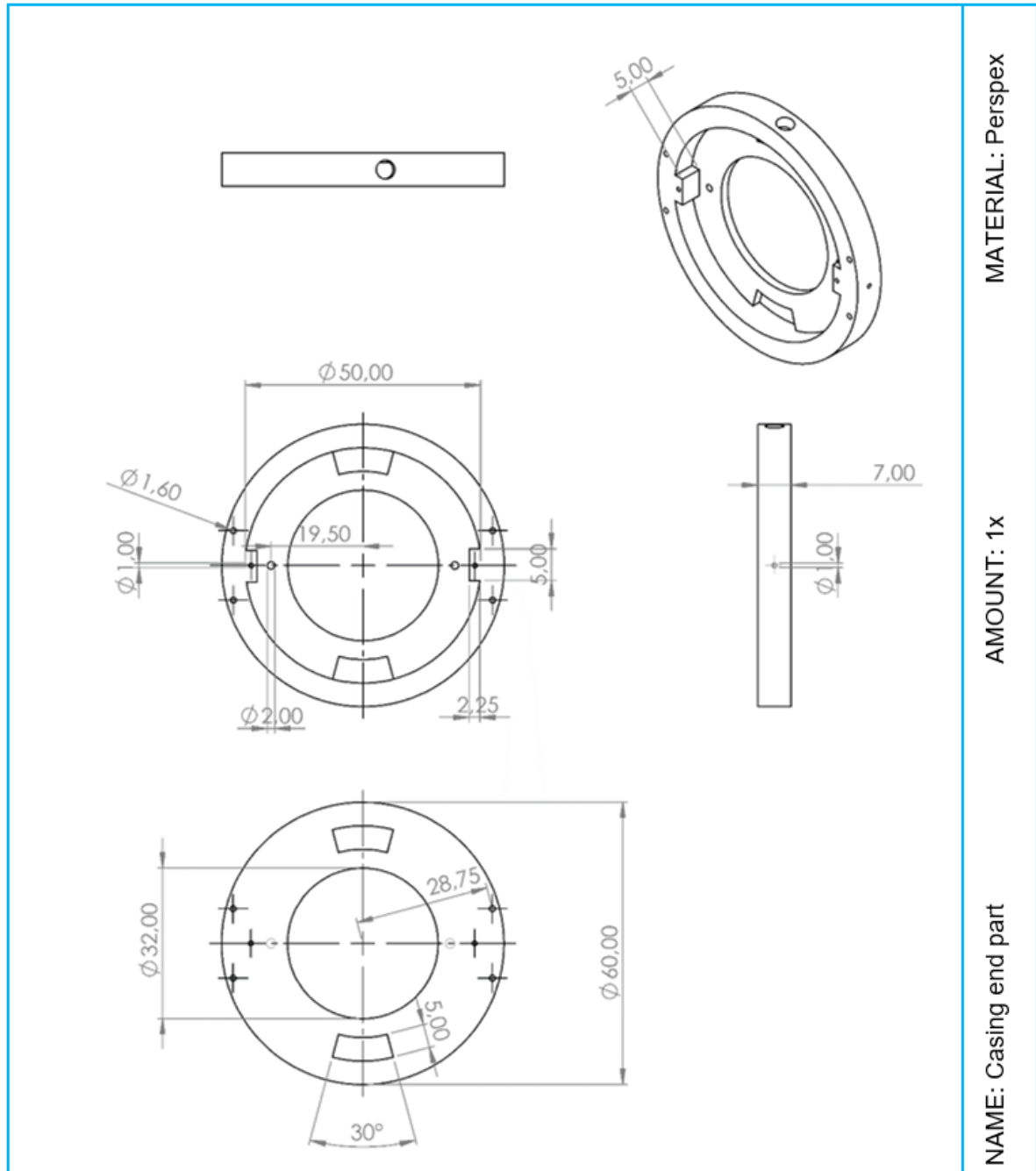


Figure D.23: Construction drawings of the casing end part - Machined prototype

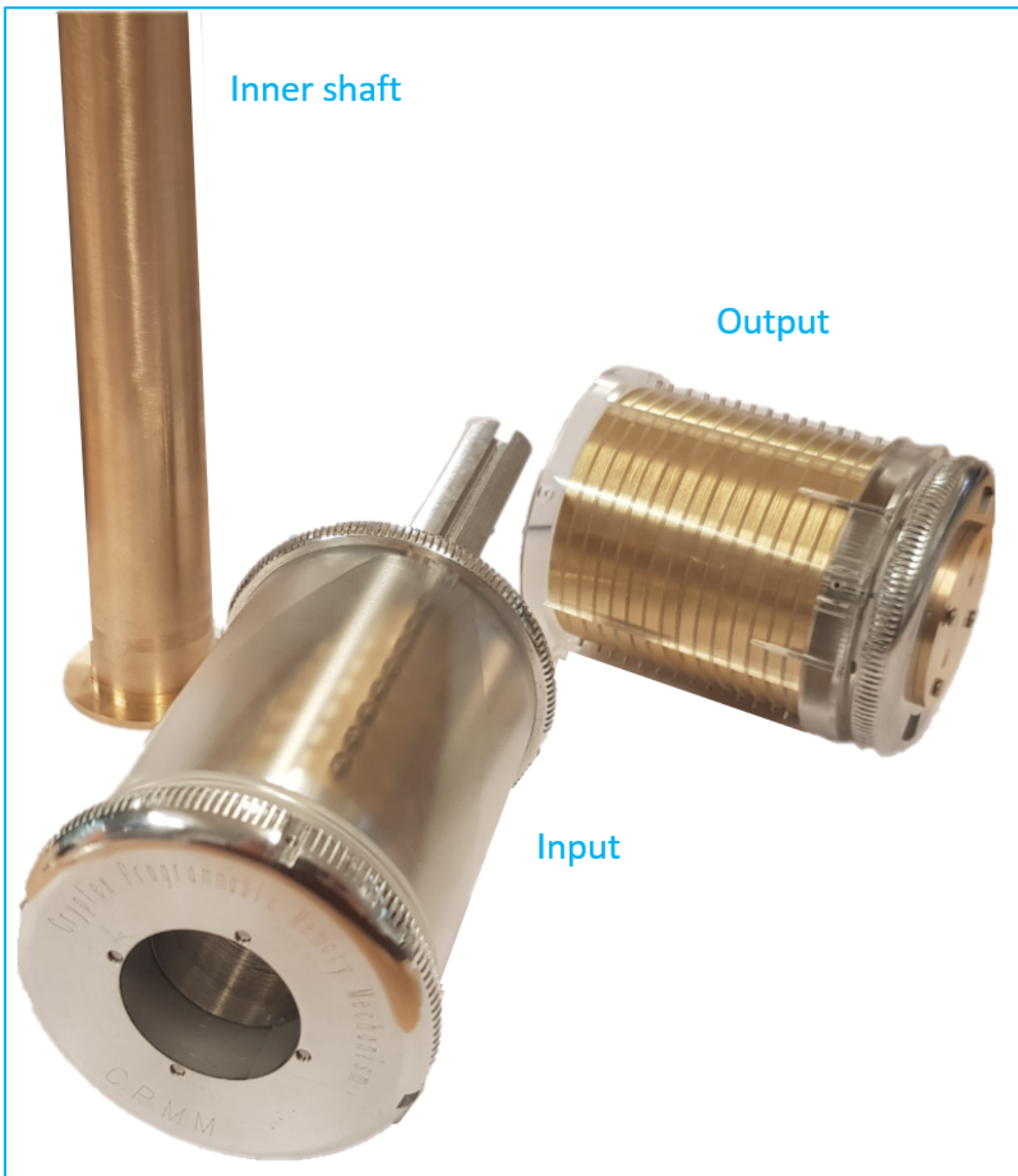


Figure D.24: Machined prototype: picture of the three building assemblies. The input includes the input knob, input shaft, translational motion mechanism, memory rings, H-beams, the front casing and the translational motion knob. The output consists out of the reading rings and their frame, the fixed shaft, end-knob, the casing middle part and casing end part.



Figure D.25: Picture of the input knob and the input shaft from the machined prototype

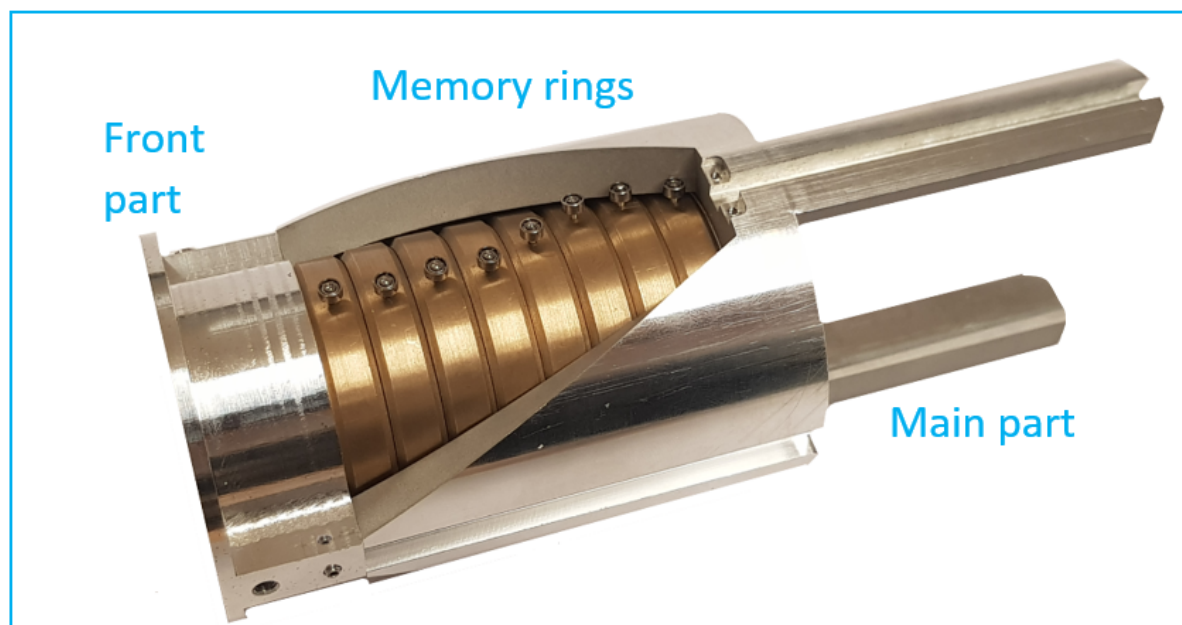


Figure D.26: Picture of the translational motion mechanism from the machined prototype



Figure D.27: Picture of the memory ring from the machined prototype

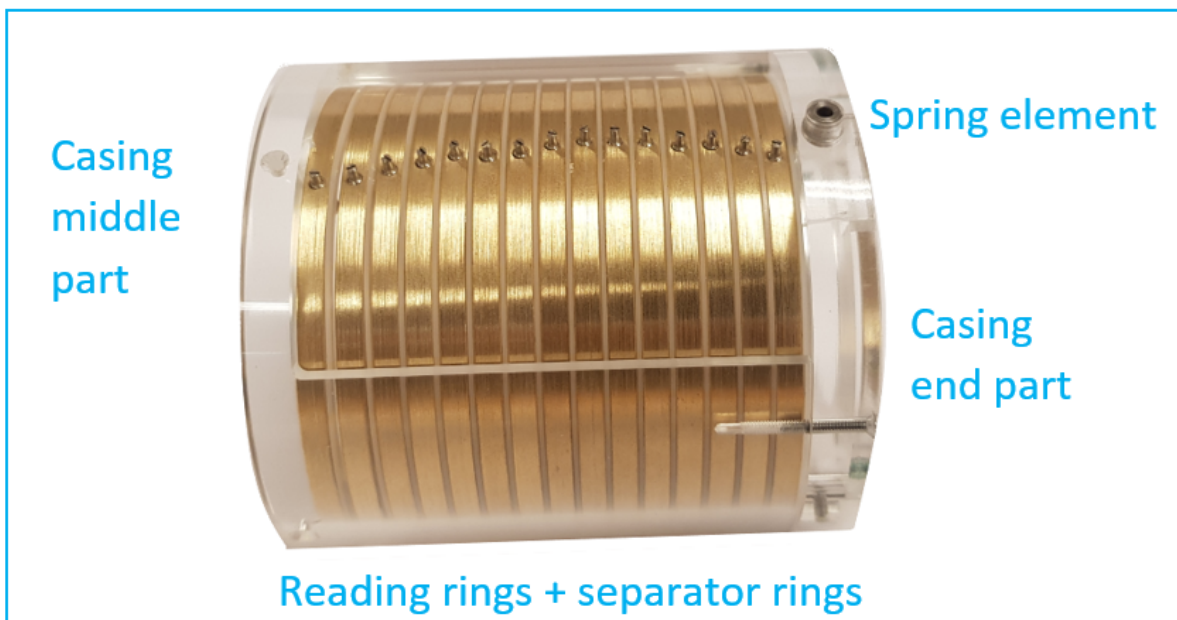


Figure D.28: Picture of the reading ring assembly from the machined prototype

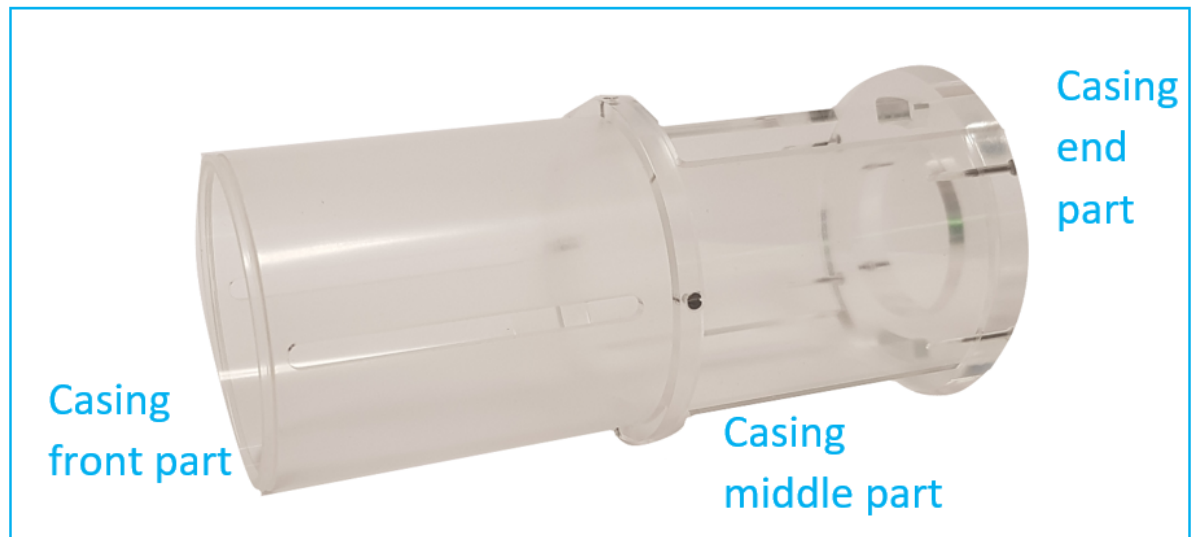
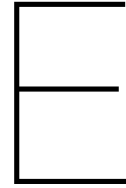


Figure D.29: Picture of the casing assembly from the machined prototype



3D printed prototype

Exploded view and BOM

The exploded view of the 3D printed prototype is provided in Figure E.1. The bill of materials for the prototype is shown in Figure E.2.

Machined vs. 3D printed prototype

The tables in Figure E.3, Figure E.4 and Figure E.5 show the main differences between the machined prototype and the 3D printed prototype. Due to the printing properties, such as the accuracy of the 3D printers available, and the material properties of the polymers, alterations were made for the 3D printed components. All parts had to be adjusted based on spacing and play between moving parts, this is not included in the figures.

Construction drawings of the parts

Construction drawings of the components are provided in Figure E.6 to Figure E.22. What must be noted is that the drawings do not have the same scale.

Dimensioning

Figure E.23 and Figure E.24 show two types of 3D printed shaft and memory ring. These prints have been used to test the spacing required for optimal performance.

Pictures of the prototype

In this section some pictures of 3D printed components are shown. Figure E.25 shows the two inner shaft components. Figure E.26 is a picture of the two shafts. The shaft and knobs are printed as one part. As can be seen in the figure, the surface of the knobs is rough. A picture of the two translational motion parts is provided in Figure E.27. Figure E.28 shows the 8 memory rings, located inside the translational motion mechanism. In Figure E.29, a closed up picture of the memory ring is shown. The memory ring includes two bearings, a pin and a slot. Similar to the machined prototype, the pin of this memory ring moves inside the slot of an adjacent ring. Therefore, it functions as a rotation limiter. The reading ring assembly is shown in Figure E.30. 3D printed rings function as separator rings in between the reading rings. Instead of ball bearings, the reading rings have M1 screws. The reading ring assembly is located inside the middle part of the casing. The casing assembly is shown in Figure E.31.

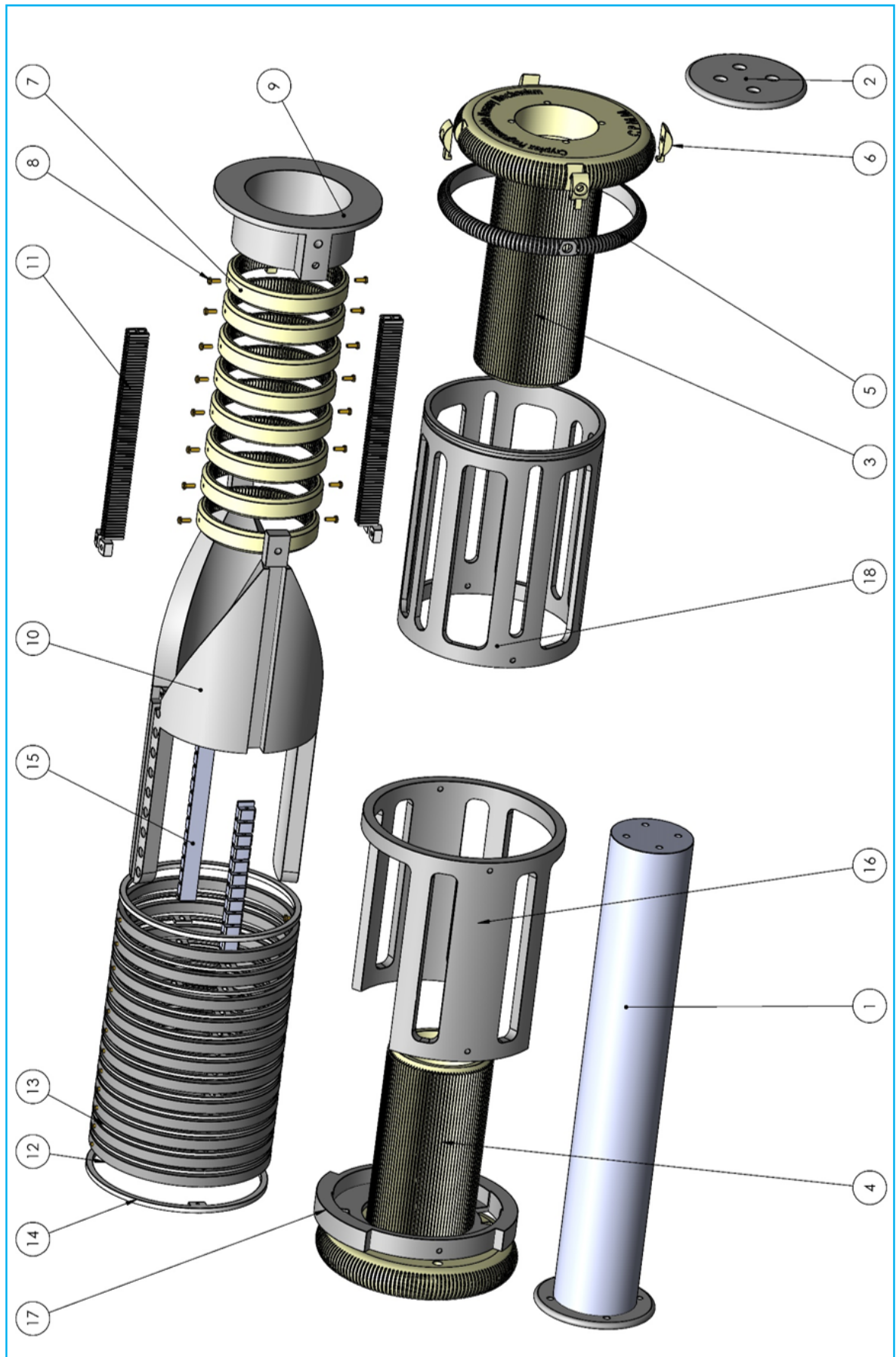


Figure E.1: Exploded view of 3D printed prototype

Number	Component name	Quantity
1	Inner shaft part 1	1
2	Inner shaft part 2	1
3	Input shaft and input knob	1
4	Fixed shaft and end knob	1
5	Translational motion knob	1
6	Input knob pin	4
7	Memory ring	8
8	M1 screw	40
9	Translational mechanism front part	1
10	Translational mechanism main part	1
11	H-beam	2
12	Reading ring	12
13	Reading ring frame ring thin	11
14	Reading ring frame ring thick	2
15	Frame holder	2
16	Casing middle part	1
17	Casing end part	1
18	Casing front part	1

Figure E.2: Bill of materials 3D printed prototype

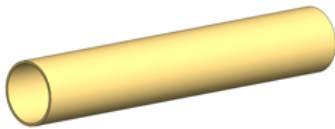

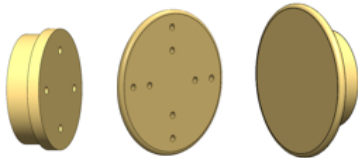

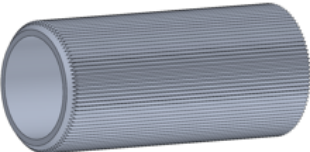
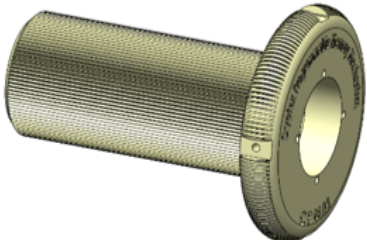

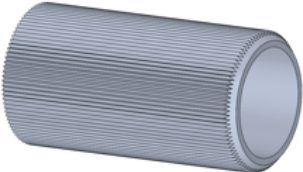
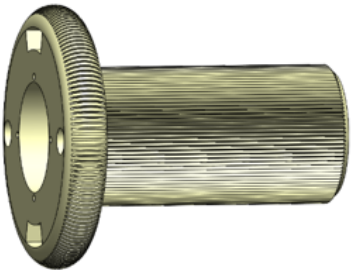
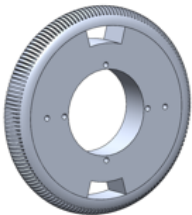
Part	Machined prototype	3D printed prototype	Changes made
Inner shaft	 <p>Part 1</p>		<p>In the machined prototype, part 2 and 4 are glued inside the shaft and part 3 is fastened against part 2. The inner shaft part 1, 2 and 3 are printed as one part. Only part 4 is printed separately. Thus part 2 in the 3D printed prototype, functions as part 4 from the machined prototype</p>
	 <p>Part 2 Part 3 Part 4</p>	<p><i>(Functions as part 4 from the machined prototype)</i></p>  <p>Part 2</p>	
Input shaft			<p>The input shaft and input-knob are printed as one part</p>
Input-knob			
Fixed shaft			<p>The fixed shaft and end-knob are printed as one part</p>
End-knob			

Figure E.3: 1/3 Machined versus 3D printed prototype. The differences in the inner shaft, input shaft and fixed shaft.



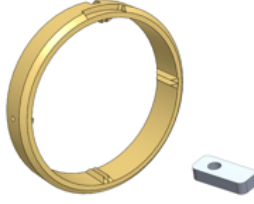





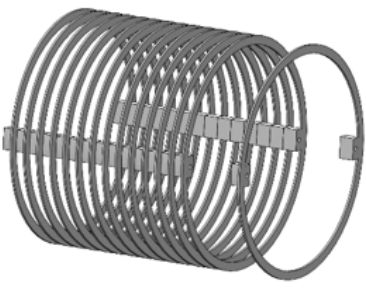
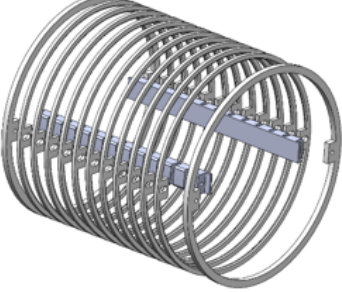
Part	Machined prototype	3D printed prototype	Changes made
Translational motion mechanism			In the machined prototype, the two parts are connected by a pin. The 3D printed parts are form fit. No additional pin, but a bigger extruded part.
Memory ring			The machined prototype has 8 teeth. The 3D printed prototype has teeth on the complete perimeter. The pin, that limits the rotation, and ring are printed as one part
Bearings			3mm ball bearings and 1 mm pins are replaced by M1x5 mm screws
Reading ring			Less rings: 12 rings instead of 15 3.2 mm thick instead of 3 mm
Reading ring frame			The separating rings are thicker: 0.9 mm instead of 0.5 mm. An additional part is printed that holds the separating rings together. A pin is going through the holder and rings. 13 separator rings instead of 16.

Figure E.4: 2/3 Machined versus 3D printed prototype. The differences in the memory rings, bearings, reading rings and reading ring frame.

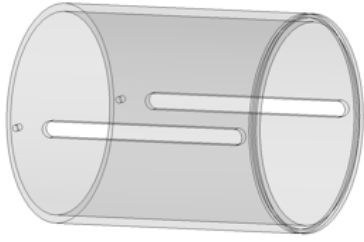

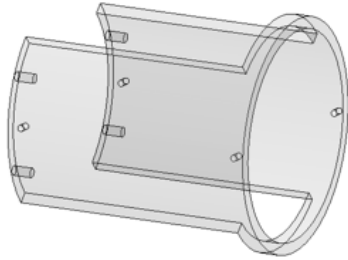
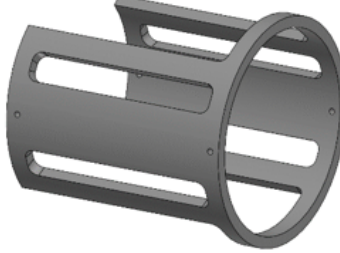
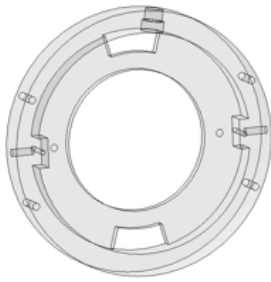

Part	Machined prototype	3D printed prototype	Changes made
Casing front part			The part is not transparent, so holes are made to be able to see the underlying components
Casing middle part			Additional gaps are made, to make the component more see-through. Also, the connection with the casing end part is adjusted.
Casing end part			The connection of the 3D printed part with the middle part of the casing is form fit, requiring a different shape. A fastener connects the parts radially. In the machined prototype, they are connected in the axially.

Figure E.5: 3/3 Machined versus 3D printed prototype. The differences in the casing components.

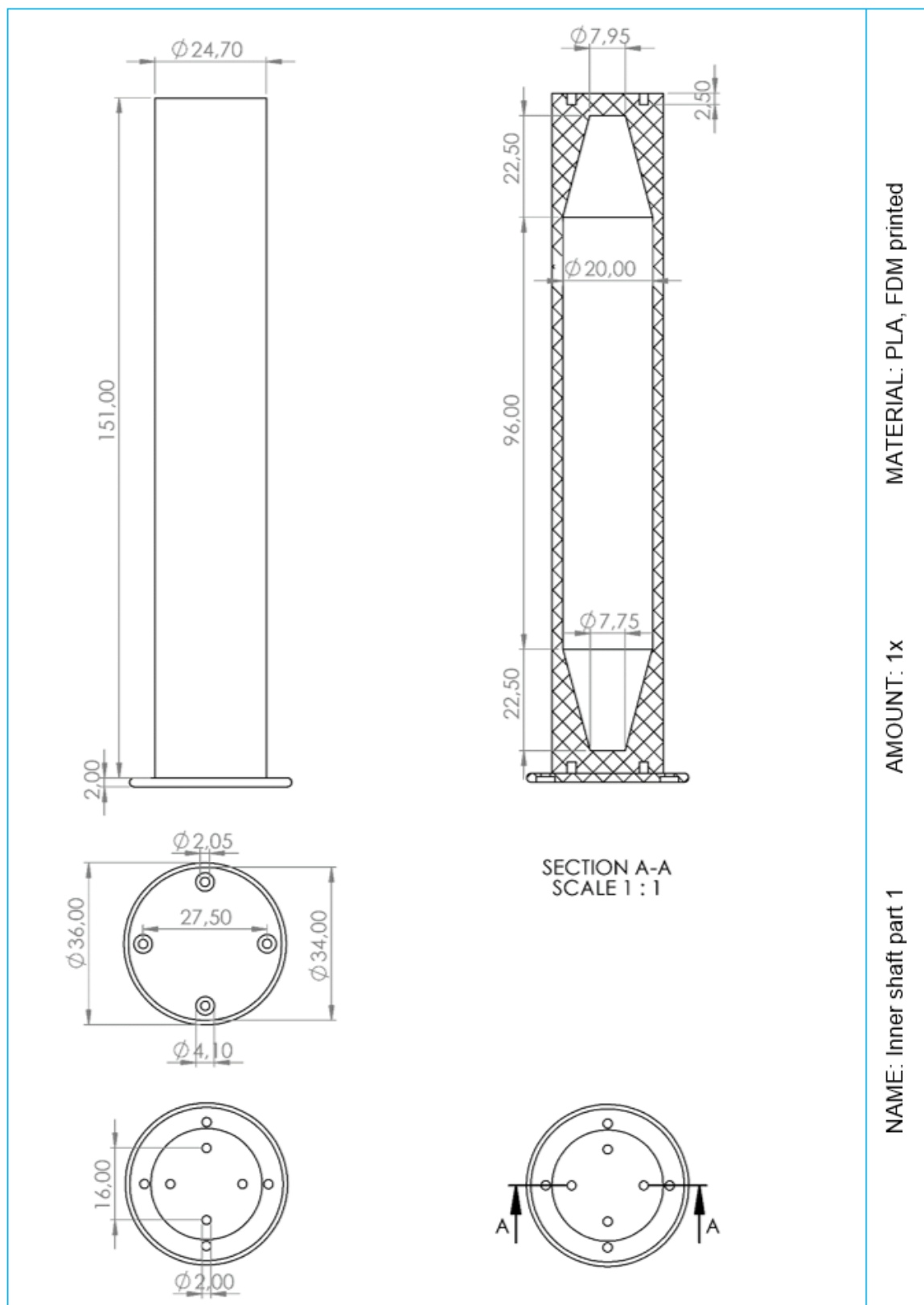


Figure E.6: Construction drawings of the inner shaft - 3D Printed prototype

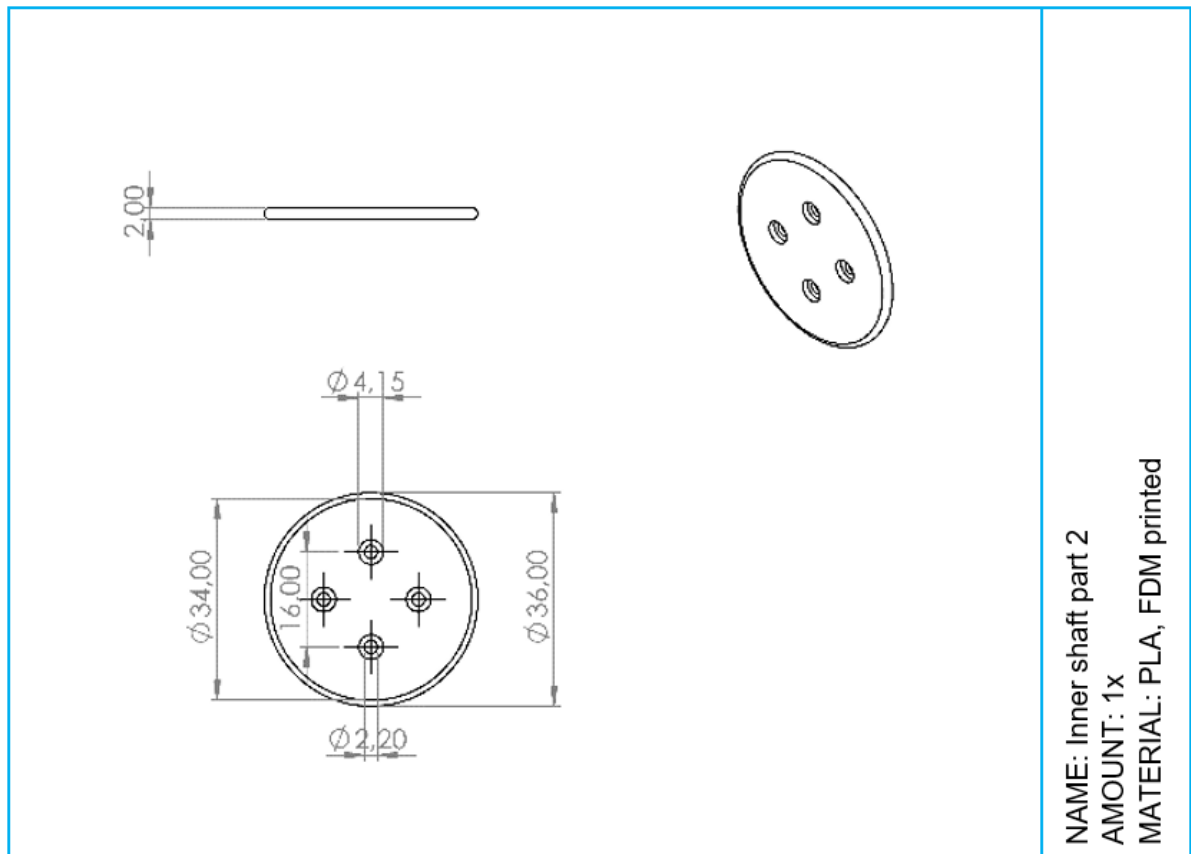


Figure E.7: Construction drawings of the inner shaft part 2 - 3D Printed prototype

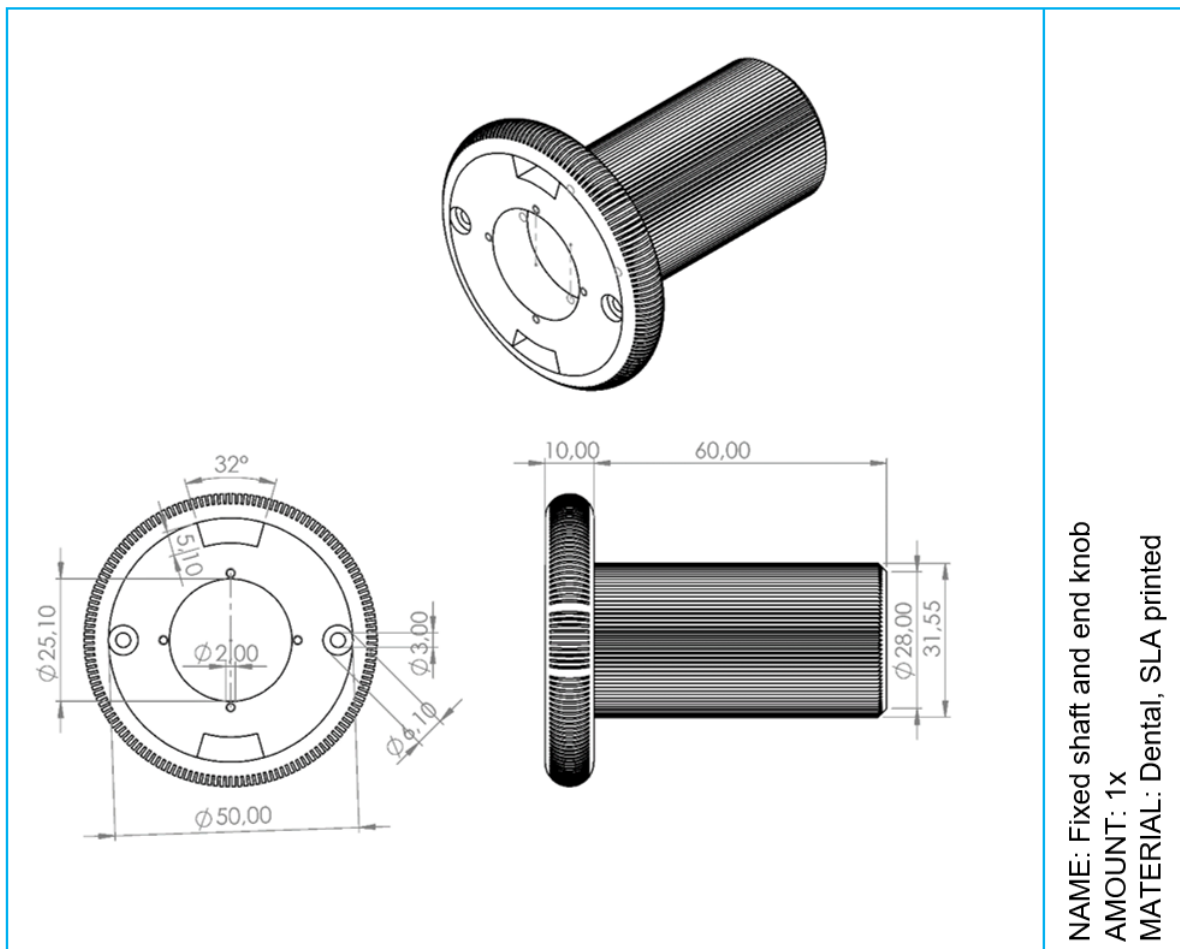


Figure E.8: Construction drawings of fixed shaft and the end knob combination - 3D Printed prototype

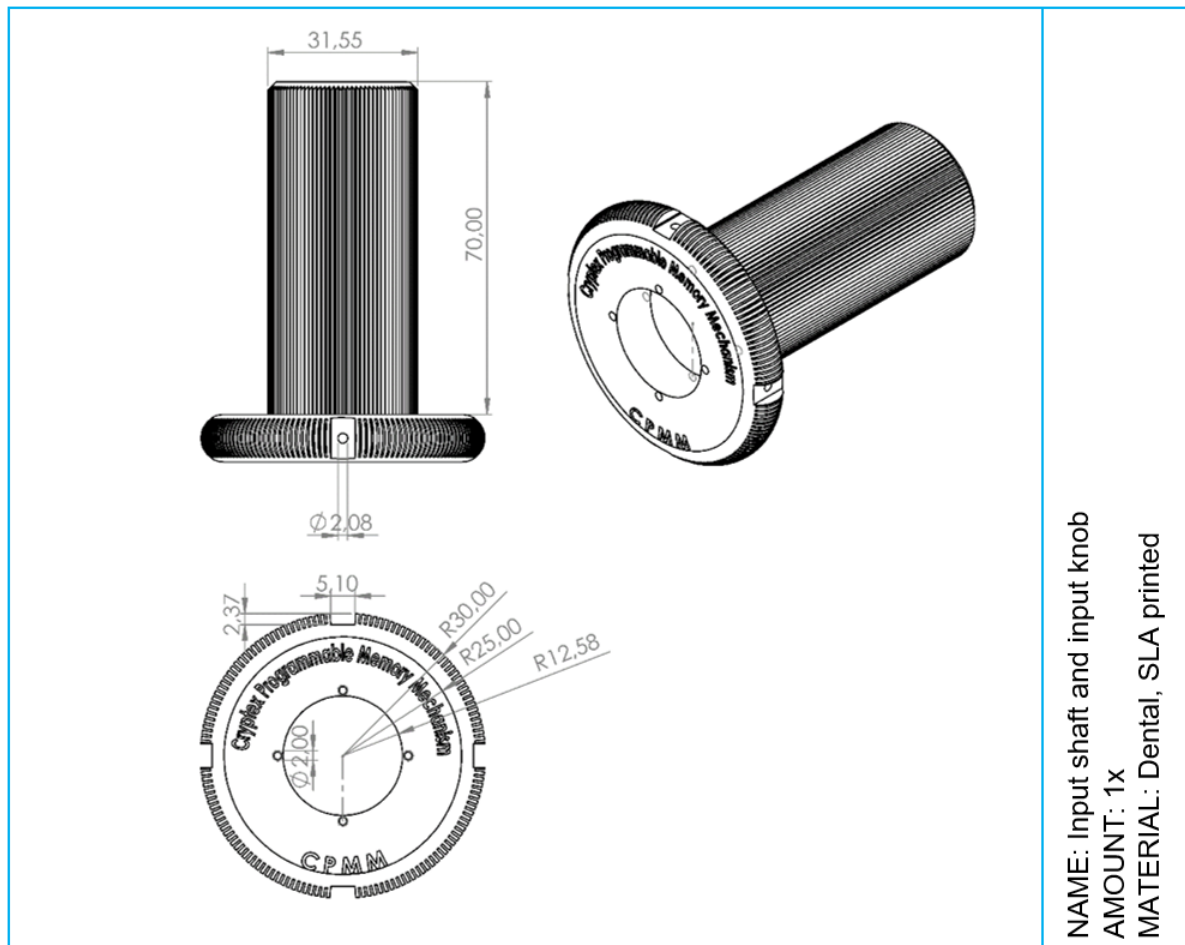


Figure E.9: Construction drawings of input shaft and the input knob combination - 3D Printed prototype

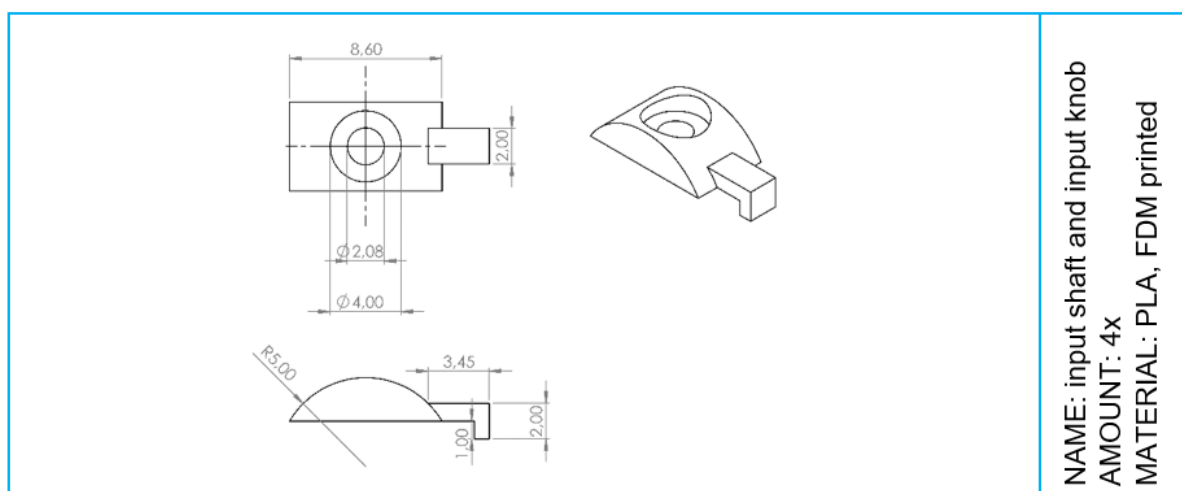


Figure E.10: Construction drawings of the pins of the input knob - 3D Printed prototype

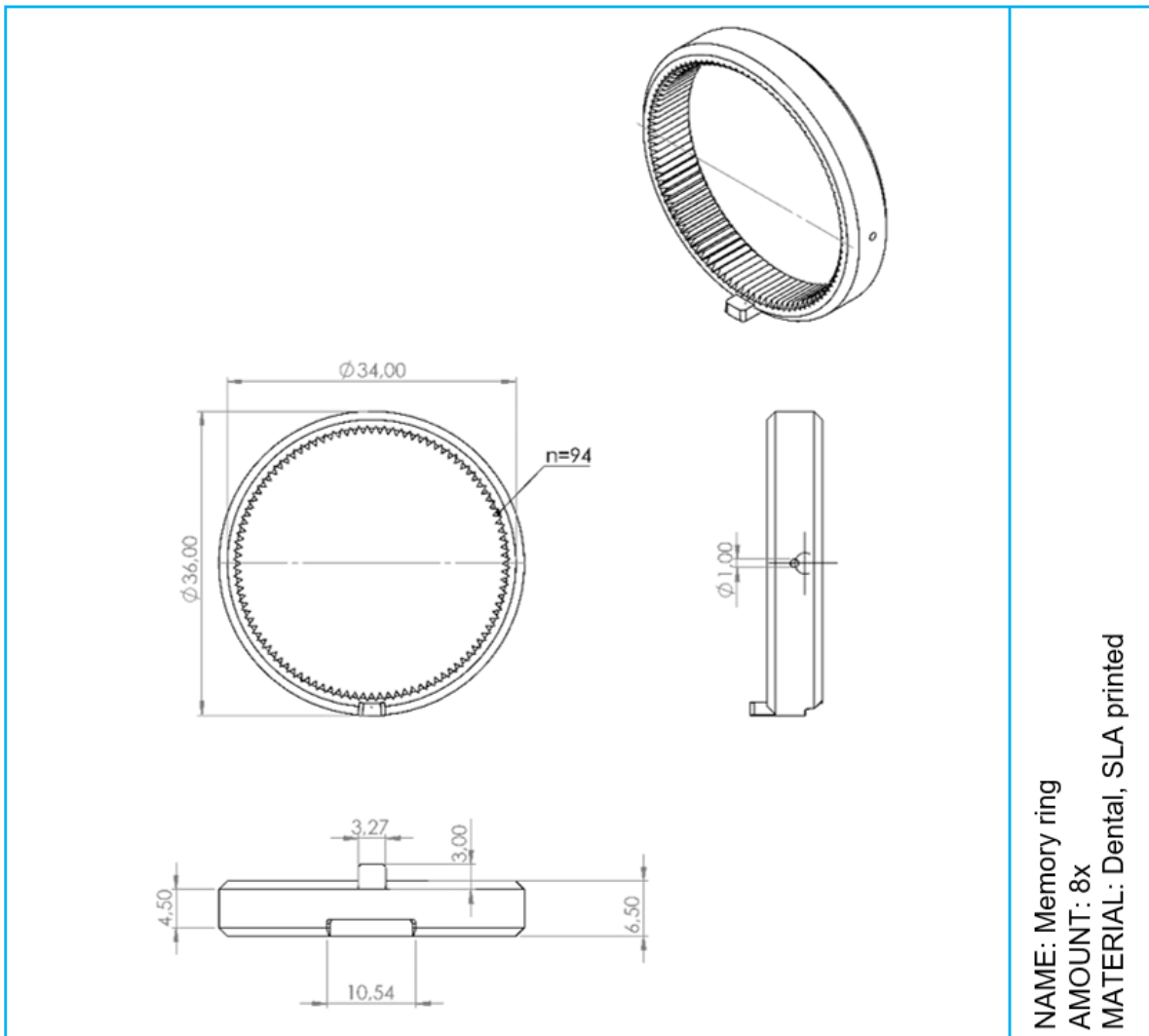


Figure E.11: Construction drawings of the memory ring- 3D Printed prototype

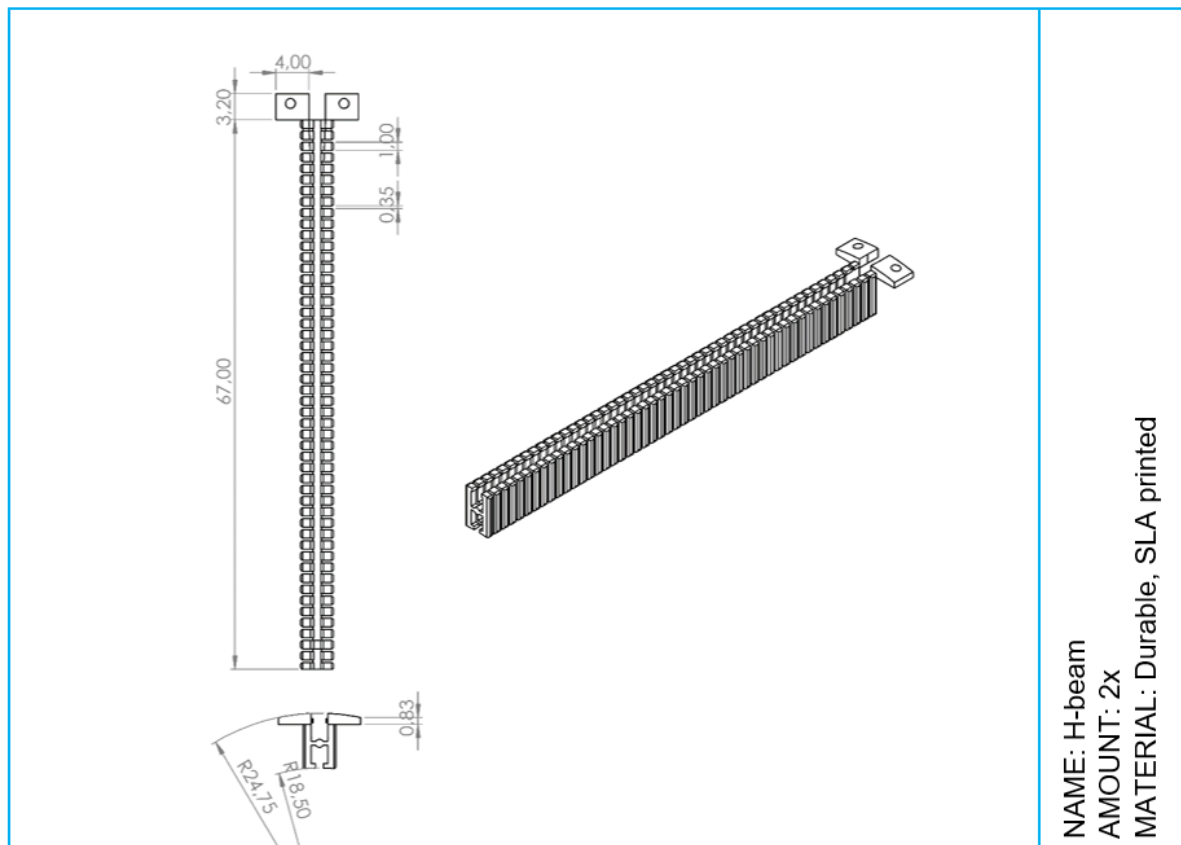


Figure E.12: Construction drawings of the H-beam - 3D Printed prototype

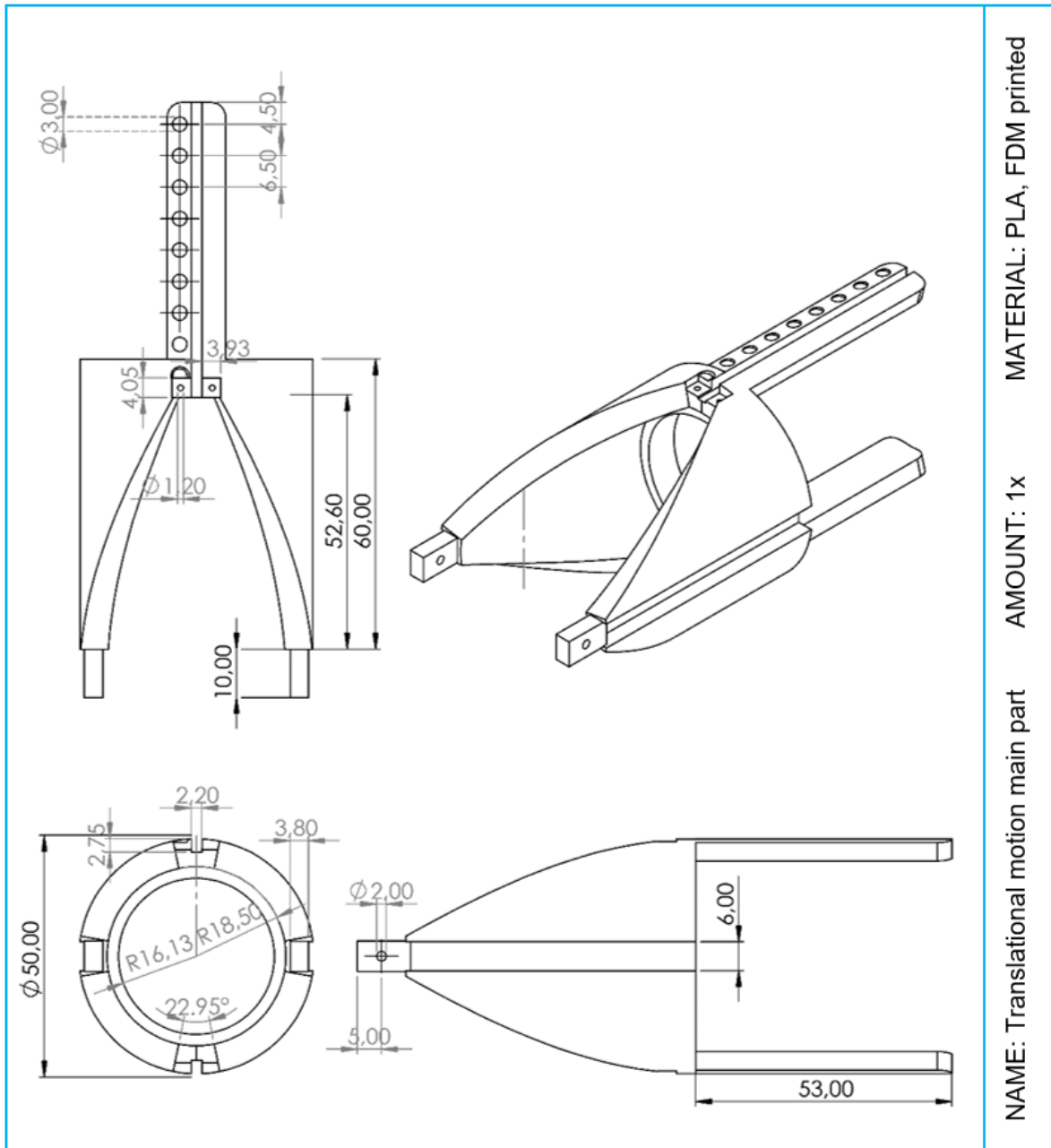


Figure E.13: Construction drawings of translational motion main part - 3D Printed prototype

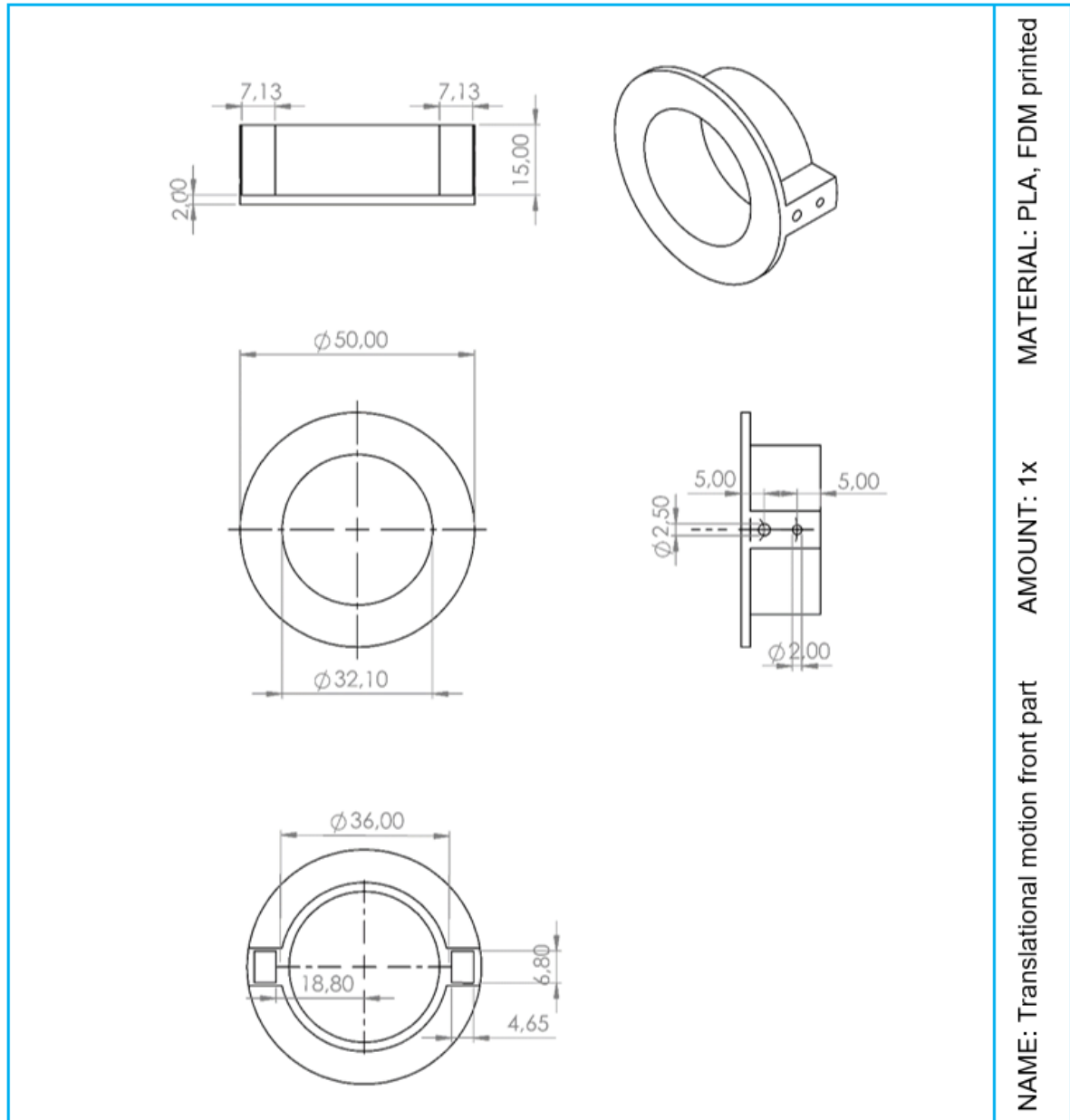


Figure E.14: Construction drawings of translational motion front part - 3D Printed prototype

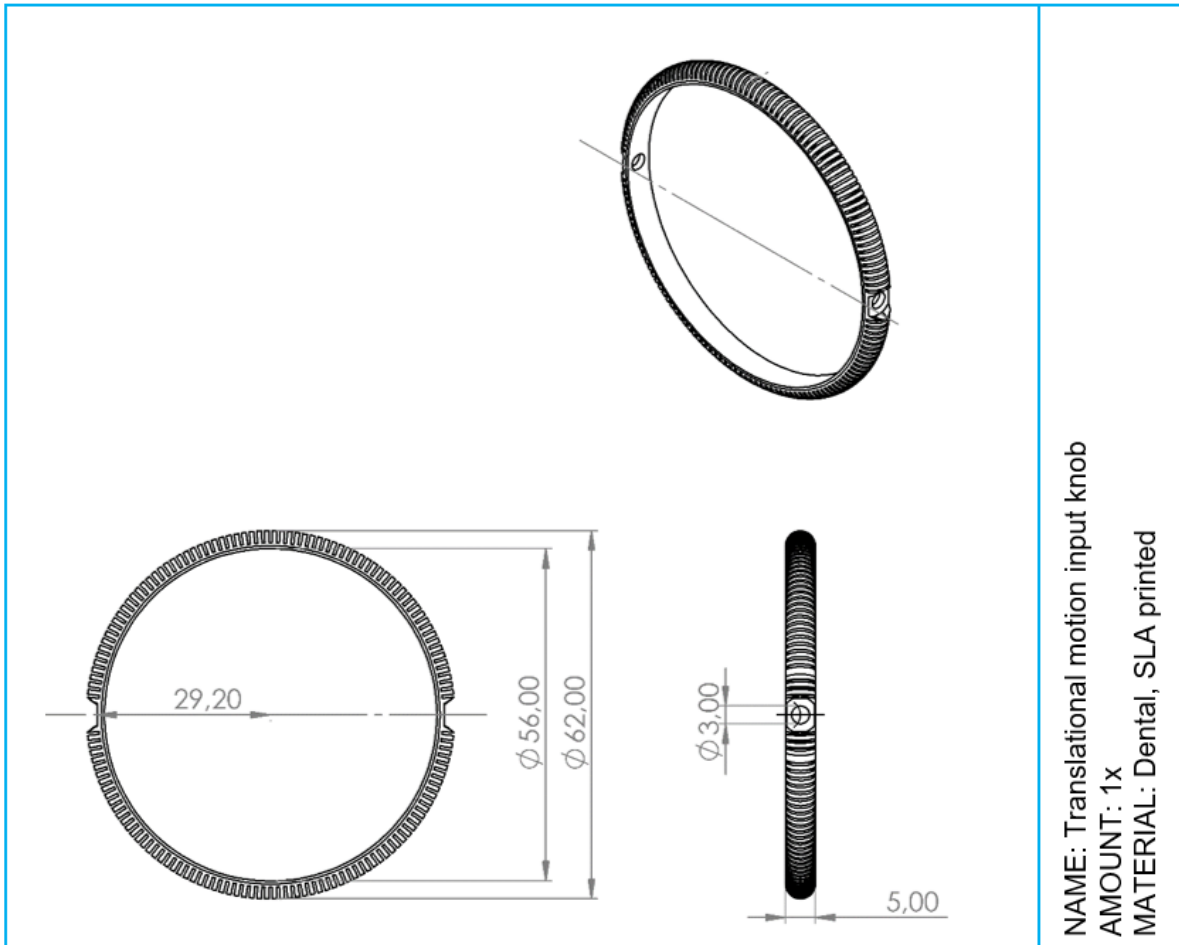


Figure E.15: Construction drawings of translational motion input knob - 3D Printed prototype

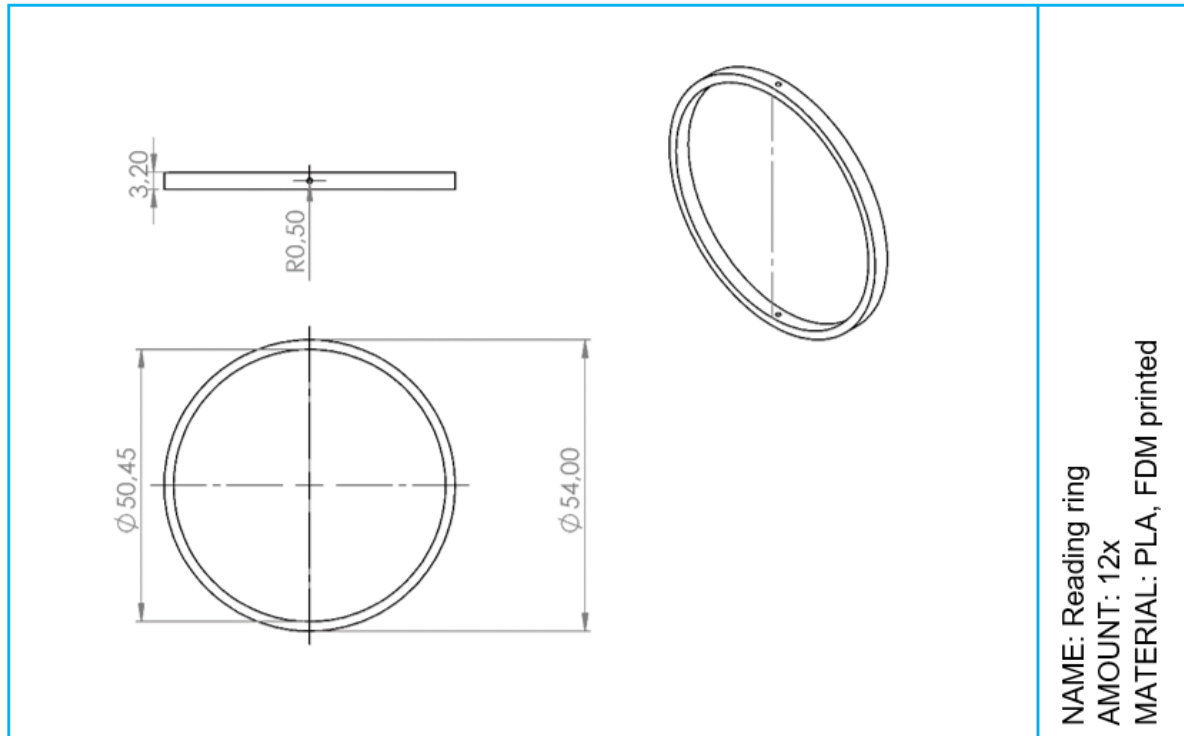


Figure E.16: Construction drawings of the reading ring - 3D Printed prototype

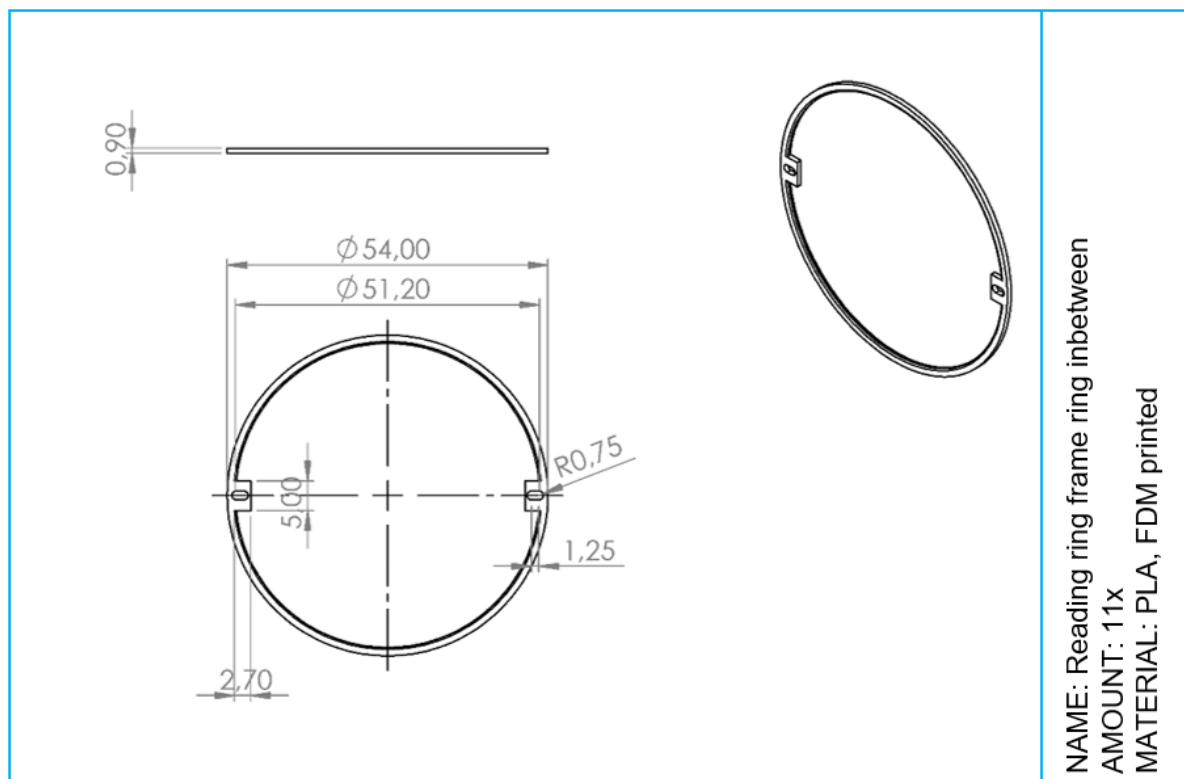


Figure E.17: Construction drawings of the reading ring frame in between - 3D Printed prototype

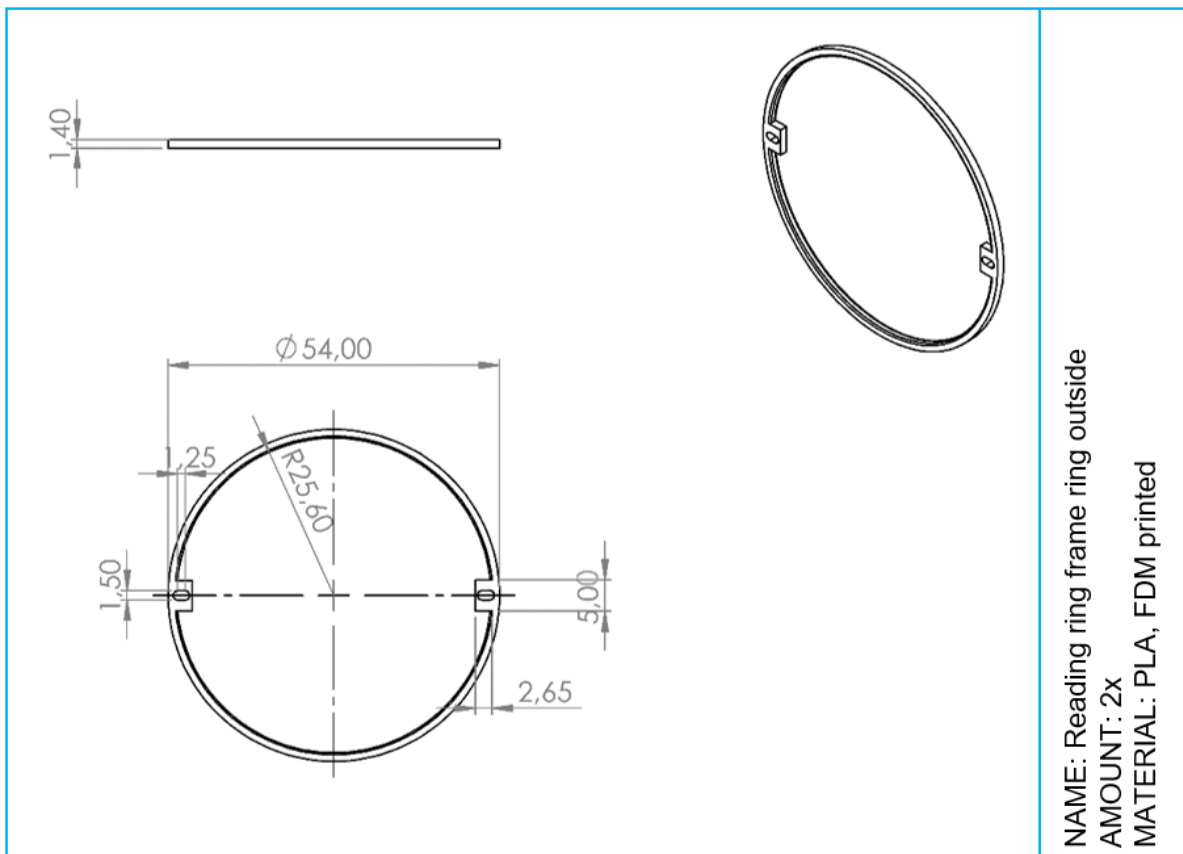


Figure E.18: Construction drawings of the reading ring frame outside rings - 3D Printed prototype

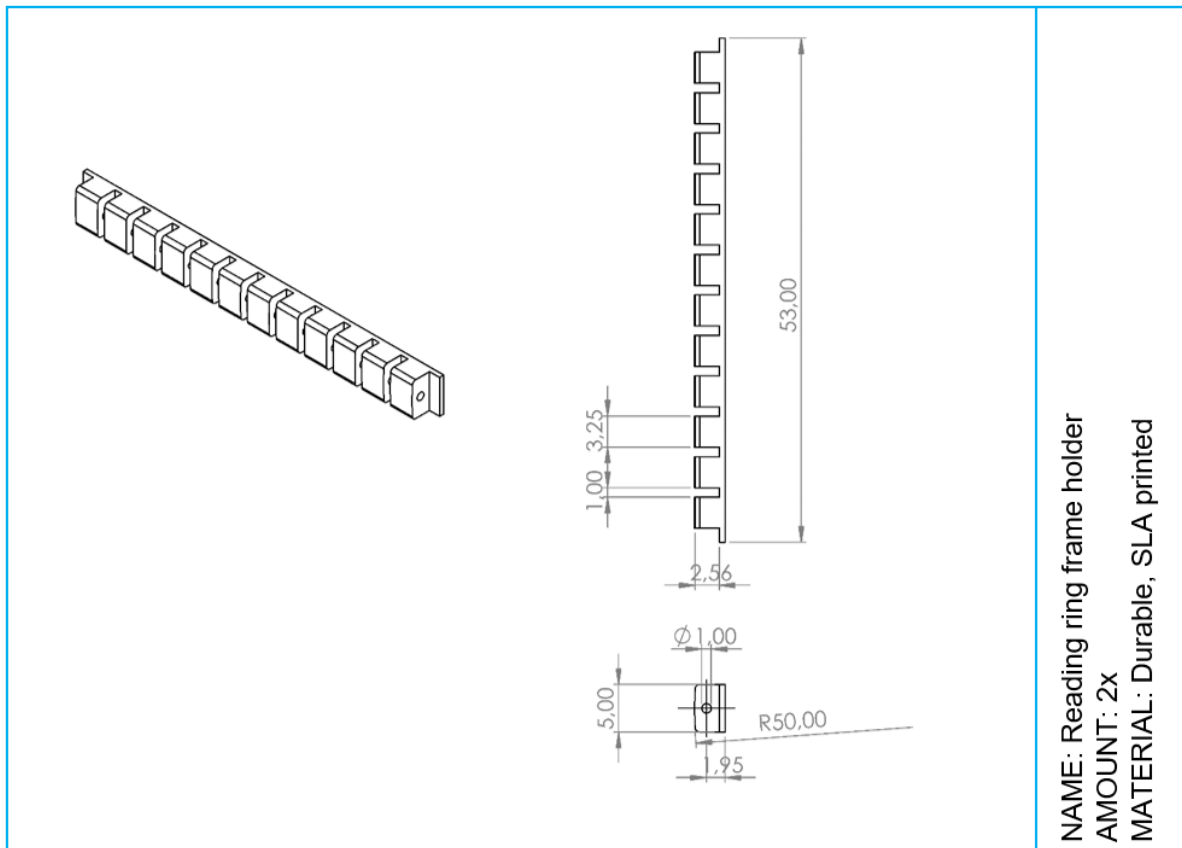


Figure E.19: Construction drawings of the reading ring frame holder - 3D Printed prototype

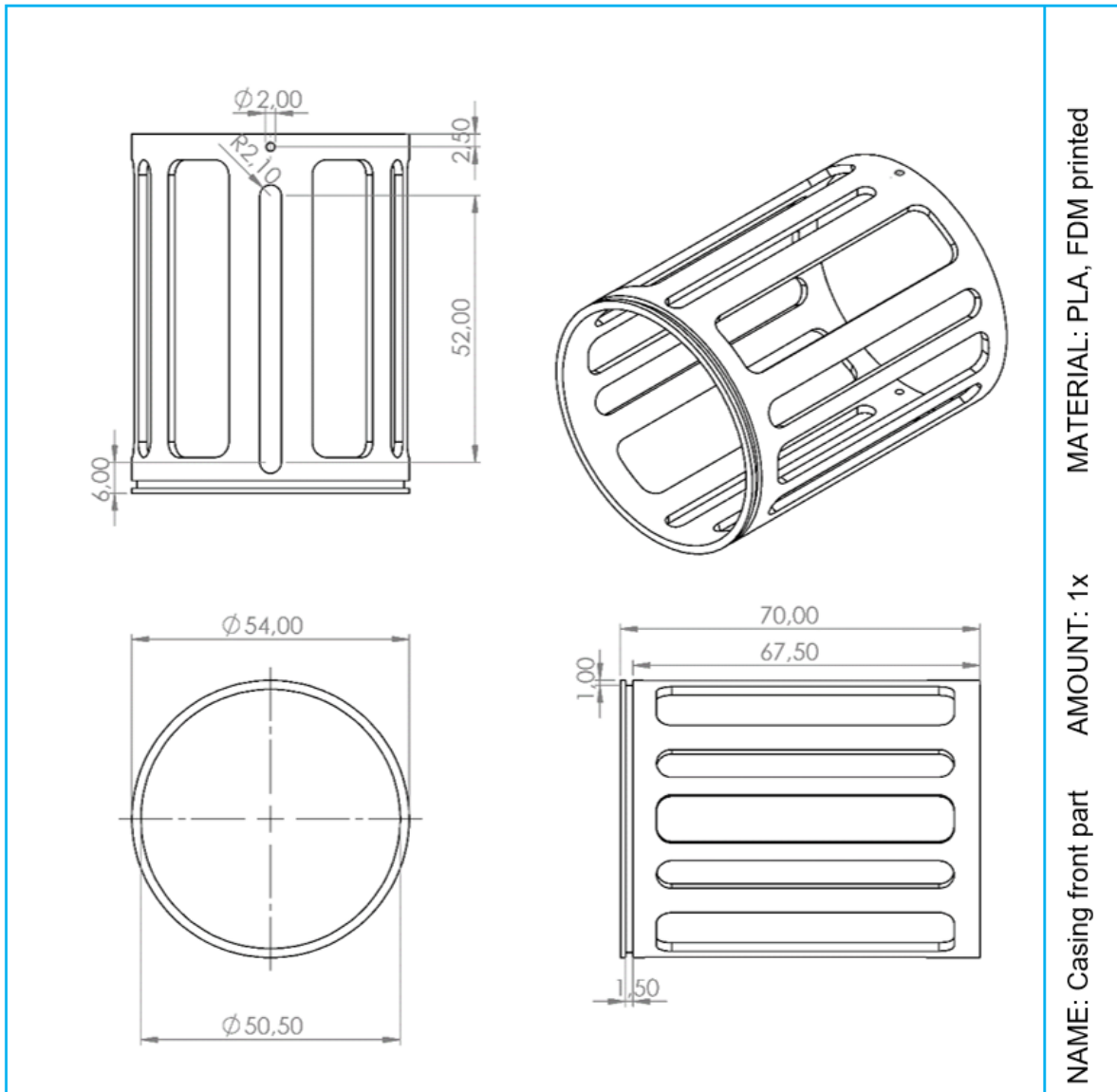


Figure E.20: Construction drawings of the casing front part - 3D Printed prototype

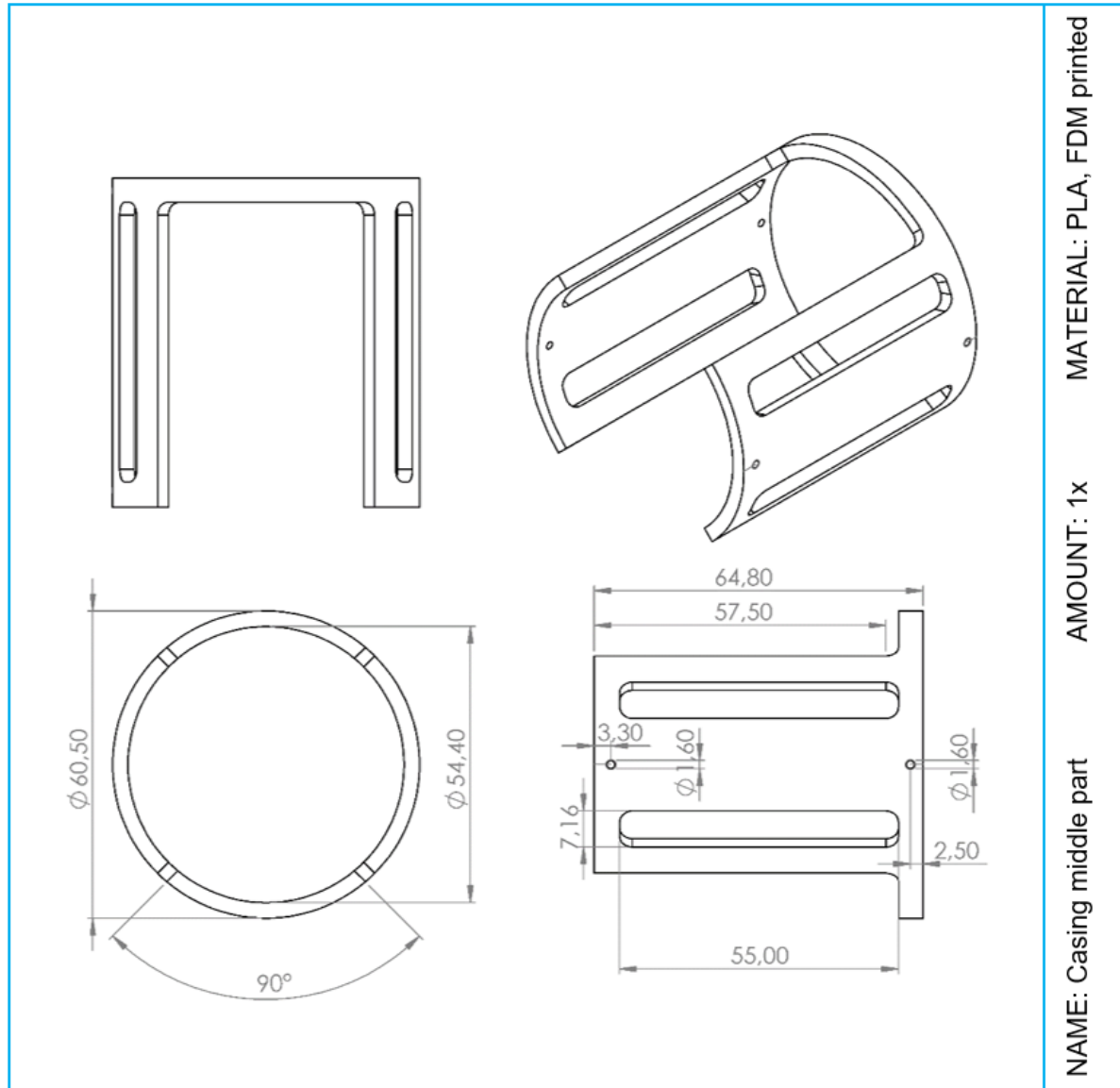


Figure E.21: Construction drawings of the casing middle part - 3D Printed prototype

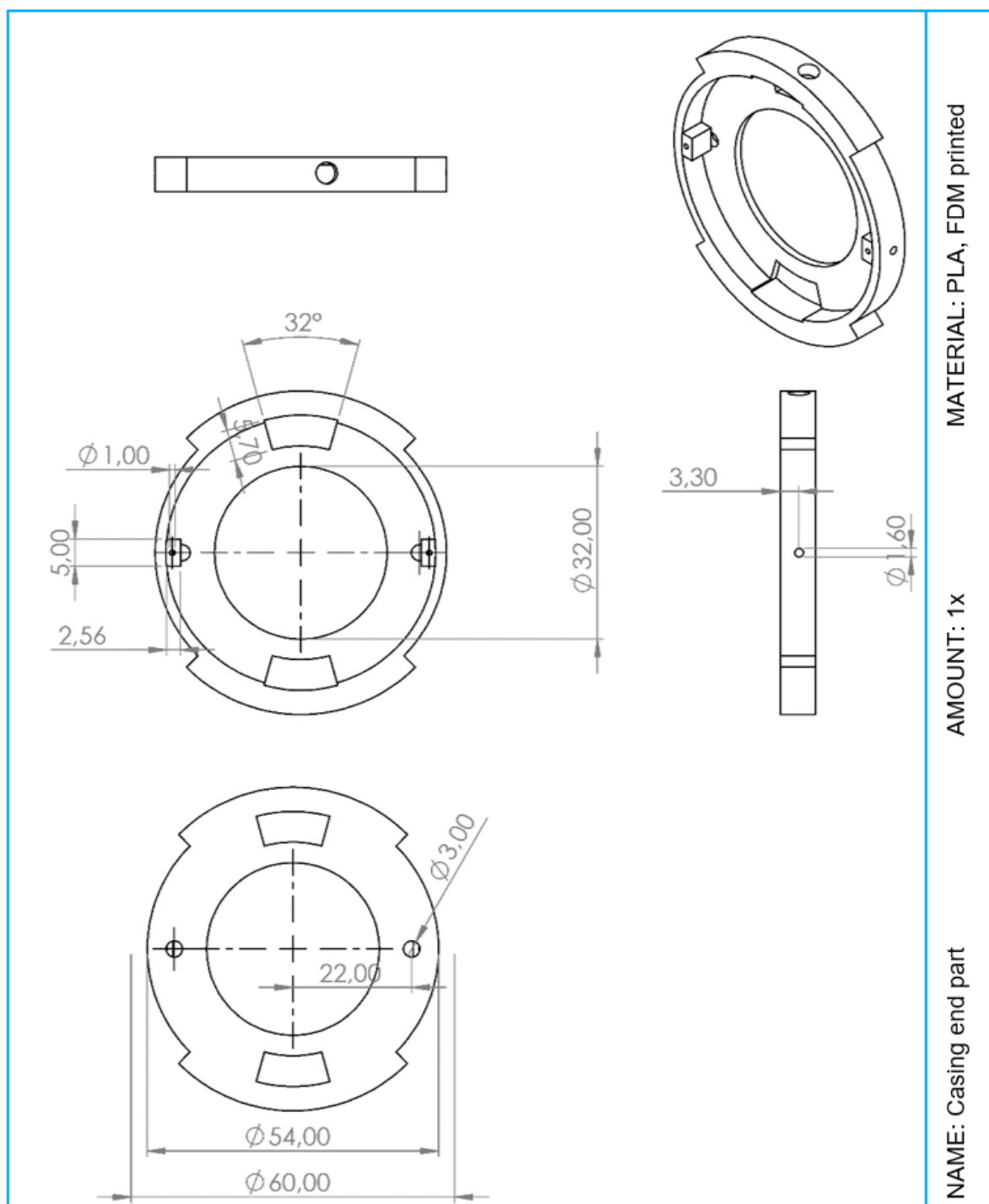


Figure E.22: Construction drawings of the casing end part - 3D Printed prototype



Figure E.23: 3D printed shaft and memory ring version 3

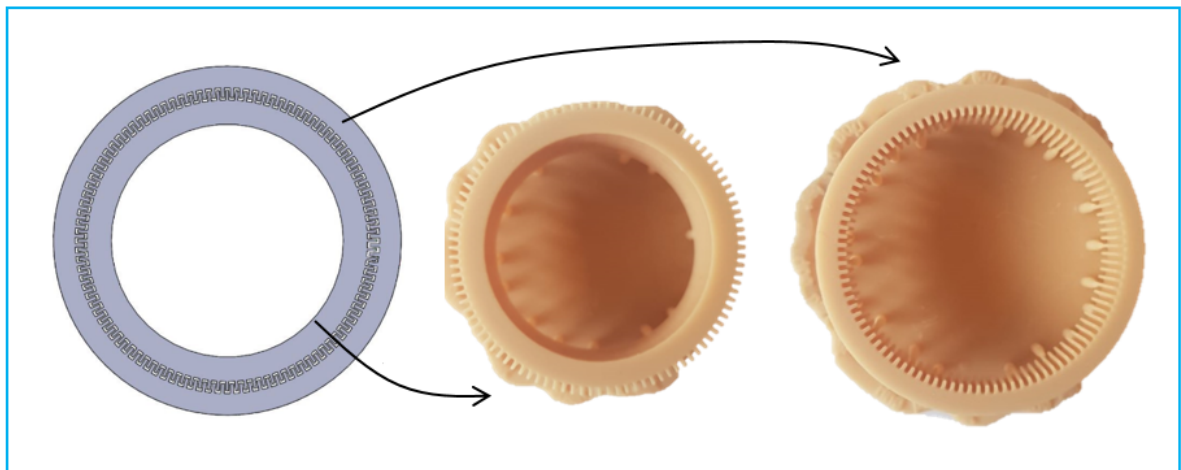


Figure E.24: 3D printed prototype, rectangular teeth.

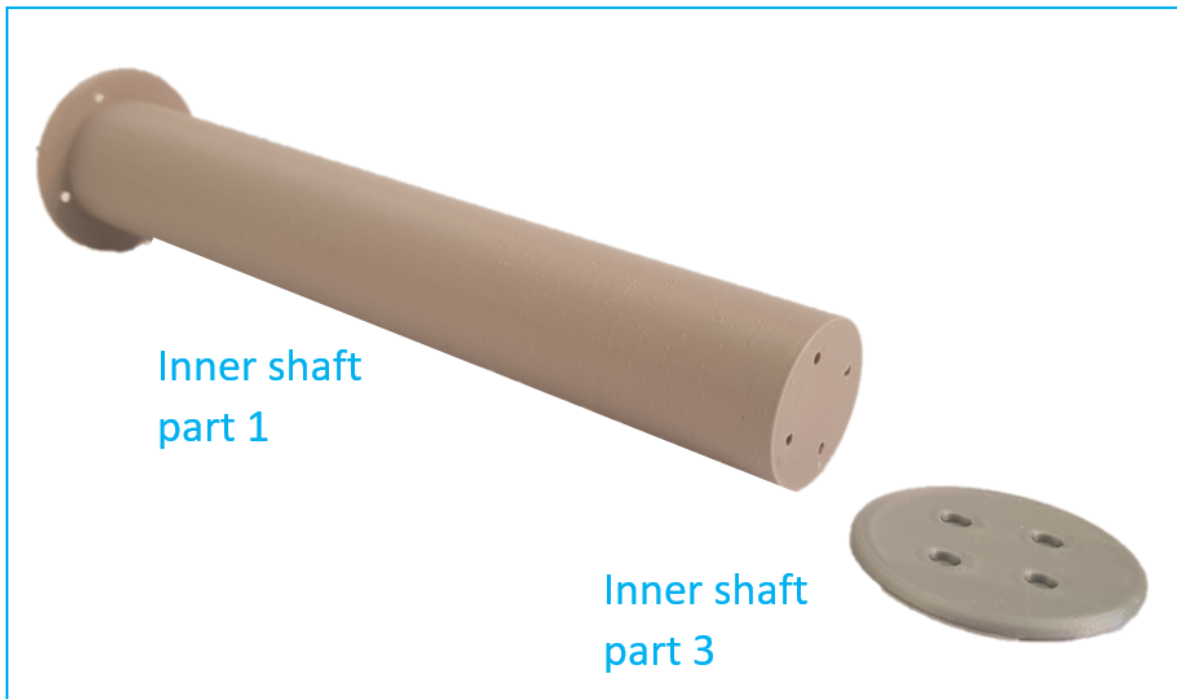


Figure E.25: Picture of the inner shaft

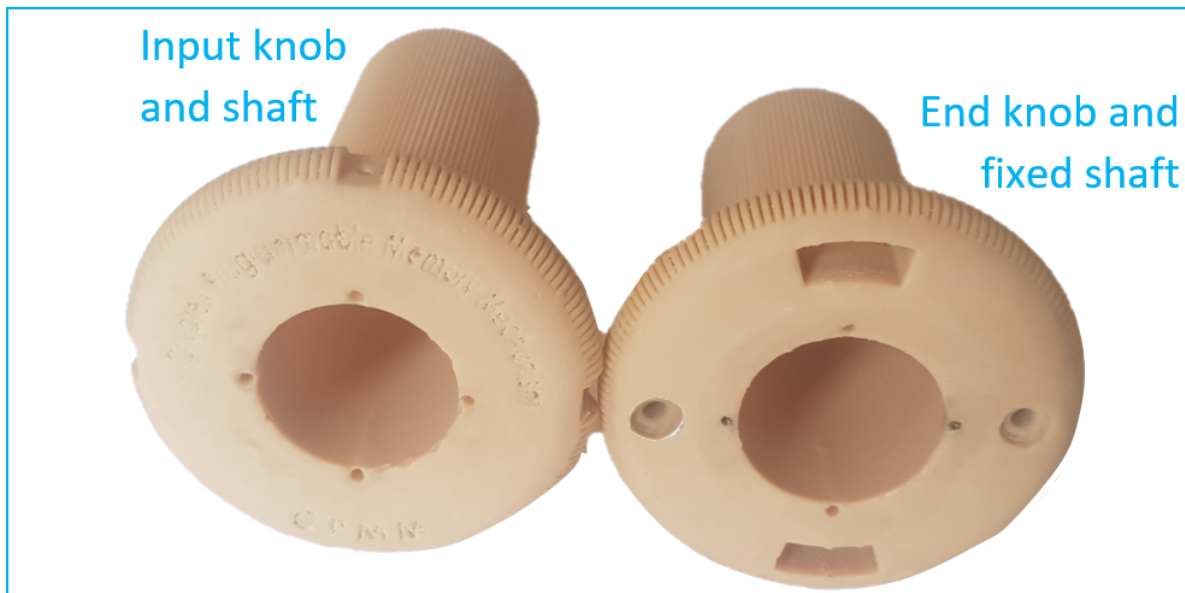


Figure E.26: Picture of the input knob-shaft and the end knob and fixed shaft from the 3D printed prototype.

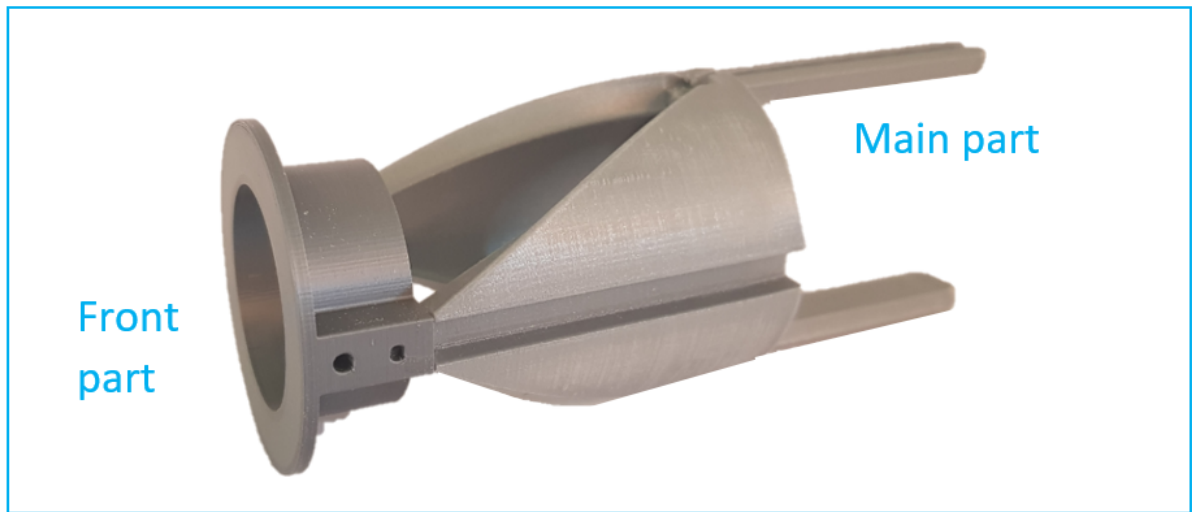


Figure E.27: Picture of the translational motion parts from the 3D printed prototype

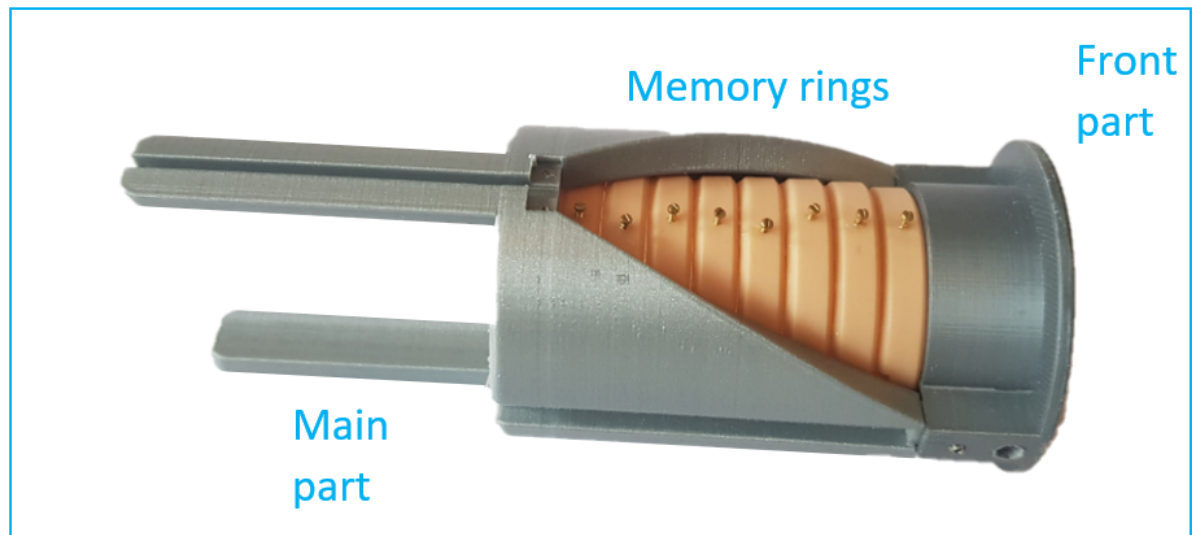


Figure E.28: Picture of the translational motion parts including the memory rings of the 3D printed prototype

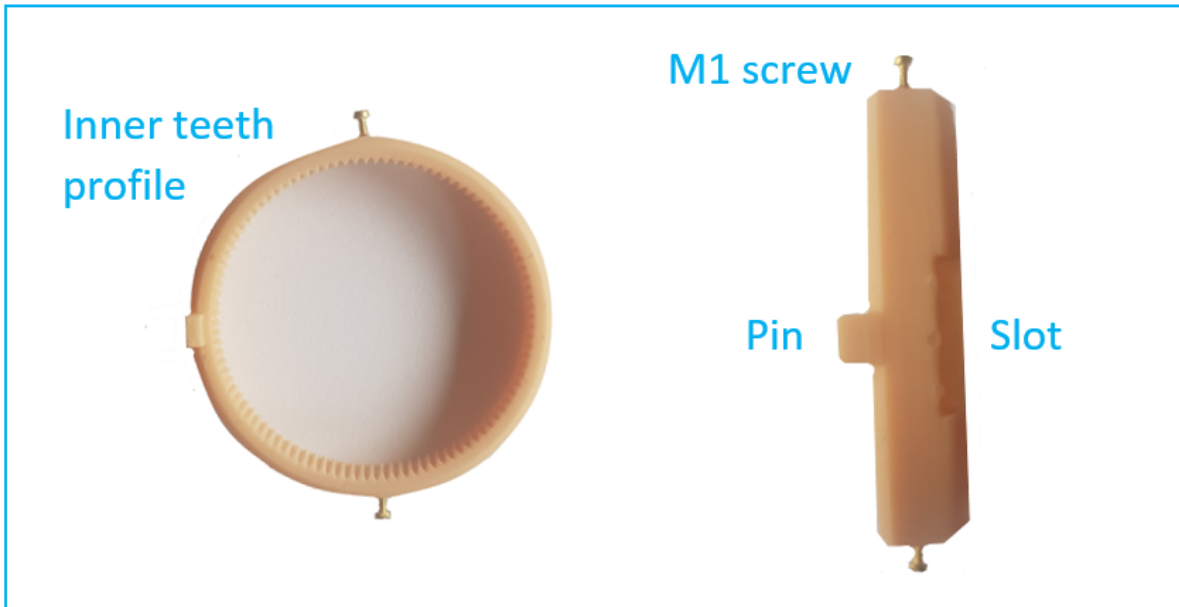


Figure E.29: Picture of a memory ring from the 3D printed prototype



Figure E.30: Picture of the reading rings in their frame from the 3D printed prototype

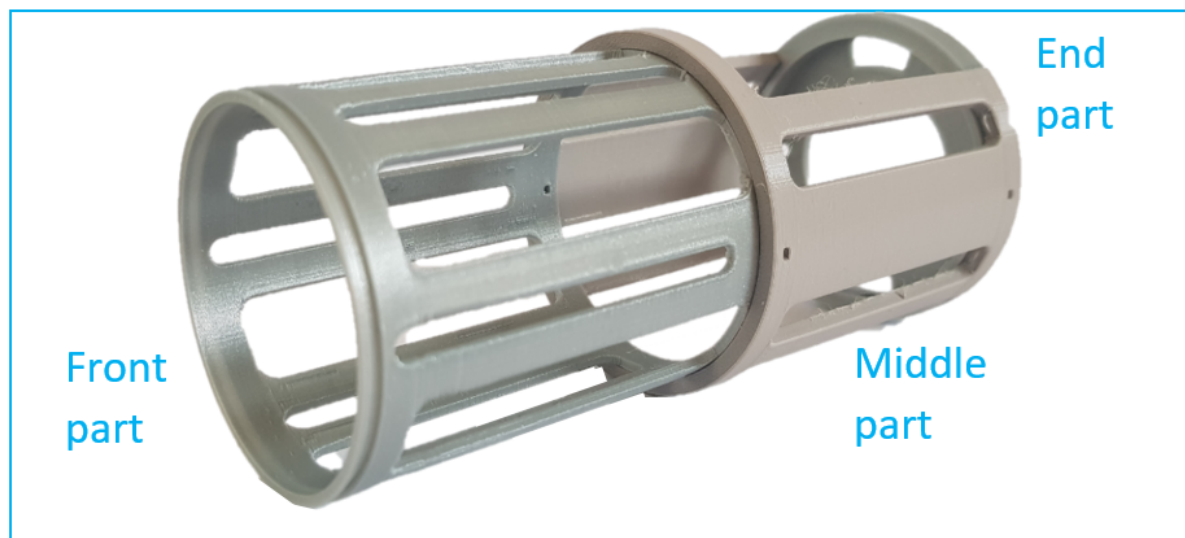
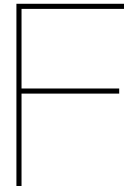


Figure E.31: Picture of the casing components of the 3D printed prototype



MATLAB scripts

MATLAB script for the input output relations of the CPMM is provided in Figure F.1.

```
%% Movement of the tool

%% Determine the input rotation with the range of angles the tool
should be able to make

alpha = linspace(-90,90,19);    % Range of angles of the tool

% Dimensions of the memory ring and reading ring
rM_i = 16;                      % Radius of yellow memory ring
                                % (inner radius)
rM_o = 18;                      % Outer radius of yellow ring
rR = 54/2;                      % Radius of blue reading ring
ri = 3;                         % Cables 3 mm away from the midline

% Calculating input and output
dL1 = 2*pi*ri*(alpha./360);    % Displacement of the cable
dL2 = -2*pi*ri*(alpha./360);   % Antagonist displacement

angle = dL1./(2*pi*rR)*360;    % angle made by rings to provide
                                % displacement

s = dL1.*(rM_i/rR);           % displacement of yellow ring (inside)

% tables
T1 = table(alpha', dL1', s', angle');
T1.Properties.VariableNames{'Var1'} = 'angle_tool'
T1.Properties.VariableNames{'Var2'} = 'dlength_cable'
T1.Properties.VariableNames{'Var3'} = 'dlength_yr'
T1.Properties.VariableNames{'Var4'} = 'angle'

%% Determine the angles the tool can make with teeth width = 1.002 mm

P = 1.002;                      % Teeth width [mm]
Step = [1,2,3,4];              % Number of steps
Pt = P.* Step;                 % Step input

dL= Pt./(rM_i/rR);             % Displacement of the cable
Angle = (dL.*360)./(2*pi*ri)   % Angle the tool makes

% tables
T2 = table(Step', dL', Angle');
T2.Properties.VariableNames{'Var1'} = 'Input_step'
T2.Properties.VariableNames{'Var2'} = 'dlength_cable'
T2.Properties.VariableNames{'Var3'} = 'Alpha'
```

Figure F.1: MATLAB script for the input output relations of the CPMM

